

AD-A185 748

INTEGRATED SYSTEMS WITH APPLICATIONS TO THE
MULTI-PHASES OF THE EPHEMERID. (U) RADEX INC CARLISLE
MA J N BASS ET AL. 27 FEB 87 RX-870227 AFGL-TR-87-0064

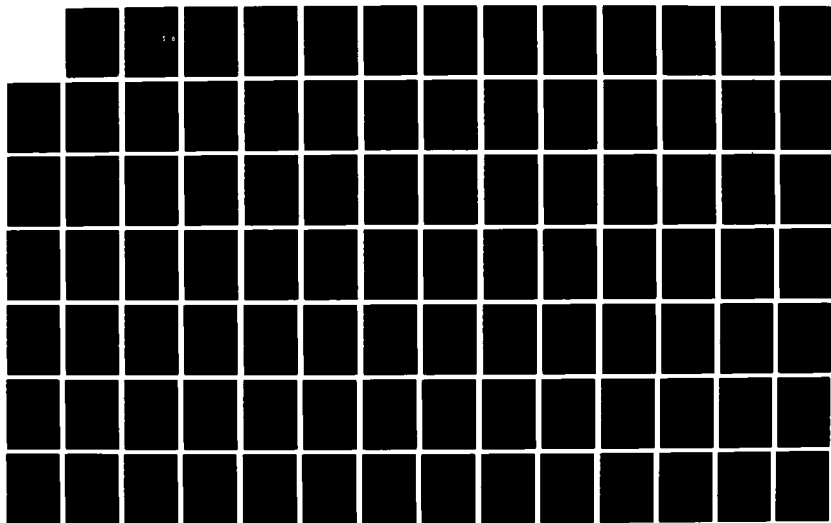
1/3

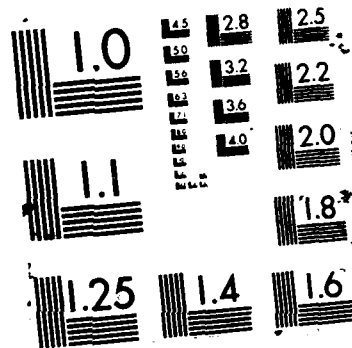
UNCLASSIFIED

F19628-83-C-0134

F/G 4/1

NL





12

AFGL-TR-87-0064

DTIC FILE COPY

Integrated Systems With Applications to the
Multi-phases of the Ephemerides, Physics and
Mathematics of the Upper Atmosphere

AD-A185 748

J.N. Bass
K.H. Bhavnani
N.A. Bonito
C.M. Bryant, Jr

W. J. McNeil
F. R. Roberts
D.A. Sannerud
A.J. Kantor

Radex, Inc
192 Log Hill Road
Carlisle, MA 01741

DTIC
ELECTE
OCT 13 1987
S D

27 February 1987

Final Report
June 1983-February 1987

APPROVED FOR PUBLIC RELEASE; DISTRIBUTION UNLIMITED

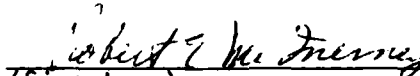
AIR FORCE GEOPHYSICS LABORATORY
AIR FORCE SYSTEMS COMMAND
UNITED STATES AIR FORCE
HANSCOM AIR FORCE BASE, MASSACHUSETTS 01731

87 10 6 052

"This technical report has been reviewed and is approved for publication"

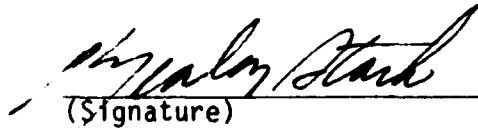

(Signature)

EDWARD C. ROBINSON
Contract Manager


(Signature)

ROBERT E. MCINERNEY
Chief
Data Systems Branch

FOR THE COMMANDER


(Signature)

C. NEALON STARK
Director
Aerospace Engineering Division

This report has been reviewed by the ESD Public Affairs Office (PA) and is releasable to the National Technical Information Service (NTIS).

Qualified requestors may obtain additional copies from the Defense Technical Information Center. All others should apply to the National Technical Information Service.

If your address has changed, or if you wish to be removed from the mailing list, or if the addressee is no longer employed by your organization, please notify AFGL/DAA, Hanscom AFB, MA 01731. This will assist us in maintaining a current mailing list.

Do not return copies of this report unless contractual obligations or notices on a specific document require that it be returned.

| | | | | | |
|--|-------|---|--|--|--------------------------------|
| 1a. REPORT SECURITY CLASSIFICATION Unclassified | | | 1b. RESTRICTIVE MARKINGS | | |
| 2a. SECURITY CLASSIFICATION AUTHORITY | | | 3. DISTRIBUTION/AVAILABILITY OF REPORT Approved for Public release; distribution unlimited | | |
| 2b. DECLASSIFICATION/DOWNGRADING SCHEDULE | | | | | |
| 4. PERFORMING ORGANIZATION REPORT NUMBER(S) RX-870227 | | | 5. MONITORING ORGANIZATION REPORT NUMBER(S) AFGL-TR-87-0064 | | |
| 6a. NAME OF PERFORMING ORGANIZATION Radex, Inc. | | 6b. OFFICE SYMBOL (if applicable) | | 7a. NAME OF MONITORING ORGANIZATION Air Force Geophysics Laboratory | |
| 6c. ADDRESS (City, State, and ZIP Code) 192 Log Hill Road Carlisle, MA 01741 | | | 7b. ADDRESS (City, State, and ZIP Code) Hanscom AFB, MA 01731 | | |
| 8a. NAME OF FUNDING/SPONSORING ORGANIZATION Aerospace Engineering Div | | 8b. OFFICE SYMBOL (if applicable) LCY | | 9. PROCUREMENT INSTRUMENT IDENTIFICATION NUMBER Contract F19628-83-C-0134 | |
| 8c. ADDRESS (City, State, and ZIP Code) AFGL/Hanscom AFB, MA 01731 | | | 10. SOURCE OF FUNDING NUMBERS | | |
| | | | PROGRAM ELEMENT NO. 62101F | PROJECT NO. 9993 | TASK NO. XX |
| | | | WORK UNIT ACCESSION NO. YG | | |
| 11. TITLE (Include Security Classification) Integrated Systems with Applications to the Multi-phases of the Ephemerides, Physics, and Mathematics of the Upper Atmosphere | | | | | |
| 12. PERSONAL AUTHOR(S) J.N. Bass, K.H. Bhavnani, N.A. Bonito, C.M. Bryant, Jr, W.J. McNeill, F.R. Roberts*, D.A. Sannerud, A.J. Kantor† | | | | | |
| 13a. TYPE OF REPORT Final | | 13b. TIME COVERED FROM 6/83 TO 2/87 | | 14. DATE OF REPORT (Year, Month, Day) 1987 FEB 27 | |
| | | | | 15. PAGE COUNT 221 | |
| 16. SUPPLEMENTARY NOTATION *Logicon, Inc., Lexington, MA †Consultant | | | | | |
| 17. COSATI CODES | | | 18. SUBJECT TERMS (Continue on reverse if necessary and identify by block number) | | |
| FIELD | GROUP | SUB-GROUP | Atmospheric density; Ionosphere; Scintillation; Magnetic field models; Trapped particles; Auroral precipitation; Interactive targeting; Celestial aspect sensor; Ephemeris | | |
| | | | | | |
| 19. ABSTRACT (Continue on reverse if necessary and identify by block number) | | | | | |
| This contract provided research, analysis and development support for integrated systems with applications to ephemerides, physics, and mathematics of the upper atmosphere. Investigations have been supported in various aspects of neutral atmospheric density, ionospheric scintillation, magnetic field models, magnetospherically trapped particles and auroral particle precipitation. Software systems have been developed for processing and analyzing data pertaining to these research areas, and for interactive targeting of the space shuttle, ephemeris computation during double thrust, and processing of celestial aspect sensor data. | | | | | |
| 20. DISTRIBUTION/AVAILABILITY OF ABSTRACT <input checked="" type="checkbox"/> UNCLASSIFIED/UNLIMITED <input type="checkbox"/> SAME AS RPT. <input type="checkbox"/> DTIC USERS | | | 21. ABSTRACT SECURITY CLASSIFICATION Unclassified | | |
| 22a. NAME OF RESPONSIBLE INDIVIDUAL Edward C. Robinson | | | 22b. TELEPHONE (Include Area Code) (617) 377-3840 | | 22c. OFFICE SYMBOL AFGL/LCY |

ACKNOWLEDGEMENTS

The work described in this report required the involvement and guidance of a number of individuals at AFGL, and their interest and encouragement is gratefully acknowledged.

Ed Robinson of the Data Systems Branch both initiated and coordinated the activities as Contract Monitor.
We also deeply appreciate the continuing and invaluable help of Bob McInerney and Bob Raistrick of the same branch.

Various investigators were involved throughout the projects, and provided essential support and the opportunity for some challenging studies in their fields:

Santimay Basu, Frank Marcos and Ed Weber
Ionospheric Effects Branch;

Sue Gussenhoven and Dave Hardy
Space Particle Environment Branch;

Dick Nadile and Tony Ratkowski
Atmospheric Backgrounds Branch.

The support of other collaborators who provided significant guidance and interaction is also highly appreciated:

Sunanda Basu Emmanuel College;

Bill Grieder and Dick Hegblom Boston College;

Henry Miranda Miranda Laboratories.

This report was developed and prepared by Deirdra Sullivan.



| | |
|--------------------|-------------------------------------|
| or | |
| %1 | <input checked="" type="checkbox"/> |
| ed | <input type="checkbox"/> |
| Availability Codes | |
| Dist | Review and/or Special |
| A-1 | |

TABLE OF CONTENTS

| | <u>Page</u> |
|--|-------------|
| 1.0 Studies of Neutral Atmospheric Density | 1 |
| 1.1 Introduction | 1 |
| 1.2 The STAT Input Description | 5 |
| 1.3 Other programs | 16 |
| 1.3.1 Data Base Construction | 16 |
| 1.3.2 PULL/CONSOL/MERGE | 19 |
| 1.3.3 HISTO | 19 |
| 1.3.4 FREQ/EDIST | 19 |
| 1.3.5 KLL | 31 |
| 1.4 PACKLIB | 31 |
| 1.5 Model Development | 38 |
| 1.5.1 Jacchia 70 Tides | 38 |
| 1.5.2 Air Force Reference Atmosphere | 39 |
| 1.6 Study of Statistical Techniques | |
| Applied to Atmospheric Density Data | 50 |
| 1.6.1 Introduction | 50 |
| 1.6.2 One Way Random Effects Analysis of Variance | 50 |
| 1.6.3 Calculation of the Autocorrelation | |
| Coefficients | 62 |
| 1.6.4 Effect of Autocorrelation on the Analysis | |
| of Satellite Data | 63 |
| 1.6.5 Conclusion | 74 |
| 1.7 AE-E Local Time Effect | 75 |
| References | 78, 79 |
| 2.0 Ionospheric Scintillation Data Processing Systems. . | 80 |
| 2.1 Overview | 80 |
| 2.2 Description of Procedures | 90 |
| 2.3 DFT Window/MEM Study | 90 |
| 2.4 Statistics Programs | 92 |
| 2.5 SDS Scintillation Processing System | |
| User's Guide | 95 |
| 2.5.1 Introduction | 95 |
| 2.5.2 SDS Tape Scan | 95 |
| 2.5.3 Normal SDS Processing | 98 |
| 2.5.4 Merging SDS Data Files | 99 |
| 2.5.5 End of the Month Statistics | 99 |
| 2.5.6 SDS Time Series Plots | 104 |
| 2.5.7 Dumping SDS Field Tapes | 107 |
| References | 108 |

TABLE OF CONTENTS (cont'd)

| | <u>Page</u> |
|---|-------------|
| 3.0 Study of Magnetic Fields | 109 |
| 3.1 Magnetic Field Models | 109 |
| 3.2 Magnetic Field Package MFP | 110 |
| 3.3 Magnetic Field Package BFLD | 111 |
| 3.4 Magnetic Field Package Tsyganenko-USmanov. | 111-3 |
| References | 116 |
| 4.0 Radiation Belt Studies | 117 |
| 4.1 Statistical Analysis | 117 |
| 4.2 Display | 120 |
| References | 126 |
| 5.0 Investigation of Auroral Electron Precipitation Data | |
| 5.1 Probabilistic Modeling of Auroral Electron Precipitation | 127 |
| 5.2 Modeling of Averaged Auroral Properties | 141 |
| References | 147 |
| 6.0 The AFGL Interactive Targeting System | 148 |
| 6.1 Introduction | 148 |
| 6.2 General Description | 149 |
| 6.2.1 System Application | 149 |
| 6.2.2 System Requirements | 150 |
| 6.3 Operations Support Functions | 151 |
| 6.3.1 Vehicle Flight Simulation | 151 |
| 6.3.2 Ephemeris Computations | 154 |
| 6.3.3 Celestial Viewing Functions | 155 |
| 6.3.4 Camera Computations | 158 |
| 6.3.5 Gimbal/Off-Track Calculations | 161 |
| 6.4 Databases | 163 |
| 6.5 Coordinate Systems | 167 |
| 6.6 User's Guide | 171 |
| References | 173 |
| 7.0 Ephemeris Computation for Double Thrust Situations | 174 |
| 7.1 Introduction | 174 |
| 7.2 Functional Description | 174 |
| 7.3 Punched Card Changes from Standard LOKANGL | 176 |
| 7.4 Output | 177 |
| 7.5 Mathematical or Logical Procedures | 178 |
| References | 184 |
| 8.0 Software for Processing Celestial Aspect | |
| Sensor Data | 185 |
| 8.1 Introduction | 185 |
| 8.2 Description of Procedures | 197 |
| References | 221 |

LIST OF FIGURES

| | <u>Page</u> |
|--|-------------|
| Studies of Neutral Atmospheric Density | |
| 1.1 STAT Flowchart | 8 |
| 1.2 Sample DATAMOD Subroutine | 10 |
| 1.3 PULL/CONSOL/MERGE Processing | 20 |
| 1.4 Histogram of SETA-1 vs Kp | 21 |
| 1.5 Histogram of SETA-1 vs Solar Flux | 22 |
| 1.6 Histogram of SETA-1 vs Altitude | 23 |
| 1.7 Histogram of SETA-1 vs Geographic Latitude | 24 |
| 1.8 Histogram of SETA-1 vs Local Time | 25 |
| 1.9 SETA-1 Relative Frequency Distribution of ln(Jacchia 71 Model Ratio) | 27 |
| 1.10 SETA-1 Relative Frequency Distribution of Percent Difference from Jacchia 71 Ratio | 28 |
| 1.11 SETA-1 Empirical Distribution Function of ln(Jacchia 71 Model Ratio) | 29 |
| 1.12 SETA-1 Empirical Distribution Function of Percent Difference from Jacchia 71 Ratio | 30 |
| 1.13 SETA-1 Kp/Latitude/Local Time Plot | 32 |
| 1.14 SETA-1 Kp/Latitude/Local Time Plot of Standard Deviation of ln(Jacchia 71) | 33 |
| 1.15 Sample Program Illustrating PACKLIB CALLS | 34,35 |
| 1.16 PACKLIB Routines | 36,37 |
| 1.17 Ratio of Forbes Density Model to MSIS-83 Density Model | 41 |
| 1.18 Schematic of AFRA-86 Model | 42 |
| 1.19 Mean MSIS-83 Density Variation With K _p | 43 |
| 1.20 Hydrostatic Equilibrium Model in Transition Region 90-120 km | 47 |
| 1.21 Ratio of Forbes Annual Mean Density at 45° N to U. S. Standard 1976 Model | 48 |
| Ionospheric Scintillation Data Processing Systems | |
| 2.1 SDS Scintillation Processing System | 84 |
| 2.2 SDS Data Reduction System | 85 |
| 2.3 SDS Period-end Statistics Processing | 86 |
| 2.4 FLT Ionospheric Scintillation Data Processing System | 87 |
| 2.5 FLT Data Reduction System | 88 |
| 2.6 FLT Period-end Statistics Processing | 89 |
| 2.7 A Typical Tape Scan Output | 96 |
| 2.8 An Example of Deck Setup for Tape Scan | 97 |
| 2.9 Example of Deck Setup for Normal SDS Processing | 100 |
| 2.10 Example of Interactive Use of MERGIT Procedure | 101 |
| 2.11 Typical End of the Month Statistics Report | 102-3 |
| 2.12 Example of Deck Setup for Month End Statistics | 105 |
| 2.13 Typical SDS Time Series Plot after FIL Proc | 106 |
| 2.14 An example of Deck Setup for SDS Time Series Plots | 107 |

LIST OF FIGURES (cont'd)

| | <u>Page</u> |
|--|-------------|
| Magnetospheric Dynamics | |
| 4.1 L-Shell Variations of Electron Counts | 122 |
| 4.2 L-Shell Variations of Ion Counts | 123 |
| 4.3 Spectrogram Depicting Electron Flux Measured by SCATHA as a Function of L-Shell and Pitch Angle . . | 124 |
| Investigation of Auroral Electron Precipitation Data | |
| 5.1 Magnetic Latitude - Local Time DMSP/F6 and F7 . . . | 130 |
| 5.2 Geometry of 50° Latitude Crossing | 132 |
| 5.3 Probabilistic Model Processing System | 135 |
| 5.4 Example of Per-Pass Probability Contours | 137 |
| 5.5 Example of Flux Event Duration Histograms | 139 |
| 5.6 Example of Contours from Original Energy Flux Data, Spherical Harmonic Model, and Fractional Deviation. | 145 |
| 5.7 Histogram of Fractional Deviation of Epstein-Fourier Model from Original Data | 146 |
| The AFGL Interactive Targeting System | |
| 6.1 Vehicle Flight Simulation (Linear Display) | 153 |
| 6.2 Station Look Angle (Example Listing #1) | 156 |
| 6.3 Camera View Simulation at an Instant | 159 |
| 6.4 Camera Celestial Target Tracking | 160 |
| 6.5 LVLH Coordinate System | 168 |
| 6.6 Vehicle Body Coordinate System and Rotation | 170 |
| 6.7 AITS Main Menu | 172 |
| Ephemeris Computation for Double Thrust Situations | |
| 7.1 TAPE4 Structure for the Case of a Single Element Set | 179 |
| 7.2 TAPE4 Structure for the Case of Two Element Sets | 179 |
| 7.3 TAPE4 Structure for a Single Thrust | 181 |
| 7.4 TAPE4 Structure for a Double Thrust | 181 |
| 7.5 Functional Flow Diagram for Double Thrust Analysis | 183 |
| Software for Processing Celestial Aspect Sensor Data | |
| 8.1 CRT Display of Field of View of CAS Showing Star Catalog Entries and 30 Detections | 188 |
| 8.2 Celestial Aspect Sensor Cut-out View | 189 |
| 8.3 Image Element Configuration | 190 |
| 8.4 PCM Telemetry Format | 192 |
| 8.5 Top Level Data Flow for Processing CAS Data | 194 |
| 8.6 Highly Schematic Representation of Manual Initiation and Subsequent Automatic Mode of CASP Operation | 199 |

LIST OF FIGURES (cont'd)

| | <u>Page</u> |
|---|-------------|
| 8.7 Flow Diagram for the Processing of a Single Frame of CAS Data | 201 |
| 8.8 Illustration of Tangent Height. | 205 |
| 8.9 Relationship Between the ECI and IFG Coordinate Systems | 207 |
| 8.10 Geometry Relating the IFG and the VEN Coordinate Systems | 208 |
| 8.11 The Body Coordinate System. | 211 |
| 8.12 Relationship Between Local VEN System and the Launcher Coordinate System (X,Y,Z). | 211 |
| 8.13 CAS Mounting Configuration | 212 |
| 8.14 Geometrical Relationship between Rocket Body Coordinates and the CAS x-y System. | 213 |
| 8.15 Implementation of Subroutine FUNCT | 216 |

LIST OF TABLES

| | <u>Page</u> |
|---|-------------|
| Studies of Neutral Atmospheric Density | |
| 1.1 Statistical Properties of Total Mass Density Log Ratios to MSIS 83: Data to 200 km | 4 |
| 1.2 Neutral Atmospheric Density Satellite Experiment Flight Histories | 4 |
| 1.3 Air Force Reference Neutral Atmospheric Density Data Base | 6 |
| 1.4 Neutral Atmospheric Density Data Base Format | 7 |
| 1.5 Packed Density Data Base Format | 18 |
| 1.6 SETA-1 Jacchia 71 Data Set. | 53-61 |
| 1.7 Autocorrelation Coefficients. | 64-73 |
| 1.8 One Way Analysis of Variance for AE-E Local Time Effect Jacchia 71 Model | 76 |
| 1.9 One Way Analysis of Variance for AE-E Local Time Effect MSIS 83B Model | 77 |
| Ionospheric Scintillation Data Processing Systems | |
| 2.1 Field Tape Data Format | 81 |
| 2.2 Unpacked Data Format | 82 |
| 2.3 SDS and FLT Plots | 83 |
| 2.4 DFT Window Candidates | 92 |
| 2.5 Sample Output of the STATSDS Program | 93,94 |
| Investigation of Auroral Electron Precipitation Data | |
| 5.1 Probabilities of Encountering a Flux Event | 140 |
| Software for Processing Celestial Aspect Sensor Data | |
| 8.1 Calibration Equations | 195 |
| 8.2 Discrete Points Defining Function f | 196 |

1.0 Studies of Neutral Atmospheric Density

1.1 Introduction

Three studies were undertaken during the contract period. These were: a) the Air Force Reference Atmosphere (AFRA) model evaluation and selection study, b) the Density Variability Study, c) revision of the Jacchia 70 Tides, and development of the Air Force Reference Atmosphere Supplements 1986. In addition, several smaller studies such as the Total Atmospheric X-ray Intensity and the Particle/Density Study were undertaken, but are not reported here.

The Air Force Reference Atmosphere model evaluation and selection process began in November 1984 by considering the MSIS 83 and Jacchia 70 Tides models. Numerous data bases were prepared during the course of this study, and a packed data base format was developed and implemented in software (See Section 1.4 below). By March 1985, the study had been expanded to include all the available data bases at the time (i.e. AE/S3-1, S3-4, SETA-1, SETA-2, and SETA-3). The models under consideration at this point were the Jacchia 70, Jacchia 70 Tides (revised), Jacchia 71, MSIS 77, MSIS 79, MSIS 83A, and MSIS 83B. The goal of this effort was to select a basic model for the reference atmosphere in the 130 to 200 kilometer region. This work was completed in April 1985, with the result that two models, the Jacchia 71⁽¹⁾ and the MSIS 83⁽²⁾, were chosen for consideration in future studies. The results of this study led into the Density Variability Study and the Air Force Reference Atmosphere Supplements 1986.

The second major work effort undertaken during the contract period was the Density Variability Study. The goal of the Density Variability Study was to recommend an atmospheric density model for operational use and to provide error bounds on the selected model. The scope of the work was outlined in October 1985, and the main objectives were:

- i) Quantify accelerometer measurement accuracy vs. altitude
- ii) Estimate accuracy of selected density models
- iii) Study spatial correlation of density errors during quiet and disturbed geomagnetic conditions.

A schedule was agreed on and the bulk of the work was completed in December 1985, continuing into early 1986. A first draft⁽³⁾ of the Density Variability Study was reviewed and commented upon in June 1986.

Two considerations are worth noting. First, it was suspected that, due to the manner in which the data were collected, the resulting estimates of atmospheric density are correlated in time (auto-correlated). A study was undertaken (See Section 1.6) to investigate this hypothesis, and this conclusion was confirmed. While this effect was shown not to affect the standard deviations as currently calculated by the STAT program, it would affect the calculation of any error bounds on predicted densities. Secondly, in January 1986, it was noted that there was an unresolved question as to the high variability in the measured to model ratios in the AE data, as indicated by the standard deviations, compared to the variability obtained for the SETA data (See Table 1.1). Hence, a study was made using the AE-E data base to see if elimination of the local time variability would bring the overall variances into agreement. The results of this study are included here in Section 1.7. This analysis shows that although there are significant unmodeled local time variations in the AE-E data base for both the MSIS 83 and Jacchia 71 models in a statistical sense, the resulting

overall standard deviation still remains at around 12%, well above the errors for the SETA satellites. Further investigative work along the lines of the analysis in Section 1.6 might help to resolve this question.

The most recent effort undertaken was the Air Force Reference Atmosphere Supplements 1986. Work began on this effort in January 1986 when the files containing the Air Force Reference Atmosphere in the 70-120 kilometer region were received⁽⁴⁾. Preliminary comparisons of the "Forbes" model with the MSIS 83 model were made. An attempt was made to develop a model which interpolated between the Forbes and the MSIS 83 models in the 104-120 km region while simultaneously satisfying hydrostatic equilibrium. When this attempt failed to produce acceptable results, and after consultation with AFGL personnel, the decision was made to drop the hydrostatic equilibrium requirement and to use cubic spline fits to interpolate in the 104-120 km region between the "Forbes" model and MSIS 83. Work on the Air Force Reference Supplements 1986 has since been completed and the results have been delivered to the initiator. These results consisted of 110 pen plots and 756 pages of tables.

Table 1.1 Statistical Properties of Total Mass Density
Log Ratios to MSIS 83 Model: Data to 200 km.

| <u>Data Set</u> | <u>N</u> | <u>\bar{x}</u> | <u>s</u> | <u>$\sqrt{b_1}$</u> | <u>b_2</u> |
|------------------|----------|-----------------------------|----------|--------------------------------|-------------------------|
| AE-C | 62,044 | 0.094 | 0.152 | -0.619 | 8.156 |
| AE-D | 29,762 | -0.029 | 0.157 | -0.775 | 10.857 |
| AE-E | 35,629 | 0.014 | 0.132 | -0.457 | 8.812 |
| S3-1 | 27,315 | 0.050 | 0.156 | -0.225 | 12.311 |
| SETA-1 | 20,923 | -0.073 | 0.087 | -0.718 | 9.946 |
| SETA-2 | 105,809 | -0.150 | 0.107 | -0.503 | 5.353 |
| SETA-3 (Jul-Nov) | 652,238 | -0.144 | 0.092 | 0.192 | 5.508 |

N is the sample size, and \bar{x} , s, $\sqrt{b_1}$, and b_2 (defined below) are the first four sample moments about the sample mean.

Table 1.2 Neutral Atmospheric Density Satellite
Experiment Flight Histories

| <u>SATELLITE</u> | <u>JULIAN</u> <u>DATE</u> | <u>SEASON</u> | <u>ALTITUDE</u> <u>RANGE (KM)</u> | <u>INCL</u> | <u>MEAN</u> <u>F10.7</u> | <u>#</u> <u>FILES</u> | <u>#</u> <u>RECS</u> | <u>#</u> <u>POINTS</u> | <u>SECS/</u> <u>CASE</u> |
|------------------|------------------------------|---------------|--------------------------------------|-------------|-----------------------------|--------------------------|-------------------------|---------------------------|-----------------------------|
| AE-C | 73353 74352 | FWSS | 135 245 | 68.4 | 86.9 | | | 62044 | 44 |
| S3-1 | 74309 75120 | FWS | 135 245 | 97 | 76.3 | | | 27315 | 44 |
| AE-D | 75281 76029 | FW | 140 245 | 90 | 75.8 | | | 29762 | 44 |
| AE-E | 75325 76322 | FWSS | 135 245 | 20 | 73.3 | | | 35629 | 44 |
| AE/S3-1 | 73353 76322 | | 135 245 | | | 23 | 12929 | 154750 | 44 |
| S3-4 | 78089 78223 | SS | 162 285 | 96* | 145.8 | 161 | 4756 | 54081 | 26 |
| SETA-1 | 79079 79100 | SPRING | 168 249 | 96* | 189.8 | 1 | 5222 | 62649 | 23 |
| SETA-2 | 82137 82332 | SSF | 168 297 | 96* | 170.0 | 114 | 37148 | 443805 | 110 |
| SETA-3 | 83201 84075 | SFWS | 163 385 | 96* | 116.0 | 150 | 246624 | 2956869 | 655 |
| S85-1 | 84177 84283 | SF | 179 257 | 96* | 81.3 | 51 | 20685 | 247330 | 113 |

* SUN SYNCHRONOUS ORBIT

1.2 The STAT program

1.2.1 Overview

The STAT program is the primary analysis tool used in studying the neutral atmospheric density data base. STAT typically breaks the data down into a set of bins, computes, and prints a report consisting of the means and standard deviations in each bin for selected satellite and model combinations. The data base consists of estimates of atmospheric density computed from accelerometer measurements of total satellite drag.^(5,6) A list of the satellites and their flight histories which make up the data base is given in Table 1.2. The current list of data base tapes in machine readable form is given in Table 1.3. The data base format is given in Table 1.4. The STAT program, based on the input, requests the appropriate data base tape (or tapes) via CALLs to PACKLIB routines (See below.), and calculates and prints the requested statistics for the requested satellite(s)/model(s) combination. Currently, the only restriction is that all the requested models (up to a maximum of four) must be stored on the same data base tape. A flowchart of the STAT program is given in Figure 1.1.

Table 1.3 Air Force Reference Atmosphere
Neutral Atmospheric Density Data Base
 (File: DBINDEX/UN=BRYANTC)

| | | | | | | |
|----------|----------|---------|-----------|--------|-----------|-------------|
| CC4494 | H | SETA-1 | 22J71 | 23J70T | 24MSIS86 | 26MSIS83B |
| CC1465GE | H | AE/S3-1 | 22J71 | 23J70T | 24MSIS77 | 26MSIS83B |
| CC5180GE | H | AE/S3-1 | 22J71 | 23J70T | 24MSIS77 | 26MSIS83B |
| CC0594GE | H | AE/S3-1 | 22J71 | 23J70T | 24MSIS77 | 26MSIS83B |
| CC0394 | H | S3-4 | 22J71 | 23J70T | 24MSIS77 | 26MSIS83B |
| CC5061 | H | SETA-1 | 22J71 | 23J70T | 24MSIS77 | 26MSIS83B |
| CC0764 | PH | SETA-2 | 22J71 | 23J70T | 24MSIS77 | 26MSIS83B |
| CC2462GE | PH | SETA-3 | 22J71 | 23J70T | 24MSIS77 | 26MSIS83B |
| CC1403GE | PH | SETA-3 | 22J71 | 23J70T | 24MSIS77 | 26MSIS83B |
| CC4274 | PH | S85-1 | 22J71 | 23J70T | 24MSIS77 | 26MSIS83B |
| CC2478 | PH | AE/S3-1 | | | 24MSIS77 | 26MSIS78/79 |
| OS0475 | SI | S3-4 | | 23J77 | 24MSIS77 | 26MSIS78/79 |
| CC4953 | SI H | SETA-1 | | 23J77 | 24MSIS77 | 26MSIS78/79 |
| CC0221 | PH | SETA-2 | | 23J77 | 24MSIS77 | 26MSIS78/79 |
| CC2466GE | H | AE/S3-1 | | 23J77 | 24MSIS83A | 26MSIS83B |
| OS0637 | SI H | S3-4 | | | 24MSIS83A | 26MSIS83B |
| CC4954 | SI H | SETA-1 | | | 24MSIS83A | 26MSIS83B |
| CC2125 | PH | SETA-2 | | | 24MSIS83A | 26MSIS83B |
| CC2484GE | H | AE/S3-1 | | | 24J70T | |
| CC0413 | H | S3-4 | | | 24J70T | |
| CC1065 | H | SETA-1 | | | 24J70T | |
| CC2165 | PH | SETA-2 | | | 24J70T | |
| CC2493GE | <AE/S3-1 | | 22J64 | 23US66 | 24J71 | 38USSR |
| OS0472 | SI | S3-4 | 22J64 | 23US66 | 24J71 | 38USSR |
| OS0492 | H | SETA-1 | 22J64 | 23US66 | 24J71 | 38USSR |
| CC0061 | PH | SETA-2 | 22J64 | 23US66 | 24J71 | 38USSR |
| CC2515GE | <AE/S3-1 | | 22JWB | 23L/N | 38US62 | |
| OS0473 | H | S3-4 | 22JWB | 23L/N | 24US62 | |
| OS0494 | H | SETA-1 | 22JWB | 23L/N | 24US62 | |
| CC0081 | PH | SETA-2 | 22JWB | 23L/N | 24US62 | |
| CC2523GE | <AE/S3-1 | | 23DENSEL | 24J70 | 38J73 | |
| OS0474 | SI | S3-4 | 22DENSEL | 23J70 | 24J73 | |
| OS0496 | H | SETA-1 | 22DENSEL | 23J70 | 24J73 | |
| CC0101 | PH | SETA-2 | 22DENSEL | 23J70 | 24J73 | |
| CC5019 | | SETA-1 | 32J71KP=1 | | | |
| OS0098 | SI | SETA-1 | 32J71KP=1 | | | |
| CC0583 | P | SETA-2 | 32J71KP=1 | | | |
| CC5108 | P | S85-1 | 32J71KP=1 | | | |

Table 1.4 Neutral Atmospheric Density Data Base Format

HEADER RECORD

| WORD# | CONTENTS |
|-------|--|
| 0.1 | WORD COUNT (40) |
| 0.2 | GROUP COUNT (1) |
| 1 | SATELLITE ID |
| 2 | EXPERIMENT NAME |
| 3 | ALTITUDE (KM) |
| 4 | 100*(NUMBER OF FILES) + (NUMBER FOR THIS FILE) |
| 5 | DATA BASE CREATION DATE (YYDDD) |
| 6-40 | BLANK |

DATA RECORD

| WORD# | CONTENTS | <u>\$BINS VARIABLE</u> <u>BIN</u> |
|-------|------------------------------|--------------------------------------|
| 0.1 | WORD COUNT (40) | |
| 0.2 | GROUP COUNT (12) | |
| 1 | ORBIT NUMBER | 'ORBIT' |
| 2 | JULIAN DATE OF DATA (YYDDD) | 'JDATE' |
| 3 | GREENWICH TIME (SECONDS) | 'UT' |
| 4 | GREENWICH HOURS | |
| 5 | GREENWICH MINUTES | |
| 6 | GREENWICH SECONDS | |
| 7 | LOCAL TIME HOURS | 'LT' |
| 8 | LOCAL TIME MINUTES | |
| 9 | LOCAL TIME SECONDS | |
| 10 | UPLEG/DOWNLEG | |
| 11 | DAY/NIGHT | |
| 12 | SPUN/DESPUN | 'SD' |
| 13 | GEOGRAPHIC LATITUDE | 'GGLAT' |
| 14 | GEOGRAPHIC LONGITUDE (EAST) | 'GGLONG' |
| 15 | GEOMAGNETIC LATITUDE | 'GMLAT' |
| 16 | GEOMAGNETIC LONGITUDE (EAST) | 'GMLONG' |
| 17 | GEOMAGNETIC LOCAL TIME | 'GMLT' |
| 18 | MEASURED DENSITY (G/CM**3) | |
| 19 | J71 MODEL DENSITY | |
| 20 | J71 MODEL DENSITY (KP=2) | |
| 21 | MSIS MODEL DENSITY | |
| 22 | MEASURED/J71 RATIO | |
| 23 | MEASURED/J71(KP=2) RATIO | |
| 24 | MEASURED/MSIS 83 RATIO | |
| 25 | AP (DAILY AVERAGE) | 'AP' |
| 26 | AP (6.7 HOUR LAG) | 'AP6.7' |
| 27 | KP (6.7 HOUR LAG) | 'KP' |
| 28 | F10.7 (1 DAY LAG) | 'F10.7' |
| 29 | F10.7 (81 DAY AVERAGE) | 'F10.7BAR' |
| 30 | ALTITUDE (KM) | 'ALT' |
| 31 | KP (3 HOUR LAG) | 'KP3' |
| 32 | KP (6 HOUR LAG) | 'KP6' |
| 33 | KP (9 HOUR LAG) | 'KP9' |
| 34 | KP (12 HOUR LAG) | 'KP12' |
| 35 | AVERAGE OF WORDS 31 - 34 | 'KPAVG' |
| 36 | | |
| 37 | J77 MODEL DENSITY | |
| 38 | MEASURED/J77 RATIO | |
| 39 | EMPIRICAL MODEL RATIO | |
| 40 | MEASURED/EMPIRICAL RATIO | |

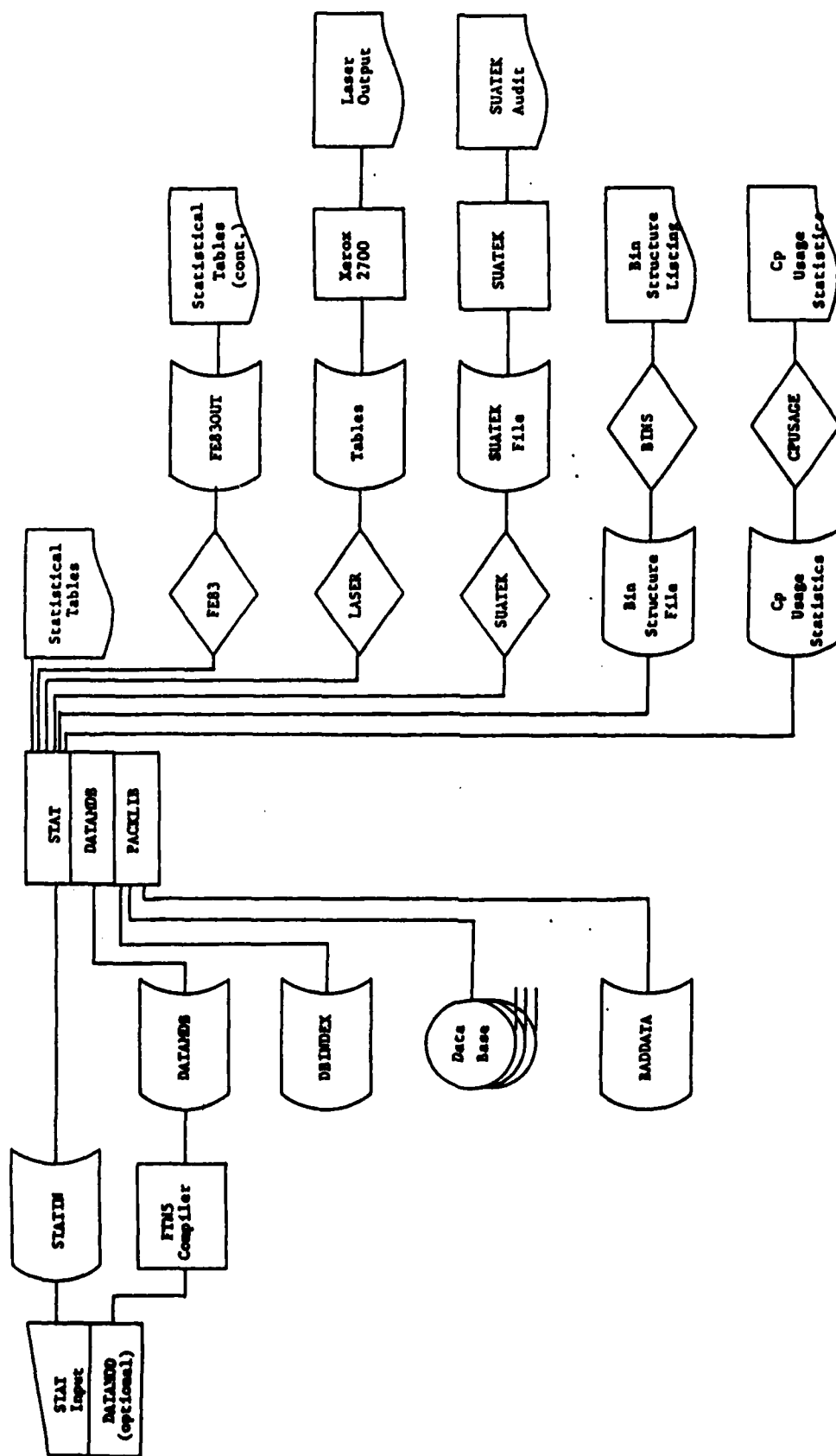


Figure 1.1 STAT Flowchart

1.2.2 STAT Input Description

The STAT program is executed via the STAT procedure which is stored under UN=BRYANTC. To get a copy of the STAT procedure, say "GET,STAT/UN=BRYANTC" at the command level while logged in under NOS 2. Parameters for the STAT procedure are:

| | |
|---------|---|
| TABLES | File name under which to store the printed tables. (May be omitted.) |
| LASER | YES or NO. Send tables to the the Xerox-2700 laser printer or not. Default is NO. |
| COPIES | Number of copies. Default is one copy. |
| TITLE | Title for laser output (1-10 characters). |
| SUATEK | File name under which to store SUATEK format file (direct access). Default is SUATEK. |
| BINS | YES or NO. Print bin structure or not. Default is NO. |
| CPUSAGE | YES or NO. Print cp usage statistics or not. Default is YES. |
| PACKED | YES, NO, or UNDEF. Packed data base or not, if known. Default is UNDEF. |
| UN | User name for laser output banner. No default. |

Input for a case consists of a single title card, followed by the NAMELIST \$INPUT input, followed by the NAMELIST \$BINS input. The user may supply a subroutine named DATAMOD as a second record of input. If the user sets the variable USERSUB true in conjunction with this, then the subroutine DATAMOD will be CALLED on every pass through the main processing loop after checks on altitude, date range and spun/despun have been made. This gives the user freedom to test and/or modify each data point prior to further processing. A sample DATAMOD subroutine is given in Figure 1.2. Cases may be stacked to any degree desired, limited only by the amount of cp time requested on the JOB card.

Figure 1.2 Sample DATAMOD Subroutine

SUBROUTINE DATAMOD (J,CASE,SKIP)

SAMPLE USER SUPPLIED SUBROUTINE FOR USE WITH THE STAT PROGRAM.
APPROPRIATE TESTS FOR ALTITUDE RANGE, DATE RANGE, AND
SPUN/DESPUN HAVE BEEN MADE, AS SELECTED BY THE USER. FILES
AND INDIVIDUAL DATA POINTS MAY BE SKIPPED BY SETTING SKIP
EQUAL TO .TRUE. (10/30/86)

| | | |
|--------------|-----------|-----------------------------------|
| INTEGER | | CASE |
| INTEGER | | BINVAR,WORD |
| LOGICAL | | SKIP |
| CHARACTER*10 | | CHEADER,CDATA |
| COMMON | /HEADER / | HEADER(40) |
| COMMON | /DATA / | DATA(40,12) |
| COMMON | /WORDNOS/ | NBINVAR,BINVAR(3),NMODELS,WORD(4) |
| DIMENSION | | IHEADER(40),CHEADER(40) |
| DIMENSION | | IDATA(40,12),CDATA(40) |
| EQUIVALENCE | | (HEADER(1),IHEADER(1)) |
| EQUIVALENCE | | (DATA(1,1),IDATA(1,1)) |

IF (J .EQ. 0) THEN
CALL TRANS (IHEADER,40,1,CHEADER)

CODE TO PROCESS HEADER OR SKIP TO NEXT HEADER RECORD

SKIP = .FALSE.

ELSE
CALL TRANS (IDATA(1,J),40,1,CDATA(1))

CODE TO PROCESS OR SKIP J'TH DATA POINT

SKIP = .FALSE.

ENDIF

RETURN

END

Description of Input

● Title card - 80 columns of case descriptive character data.

● NAMELIST \$INPUT -

The NAMELIST \$INPUT describes all of the relevant information for a case except for the description of the bin structure (and the title card).

| <u>\$INPUT</u> <u>Variable</u> | <u>Size</u> | <u>Type</u> | <u>Description</u> | <u>Default</u> |
|-----------------------------------|-------------|-------------|--------------------|----------------|
| SAT (required) | 9 | CHAR*10 | satellite | None |
| MODEL | 4 | INTEGER | model number (1-4) | None |
| WORD | 4 | INTEGER | word number | None |
| MODNAME | 4 | CHAR*10 | model name | Predefined |
| MODABBR | 4 | CHAR*10 | model abbreviation | None |

The user should specify either MODEL, WORD, or MODDABBR. MODDABBR is usually the most convenient when doing statistics on model ratios. (See Table 1.3 for model abbreviations.) WORD gives the flexibility to do statistics on any variable in the data base. (See Table 1.4)

| <u>Variable</u> | <u>Size</u> | <u>Type</u> | <u>Description</u> | <u>Default</u> |
|-----------------------|-------------|-------------|---|----------------|
| MODHEAD (optional) | 4 | CHAR*16 | heading for model column | Predefined |
| MODFMT (optional) | 4 | CHAR*20 | format under which to print model statistics | Predefined |
| MRSTATS | 1 | LOGICAL | true if model ratio statistics are being calculated, false o.w. | |
| ALLDATA | 1 | LOGICAL | true if "all data" case is to be calculated | TRUE |
| ALT | 2 | REAL | altitude range min & max | 0-600 |
| DAYNITE | 1 | LOGICAL | true for day/night partitioning, false o.w. | FALSE |
| GMLT | 1 | LOGICAL | true for geomagnetic local time, if false, solar local time is used | |
| DAYLT | 2 | INTEGER | local time range for day (hhmm format) | 0800-1800 |
| NITELT | 2 | INTEGER | local time range for night (hhmm format) | 1800-2400 |
| ILT | 1 | LOGICAL | true if local time is to be calculated (packed data bases only) | |
| IGMCO | 1 | LOGICAL | true if geomagnetic coordinates are to be calculated (packed data bases only) | |
| IGMLT | 1 | LOGICAL | true if geomagnetic local time is to be calculated (packed data bases only) | |

| <u>Variable</u> | <u>Size</u> | <u>Type</u> | <u>Description</u> | <u>Default</u> |
|-----------------|-------------|-------------|--|----------------|
| YYDDD | 2 | INTEGER | date range (yyddd format) | None |
| YRMODA | 2 | INTEGER | date range (yymmdd format) | None |
| DATES | 50 | INTEGER | set of up to 50 dates in yyddd format | None |
| SPUN | 1 | LOGICAL | true if spun data only (AE satellites only) | FALSE |
| DESPUN | 1 | LOGICAL | true if despun data only (AE satellites only) | FALSE |
| MEANKP | 1 | LOGICAL | calculate and print average Kp in each bin | TRUE |
| MEANF | 1 | LOGICAL | calculate and print average $F_{10.7}$ in each bin | TRUE |
| MEANZ | 1 | LOGICAL | calculate and print average altitude in each bin | TRUE |
| MEANLT | 1 | LOGICAL | calculate and print average local time in each bin | TRUE |
| MEANUT | 1 | LOGICAL | calculate and print average universal time in each bin | TRUE |
| MEANALL | 1 | LOGICAL | calculate and print average of each of the 5 variables, Kp, $F_{10.7}$, altitude, local time, and universal time in each bin | TRUE |
| MEAN | 1 | LOGICAL | calculate and print averages of the dependent variables | TRUE |
| SD | 1 | LOGICAL | calculate and print standard deviations of the dependent variables | TRUE |
| MEANCL | 1 | LOGICAL | calculate and print confidence limits on the mean of the dependent variables | FALSE |
| SDCL | 1 | LOGICAL | calculate and print confidence limits on the standard deviation of the dependent variables | TRUE |
| ANOVA | 1 | LOGICAL | Do a one-way analysis of variance on the dependent variable | FALSE |
| ALPHA | 1 | LOGICAL | significance level for F-test in one-way ANOVA | .05 |

| <u>Variable</u> | <u>Size</u> | <u>Type</u> | <u>Description</u> | <u>Default</u> |
|-----------------|-------------|-------------|---|----------------|
| LNRATIO | 1 | LOGICAL | calculate statistics using natural logarithms of dependent variables | TRUE |
| LINEAR | 1 | LOGICAL | calculate statistics using dependent variable directly | FALSE |
| PCTSD | 1 | LOGICAL | print standard deviation as a percentage of the mean | FALSE |
| SUATEK | 1 | LOGICAL | Write a SUATEK format file and save it as a direct access file | FALSE |
| SUABINS | 1 | CHAR*10 | 'MINMAX': write bin mins & maxs to SUATEK file; 'AVERAGE': write bin averages to SUATEK file. | MINMAX |
| SUAMEAN | 1 | LOGICAL | Write the mean Kp, F _{10.7} , altitude, local time, and universal time to the SUATEK format file | FALSE |
| SUACL | 1 | LOGICAL | Write confidence limits on the mean to the SUATEK format file | FALSE |
| USERSUB | 1 | LOGICAL | CALL the user supplied subroutine DATAMOD in the main processing loop | FALSE |
| RAWDATA | 1 | LOGICAL | true for "raw data" print out, false o.w. | FALSE |
| NLPAGE | 1 | INTEGER | number of lines per page (18≤NLPAGE≤48, not including headings) | 36 |
| RESET | 1 | LOGICAL | Reset the \$INPUT variables to their defaults at the beginning of the next case | FALSE |

Character input must be enclosed in single quotes ('). The pairs of variables, LNRATIO and LINEAR, and SD and PCTSD are logical complements of each other.

● NAMELIST \$BINS -

The user may specify up to three (3) separate binning variables. These, along with day/night partitioning allow for a up to four-way breakdown of the data. (In the following, "I" refers to the bin number, 1, 2, or 3.)

SBINS

| <u>Variable</u> | <u>Size</u> | <u>Type</u> | <u>Description</u> | <u>Default</u> |
|-----------------|-------------|-------------|--------------------|----------------|
|-----------------|-------------|-------------|--------------------|----------------|

The user may specify a particular bin variable using one of the following two variables.

| | | | |
|--------|---|---------|---|
| BIN | 3 | CHAR*10 | abbreviated bin variable name (See Table 1.4) |
| BINVAR | 3 | INTEGER | bin variable number (See Table 1.4) |

The user has a choice of one of the following six methods for specifying each bin. (KP2, KP3, and KP4 count a one method.)

| | | | |
|---------|--------|---------|--|
| FROM | 3 | REAL | These three variables together specify the bin structure for the bin variable named by BIN(I) OR BINVAR(I) |
| TO | 3 | REAL | |
| BY | 3 | REAL | |
| BMINMAX | 2,36,3 | REAL | Explicit enumeration of bin structure for bin I |
| KP2 | 1 | INTEGER | KP2=I selects standard 2 Kp bins, (0 to 3+ and 4- to 9) for bin variable I |
| KP3 | 1 | INTEGER | KP3=I selects standard 3 Kp bins (0 to 3, 3+ to 4+, and 5- to 9) for bin variable I |
| KP4 | 1 | INTEGER | KP4=I selects standard 4 Kp bins (0 to 1+, 2- to 3+, 4- to 5+, and 6- to 9) for bin variable I |
| MONTH | 1 | INTEGER | MONTH=I selects monthly binning for bin I |
| SEASON | 1 | INTEGER | SEASON=I selects seasonal binning for bin I |
| ORBIT | 2000 | INTEGER | set of up to 2000 orbit numbers |

(Only one bin is allowed when ORBIT is specified.)

| <u>Variable</u> | <u>Size</u> | <u>Type</u> | <u>Description</u> | <u>Default</u> |
|-----------------------|-------------|-------------|--|----------------|
| BINNAME (optional) | 40 | CHAR*14 | bin name for column heading | Predefined |
| BINFMT (optional) | 40 | CHAR*20 | format under which to print out bin variable | Predefined |
| ILT (optional) | 1 | LOGICAL | true if local time is to be calculated (packed data bases only) | |
| IGMCO (optional) | 1 | LOGICAL | true if geomagnetic coordinates are to be calculated (packed data bases only) | |
| IGMLT (optional) | 1 | LOGICAL | true if geomagnetic local time is to be calculated (packed data bases only) | |
| RESET (optional) | 1 | LOGICAL | Reset the \$BINS variables to their defaults at the beginning of the next case | |

1.3 Other Programs

1.3.1 Data Base Construction

The construction of the neutral atmospheric density data bases described in Tables 1.3 and 1.4 is accomplished with updated versions of programs FOURMOD and DENDB.⁽⁷⁾ Both these programs have been updated to produce on option the packed versions of the data bases shown in those tables. This format is produced and accessed with the PACKLIB library to be discussed in Section 1.4. In summary it consists of 15-bit integer data words packed 4 per full CDC 60-bit word. For completeness we provide the detailed contents of these data bases in Table 1.5. Note that only a subset of the full unpacked data base is contained. The remaining quantities are easily derived. The implementation of this packed data base structure was motivated by the increasing amounts of data to be handled. Program DENDB has also been modified from time to time by substitution of density computation modules for computation of models other than those present in the original package.

The complexity of the thermospheric response to geomagnetic activity has motivated special studies which have required special processing. Program MRDB was written to produce data bases containing the ratios of the measured density to the Jacchia 71 model at fixed $K_p=1$. These ratios contain the unattenuated density variations related to geomagnetic activity, while the other variations (altitude, latitude, solar flux, etc.) are "damped out" by the approximately correct variations contained in the Jacchia 71 model.

MRDB produces both packed and unpacked data base formats similar to those described in Tables 1.3-1.5, with the addition of the K_p index at lags of -3 hr to +15 hr to permit study of density variations versus lag time relative to K_p variations. Program OADB uses these data bases to produce averaged ratio per latitude bin per orbit, and program PERCENT computes the percent changes of these averaged ratios during period of high geomagnetic activity relative to the values found during the preceding quiet period. All these results are output onto data files suitable for display by program SUATEK.⁽⁸⁾ Display of these results, along with proposed new geomagnetic activity indices, such as the Total Atmospheric X-ray Intensity (TAXI) index, permitted evaluation of these indices as possible improvements over K_p for use in density modelling.

Table 1.5 Packed Density Data Base Format

Header Record 1: Same as for unpacked data bases.

Header Record 2: Unpacked offsets and scale values to be used to convert the packed data words to the equivalent 60 bit real unpacked values.

Data records: 15-bit data words, packed 4 per 60-bit full word; these are preceded by a real 60 bit word containing the time in the form YYDDD.XXXXXX where YY = the last two digits of the year;
DDD = the day number in the year;
XXXXX = fraction of the day from UT midnight.

The 15-bit packed data words are:

| <u>Word #</u> | <u>Variable</u> |
|---------------|-------------------------------|
| 1 | Orbit Number |
| 2 | Latitude ($^{\circ}$ N) |
| 3 | Longitude ($^{\circ}$ E) |
| 4 | Altitude (km) |
| 5 | $F_{10.7}$ |
| 6 | $F_{10.7}$ smoothed |
| 7 | K_p |
| 8 | Measured density (g/cc) |
| 9-12 | Measured/model density ratios |

1.3.2 PULL/CONSOL/MERGE

Three software programs, PULL, CONSOL, and MERGE, have been developed to consolidate selected models, originally residing on different tapes onto a single tape. PULL "pulls" the data-to-model ratios for selected models from a full data base and packs them, time-tagged, onto a temporary disk file. CONSOL consolidates the model ratios on two or three files into one. MERGE merges the ratios residing on a packed temporary disk into a full data base. A flowchart of the PULL/CONSOL/MERGE operation is given in Figure 1.3.

1.3.3 HISTO

HISTO plots histograms of the number of data points versus K_p , solar flux, altitude, geographic latitude, and solar local time for a given satellite. Sample histograms are shown in Figures 1.4-1.8. Such histograms are useful in showing the distribution of the data.

1.3.4 FREQ/EDIST

FREQ plots the relative frequency distribution as a function of model or $\ln(\text{model ratio})$ and superimposes the normal frequency distribution based on the sample mean and standard deviation. The relative frequency, f_i , for a given interval is defined as the fraction of the total sample falling within that interval. The first four sample moments, the mean, standard deviation, skewness, and kurtosis are calculated

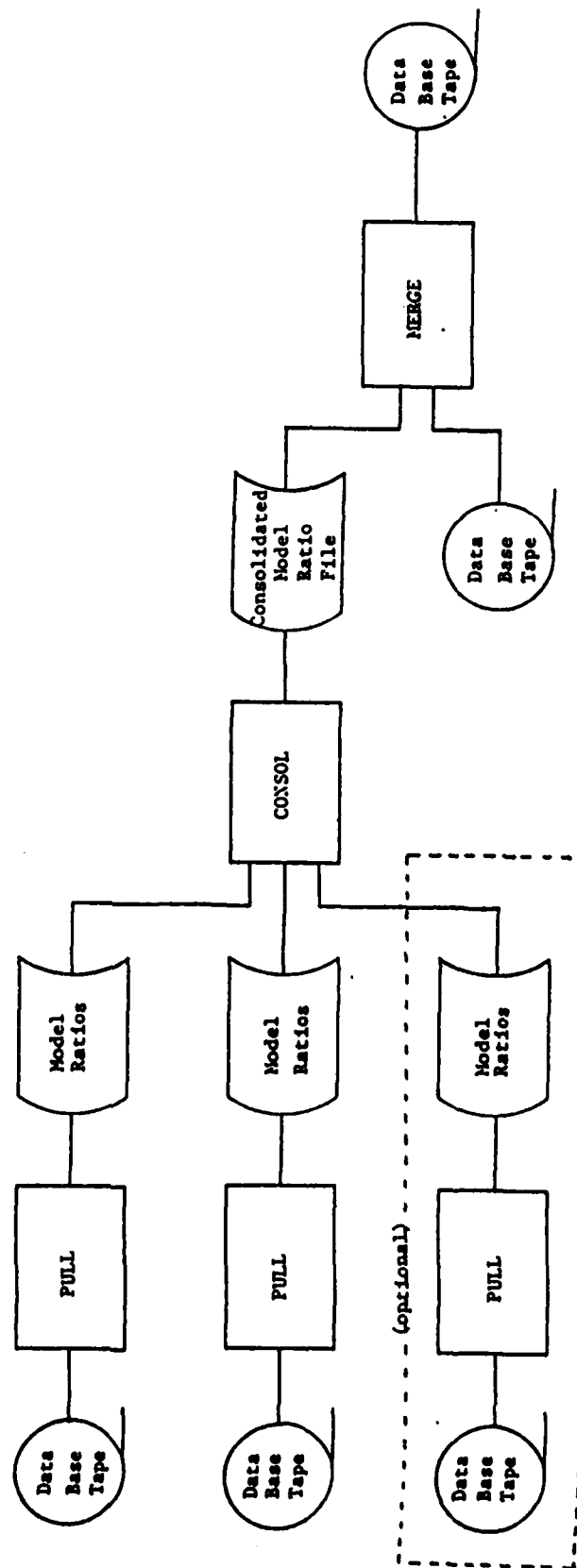


Figure 1.3 PULL/CONSOL/MERGE Processing

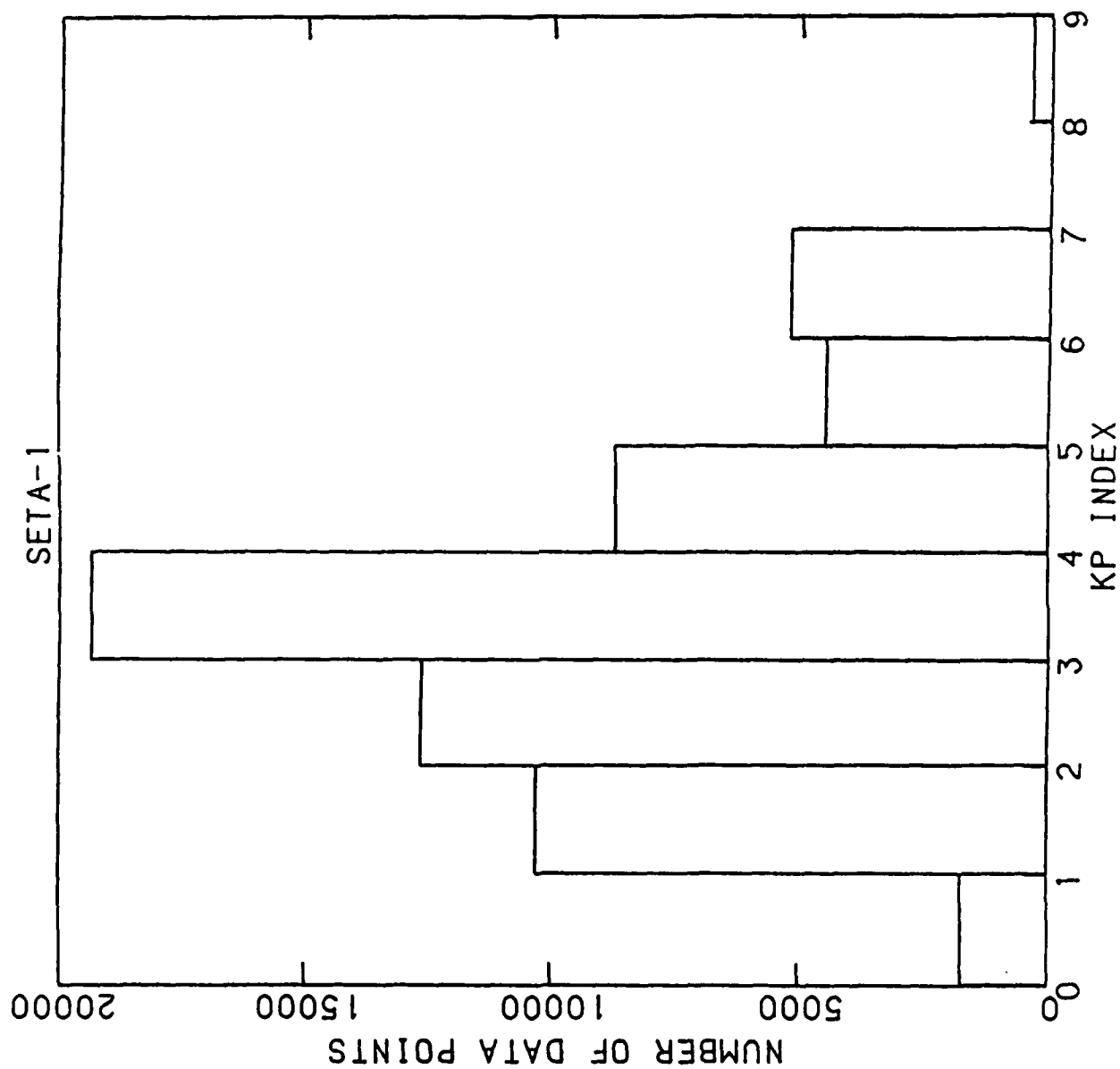


Figure 1.4 Histogram of SETA-1 vs Kp

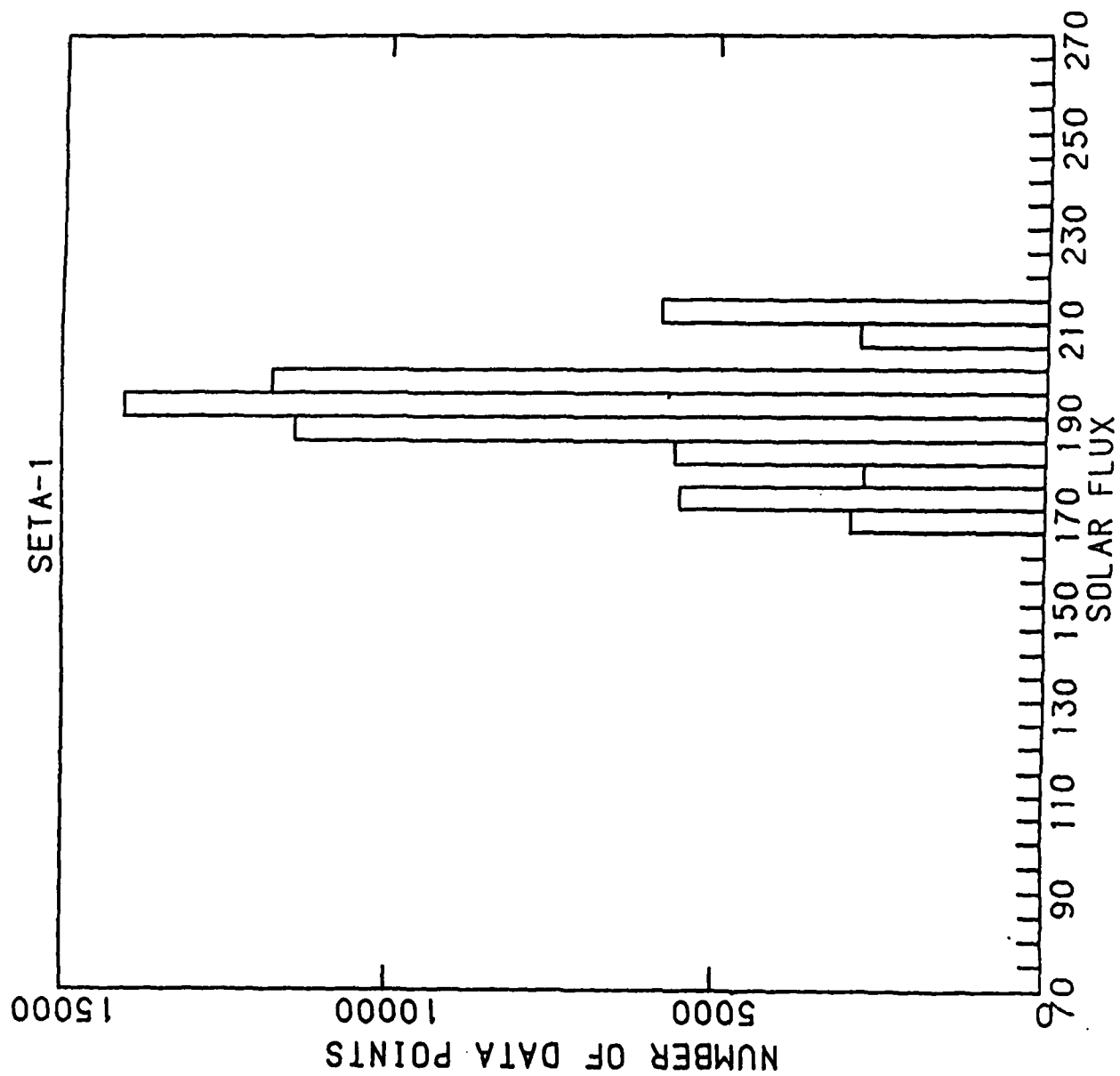


Figure 1.5 Histogram of SETA-1 vs Solar Flux

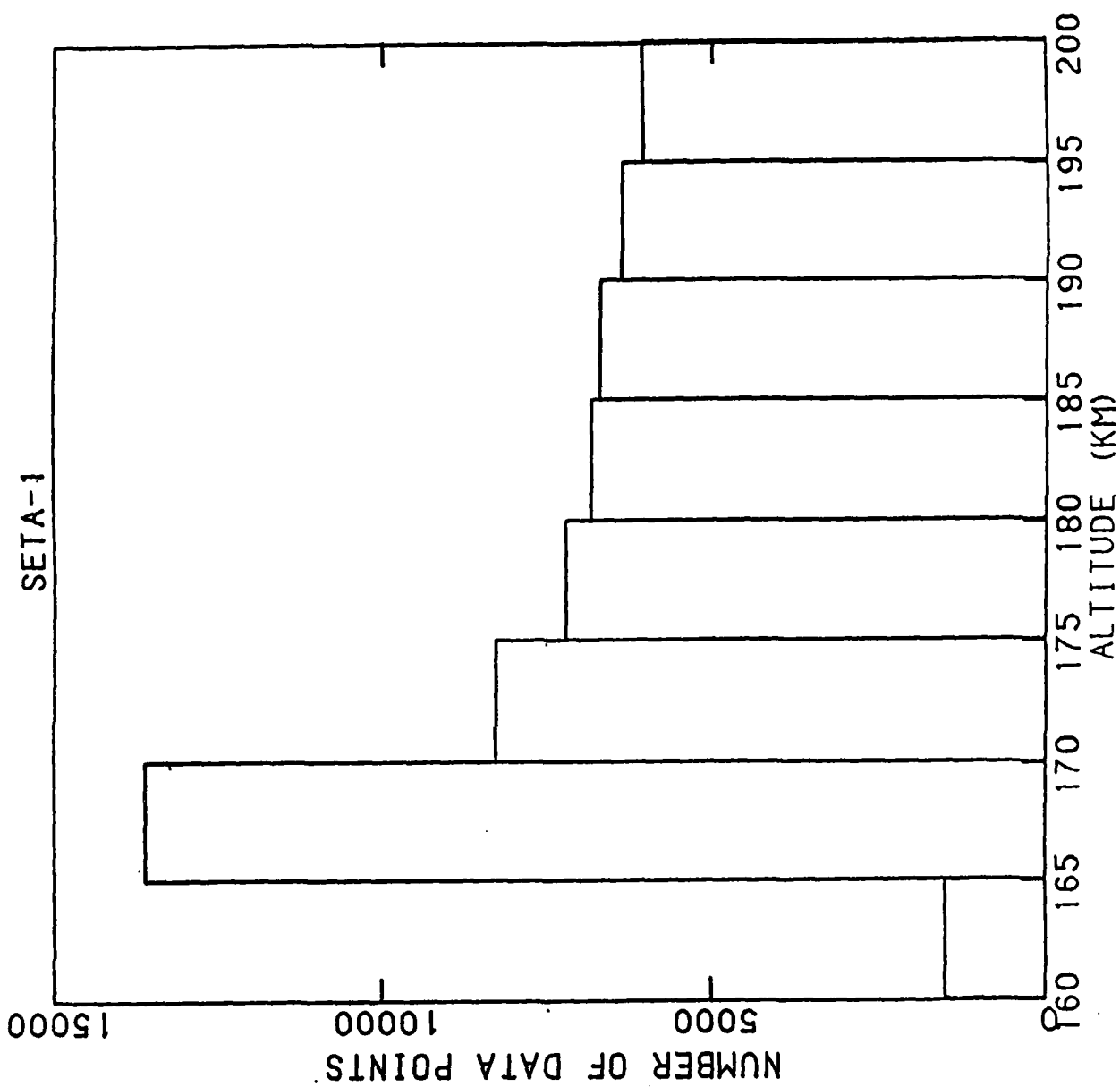


Figure 1.6 Histogram of SETA-1 vs Altitude

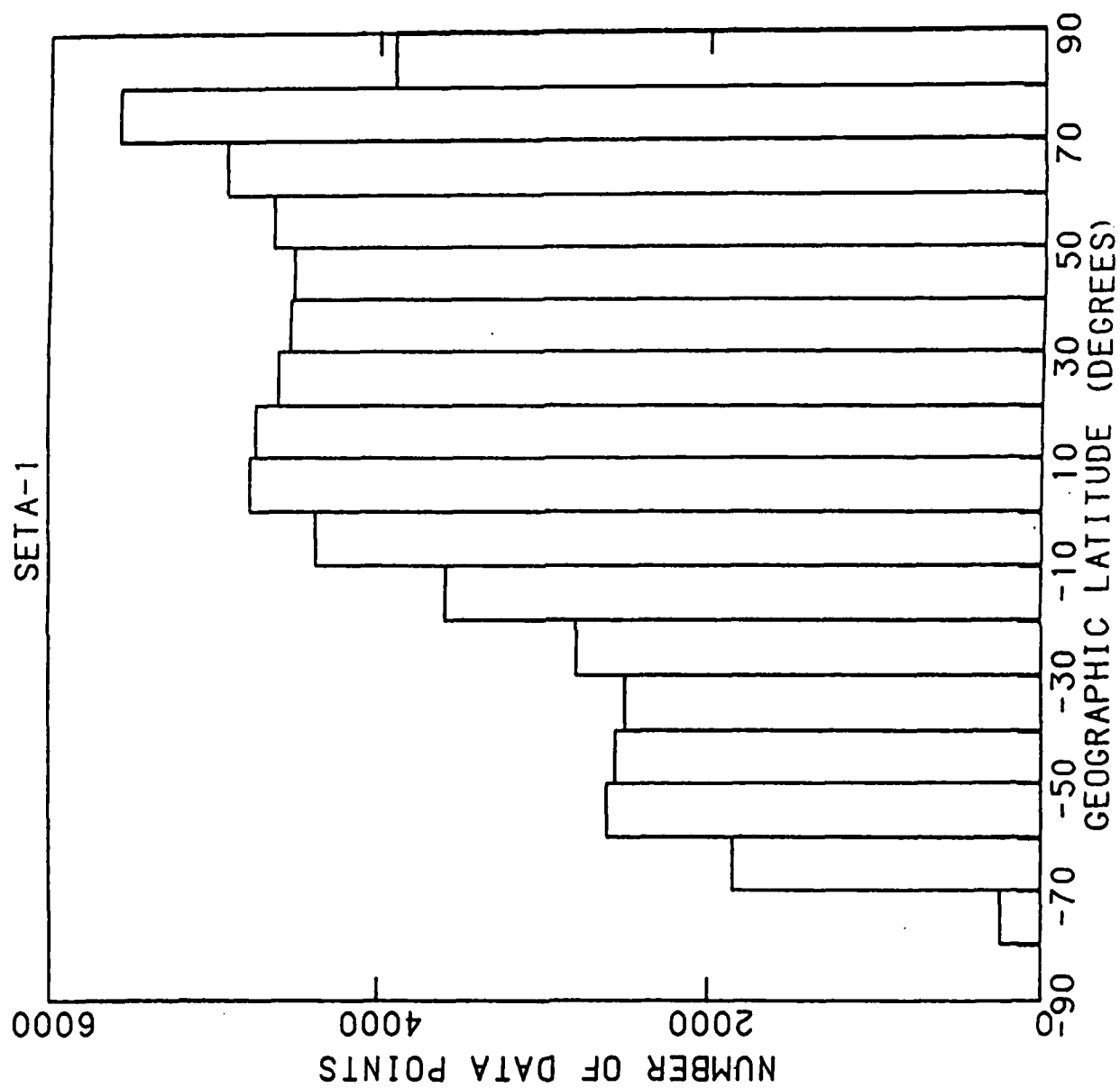


Figure 1.7 Histogram of SETA-1 vs Geographic Latitude

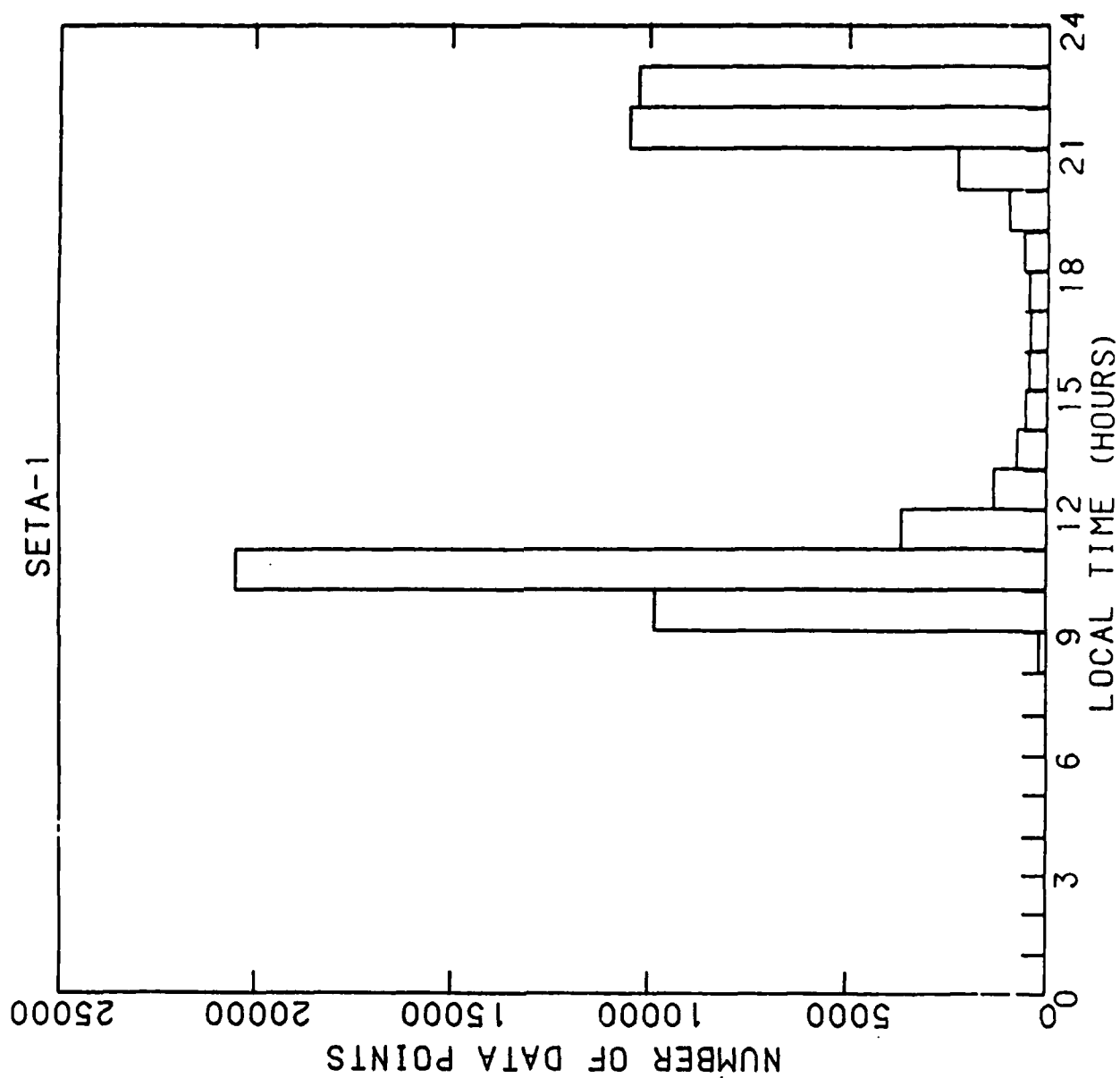


Figure 1.8 Histogram of SETA-1 vs Local Time

and displayed in a corner of the plot. Sample plots from the FREQ program are shown in Figures 1.9 and 1.10.

The mean, standard deviation, skewness, and kurtosis are defined as follows ⁽⁹⁾:

$$\text{mean} \quad \bar{x} = (1/n) \sum_{i=1}^n x_i$$

$$\text{standard deviation} \quad s = [1/(n-1) \sum_{i=1}^n (x_i - \bar{x})^2]^{1/2}$$

$$\text{skewness} \quad \sqrt{b_1} = (1/n) \sum_{i=1}^n ((x_i - \bar{x})/s)^3$$

$$\text{kurtosis} \quad b_2 = (1/n) \sum_{i=1}^n ((x_i - \bar{x})/s)^4$$

EDIST plots the empirical distribution function, $S_n(x)$, for selected satellite/density model combinations. The empirical distribution function, $S_n(x)$, is defined as ⁽¹⁰⁾:

$$S_n(x) = \begin{cases} 0, & \text{if } x < X_{(1)}, \\ k/n, & \text{if } X_{(k)} \leq x < X_{(k+1)}, \\ 1, & \text{if } x \geq X_{(n)}. \end{cases} \quad k=1, \dots, n-1,$$

where $X_{(1)}, \dots, X_{(n)}$ denotes the order statistics of a sample of size n .

The empirical distribution function is plotted on an inverse normal probability scale versus a standardized abscissa so that normally distributed data plot as a straight line. Let

$$\Phi(x) = 1/\sqrt{2\pi}\sigma \int_{-\infty}^x \exp[-(t - \mu)/\sigma]^2 dt,$$

$$\begin{aligned} \text{let} \quad \mu &= \bar{x}, \\ \text{and} \quad \sigma &= s. \end{aligned}$$

Then $\Phi^{-1}(x)$ is plotted against $z = (x - \bar{x})/s$, a standardized deviate. The x and y axes are labeled in terms of the original scale of the variable of interest and cumulative probability, respectively. ⁽¹¹⁾ Sample EDIST plots are shown in Figures 1.11 and 1.12.

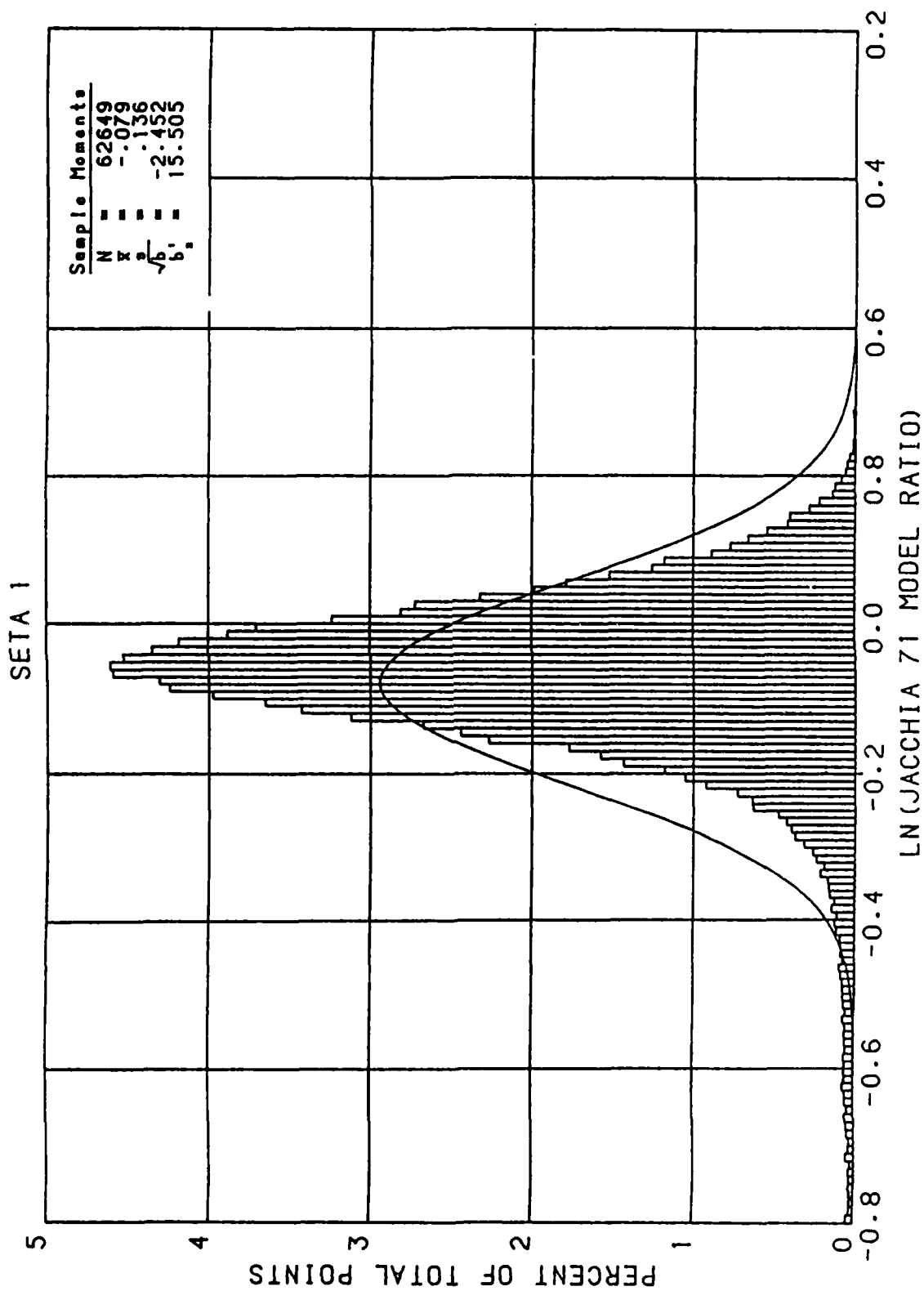


Figure i.9 SETA-1 Relative Frequency Distribution of
ln(Jacchia 71 Model Ratio)

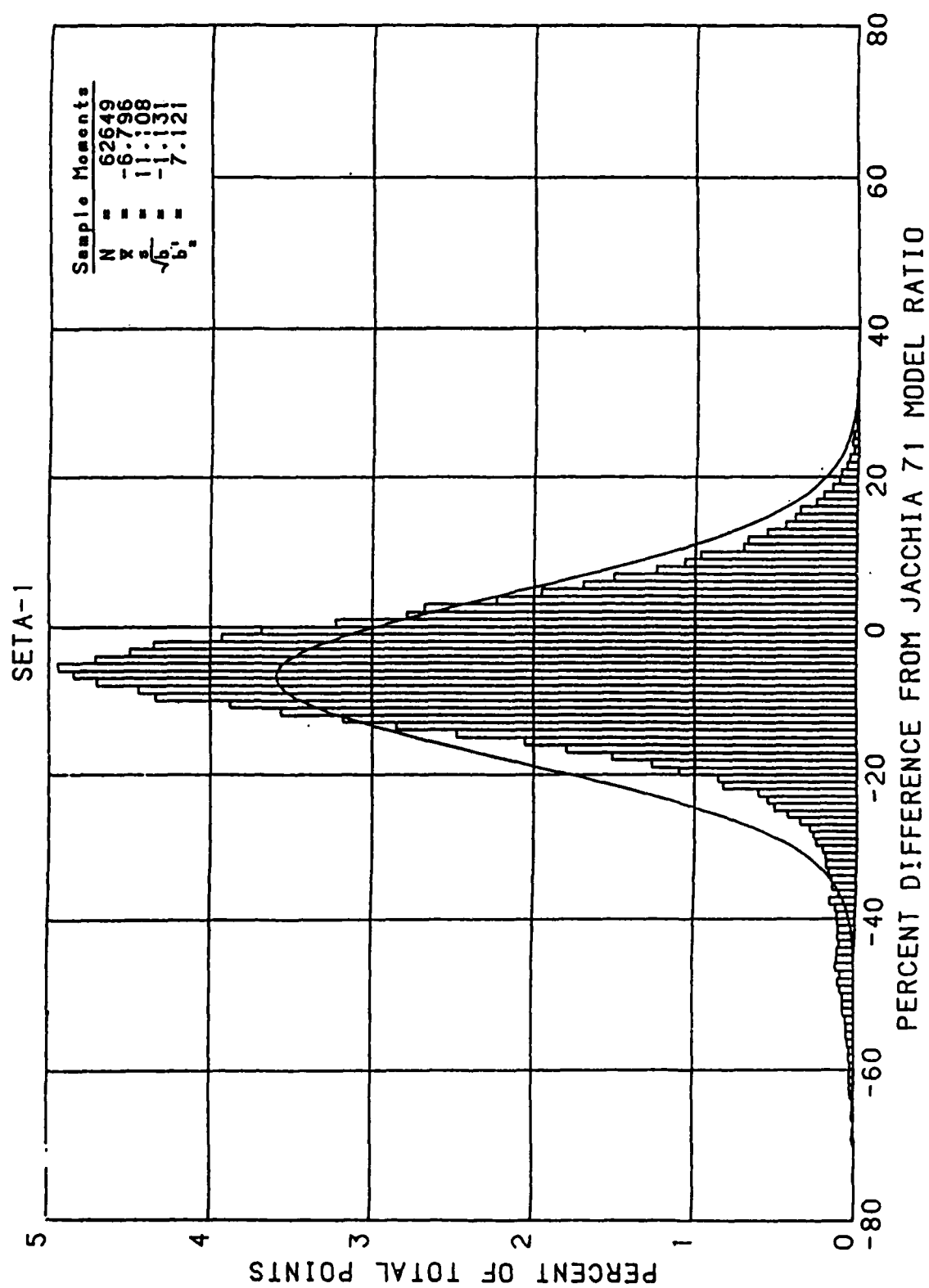


Figure 1.10 SETA-1 Relative Frequency Distribution of Percent Difference from JACCHIA 71 Ratio

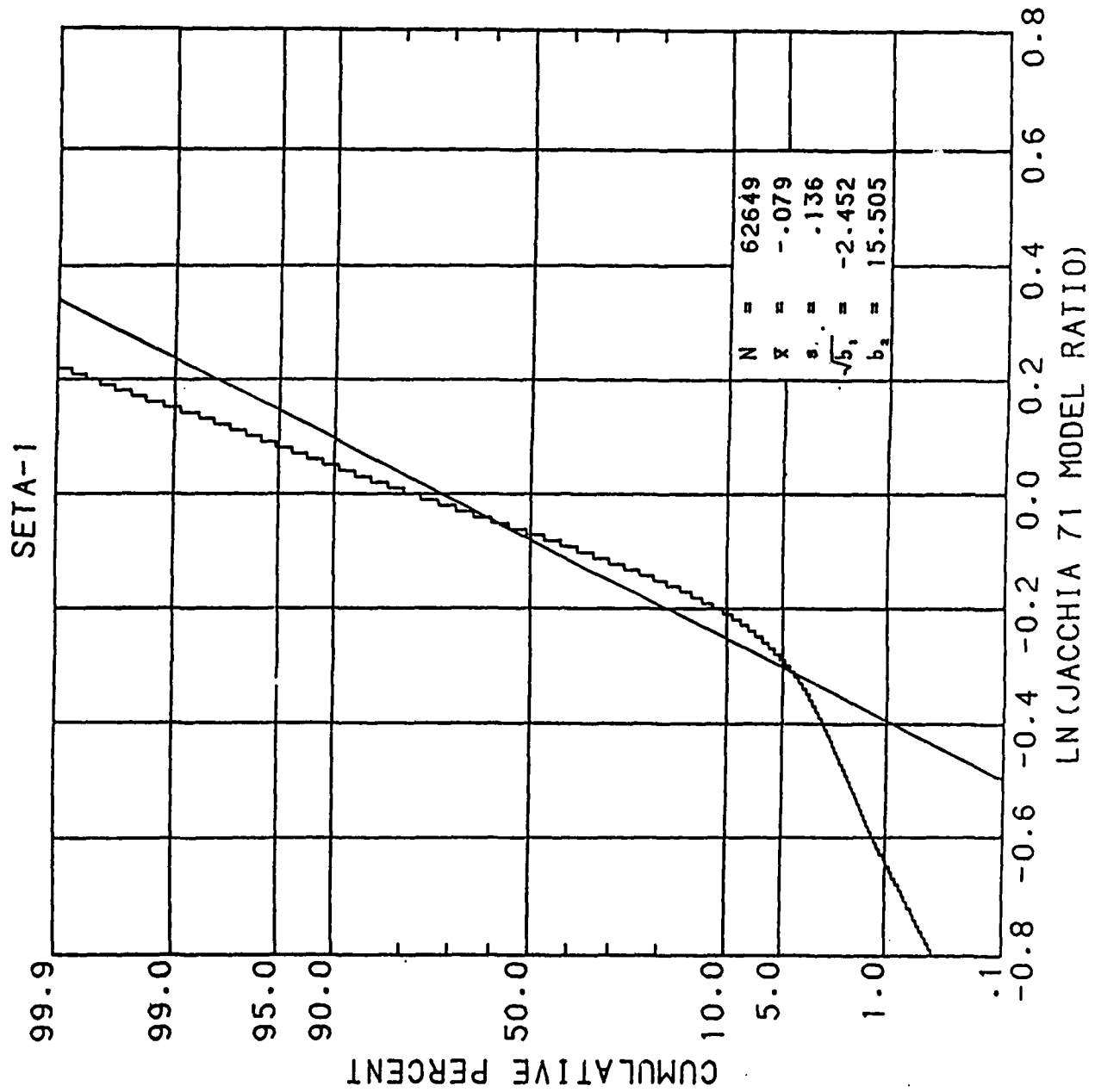


Figure 1.11 SETA-1 Empirical Distribution Function of $\ln(\text{Jacchia 71 Model Ratio})$

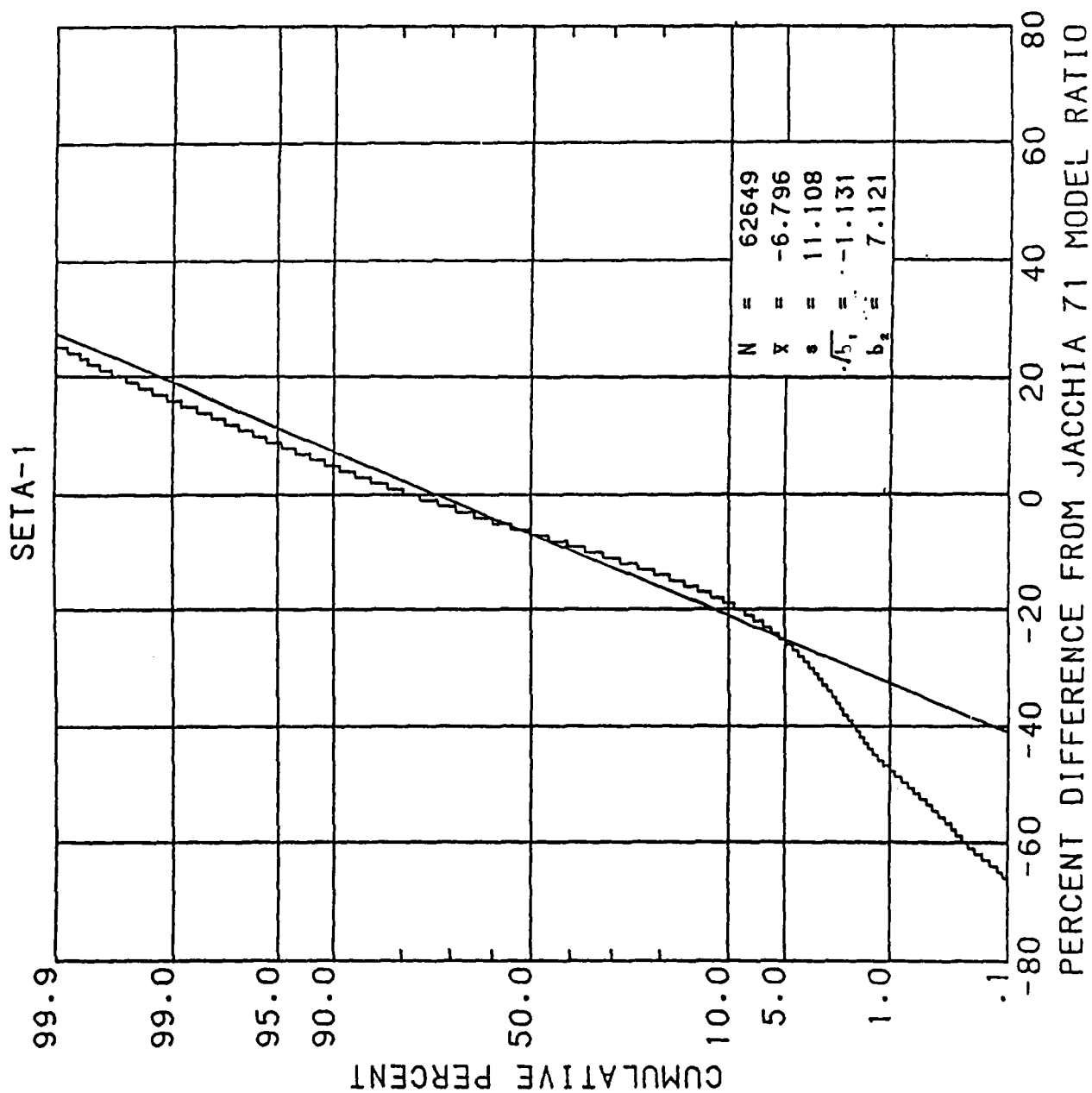


Figure 1.12 SETA-1 Empirical Distribution Function of Percent Difference from Jacchia 71 Ratio

1.3.5 KLL

KLL generates Kp/latitude/local time plots from SUATEK format files produced by the STAT program. The interesting feature of the KLL plots is that the abscissa is non-monotonic. The x-axis, from left to right, spans the dayside latitude range -90 to 90 degrees and continues over into the nightside +90 to -90 degrees latitude with appropriate axis labeling. The four Kp ranges are plotted with different symbols. Sample KLL plots are shown in Figures 1.13 and 1.14.

1.4 PACKLIB

PACKLIB is a collection of Radex written routines, originally developed to read the "packed" data base format tapes. PACKLIB has since been enhanced and added to, so that the relevant routines are capable of reading both the packed and unpacked data base format using a handful of user friendly CALLs. The standard CALLing sequence for processing atmospheric density data base tapes is shown in Figure 1.15. A number of other routines useful in routine programming applications have been included in PACKLIB as a convenient repository. A list of the PACKLIB routines, along with their argument lists is shown in Figure 1.16.

SETA-1 SATELLITE ACCELEROMETER DATA
 MEAN LN(RATIO): JACCHIA 71 MODEL
 . ALL DATA. MAX. ALT. = 200 KM.

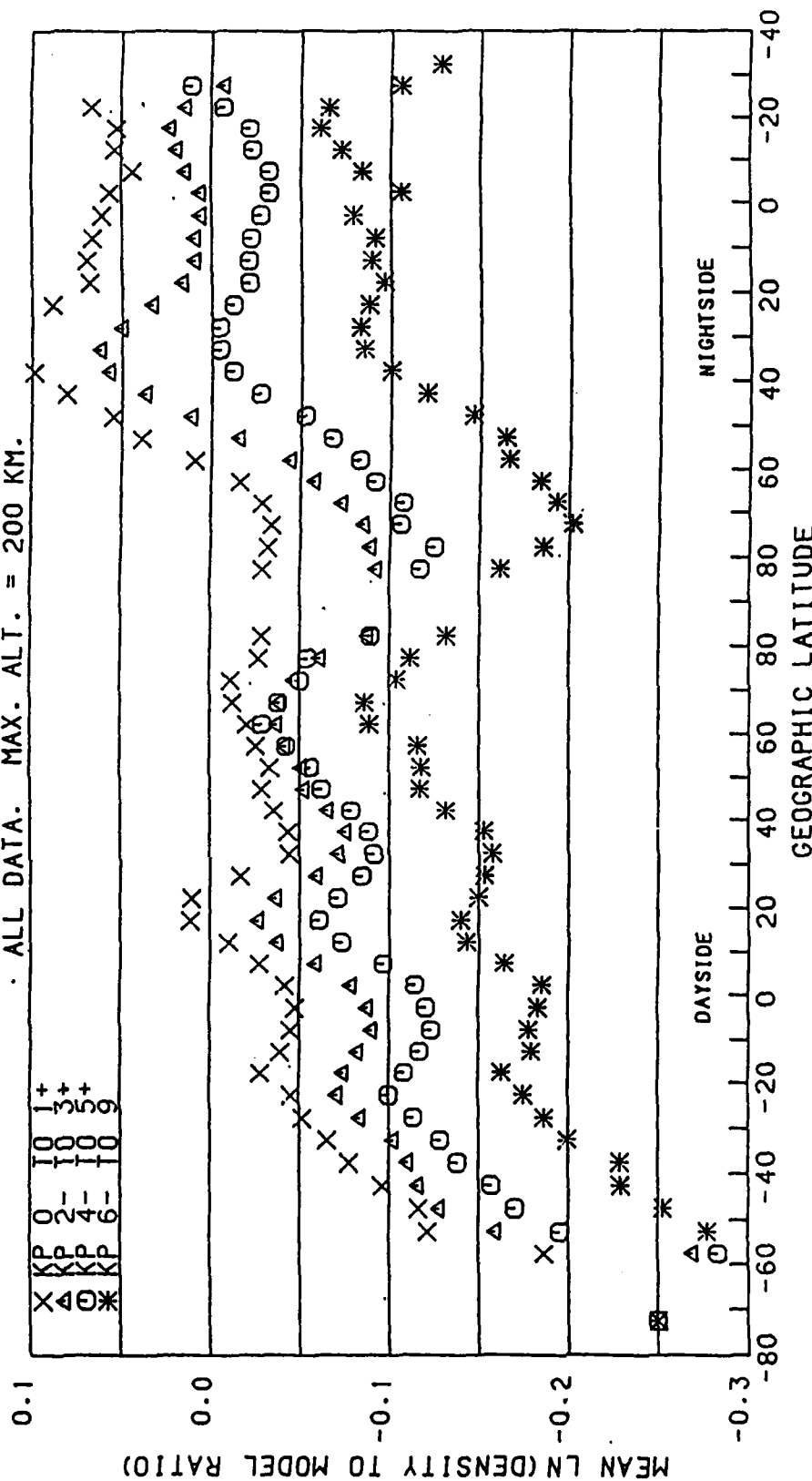


Figure 1.13 SETA-1 Kp/Latitude/Local Time Plot of
 ln(Jacchia 71 Model Ratio)

SETA-1 SATELLITE ACCELEROMETER DATA
 STANDARD DEVIATION: JACCHIA 71 MODEL
 ALL DATA. MAX. ALT. = 200 KM.

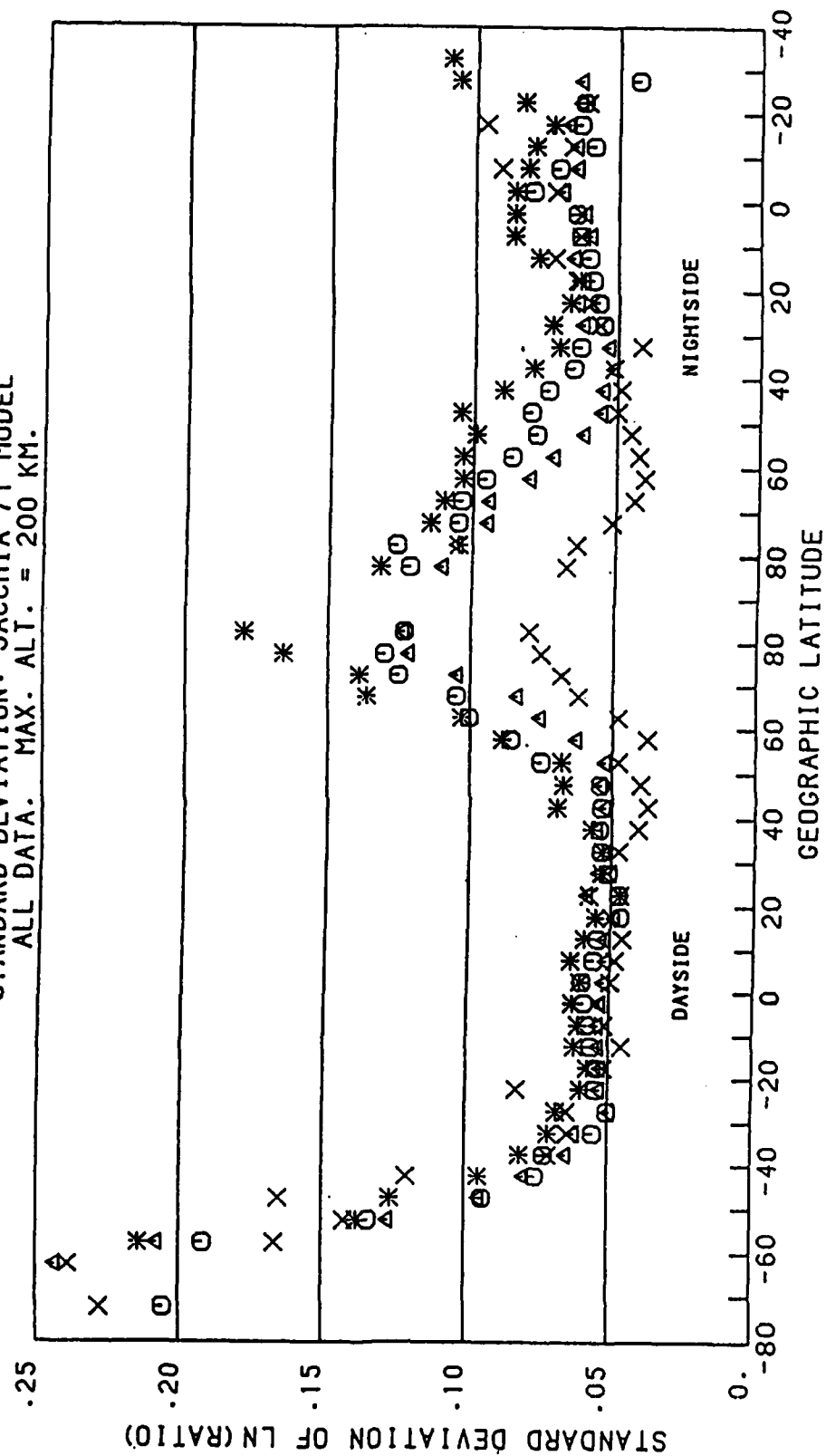


Figure 1.14 SETA-1 Kp/Latitude/Local Time Plot of
 Standard Deviation of $\ln(\text{Jacchia 71})$

Figure 1.15 Sample Program Illustrating PACKLIB CALLs

PROGRAM SAMPLE

SAMPLE PROGRAM ILLUSTRATING THE USUAL SEQUENCE OF CALLS TO
PACKLIB ROUTINES WHEN PROCESSING ATMOSPHERIC DENSITY DATA BASES.

```
INTEGER          DBUNIT
LOGICAL          SELECT, ILT, IGMCO, IGMLT
CHARACTER*10     SAT, MODABBR, MODNAME, CHEADER, CDATA
COMMON /HEADER / HEADER(40)
COMMON /DATA    / DATA(40,12)
DIMENSION        MODABBR(4), MRWORD(4), MODNAME(4)
DIMENSION        IHEADER(40), CHEADER(40)
DIMENSION        IDATA(40,12), CDATA(40,12)
EQUIVALENCE      (HEADER(1), IHEADER(1)), (DATA(1,1), IDATA(1,1))
```

```
DATA ILT/.TRUE./, IGMCO/.FALSE./, IGMLT/.FALSE./
```

```
DBUNIT      = 1
SAT         = 'SETA-1'
NMODELS     = 2
MODABBR(1)  = 'MSIS83'
MODABBR(2)  = 'J71'
```

THE CALL TO DBTAPE REQUESTS THE DATA BASE TAPE CONTAINING THE
NAMED SATELLITE (SAT) AND MODELS (MODABBR) AND ASSIGNS IT TO
UNIT NUMBER DBUNIT. DBTAPE SEARCHES THE FILE
DBINDEX/UN=BRYANTC. THE WORD NUMBERS OF THE REQUESTED MODELS
IN THE DATA RECORD ARE RETURNED IN THE ARRAY MRWORD AND THE
FULL MODEL NAMES ARE RETURNED IN THE ARRAY MODNAME.

```
CALL DBTAPE (DBUNIT, SAT, NMODELS, MODABBR, MRWORD, MODNAME)
```

THE CALL TO HEADIN READS THE HEADER RECORD INTO THE COMMON BLOCK
/HEADER/. THE FIRST ALTERNATE RETURN IS TAKEN IF END-OF-FILE
IS ENCOUNTERED, THE SECOND IF PARITY.

```
1000 CALL HEADIN (*9998, *9999)
```

TRANS IS USED TO DO A BOOLEAN TO BOOLEAN TRANSFER OF DATA FROM
ONE ARRAY TO ANOTHER. THIS IS DONE IF CHARACTER DATA IN THE
HEADER IS NEEDED.

```
CALL TRANS (HEADER, 40, 1, CHEADER)
```

Figure 1.15 Sample Program Illustrating PACKLIB CALLs (cont'd)

THE CALL TO DATAIN READS A RECORD OF DATA INTO THE COMMON BLOCK /DATA/. ILT, IGMCO, AND IGMLT SHOULD BE SET TO .TRUE. IF LOCAL TIME, GEOMAGNETIC CORDINATES, OR GEOMAGNETIC LOCAL TIME ARE NEEDED, RESPECTIVELY. (FOR PACKED DATA BASES ONLY) JG IS THE NUMBER OF DATA POINTS IN THE DATA RECORD. THE ALTERNATE RETURNS ARE THE SAME AS FOR HEADIN. IN THIS CASE, ON END-OF-FILE, NORMAL PROCESSING RETURNS TO HEADIN TO READ IN THE NEXT HEADER RECORD.

```
1200  CALL DATAIN (ILT,IGMCO,IGMLT,JG,*1000,*9998)
      CALL TRANS  (DATA,40,JG,CDATA)
```

BEGINNING OF MAIN PROCESSING LOOP.

```
DO 1500 J=1,JG
```

SELECT DETERMINES IF DATA POINT J COMES FROM SATELLITE SAT. (APPLICABLE TO AE/S3-1 SATELLITES ONLY. FOR SETA SATELLITES, SELECT IS ALWAYS TRUE. NOTE: SELECT MUST BE DECLARED TYPE LOGICAL.)

```
IF (.NOT.SELECT(J,SAT)) GOTO 1500
```

```
- - - - -
```

PROCESS DATA POINT J.

```
- - - - -
```

```
1500  CONTINUE
```

GO BACK AND READ THE NEXT DATA RECORD.

```
GOTO 1200
```

END OF DATA SET. FINISH UP PROCESSING (OR GO BACK AND GET ANOTHER SATELLITE'S WORTH OF DATA).

```
9998  CONTINUE
```

```
STOP
```

PARITY ERROR.

```
9999  STOP 'PARITY'
```

END

Figure 1.16 PACKLIB Routines

PACKLIB SUBROUTINES, FUNCTIONS, & ALTERNATE ENTRY POINTS WITH
THEIR ARGUMENT LISTS. (12/30/86)

SUBROUTINES:

```

SUBROUTINE DBTAPE (DBUNIT, SAT, NMODELS, MODABBR, MRWORD, MODNAME)
SUBROUTINE INIT (NTAPE, *, *)
SUBROUTINE HEADIN (*, *)
SUBROUTINE HEADOUT (NT, HEADER)
SUBROUTINE DATAIN (ILT, IGMCO, IGMLT, JG, *, *)
ENTRY READAT (ILT, IGMCO, IGMLT, JG, *, *)
SUBROUTINE DATAOUT (NT, DATA, JG)
ENTRY WRITDAT (NT, DATA, JG)
SUBROUTINE TRANS (BOOL1, NROWS, NCOLS, BOOL2)
SUBROUTINE DATAMOD (J, CASE, SKIP)
SUBROUTINE S851ORB
SUBROUTINE PACKER (IT, IU, IA, NIA, LN, L, *, *)
ENTRY NUTP
ENTRY OLTP (IT)
ENTRY WRTP
ENTRY PKTP
ENTRY OUTP
ENTRY ENTP
ENTRY RETP
ENTRY RDTP
ENTRY UPTP (IT, IU, IA, NIA, LN, *, *)
ENTRY INTF
ENTRY WRHEAD
ENTRY RDHEAD (IT, IU, IA, NIA, *, *)
ENTRY BSTP
SUBROUTINE REWDB
SUBROUTINE DBCREAT (CHEADER, DBDATE)
SUBROUTINE TIMAG1 (GLAT, GLONE, TIME, HRMNSC, GMLAT, GMLONE, GMLT)
SUBROUTINE XLOCTIM (TIME, XLONG, HRMNSC)
SUBROUTINE HMS (SEC, HRMNSC)
SUBROUTINE TIMAG (GLAT, GLONE, AMJD, GMLAT, GMLONE, GMLT)
SUBROUTINE DIMAG (GLAT, GLONE, GMLAT, GMLONG)
SUBROUTINE SOLONG (AMJD, ALONG)
SUBROUTINE YRMODAF (JDATE, YEAR, MONTH, DAY)
SUBROUTINE BHWIN
SUBROUTINE SKIPF (UNITNO, FORM, *)
SUBROUTINE COPYCF (FROM, TO, *)
SUBROUTINE DESPACE (ALPHA)
SUBROUTINE DECOMMA (ALPHA)
SUBROUTINE PACK (ALPHA)

```

Figure 1.16 PACKLIB Routines (cont'd)

```

SUBROUTINE LJJUST (ALPHAI,ALPHAO,NCHAR)
SUBROUTINE RJJUST (ALPHAI,ALPHAO,NCHAR)
SUBROUTINE POWER10 (X,Y,CHSIZ,ORIENT,EXP)
SUBROUTINE SQRTSYM (X,Y,CHSIZ,ANCHAR)
SUBROUTINE ITOI (IA,A,NA)
  ENTRY RTOI (A,IA,NA)
SUBROUTINE JOBINFO (PARAM,VALUE)
SUBROUTINE SETIND (BOOLVAR)
  ENTRY SETINF (BOOLVAR)
  ENTRY SETNINF (BOOLVAR)

```

FUNCTIONS:

```

LOGICAL      FUNCTION SELECT (J,SAT)
LOGICAL      FUNCTION ALTDBF (SAT)
INTEGER      FUNCTION MJDATEF (JDATE)
  ENTRY      AMJDF (AJDATE)
INTEGER      FUNCTION JDATEF (MONTH)
INTEGER      FUNCTION MONTHF (JDATE)
INTEGER      FUNCTION SEASONF (JDATE)
INTEGER      FUNCTION NDTOD (YEAR,MONTH,DAY)
INTEGER      FUNCTION NDINYR (JDATE)
INTEGER      FUNCTION NDINMO (JDATE)
REAL         FUNCTION UTF (LT,LON)
REAL         FUNCTION LTF (UT,LON)
REAL         FUNCTION LONF (UT,LT)
INTEGER      FUNCTION HHMMF (HOURS)
CHARACTER*(*) FUNCTION CENTER (ALPHA,NCHAR,FIELDWD)
CHARACTER*(*) FUNCTION ENCODEI (I,W)
CHARACTER*(*) FUNCTION ENCODEF (X,W,D,DTRAIL0)
CHARACTER*(*) FUNCTION ENCODEE (X,W,D)
CHARACTER*10 FUNCTION PLOTDEV ( )
INTEGER      FUNCTION LOWERF (LETTER)
REAL         FUNCTION XMAXF ( )
REAL         FUNCTION YMAXF ( )
LOGICAL      FUNCTION IAOF ( )
LOGICAL      FUNCTION IOUNITF ( )
CHARACTER*10 FUNCTION TYPE (BOOLVAR)
LOGICAL      FUNCTION MINUSOF (BOOLVAR)
REAL         FUNCTION SIGNUMF (X)
REAL         FUNCTION RGASF ( )
REAL         FUNCTION DELETF ( )
REAL         FUNCTION IGNOREF ( )

```

1.5 Model Development

1.5.1 Jacchia 70 Tides

The early Jacchia models are based largely on high altitude satellite orbital decay data, and thus reflect the dominance of the diurnal (one oscillation per day) tidal modes at these altitudes, ignoring competition from the semidiurnal (twice per day oscillations) which occur at lower altitudes. These early models nevertheless enjoy the advantage of computational simplicity in comparison with more elaborate recent models if only the total density is being computed, as opposed to composition. This is because the total density could be stored for convenient retrieval from two-dimensional lookup tables. Except for this principal weakness of the simpler early models with regard to their low-altitude local time variations, these models have achieved accuracies comparable to those of the more recent models, according to data/model comparisons. The Jacchia 70 Tides model^(7,12) represents an attempt to correct the local time variation in the Jacchia 70 model. Polynomial fits in altitude and latitude were constructed to the total density diurnal and semidiurnal results of Forbes, et. al. (see References 7 and 12, and references therein, for details), and added to the diurnally averaged Jacchia 70 model.

In statistical evaluations using accelerometer data, as described in previous sections of this chapter, the Jacchia 70 Tides model yielded lower variability (standard deviations) than the original model for the satellite with the most extensive local time coverage (AE-E), about the same variability for the other AE/S3-1 satellites, and somewhat higher variability for the SETA series. This indicates that probably the local time representation in the Jacchia 70 Tides model is accurate, at least at low latitudes and low solar activity, but degrades for the SETA satellites because

of inaccurate representation of latitudinal and/or solar cycle dependencies of the diurnal and semidiurnal parameters. A polar-orbiting satellite at high solar activity, rotated 6 hours in local time from the SETA satellites, could possibly resolve this issue and lead to improved modelling.

1.5.2 Air Force Reference Atmosphere Supplements 1986

The Air Force Reference Atmosphere Supplements 1986 Model (AFRA-86) has as its objective the specification of various atmospheric properties in the altitude region 80-200 km. Early on it was decided that the model would be put together from the MSIS-83 model and the lower altitude model reported by Forbes in previous sections of this report. Two factors become immediately obvious:

- 1) The Forbes model is defined only up to 120 km, and contains dependencies on only altitude, latitude, and month;
- 2) The MSIS-83 model is defined from 85 km up and contains far more dependencies, such as local time, solar activity, and geomagnetic activity.

Thus it is apparent that the Forbes model should be used in the lower portion of the AFRA-86 altitude range (80-200 km), while the MSIS-83 model should be used in the upper portion.

To determine precisely what the boundaries should be for these respective portions, and how to effect the transition between them, we made some comparisons between the two models in the overlap region 90-120 km. In these comparisons we deleted from the MSIS-83 model the dependencies not included in the Forbes model. It was hoped that the two models would be in close agreement over a large enough altitude range that

the joining could be effected by a small adjustment in one or both models (for example, modifying selected MSIS-83 low altitude parameters) without compromising either model in its region of dominant application. Unfortunately we found this not to be the case, as shown for example in Fig. 1.17. In general it was found that the Forbes-MSIS disagreement worsens as one goes from low to middle latitudes, an effect apparently related to differences in the mid latitude data sets used in their respective derivations. We therefore concluded that the models could not be brought into agreement in their overlap region by any simple adjustment without jeopardizing their validities in their separate altitude regions of application (low altitudes for the Forbes model, high altitudes for the MSIS-83 model).

We have thus adopted a model definition (Figure 1.18) which employs strictly the Forbes model below a prescribed altitude h_1 , the MSIS-83 model above another prescribed altitude h_2 , and a connecting model which matches continuously and smoothly the Forbes model at h_1 and the MSIS-83 model at h_2 . The value of h_2 was chosen to be 120 km, since it was found (Fig. 1.19) that the MSIS-83 density dependence on geomagnetic activity is minimal at this altitude, thus easing the transition to the lower altitude Forbes model, which, as mentioned previously, contains no dependence on geomagnetic activity. This near independence of the MSIS-83 model density on geomagnetic activity is evidently due to the vanishing of the coefficients k_{00}^a and k_{20}^a specifying the N_2 dependence at 120 km on geomagnetic activity [see Hedin's paper ⁽²⁾, Table 2d]. The simplest type of connecting function meeting the requirements of continuous and smooth joining at two points would be a cubic polynomial possessing the required values and derivatives. Due to practical difficulties in computing derivatives, we have chosen to approximate this by a cubic polynomial matching the Forbes model values at $h_1 - 2$ km and h_1 , and the MSIS-83 model values at h_2 and $h_2 + 2$ km.

FORBES/MSIS-83 DENSITY RATIOS
 LAT = 30 DEG KP = 1 F10.7 = 75.

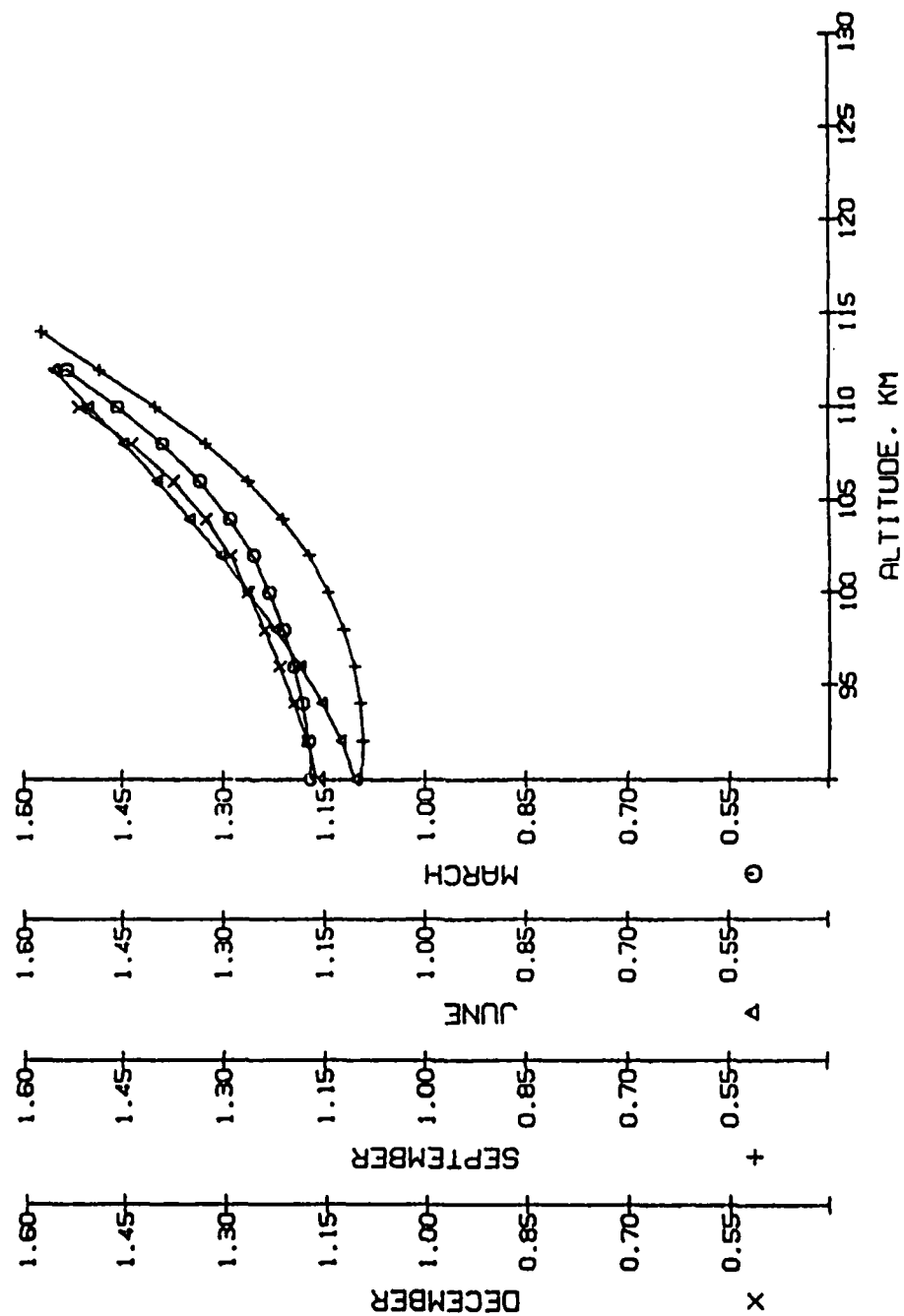


Figure 1.17 Ratio of Forbes Density Model to MSIS-83 Density Model

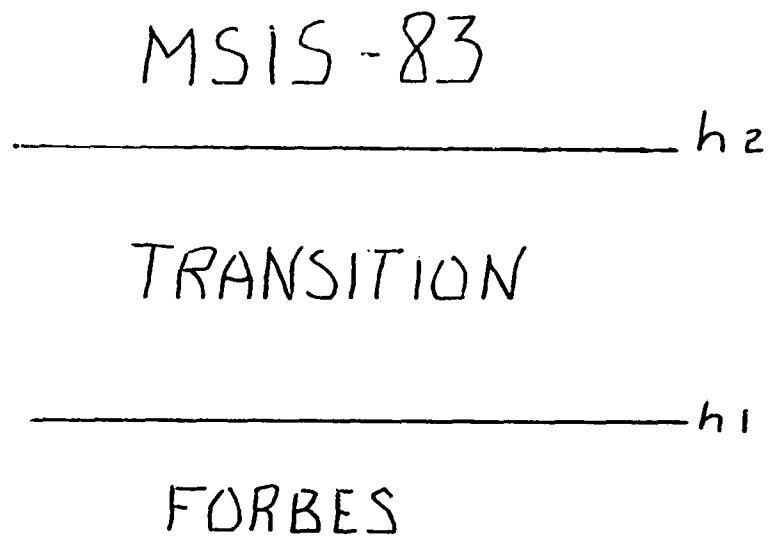


Figure 1.18 Schematic of AFRA-86 Model

MEAN MSIS-83 DENSITY VARIATION WITH K_p .
RATIO OF DENSITY AT K_p TO DENSITY AT $K_p=1$

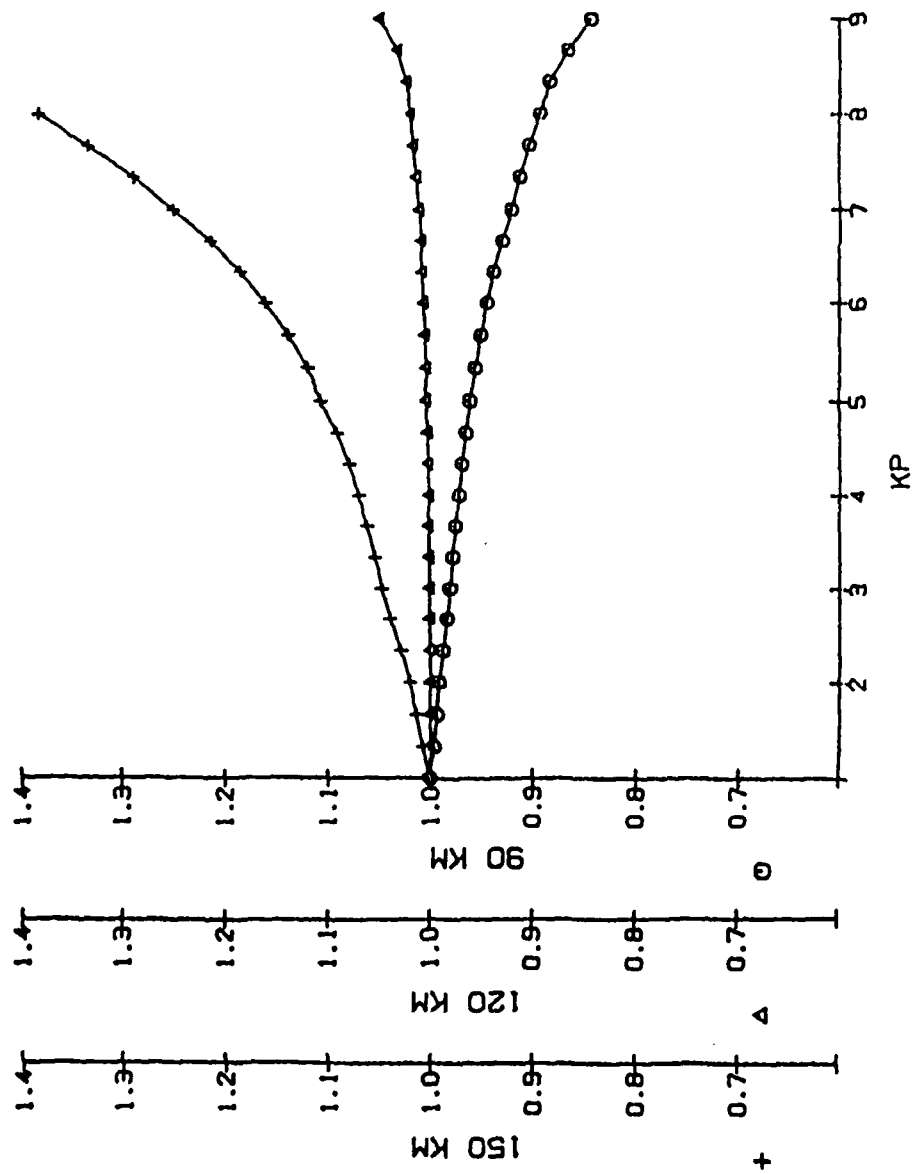


Figure 1.19 Mean MSIS-83 Density Variation With K_p

It was also desirable, but not mandatory, that the connection model be consistent with basic physics, i. e., satisfy hydrostatic equilibrium. The problem with this is that the solutions to the equation for hydrostatic equilibrium are specified by boundary conditions at only one altitude, and we have to satisfy boundary conditions (the matching conditions discussed in the last paragraph) at two points. We attempted to do this by modifying the temperature or molecular weight so that the resulting equations would yield solutions providing the required matches.

The equation for hydrostatic equilibrium is:

$$d(\ln P)/dz = -Mg/(RT), \quad (1)$$

where:

P = pressure;
 z = altitude;
 M = molecular weight;
 g = acceleration of gravity;
 R = universal gas constant
 = 8.31432×10^7 g cm²/(sec² mole K);
 T = temperature.

The acceleration of gravity g is commonly given by:

$$g = g_s / (1 + z/R_p)^2.$$

where,

$g_s = 9.80665$ m/s²;
 $R_p = 6356.766$ km.

from the geometric altitude z to the geopotential altitude:

$$y = (z - z_1)(R_p + z_1)/(R_p + z),$$

where z_1 is an arbitrary altitude. Equation (1) then becomes:

$$d(\ln P)/dy = -Mg_1/(RT),$$

where g_1 is the acceleration of gravity at $z=h_1$.

It is convenient to set z_1 to h_1 and expand the molecular weight and the inverse temperature in powers of y :

$$M = \sum_{i=0}^3 m_i y^i;$$
$$1/T = \sum_{i=0}^3 t_i y^i + s y^2 (y - y_2)^2,$$

where the m_i and t_i are the coefficients of the matching cubic polynomials for M and $1/T$, s is an adjustable parameter, and y_2 is the geopotential altitude at $z = h_2$. Note that the form of the term multiplied by s preserves the match in $1/T$ at $y = y_1 = 0$ and $y = y_2$. The solution P can be generated analytically which satisfies the matching conditions at both boundaries y_1 and y_2 provided s is chosen so that

$$s = [-\ln(P_2/P_1) - (g_1 F/R)]/(g_1 G/R),$$

where:

P_1 = pressure at y_1 ;

P_2 = pressure at y_2 ;

$$F = y_2 \sum_{i=0}^6 q_i y_2^i;$$

$$G = y_2^5 \sum_{i=0}^3 m_i r_i y_2^i,$$

where:

$$q_i = \left(\sum_{j=0}^i m_j t_{i-j} \right) / (i+1);$$

$$r_i = 1/(1+5) - 2/(i+4) + 1/(1+3).$$

Given P , T , and M over the interval y_1 to y_2 we can calculate the density ρ from the perfect gas law:

$$\rho = PM/(RT).$$

A similar formulation can be developed for adjusting the molecular weight M rather than $1/T$, i. e., we add a term to the polynomial for M containing a coefficient which is adjusted to make the required match.

We examined these approaches for various cases. Unfortunately we found some cases, as in Figure 1.20, where either the temperature had to go through at minimum at an unrealistically high altitude (normally it should minimize near 90 km) or the mass attained unrealistically high or low values. Broadening the transition region did not help, nor was it felt feasible to add more terms to the expansions, since this would complicate the calculations unduly and most likely would simply result in solutions containing more severe undulations.

JUN. LAT = 30.. KP = 3.. F10.7 = 100.
MATCHING REGION = 90 TO 120 KM.

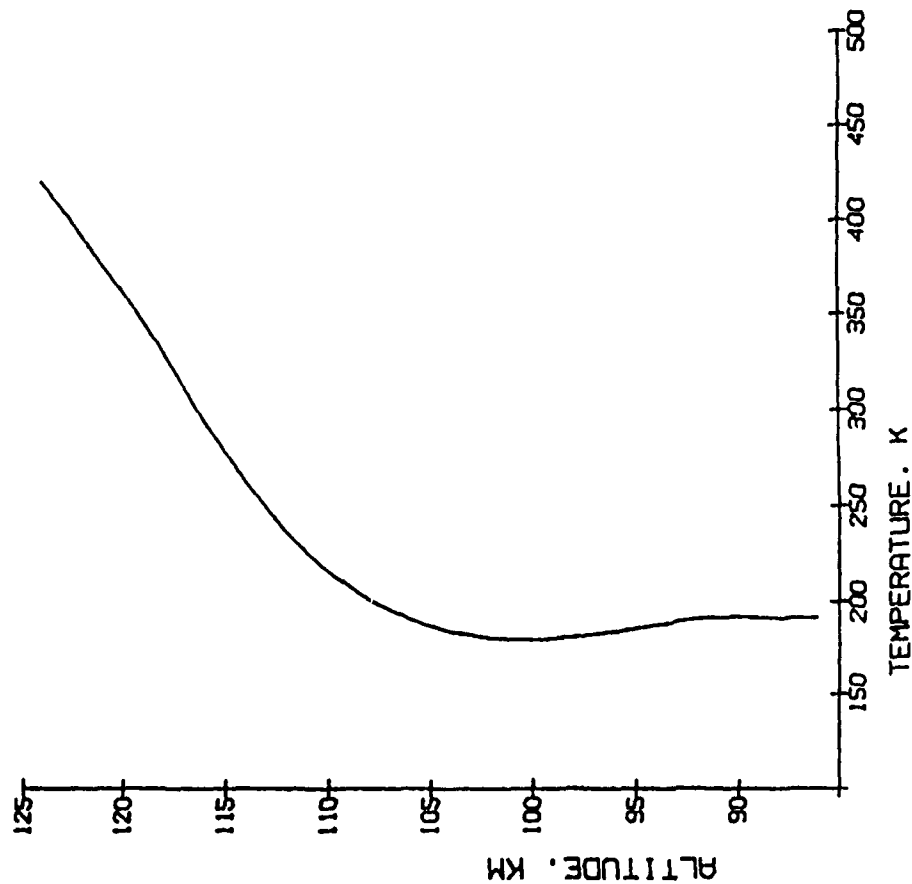


Figure 1.20 Hydrostatic Equilibrium Model in Transition
Region 90-120 km

FORBES ANNUAL MEAN DENSITY AT 45 DEG N.
(RATIO TO U. S. STANDARD 1976)

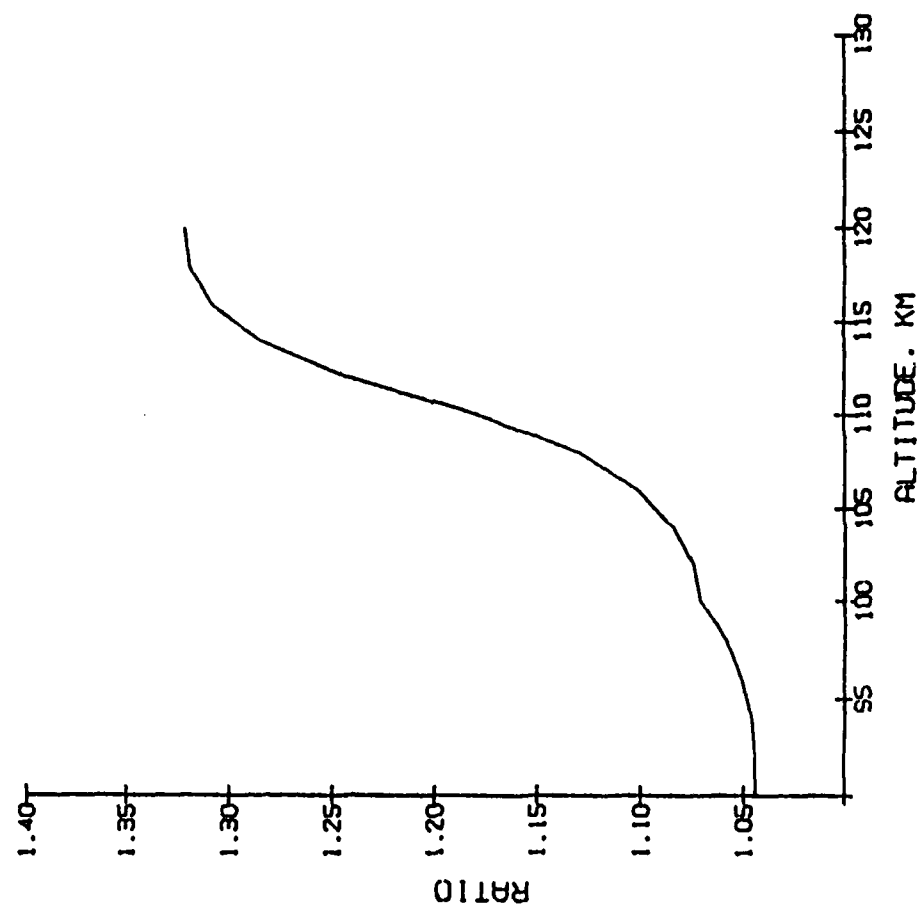


Figure 1.21 Ratio of Forbes Annual Mean Density at 45° N to
U. S. Standard 1976 Model

Therefore we have chosen to drop the requirement of static equilibrium and define the Forbes-MSIS transition strictly by matching cubic polynomials. After examination of typical results we chose 104 km as the lower boundary of the transition region. This amounts to a compromise between 110 km suggested by Forbes as the upper limit of validity of his model and a more conservative upper limit at 100 km, which arose out of our preliminary studies (we found in particular severe disagreement between Forbes and the U. S. Standard 76 Atmosphere at 110 km, 45 degrees latitude, as shown in Figure 1.21).

In conclusion, we give the final definition for the Air Force Reference Atmosphere 1986 (AFRA-86):

Region 1 (70-104 km): Forbes model;

Region 2 (104-120 km):

compute the density, temperature and molecular weight from cubic polynomials matching the Forbes model at 102 km and 104 km, and matching the MSIS-83 model at 120 km and 122 km; then compute the pressure from the perfect gas law;

Region 3 (120-200 km): MSIS-83 model.

1.6 Study of Statistical Techniques Applied to Atmospheric Density Data

1.6.1 Introduction

It was suggested that the neutral mass density to model ratios may be correlated in time. An investigation was undertaken to evaluate this possibility and to assess it's effect on the statistics currently being calculated for Air Force Reference Atmosphere purposes. Two approaches were used: one was to do a one way random effects analysis of variance, separating the variation into between and within orbit components, the second was to calculate the auto-correlation coefficients for various lags and compare them with their standard errors. The Durbin-Watson statistic for serial correlation was also calculated.

1.6.2 One Way Random Effects Analysis of Variance

The STAT program was modified to do a one way random effects analysis of variance calculation. The Jacchia 1971 model ratios were analyzed from the SETA-1 data set spanning days 79 through 100 of 1979. The data were binned on 4 Kp bins (0 to 1+, 2- to 3+, 4- to 5+, and 6- to 9) and 5 geographic latitude bins. The variation within each bin was divided into between and within orbit variance components.

The one way random effects model is:

$$y_{ij} = \mu + \alpha_i + \epsilon_{ij}$$

where y_{ij} is the mean ratio,

μ is the overall mean in each bin

α_i is a random component due to orbit to orbit variability and,

ϵ_{ij} is a random component due to variability within orbits

(See References 15 and 16)

Note that

$$E[\alpha_i] = 0, \quad V[\alpha_i] = \sigma_\alpha^2$$

$$E[\epsilon_{ij}] = 0, \quad V[\epsilon_{ij}] = \sigma^2$$

so that

$$E[y_{ij}] = \mu$$

$$V[y_{ij}] = \sigma_\alpha^2 + \sigma^2$$

where $E[.]$ is the expected value, and $V[.]$ is the

variance. We want to test if $\sigma_\alpha^2 = 0$. If the data are correlated in time, one would expect σ^2 to be much less than σ_α^2 .

We construct the following analysis of variance table.

One way Random Effects Analysis of Variance Table

| Source | Sum of Squares | Degrees Freedom | Mean Square | Expected Mean Square |
|---------|----------------|-----------------|-------------|----------------------------------|
| Total | SST | N-1 | | |
| Between | SSB | $n_o - 1$ | MSB | $\sigma^2 + n_e \sigma_\alpha^2$ |
| Within | SSW | $N - n_o$ | MSW | σ^2 |

where N = total number of points,

n_o = number of orbits,

MSB = $\frac{SSB}{n_o - 1}$ and,

MSW = $\frac{SSW}{N - n_o}$.

The total sum of squares can be partitioned into its between and within components.

$$\begin{aligned}
 SST &= \sum_{j=1}^{n_o} \sum_{i=1}^{n_j} (y_{ij} - \bar{y})^2 \\
 &= \sum_{j=1}^{n_o} n_j (\bar{y}_{.j} - \bar{y})^2 + \sum_{j=1}^{n_o} \sum_{i=1}^{n_j} (y_{ij} - \bar{y}_{.j})^2 \\
 &= SSB + SSW
 \end{aligned}$$

where $\bar{y}_{.j}$ is the average over $i=1, n_j$.

Note that $E[MSB] = \sigma^2 + n_e \sigma_\alpha^2$

and $E[MSW] = \sigma^2$.

n_e is equal to or less than the number of points per bin per orbit with equality holding when there are an equal number of points per bin per orbit (See Reference 17).

To test that $\sigma_\alpha^2 = 0$, we can test the F ratio,

$$F = \frac{MSB}{MSW}$$

for significance. Table 1.6 shows the calculation for the SETA-1, Jacchia 71 data set. The value in the column "1-P" is the probability of exceeding the calculated F ratio.

- ALL DATA -
 AIR FORCE REFERENCE ATMOSPHERE
 ONE WAY RANDOM EFFECTS ANALYSIS OF VARIANCE
 NEUTRAL MASS DENSITY RATIO TO MODEL STATISTICS

86/02/24

SATELLITE(S): SETA-1
 ALTITUDE RANGE SAMPLED: 0 TO 200 KM. DATE RANGE: 79/79 TO 79/100.
 LINEAR MODEL RATIOS.

| | | | | | | | |
|------------|--------------|-----------|--------------|--------------|----------------|--------------------|--------------------|
| MEAN KP | MEAN FLUX | MEAN Z | MEAN L.T. | MEAN U.T. | # OF POINTS | JACCHIA 71 MEAN | JACCHIA 71 S.D. |
| 3.34 | 189.9 | 181.7 | 12.32 | 12.45 | 30585 | .932 | .081 |

Table 1.6: SETA-1 Jacchia 71
Data Set

AIR FORCE REFERENCE ATMOSPHERE
ONE WAY RANDOM EFFECTS ANALYSIS OF VARIANCE
NEUTRAL MASS DENSITY RATIO TO MODEL STATISTICS

SATELLITE(S): SETA-1
ALTITUDE RANGE SAMPLED: 0 TO 200 KM. DATE RANGE: 79/79 TO 79/100.
SOLAR DAY LOCAL TIME FROM 0800 TO 1800 HOURS.
LINEAR MODEL RATIOS.

| KP | GG LAT | | MEAN KP | MEAN FLUX | MEAN Z | MEAN L.T. | MEAN U.T. | # OF POINTS | MEAN | S.D. | D.F. | JACCHIA 71 | | NE | 1-P |
|----|--------|------|------------|--------------|-----------|--------------|--------------|----------------|-------|------|------|------------|--------|---------|-----|
| | MIN | MAX | | | | | | | | | | S.D. B | S.D. W | | |
| 0 | -90. | -85. | .99 | 190.8 | 198.8 | 10.02 | 13.62 | 32 | .952 | .057 | 19 | .057 | 1.52 | 2.6E-07 | |
| | -85. | -80. | 1.05 | 190.4 | 195.9 | 10.06 | 13.00 | 83 | .960 | .059 | 25 | .056 | 2.95 | .0E+00 | |
| | -80. | -75. | 1.06 | 185.6 | 193.0 | 10.10 | 13.08 | 130 | .973 | .051 | 32 | .049 | 3.71 | .0E+00 | |
| | -75. | -70. | 1.06 | 185.7 | 188.5 | 10.14 | 13.07 | 124 | .963 | .043 | 31 | .040 | 3.54 | .0E+00 | |
| | -70. | -65. | 1.08 | 185.9 | 184.3 | 10.18 | 13.13 | 127 | .957 | .049 | 33 | .046 | 3.52 | .0E+00 | |
| | -65. | -60. | 1.06 | 185.6 | 180.7 | 10.22 | 13.15 | 130 | .955 | .051 | 34 | .050 | 3.51 | .0E+00 | |
| | -60. | -55. | 1.06 | 185.7 | 177.7 | 10.25 | 13.31 | 130 | .960 | .047 | 33 | .046 | 3.61 | 3.6E-14 | |
| | -55. | -50. | 1.06 | 185.6 | 175.1 | 10.29 | 13.27 | 130 | .974 | .047 | 33 | .044 | 3.51 | .0E+00 | |
| | -50. | -45. | 1.08 | 186.0 | 173.2 | 10.33 | 13.14 | 128 | .991 | .046 | 33 | .043 | 3.55 | .0E+00 | |
| | -45. | -40. | 1.06 | 186.2 | 171.6 | 10.37 | 13.47 | 125 | 1.012 | .050 | 89 | .048 | 3.47 | .0E+00 | |
| | -40. | -35. | 1.03 | 185.8 | 170.8 | 10.41 | 13.49 | 125 | 1.012 | .058 | 32 | .056 | 3.57 | .0E+00 | |
| | -35. | -30. | 1.04 | 186.1 | 170.3 | 10.45 | 13.62 | 120 | .985 | .051 | 29 | .046 | 3.53 | .0E+00 | |
| | -30. | -25. | 1.04 | 185.7 | 170.4 | 10.50 | 13.55 | 111 | .958 | .046 | 28 | .044 | 3.58 | .0E+00 | |
| | -25. | -20. | 1.01 | 185.3 | 170.8 | 10.56 | 13.57 | 108 | .958 | .039 | 28 | .036 | 3.27 | .0E+00 | |
| | -20. | -15. | 1.03 | 184.2 | 171.7 | 10.62 | 13.93 | 106 | .966 | .036 | 25 | .033 | 3.65 | .0E+00 | |
| | -15. | -10. | 1.03 | 183.7 | 173.1 | 10.70 | 13.68 | 99 | .972 | .039 | 26 | .037 | 3.41 | .0E+00 | |
| | -10. | -5. | 1.05 | 184.2 | 174.6 | 10.79 | 13.79 | 107 | .968 | .045 | 27 | .043 | 3.56 | .0E+00 | |
| | 0 | 5. | 1.02 | 184.0 | 176.7 | 10.91 | 13.83 | 109 | .975 | .037 | 29 | .036 | 3.51 | .0E+00 | |
| | 5. | 10. | 1.03 | 184.4 | 179.0 | 11.06 | 13.63 | 111 | .981 | .048 | 29 | .046 | 3.58 | .0E+00 | |
| | 10. | 15. | 1.06 | 185.0 | 181.1 | 11.28 | 13.45 | 119 | .990 | .064 | 31 | .062 | 3.60 | .0E+00 | |
| | 15. | 20. | 1.03 | 185.2 | 183.7 | 11.63 | 13.38 | 129 | .991 | .070 | 30 | .066 | 3.79 | .0E+00 | |
| | 20. | 25. | 1.05 | 185.4 | 186.2 | 12.31 | 13.17 | 141 | .976 | .076 | 106 | .075 | 4.03 | .0E+00 | |
| | 25. | 30. | 1.06 | 185.3 | 189.6 | 15.02 | 12.63 | 275 | .978 | .075 | 34 | .068 | 7.43 | .0E+00 | |
| | 30. | 35. | | | | | | 0 | | | | | | | |
| | 35. | 40. | | | | | | | | | | | | | |
| | 40. | 45. | | | | | | | | | | | | | |
| | 45. | 50. | | | | | | | | | | | | | |
| | 50. | 55. | | | | | | | | | | | | | |
| | 55. | 60. | | | | | | | | | | | | | |
| | 60. | 65. | | | | | | | | | | | | | |
| | 65. | 70. | | | | | | | | | | | | | |
| | 70. | 75. | | | | | | | | | | | | | |
| | 75. | 80. | | | | | | | | | | | | | |
| | 80. | 85. | | | | | | | | | | | | | |
| | 85. | 90. | | | | | | | | | | | | | |

Table 1.6 cont.

AIR FORCE REFERENCE ATMOSPHERE
ONE WAY RANDOM EFFECTS ANALYSIS OF VARIANCE
NEUTRAL MASS DENSITY RATIO TO MODEL STATISTICS

86/02/24

SATELLITE(S): SETA-1
ALTITUDE RANGE SAMPLED: 0 TO 200 KM. DATE RANGE: 79/79 TO 79/100.
SOLAR DAY LOCAL TIME FROM 0800 TO 1800 HOURS.
LINEAR MODEL RATIOS.

| KP | GG LAT | MEAN KP | MEAN FLUX | MEAN Z | MEAN L.T. | MEAN U.T. | # OF POINTS | MEAN | S.D. | D.F. B | S.D. B | JACCHIA 71 | D.F. W | S.D. W | NE | 1-P |
|-------|-----------|---------|-----------|--------|-----------|-----------|-------------|------|------|--------|--------|------------|--------|--------|---------|-----|
| 2- 3+ | MIN MAX | | | | | | | | | | | | | | | |
| | -90. -85. | 2.33 | 188.6 | 199.0 | 10.02 | 10.70 | 63 | .939 | .047 | 37 | .045 | 19 | .015 | 1.43 | 4.9E-08 | |
| | -85. -80. | 2.60 | 188.1 | 196.9 | 10.06 | 11.86 | 273 | .940 | .048 | 96 | .045 | 165 | .017 | 2.52 | .0E+00 | |
| | -80. -75. | 2.60 | 186.5 | 194.9 | 10.10 | 12.04 | 617 | .929 | .049 | 165 | .047 | 439 | .016 | 3.47 | .0E+00 | |
| | -75. -70. | 2.61 | 187.0 | 190.5 | 10.14 | 12.10 | 627 | .922 | .050 | 166 | .048 | 450 | .015 | 3.54 | .0E+00 | |
| | -70. -65. | 2.60 | 186.7 | 186.3 | 10.18 | 12.00 | 637 | .915 | .050 | 171 | .048 | 458 | .013 | 3.56 | .0E+00 | |
| | -65. -60. | 2.60 | 186.8 | 182.5 | 10.22 | 11.94 | 641 | .917 | .049 | 169 | .047 | 463 | .014 | 3.60 | .0E+00 | |
| | -60. -55. | 2.61 | 186.8 | 179.1 | 10.25 | 12.04 | 620 | .926 | .048 | 167 | .046 | 443 | .014 | 3.50 | .0E+00 | |
| | -55. -50. | 2.60 | 186.8 | 176.4 | 10.29 | 12.23 | 613 | .944 | .049 | 159 | .046 | 442 | .016 | 3.58 | .0E+00 | |
| | -50. -45. | 2.62 | 186.7 | 174.2 | 10.33 | 12.43 | 589 | .964 | .050 | 155 | .048 | 423 | .016 | 3.55 | .0E+00 | |
| | -45. -40. | 2.61 | 186.5 | 172.6 | 10.37 | 12.42 | 570 | .975 | .048 | 147 | .044 | 407 | .019 | 3.50 | .0E+00 | |
| | -40. -35. | 2.64 | 186.8 | 171.4 | 10.41 | 12.56 | 543 | .965 | .057 | 146 | .055 | 388 | .017 | 3.50 | .0E+00 | |
| | -35. -30. | 2.63 | 186.5 | 170.7 | 10.46 | 12.59 | 537 | .944 | .051 | 142 | .048 | 383 | .017 | 3.49 | .0E+00 | |
| | -30. -25. | 2.63 | 186.7 | 170.4 | 10.51 | 12.86 | 541 | .932 | .049 | 139 | .046 | 391 | .016 | 3.61 | .0E+00 | |
| | -25. -20. | 2.63 | 186.5 | 170.7 | 10.56 | 13.01 | 531 | .928 | .052 | 144 | .050 | 379 | .014 | 3.49 | .0E+00 | |
| | -20. -15. | 2.61 | 186.4 | 171.3 | 10.62 | 13.43 | 528 | .938 | .050 | 140 | .047 | 378 | .016 | 3.52 | 2.7E-13 | |
| | -15. -10. | 2.61 | 186.9 | 172.4 | 10.70 | 13.43 | 524 | .950 | .052 | 141 | .050 | 376 | .014 | 3.54 | .0E+00 | |
| | -10. -5. | 2.61 | 186.1 | 173.8 | 10.79 | 13.57 | 531 | .951 | .050 | 141 | .049 | 383 | .014 | 3.59 | .0E+00 | |
| | 0. 5. | 2.63 | 186.7 | 175.5 | 10.91 | 13.41 | 541 | .961 | .061 | 140 | .059 | 393 | .017 | 3.65 | .0E+00 | |
| | 5. 10. | 2.61 | 186.3 | 177.5 | 11.06 | 13.36 | 563 | .966 | .074 | 147 | .071 | 407 | .022 | 3.61 | .0E+00 | |
| | 10. 15. | 2.62 | 186.3 | 179.8 | 11.28 | 13.00 | 596 | .965 | .081 | 155 | .078 | 433 | .023 | 3.66 | .0E+00 | |
| | 15. 20. | 2.61 | 186.5 | 182.1 | 11.62 | 12.64 | 642 | .959 | .096 | 160 | .092 | 474 | .027 | 3.82 | 1.8E-13 | |
| | 20. 25. | 2.62 | 186.7 | 184.8 | 12.31 | 12.28 | 734 | .947 | .108 | 164 | .103 | 561 | .032 | 4.24 | .0E+00 | |
| | 25. 30. | 2.62 | 186.5 | 188.8 | 15.12 | 12.27 | 1346 | .923 | .111 | 166 | .101 | 1170 | .046 | 7.65 | .0E+00 | |
| | 30. 35. | | | | | | 0 | | | | | | | | | |
| | 35. 40. | | | | | | | | | | | | | | | |
| | 40. 45. | | | | | | | | | | | | | | | |
| | 45. 50. | | | | | | | | | | | | | | | |
| | 50. 55. | | | | | | | | | | | | | | | |
| | 55. 60. | | | | | | | | | | | | | | | |
| | 60. 65. | | | | | | | | | | | | | | | |
| | 65. 70. | | | | | | | | | | | | | | | |
| | 70. 75. | | | | | | | | | | | | | | | |
| | 75. 80. | | | | | | | | | | | | | | | |
| | 80. 85. | | | | | | | | | | | | | | | |
| | 85. 90. | | | | | | | | | | | | | | | |

Table 1.6 cont.

86/02/24

AIR FORCE REFERENCE ATMOSPHERE
ONE WAY RANDOM EFFECTS ANALYSIS OF VARIANCE
NEUTRAL MASS DENSITY RATIO TO MODEL STATISTICS

SATELLITE(S): SETA-1
ALTITUDE RANGE SAMPLED: 0 TO 200 KM. DATE RANGE: 79/79 TO 79/100.
SOLAR DAY LOCAL TIME FROM 0800 TO 1800 HOURS.
LINEAR MODEL RATIOS.

| KP | | GG LAT | MEAN KP | MEAN FLUX | MEAN Z | MEAN L.T. | MEAN U.T. | # OF POINTS | MEAN | S.D. | D.F. B | S.D. B | JACCHIA 71 | D.F. W | S.D. W | NE | 1-P |
|------|------|--------|---------|-----------|--------|-----------|-----------|-------------|------|------|--------|--------|------------|--------|--------|----|---------|
| MIN | MAX | MIN | MAX | | | | | | | | | | | | | | |
| -90. | -85. | | 3.92 | 187.0 | 199.2 | 10.03 | 7.69 | 8 | .913 | .035 | | | | | | | |
| -85. | -80. | | 4.23 | 190.1 | 197.6 | 10.06 | 10.10 | 184 | .907 | .046 | 56 | .043 | 121 | .017 | 2.92 | | .0E+00 |
| -80. | -75. | | 4.29 | 193.9 | 194.7 | 10.10 | 10.97 | 339 | .899 | .049 | 92 | .047 | 240 | .015 | 3.42 | | .0E+00 |
| -75. | -70. | | 4.29 | 194.6 | 190.2 | 10.14 | 11.12 | 358 | .891 | .050 | 94 | .049 | 259 | .014 | 3.62 | | .0E+00 |
| -70. | -65. | | 4.28 | 194.6 | 185.9 | 10.18 | 10.98 | 352 | .885 | .052 | 95 | .050 | 252 | .014 | 3.52 | | .0E+00 |
| -65. | -60. | | 4.28 | 194.6 | 182.3 | 10.22 | 11.33 | 360 | .888 | .053 | 96 | .051 | 259 | .013 | 3.56 | | .0E+00 |
| -60. | -55. | | 4.26 | 194.4 | 178.9 | 10.25 | 11.22 | 350 | .893 | .053 | 95 | .052 | 250 | .014 | 3.50 | | .0E+00 |
| -55. | -50. | | 4.26 | 194.1 | 176.3 | 10.29 | 11.22 | 346 | .909 | .051 | 93 | .049 | 247 | .015 | 3.49 | | .0E+00 |
| -50. | -45. | | 4.25 | 194.9 | 174.1 | 10.33 | 11.37 | 346 | .931 | .050 | 87 | .047 | 250 | .018 | 3.60 | | .0E+00 |
| -45. | -40. | | 4.27 | 194.6 | 172.5 | 10.37 | 11.42 | 334 | .942 | .044 | 88 | .042 | 238 | .015 | 3.48 | | .0E+00 |
| -40. | -35. | | 4.28 | 194.6 | 171.3 | 10.41 | 11.75 | 327 | .932 | .044 | 85 | .041 | 232 | .017 | 3.44 | | .0E+00 |
| -35. | -30. | | 4.30 | 194.9 | 170.7 | 10.46 | 11.69 | 314 | .920 | .047 | 80 | .043 | 224 | .019 | 3.49 | | 1.4E-13 |
| -30. | -25. | | 4.31 | 195.1 | 170.4 | 10.50 | 12.13 | 305 | .914 | .049 | 81 | .046 | 217 | .016 | 3.46 | | .0E+00 |
| -25. | -20. | | 4.33 | 195.9 | 170.7 | 10.56 | 12.26 | 292 | .917 | .050 | 77 | .047 | 209 | .016 | 3.52 | | .0E+00 |
| -20. | -15. | | 4.35 | 196.1 | 171.3 | 10.62 | 12.73 | 278 | .926 | .050 | 73 | .047 | 198 | .018 | 3.47 | | 1.1E-13 |
| -15. | -10. | | 4.32 | 196.5 | 172.4 | 10.70 | 12.81 | 300 | .941 | .051 | 76 | .049 | 217 | .018 | 3.61 | | .0E+00 |
| -10. | -5. | | 4.33 | 196.3 | 174.0 | 10.79 | 12.80 | 291 | .948 | .072 | 78 | .069 | 209 | .019 | 3.55 | | .0E+00 |
| 0. | 5. | | 4.33 | 196.1 | 175.5 | 10.91 | 12.72 | 299 | .962 | .083 | 80 | .082 | 216 | .018 | 3.60 | | .0E+00 |
| 5. | 10. | | 4.31 | 196.1 | 177.5 | 11.06 | 12.35 | 313 | .976 | .100 | 82 | .098 | 228 | .022 | 3.68 | | .0E+00 |
| 10. | 15. | | 4.29 | 195.9 | 178.9 | 11.28 | 12.02 | 328 | .968 | .101 | 84 | .095 | 237 | .035 | 3.60 | | .0E+00 |
| 15. | 20. | | 4.28 | 194.9 | 182.3 | 11.63 | 11.53 | 370 | .958 | .113 | 93 | .109 | 272 | .029 | 3.77 | | 1.4E-14 |
| 20. | 25. | | 4.27 | 194.9 | 184.9 | 12.31 | 11.59 | 427 | .955 | .116 | 97 | .112 | 325 | .032 | 4.19 | | .0E+00 |
| 25. | 30. | | 4.27 | 194.7 | 189.1 | 15.10 | 11.24 | 801 | .922 | .111 | 97 | .101 | 697 | .047 | 7.70 | | .0E+00 |
| 30. | 35. | | | | | | | 0 | | | | | | | | | |
| 35. | 40. | | | | | | | | | | | | | | | | |
| 40. | 45. | | | | | | | | | | | | | | | | |
| 45. | 50. | | | | | | | | | | | | | | | | |
| 50. | 55. | | | | | | | | | | | | | | | | |
| 55. | 60. | | | | | | | | | | | | | | | | |
| 60. | 65. | | | | | | | | | | | | | | | | |
| 65. | 70. | | | | | | | | | | | | | | | | |
| 70. | 75. | | | | | | | | | | | | | | | | |
| 75. | 80. | | | | | | | | | | | | | | | | |
| 80. | 85. | | | | | | | | | | | | | | | | |
| 85. | 90. | | | | | | | | | | | | | | | | |

Table 1.6 cont.

SATELLITE(S): SETA-1
ALTITUDE RANGE SAMPLED: 0 TO 200 KM. DATE RANGE: 79/79 TO 79/100.
SOLAR DAY LOCAL TIME FROM 0800 TO 1800 HOURS.
LINEAR MODEL RATIOS.

| KP | MIN | MAX | GG MIN | LAT MAX | MEAN KP | MEAN FLUX | MEAN Z | MEAN L.T. | MEAN U.T. | # OF POINTS | MEAN | S.D. | O.F. | JACCHIA 71 | | S.D. W | NE | 1-P |
|----|-----|-----|-----------|------------|------------|--------------|-----------|--------------|--------------|----------------|------|------|------|------------|--------|--------|------|---------|
| | | | | | | | | | | | | | | S.D. B | D.F. B | | | |
| 6- | 9 | | -90. | -85. | 6.33 | 193.0 | 198.9 | 10.03 | 19.23 | 0 | | | | | | | | |
| | | | -85. | -80. | 6.23 | 191.6 | 196.9 | 10.06 | 15.20 | 0 | | | | | | | | |
| | | | -80. | -75. | 6.40 | 194.4 | 194.7 | 10.10 | 12.60 | 0 | | | | | | | | |
| | | | -75. | -70. | 6.42 | 194.5 | 190.1 | 10.14 | 12.48 | 0 | | | | | | | | |
| | | | -70. | -65. | 6.42 | 194.7 | 185.9 | 10.18 | 12.44 | 0 | | | | | | | | |
| | | | -65. | -60. | 6.41 | 194.7 | 182.2 | 10.22 | 12.54 | 0 | | | | | | | | |
| | | | -60. | -55. | 6.41 | 194.7 | 178.9 | 10.25 | 12.52 | 0 | | | | | | | | |
| | | | -55. | -50. | 6.41 | 193.9 | 176.1 | 10.29 | 13.10 | 0 | | | | | | | | |
| | | | -50. | -45. | 6.43 | 194.1 | 174.0 | 10.33 | 12.94 | 0 | | | | | | | | |
| | | | -45. | -40. | 6.45 | 193.8 | 172.3 | 10.37 | 13.29 | 0 | | | | | | | | |
| | | | -40. | -35. | 6.43 | 193.8 | 171.2 | 10.41 | 13.40 | 0 | | | | | | | | |
| | | | -35. | -30. | 6.44 | 194.4 | 170.5 | 10.46 | 13.03 | 0 | | | | | | | | |
| | | | -30. | -25. | 6.44 | 194.3 | 170.4 | 10.51 | 12.98 | 0 | | | | | | | | |
| | | | -25. | -20. | 6.42 | 194.7 | 170.6 | 10.56 | 12.95 | 0 | | | | | | | | |
| | | | -20. | -15. | 6.41 | 194.2 | 171.5 | 10.62 | 13.41 | 0 | | | | | | | | |
| | | | -15. | -10. | 6.39 | 194.1 | 172.3 | 10.70 | 13.19 | 0 | | | | | | | | |
| | | | -10. | -5. | 6.41 | 194.0 | 173.8 | 10.79 | 13.24 | 0 | | | | | | | | |
| | | | 0. | 5. | 6.41 | 193.7 | 175.6 | 10.91 | 13.52 | 0 | | | | | | | | |
| | | | 5. | 10. | 6.42 | 193.7 | 177.3 | 11.06 | 13.09 | 0 | | | | | | | | |
| | | | 10. | 15. | 6.44 | 194.3 | 179.4 | 11.28 | 12.77 | 0 | | | | | | | | |
| | | | 15. | 20. | 6.45 | 194.1 | 181.9 | 11.63 | 13.05 | 0 | | | | | | | | |
| | | | 20. | 25. | 6.45 | 194.7 | 183.9 | 12.31 | 12.65 | 0 | | | | | | | | |
| | | | 25. | 30. | 6.42 | 194.7 | 187.9 | 15.13 | 12.57 | 0 | | | | | | | | |
| | | | 30. | 35. | | | | | | 9 | .826 | .068 | 5 | .071 | 3 | .003 | 1.47 | 8.4E-05 |
| | | | 35. | 40. | | | | | | 59 | .851 | .051 | 17 | .049 | 40 | .017 | 3.09 | .0E+00 |
| | | | 40. | 45. | | | | | | 108 | .851 | .049 | 28 | .047 | 77 | .017 | 3.48 | .0E+00 |
| | | | 45. | 50. | | | | | | 116 | .838 | .053 | 29 | .051 | 84 | .016 | 3.62 | .0E+00 |
| | | | 50. | 55. | | | | | | 117 | .839 | .051 | 30 | .050 | 84 | .015 | 3.54 | .0E+00 |
| | | | 55. | 60. | | | | | | 118 | .834 | .053 | 31 | .052 | 85 | .010 | 3.57 | .0E+00 |
| | | | 60. | 65. | | | | | | 124 | .832 | .050 | 31 | .048 | 90 | .014 | 3.65 | 6.4E-14 |
| | | | 65. | 70. | | | | | | 113 | .850 | .053 | 31 | .052 | 80 | .014 | 3.42 | .0E+00 |
| | | | 70. | 75. | | | | | | 117 | .868 | .051 | 31 | .049 | 83 | .015 | 3.44 | .0E+00 |

Table 1.6 cont.

SATELLITE(S): SEYA-1
ALTITUDE RANGE SAMPLED: 0 TO 200 KM. DATE RANGE: 79/79 TO 79/100.
SOLAR NIGHT LOCAL TIME FROM 1800 TO 2400 HOURS.
LINEAR MODEL RATIOS.

| KP | | GG LAT | | MEAN KP | MEAN FLUX | MEAN Z | MEAN L.T. | MEAN U.T. | # OF POINTS | MEAN | S.O. | D.F. B | JACCHIA 71 | S.D. W | NE | 1-P |
|-----|-----|--------|------|---------|-----------|--------|-----------|-----------|-------------|------|------|--------|------------|--------|------|---------|
| MIN | MAX | MIN | MAX | | | | | | | | | | | | | |
| 0 | 1+ | -90. | -85. | | | | | | 0 | | | | | | | |
| | | -85. | -80. | | | | | | 0 | | | | | | | |
| | | -80. | -75. | | | | | | 0 | | | | | | | |
| | | -75. | -70. | | | | | | 0 | | | | | | | |
| | | -70. | -65. | | | | | | 0 | | | | | | | |
| | | -65. | -60. | | | | | | 0 | | | | | | | |
| | | -60. | -55. | | | | | | 0 | | | | | | | |
| | | -55. | -50. | | | | | | 0 | | | | | | | |
| | | -50. | -45. | | | | | | 0 | | | | | | | |
| | | -45. | -40. | | | | | | 0 | | | | | | | |
| | | -40. | -35. | | | | | | 0 | | | | | | | |
| | | -35. | -30. | | | | | | 0 | | | | | | | |
| | | -30. | -25. | | | | | | 0 | | | | | | | |
| | | -25. | -20. | | | | | | 0 | | | | | | | |
| | | -20. | -15. | | | | | | 0 | | | | | | | |
| | | -15. | -10. | | | | | | 0 | | | | | | | |
| | | -10. | -5. | | | | | | 0 | | | | | | | |
| | | -5. | 0. | | | | | | 0 | | | | | | | |
| | | 0. | 5. | | | | | | 0 | | | | | | | |
| | | 5. | 10. | | | | | | 0 | | | | | | | |
| | | 10. | 15. | | | | | | 0 | | | | | | | |
| | | 15. | 20. | | | | | | 0 | | | | | | | |
| | | 20. | 25. | | | | | | 0 | | | | | | | |
| | | 25. | 30. | | | | | | 0 | | | | | | | |
| | | 30. | 35. | | | | | | 0 | | | | | | | |
| | | 35. | 40. | | | | | | 0 | | | | | | | |
| | | 40. | 45. | | | | | | 0 | | | | | | | |
| | | 45. | 50. | | | | | | 0 | | | | | | | |
| | | 50. | 55. | | | | | | 0 | | | | | | | |
| | | 55. | 60. | | | | | | 0 | | | | | | | |
| | | 60. | 65. | 1.30 | 193.6 | 199.2 | 21.38 | 13.51 | 10 | .937 | .018 | 1 | .011 | .015 | 1.90 | 2.3E-01 |
| | | 65. | 70. | 1.24 | 184.4 | 198.2 | 21.17 | 11.78 | 41 | .945 | .041 | 12 | .039 | .016 | 2.69 | 2.4E-09 |
| | | 70. | 75. | 1.03 | 181.4 | 197.0 | 20.83 | 12.66 | 78 | .956 | .049 | 17 | .041 | .029 | 3.38 | 3.0E-10 |
| | | 75. | 80. | 1.06 | 183.5 | 195.1 | 20.18 | 12.63 | 118 | .972 | .063 | 26 | .059 | .023 | 4.07 | .0E+00 |
| | | 80. | 85. | 1.06 | 184.3 | 192.9 | 18.90 | 12.78 | 100 | .977 | .060 | 29 | .058 | .018 | 3.12 | .0E+00 |
| | | 85. | 90. | | | | | | 0 | | | | | | | |

Table 1.6 cont.

AIR FORCE REFERENCE ATMOSPHERE
ONE WAY RANDOM EFFECTS ANALYSIS OF VARIANCE
NEUTRAL MASS DENSITY RATIO TO MODEL STATISTICS

86/02/24

SATELLITE(S): SETA-1
ALTITUDE RANGE SAMPLED: 0 TO 200 KM. DATE RANGE: 79/79 TO 79/100.
SOLAR NIGHT LOCAL TIME FROM 1800 TO 2400 HOURS.
LINEAR MODEL RATIOS.

| KP | MIN | MAX | GG LAT MIN MAX | MEAN KP | MEAN FLUX | MEAN Z | MEAN L.T. U.T. | MEAN U.T. | # OF POINTS | S.D. | JACCHIA 71 | | D.F. W | S.D. W | NE | 1-P |
|----|-----|-----|-------------------|------------|--------------|-----------|-------------------|--------------|----------------|-------|------------|--------|--------|--------|------|---------|
| | | | | | | | | | | | O.F. B | S.O. B | | | | |
| 2- | 3+ | | -90. | -85. | | | | | 0 | | | | | | | |
| | | | -85. | -80. | | | | | 0 | | | | | | | |
| | | | -80. | -75. | | | | | 0 | | | | | | | |
| | | | -75. | -70. | | | | | 0 | | | | | | | |
| | | | -70. | -65. | | | | | 0 | | | | | | | |
| | | | -65. | -60. | | | | | 0 | | | | | | | |
| | | | -60. | -55. | | | | | 0 | | | | | | | |
| | | | -55. | -50. | | | | | 0 | | | | | | | |
| | | | -50. | -45. | | | | | 0 | | | | | | | |
| | | | -45. | -40. | | | | | 0 | | | | | | | |
| | | | -40. | -35. | | | | | 0 | | | | | | | |
| | | | -35. | -30. | | | | | 0 | | | | | | | |
| | | | -30. | -25. | | | | | 0 | | | | | | | |
| | | | -25. | -20. | | | | | 0 | | | | | | | |
| | | | -20. | -15. | | | | | 0 | | | | | | | |
| | | | -15. | -10. | | | | | 0 | | | | | | | |
| | | | -10. | -5. | | | | | 0 | | | | | | | |
| | | | -5. | 0. | | | | | 0 | | | | | | | |
| | | | 0. | 5. | | | | | 0 | | | | | | | |
| | | | 5. | 10. | | | | | 0 | | | | | | | |
| | | | 10. | 15. | | | | | 0 | | | | | | | |
| | | | 15. | 20. | | | | | 0 | | | | | | | |
| | | | 20. | 25. | | | | | 0 | | | | | | | |
| | | | 25. | 30. | | | | | 0 | | | | | | | |
| | | | 30. | 35. | | | | | 0 | | | | | | | |
| | | | 35. | 40. | | | | | 0 | | | | | | | |
| | | | 40. | 45. | | | | | 0 | | | | | | | |
| | | | 45. | 50. | | | | | 0 | | | | | | | |
| | | | 50. | 55. | | | | | 5 | 1.002 | .013 | .012 | 1 | .008 | 2.40 | 8.0E-02 |
| | | | 55. | 60. | | | | | 14 | 1.001 | .082 | .089 | 5 | .009 | 2.20 | 2.2E-08 |
| | | | 60. | 65. | | | | | 63 | .972 | .070 | .065 | 21 | .028 | 2.50 | 1.5E-12 |
| | | | 65. | 70. | | | | | 149 | .943 | .075 | .072 | 42 | .023 | 3.23 | .0E+00 |
| | | | 70. | 75. | | | | | 245 | .932 | .095 | .089 | 70 | .033 | 3.18 | .0E+00 |
| | | | 75. | 80. | | | | | 394 | .919 | .089 | .085 | 111 | .028 | 3.28 | .0E+00 |
| | | | 80. | 85. | | | | | 612 | .920 | .098 | .092 | 151 | .033 | 3.78 | .0E+00 |
| | | | 85. | 90. | | | | | 548 | .917 | .101 | .097 | 160 | .031 | 3.20 | .0E+00 |
| | | | | | | | | | 0 | | | | | | | |

Table 1.6 cont.

SATELLITE(S): SETA-1
ALTITUDE RANGE SAMPLED: 0 TO 200 KM. DATE RANGE: 79/79 TO 79/100.
SOLAR NIGHT LOCAL TIME FROM 1800 TO 2400 HOURS.
LINEAR MODEL RATIOS.

| KP | MIN | MAX | GG LAT | MIN | MAX | MEAN KP | MEAN FLUX | MEAN Z | MEAN L.T. | MEAN U.T. | # OF POINTS | MEAN | S.D. | JACCHIA 71 | | D.F. W | S.D. W | NE | I-P |
|----|-----|-----|--------|------|------|---------|-----------|--------|-----------|-----------|-------------|-------|------|------------|------|--------|--------|------|---------|
| | | | | | | | | | | | | | | | | | | | |
| 4- | 5+ | | | | | | | | | | | | | | | | | | |
| | | | -90. | -85. | -85. | 3.67 | 210.0 | 199.4 | 21.83 | 18.72 | 6 | 1.101 | .067 | 2 | .075 | 3 | .021 | 1.83 | 1.4E-02 |
| | | | -85. | -80. | -80. | 4.06 | 201.3 | 198.7 | 21.76 | 15.05 | 22 | 1.038 | .059 | 8 | .059 | 12 | .015 | 2.16 | 3.1E-07 |
| | | | -80. | -75. | -75. | 4.21 | 199.7 | 197.3 | 21.68 | 13.14 | 42 | .980 | .064 | 11 | .065 | 30 | .012 | 3.49 | .0E+00 |
| | | | -75. | -70. | -70. | 4.24 | 200.0 | 196.1 | 21.56 | 14.74 | 67 | .950 | .060 | 18 | .058 | 47 | .020 | 3.33 | .0E+00 |
| | | | -70. | -65. | -65. | 4.47 | 201.4 | 195.7 | 21.40 | 13.95 | 98 | .941 | .079 | 29 | .077 | 66 | .021 | 3.05 | 7.1E-15 |
| | | | -65. | -60. | -60. | 4.45 | 201.5 | 195.1 | 21.19 | 12.85 | 156 | .906 | .083 | 44 | .079 | 108 | .026 | 3.24 | 1.4E-14 |
| | | | -60. | -55. | -55. | 4.40 | 198.6 | 193.9 | 20.84 | 12.89 | 214 | .918 | .087 | 56 | .081 | 152 | .032 | 3.45 | 2.8E-14 |
| | | | -55. | -50. | -50. | 4.41 | 197.9 | 192.8 | 20.19 | 12.10 | 299 | .895 | .113 | 71 | .107 | 222 | .038 | 3.88 | .0E+00 |
| | | | -50. | -45. | -45. | 4.35 | 195.6 | 191.7 | 18.90 | 11.87 | 301 | .892 | .108 | 90 | .104 | 205 | .031 | 3.13 | .0E+00 |
| | | | -45. | -40. | -40. | | | | | | 0 | | | | | | | | |
| | | | -40. | -35. | -35. | | | | | | 0 | | | | | | | | |
| | | | -35. | -30. | -30. | | | | | | 0 | | | | | | | | |
| | | | -30. | -25. | -25. | | | | | | 0 | | | | | | | | |
| | | | -25. | -20. | -20. | | | | | | 0 | | | | | | | | |
| | | | -20. | -15. | -15. | | | | | | 0 | | | | | | | | |
| | | | -15. | -10. | -10. | | | | | | 0 | | | | | | | | |
| | | | -10. | -5. | -5. | | | | | | 0 | | | | | | | | |
| | | | -5. | 0. | 0. | | | | | | 0 | | | | | | | | |
| | | | 0. | 5. | 5. | | | | | | 0 | | | | | | | | |
| | | | 5. | 10. | 10. | | | | | | 0 | | | | | | | | |
| | | | 10. | 15. | 15. | | | | | | 0 | | | | | | | | |
| | | | 15. | 20. | 20. | | | | | | 0 | | | | | | | | |
| | | | 20. | 25. | 25. | | | | | | 0 | | | | | | | | |
| | | | 25. | 30. | 30. | | | | | | 0 | | | | | | | | |
| | | | 30. | 35. | 35. | | | | | | 0 | | | | | | | | |
| | | | 35. | 40. | 40. | | | | | | 0 | | | | | | | | |
| | | | 40. | 45. | 45. | | | | | | 0 | | | | | | | | |
| | | | 45. | 50. | 50. | | | | | | 0 | | | | | | | | |
| | | | 50. | 55. | 55. | | | | | | 0 | | | | | | | | |
| | | | 55. | 60. | 60. | | | | | | 0 | | | | | | | | |
| | | | 60. | 65. | 65. | | | | | | 0 | | | | | | | | |
| | | | 65. | 70. | 70. | | | | | | 0 | | | | | | | | |
| | | | 70. | 75. | 75. | | | | | | 0 | | | | | | | | |
| | | | 75. | 80. | 80. | | | | | | 0 | | | | | | | | |
| | | | 80. | 85. | 85. | | | | | | 0 | | | | | | | | |
| | | | 85. | 90. | 90. | | | | | | 0 | | | | | | | | |

Table 1.6 cont.

AIR FORCE REFERENCE ATMOSPHERE
ONE WAY RANDOM EFFECTS ANALYSIS OF VARIANCE
NEUTRAL MASS DENSITY RATIO TO MODEL STATISTICS

SATELLITE(S): SETA-1
ALTITUDE RANGE SAMPLED: 0 TO 200 KM. DATE RANGE: 79/79 TO 79/100.
SOLAR NIGHT LOCAL TIME FROM 1800 TO 2400 HOURS.
LINEAR MODEL RATIOS.

| KP | MIN | MAX | GG | LAT | MIN | MAX | MEAN | FLUX | MEAN | Z | MEAN | L.T. | MEAN | U.T. | # OF | POINTS | MEAN | S.D. | D.F. | B | S.D. | B | D.F. | W | S.D. | W | NE | I-P |
|----|-----|-----|------|------|-----|-----|------|------|-------|-------|-------|-------|------|------|------|--------|------|------|------|----|------|----|------|------|---------|---|----|-----|
| 6- | 9 | | -90. | -85. | | | | | | | | | | | 0 | | | | | | | | | | | | | |
| | | | -85. | -80. | | | | | | | | | | | 0 | | | | | | | | | | | | | |
| | | | -80. | -75. | | | | | | | | | | | 0 | | | | | | | | | | | | | |
| | | | -75. | -70. | | | | | | | | | | | 0 | | | | | | | | | | | | | |
| | | | -70. | -65. | | | | | | | | | | | 0 | | | | | | | | | | | | | |
| | | | -65. | -60. | | | | | | | | | | | 0 | | | | | | | | | | | | | |
| | | | -60. | -55. | | | | | | | | | | | 0 | | | | | | | | | | | | | |
| | | | -55. | -50. | | | | | | | | | | | 0 | | | | | | | | | | | | | |
| | | | -50. | -45. | | | | | | | | | | | 0 | | | | | | | | | | | | | |
| | | | -45. | -40. | | | | | | | | | | | 0 | | | | | | | | | | | | | |
| | | | -40. | -35. | | | | | | | | | | | 0 | | | | | | | | | | | | | |
| | | | -35. | -30. | | | | | | | | | | | 0 | | | | | | | | | | | | | |
| | | | -30. | -25. | | | | | | | | | | | 0 | | | | | | | | | | | | | |
| | | | -25. | -20. | | | | | | | | | | | 0 | | | | | | | | | | | | | |
| | | | -20. | -15. | | | | | | | | | | | 0 | | | | | | | | | | | | | |
| | | | -15. | -10. | | | | | | | | | | | 0 | | | | | | | | | | | | | |
| | | | -10. | -5. | | | | | | | | | | | 0 | | | | | | | | | | | | | |
| | | | -5. | 0. | | | | | | | | | | | 0 | | | | | | | | | | | | | |
| | | | 0. | 5. | | | | | | | | | | | 0 | | | | | | | | | | | | | |
| | | | 5. | 10. | | | | | | | | | | | 0 | | | | | | | | | | | | | |
| | | | 10. | 15. | | | | | | | | | | | 0 | | | | | | | | | | | | | |
| | | | 15. | 20. | | | | | | | | | | | 0 | | | | | | | | | | | | | |
| | | | 20. | 25. | | | | | | | | | | | 0 | | | | | | | | | | | | | |
| | | | 25. | 30. | | | | | | | | | | | 0 | | | | | | | | | | | | | |
| | | | 30. | 35. | | | | | | | | | | | 0 | | | | | | | | | | | | | |
| | | | 35. | 40. | | | | | | | | | | | 0 | | | | | | | | | | | | | |
| | | | 40. | 45. | | | | 6.53 | 186.0 | 199.4 | 21.83 | 20.43 | | | 5 | | .911 | .041 | .044 | 2 | .044 | 2 | .011 | 1.60 | 3.4E-02 | | | |
| | | | 45. | 50. | | | | 6.33 | 186.0 | 198.2 | 21.77 | 18.86 | | | 16 | | .904 | .050 | .053 | 4 | .053 | 11 | .012 | 3.19 | 1.9E-07 | | | |
| | | | 50. | 55. | | | | 6.33 | 195.0 | 197.1 | 21.68 | 13.97 | | | 32 | | .856 | .074 | .076 | 8 | .076 | 23 | .016 | 3.54 | 7.1E-15 | | | |
| | | | 55. | 60. | | | | 6.33 | 196.6 | 194.9 | 21.56 | 12.97 | | | 34 | | .859 | .103 | .105 | 8 | .105 | 25 | .024 | 3.77 | .0E+00 | | | |
| | | | 60. | 65. | | | | 6.36 | 196.9 | 194.0 | 21.40 | 12.30 | | | 38 | | .840 | .094 | .095 | 12 | .095 | 25 | .017 | 2.91 | .0E+00 | | | |
| | | | 65. | 70. | | | | 6.62 | 197.8 | 193.9 | 21.19 | 9.78 | | | 67 | | .819 | .098 | .098 | 17 | .098 | 48 | .023 | 3.51 | .0E+00 | | | |
| | | | 70. | 75. | | | | 6.56 | 196.8 | 192.6 | 20.84 | 10.29 | | | 84 | | .821 | .097 | .095 | 21 | .095 | 61 | .025 | 3.64 | .0E+00 | | | |
| | | | 75. | 80. | | | | 6.50 | 196.0 | 191.1 | 20.18 | 10.37 | | | 100 | | .841 | .082 | .078 | 22 | .078 | 75 | .029 | 4.00 | .0E+00 | | | |
| | | | 80. | 85. | | | | 6.42 | 194.9 | 190.0 | 18.93 | 11.75 | | | 92 | | .879 | .095 | .089 | 26 | .089 | 62 | .034 | 3.06 | .0E+00 | | | |
| | | | 85. | 90. | | | | | | | | | | | 0 | | | | | | | | | | | | | |

Table 1.6 cont.

It is readily apparent that nearly every case showed statistical significance leading one to reject the hypothesis that $\sigma_{\alpha}^2 = 0$. The tabulated values of S.D.B and S.D.W are the square roots of the variance components σ_{α}^2 and σ^2 (i.e. standard deviations) respectively. It can be seen that the standard deviation within orbits is less than the standard deviation between orbits which would lead one to conclude that the data are correlated within orbits.

1.6.3 Calculation of the Autocorrelation Coefficients

Next, 20 random samples of 100 consecutive data points were taken from the SETA-1, Jacchia 71, 21 day data set. The Durbin-Watson statistic was calculated and the autocorrelations and their standard errors were calculated for lags up to lag 25 for each sample.

The Durbin-Watson statistic is defined as:

$$d = \frac{\sum_{i=2}^N (y_i - y_{i-1})^2}{\sum_{i=1}^N (y_i - \bar{y})^2}$$

where y_i is the model ratio.

In this case we are testing for $\rho > 0$ and small values of d are significant (See Reference 14).

The sample auto correlation coefficient at lag 1 is defined as

$$r_1 = \frac{\sum_{i=1}^{N-1} (y_i - \bar{y})(y_{i+1} - \bar{y})}{\sum_{i=1}^N (y_i - \bar{y})^2}$$

where y_i is the model ratio.

The large lag standard error of the auto correlation coefficient is defined as:

$$V[r_1] = \frac{1}{N} (1 + 2\sum_{i=1}^q r_i^2) \quad l > q$$

where r_i is the sample auto correlation coefficient at lag i .
(see Reference 13)

The results of this calculation are given in Table 1.7. The Durbin-Watson statistic was significant at the 5% and 1% levels for all 20 samples indicating evidence of positive serial correlation. Inspecting Table 1.7, one notices that the auto correlations die out so that they are typically on the order of one or two times their standard errors by fourth or fifth lag. This would indicate that to achieve independence in sampling one should sample at most only every fourth or fifth data point.

1.6.4 Effect of Autocorrelation on Analysis of Satellite Data

Assume that on average N samples are taken during each orbit, and that n_o orbits of data are collected. Assume the n samples per orbit are "perfectly" correlated. Since the n samples per orbit are essentially repeats we obtain a standard deviation of

$$s = \sqrt{\frac{n \sum_{j=1}^{n_o} (\bar{Y}_{.j} - \bar{Y})^2}{N - 1}}$$

where $N = n.n_o$

SAMPLE NUMBER 1

MEAN RATIOS

.999 .967 .955 .937 .906 .892 .901 .945 .955 .968 .968 .963 .977 .998 .963 .975 1.006 .970 .924
 .875 .807 .768 .756 .785 .852 .929 1.152 1.146 1.125 1.094 1.068 1.062 1.062 1.049 1.036 .982 .898 .884
 .907 .946 .998 1.007 1.032 1.008 .982 .968 .984 .986 .971 .978 .991 1.031 1.043 1.003 .987 1.022 1.021 1.002
 .992 1.011 1.033 1.037 1.035 .997 1.002 1.019 1.043 1.095 1.101 1.095 1.089 1.075 1.045 .982 .957 .939 .926 .933
 .972 .958 .947 .943 .949 .973 .987 .951 .933 .990 1.063 1.103 1.111 1.099 1.088 1.081 1.075 1.071 1.056 1.025

MEAN = .990
 S.D. = .076
 D = .231
 4-D = 3.769

AUTOCORRELATION COEFFICIENTS

| LAG | R(L) | S.E. | LAG | R(L) | S.E. | LAG | R(L) | S.E. | LAG | R(L) | S.E. |
|-----|--------|---------|-----|--------|---------|-----|--------|---------|-----|--------|---------|
| 1 | .8743 | (.1000) | 2 | .6521 | (.1580) | 3 | .4028 | (.1838) | 4 | -.1782 | (.1925) |
| 6 | -.1260 | (.1941) | 7 | -.1986 | (.1949) | 8 | -.2318 | (.1969) | 9 | -.2314 | (.1997) |
| 11 | -.1898 | (.2045) | 12 | -.1512 | (.2062) | 13 | -.0803 | (.2073) | 14 | .0120 | (.2076) |
| 16 | .1675 | (.2082) | 17 | .1988 | (.2095) | 18 | .1841 | (.2114) | 19 | .1463 | (.2130) |
| 21 | .0550 | (.2145) | 22 | .0179 | (.2146) | 23 | -.0016 | (.2146) | 24 | .0070 | (.2146) |
| | | | | | | | | | 25 | .0307 | (.2146) |

SAMPLE NUMBER 2

MEAN RATIOS

.819 .819 .816 .822 .817 .764 .637 .540 .523 .552 .613 .711 1.099 1.090 1.041 1.042 1.039 1.040 1.072 1.130
 1.114 1.119 1.137 1.136 1.092 1.087 1.078 1.056 1.029 1.031 1.082 1.061 1.029 1.011 .986 .989 .997 1.002 .993 .985
 .982 .983 .979 .972 .973 .979 .979 .947 .942 .994 1.009 1.007 1.003 1.018 .992 1.004 1.046 1.055 1.052 1.034
 1.029 1.028 1.013 1.005 1.009 1.005 .986 .964 .951 .955 .959 .961 .952 .943 .941 .936 .927 .919 .902 .880
 .883 .889 .867 .854 .858 .832 .800 .809 .823 .814 .820 .836 .849 .879 .910 .922 .979 1.020 .989

MEAN = .948
 S.D. = .125
 D = .148
 4-D = 3.852

AUTOCORRELATION COEFFICIENTS

| LAG | R(L) | S.E. | LAG | R(L) | S.E. | LAG | R(L) | S.E. | LAG | R(L) | S.E. |
|-----|--------|---------|-----|--------|---------|-----|--------|---------|-----|--------|---------|
| 1 | .9110 | (.1000) | 2 | .7854 | (.1631) | 3 | .6578 | (.1873) | 4 | .5325 | (.2182) |
| 6 | .3446 | (.2384) | 7 | .2837 | (.2433) | 8 | .2051 | (.2466) | 9 | .1210 | (.2483) |
| 11 | -.0466 | (.2489) | 12 | -.1204 | (.2490) | 13 | -.1451 | (.2496) | 14 | -.1610 | (.2504) |
| 16 | -.1829 | (.2527) | 17 | -.1777 | (.2540) | 18 | -.1701 | (.2553) | 19 | -.1740 | (.2564) |
| 21 | -.1764 | (.2588) | 22 | -.1729 | (.2600) | 23 | -.1615 | (.2611) | 24 | -.1442 | (.2621) |
| | | | | | | | | | 25 | -.1270 | (.2629) |

Table 1.7: Autocorrelation Coefficients

SAMPLE NUMBER 3

MEAN RATIOS

| | | | | | | | | | | | | | | | | | | | |
|-------|-------|------|------|------|------|------|------|------|------|------|------|------|------|------|------|------|------|-------|-------|
| .807 | .821 | .797 | .789 | .804 | .818 | .818 | .796 | .789 | .820 | .842 | .841 | .859 | .889 | .698 | .886 | .874 | .873 | .880 | .893 |
| .903 | .902 | .894 | .893 | .905 | .914 | .904 | .887 | .875 | .864 | .851 | .840 | .831 | .817 | .809 | .812 | .817 | .816 | .824 | .840 |
| .855 | .877 | .902 | .907 | .899 | .902 | .921 | .943 | .959 | .966 | .938 | .939 | .945 | .959 | .972 | .974 | .976 | .995 | 1.007 | 1.007 |
| 1.007 | 1.007 | .997 | .981 | .965 | .953 | .948 | .944 | .930 | .900 | .872 | .865 | .875 | .885 | .886 | .880 | .876 | .881 | .915 | .913 |
| .902 | .897 | .906 | .876 | .865 | .859 | .861 | .863 | .873 | .883 | .889 | .895 | .892 | .882 | .878 | .886 | .909 | .889 | .897 | .931 |

MEAN = .890
S.D. = .054
D = .068
4-D = 3.932

AUTOCORRELATION COEFFICIENTS

| LAG | R(L) | S.E. | LAG | R(L) | S.E. | LAG | R(L) | S.E. | LAG | R(L) | S.E. |
|-----|--------|---------|-----|--------|---------|-----|--------|---------|-----|--------|---------|
| 1 | .9413 | (.1000) | 2 | .8743 | (.1665) | 3 | .8046 | (.2074) | 4 | .7294 | (.2366) |
| 6 | .5664 | (.2740) | 7 | .4773 | (.2854) | 8 | .3827 | (.2933) | 9 | .2903 | (.2983) |
| 11 | .1474 | (.3026) | 12 | .0864 | (.3033) | 13 | .0362 | (.3035) | 14 | -.0010 | (.3036) |
| 16 | -.0688 | (.3036) | 17 | -.0989 | (.3038) | 18 | -.1293 | (.3041) | 19 | -.1534 | (.3047) |
| 21 | -.1837 | (.3064) | 22 | -.1950 | (.3075) | 23 | -.1943 | (.3087) | 24 | -.1839 | (.3099) |
| | | | | | | | | | 25 | -.1646 | (.3110) |

SAMPLE NUMBER 4

MEAN RATIOS

| | | | | | | | | | | | | | | | | | | | |
|------|------|-------|-------|-------|-------|-------|------|------|-------|-------|------|------|------|------|------|------|------|------|------|
| .855 | .845 | .861 | .870 | .841 | .726 | .572 | .467 | .444 | 1.018 | .978 | .962 | .949 | .939 | .931 | .916 | .900 | .895 | .905 | .922 |
| .935 | .927 | .908 | .902 | .910 | .912 | .913 | .947 | .952 | .958 | .966 | .965 | .959 | .929 | .952 | .939 | .945 | .965 | .977 | .978 |
| .984 | .994 | 1.001 | 1.003 | 1.006 | 1.018 | 1.024 | .975 | .963 | .972 | 1.001 | .989 | .982 | .975 | .971 | .966 | .946 | .926 | .913 | .913 |
| .919 | .922 | .919 | .915 | .909 | .904 | .906 | .908 | .907 | .914 | .917 | .920 | .924 | .906 | .868 | .877 | .945 | .979 | .970 | .983 |
| .984 | .952 | .962 | .992 | .971 | .941 | .945 | .947 | .929 | .908 | .894 | .894 | .905 | .911 | .912 | .918 | .916 | .900 | .895 | .905 |

MEAN = .921
S.D. = .088
D = .527
4-D = 3.473

AUTOCORRELATION COEFFICIENTS

| LAG | R(L) | S.E. | LAG | R(L) | S.E. | LAG | R(L) | S.E. | LAG | R(L) | S.E. |
|-----|--------|---------|-----|--------|---------|-----|--------|---------|-----|--------|---------|
| 1 | .7261 | (.1000) | 2 | .4495 | (.1433) | 3 | .2458 | (.1568) | 4 | .1587 | (.1606) |
| 6 | .1540 | (.1636) | 7 | .1391 | (.1650) | 8 | .1034 | (.1662) | 9 | .0743 | (.1668) |
| 11 | .0665 | (.1676) | 12 | .0364 | (.1678) | 13 | .0166 | (.1679) | 14 | .0222 | (.1679) |
| 16 | .0471 | (.1680) | 17 | .0427 | (.1682) | 18 | .0336 | (.1683) | 19 | .0016 | (.1683) |
| 21 | -.0439 | (.1684) | 22 | -.0590 | (.1685) | 23 | -.0676 | (.1687) | 24 | -.0716 | (.1690) |
| | | | | | | | | | 25 | -.0491 | (.1693) |

Table 1.7 cont.

SAMPLE NUMBER 5

MEAN RATIOS

| | | | | | | | | | | | | | | | | | | | |
|------|------|------|------|------|------|------|------|------|------|------|------|------|------|------|------|------|------|------|------|
| .913 | .920 | .918 | .923 | .929 | .923 | .921 | .937 | .963 | .982 | .985 | .938 | .921 | .914 | .921 | .966 | .973 | .967 | .958 | .956 |
| .963 | .978 | .990 | .980 | .955 | .932 | .920 | .898 | .921 | .940 | .972 | .964 | .965 | .971 | .965 | .955 | .925 | .914 | .897 | .886 |
| .884 | .886 | .919 | .916 | .885 | .874 | .853 | .833 | .841 | .866 | .872 | .867 | .766 | .697 | .592 | .556 | .598 | .706 | .782 | .845 |
| .866 | .861 | .841 | .831 | .832 | .938 | .959 | .952 | .953 | .919 | .883 | .839 | .830 | .850 | .880 | .909 | .943 | .957 | .964 | .911 |
| .899 | .936 | .944 | .946 | .959 | .961 | .923 | .922 | .926 | .924 | .962 | .866 | .965 | .974 | .987 | .982 | .971 | .946 | .972 | .968 |

MEAN = .907
 S.D. = .081
 D = .150
 4-D = 3.850

AUTOCORRELATION COEFFICIENTS

| LAG | R(L) | S.E. | LAG | R(L) | S.E. | LAG | R(L) | S.E. | LAG | R(L) | S.E. | LAG | R(L) | S.E. |
|-----|--------|---------|-----|--------|---------|-----|--------|---------|-----|--------|---------|-----|--------|---------|
| 1 | .9131 | (.1000) | 2 | .7580 | (.1633) | 3 | .5857 | (.1954) | 4 | .4472 | (.2122) | 5 | .3758 | (.2214) |
| 6 | .3655 | (.2277) | 7 | .3781 | (.2335) | 8 | .3713 | (.2396) | 9 | .3140 | (.2452) | 10 | .2225 | (.2492) |
| 11 | .1376 | (.2512) | 12 | .0855 | (.2520) | 13 | .0756 | (.2522) | 14 | .1044 | (.2525) | 15 | .1454 | (.2528) |
| 16 | .1671 | (.2537) | 17 | .1448 | (.2548) | 18 | .0774 | (.2557) | 19 | -.0144 | (.2559) | 20 | -.1044 | (.2558) |
| 21 | -.1797 | (.2563) | 22 | -.2198 | (.2576) | 23 | -.2237 | (.2595) | 24 | -.2095 | (.2614) | 25 | -.1877 | (.2631) |

SAMPLE NUMBER 6

MEAN RATIOS

| | | | | | | | | | | | | | | | | | | | |
|-------|-------|-------|-------|-------|-------|------|------|------|------|------|------|------|------|------|------|------|-------|-------|-------|
| .938 | .947 | .949 | .940 | .932 | .900 | .889 | .875 | .869 | .865 | .888 | .893 | .909 | .919 | .922 | .916 | .906 | .906 | .909 | .912 |
| .911 | .912 | .932 | .961 | .961 | .937 | .931 | .952 | .976 | .978 | .967 | .963 | .978 | .987 | .971 | .962 | .984 | 1.019 | 1.058 | 1.083 |
| 1.096 | 1.070 | 1.046 | 1.034 | 1.021 | 1.002 | .983 | .970 | .961 | .956 | .951 | .943 | .939 | .941 | .948 | .957 | .965 | .968 | .965 | .957 |
| .944 | .939 | .937 | .931 | .934 | .938 | .922 | .895 | .852 | .851 | .863 | .867 | .862 | .867 | .883 | .894 | .892 | .876 | .867 | .878 |
| .893 | .904 | .916 | .925 | .937 | .953 | .961 | .959 | .959 | .953 | .972 | .961 | .952 | .912 | .904 | .893 | .885 | .910 | .908 | .903 |

MEAN = .937
 S.D. = .050
 D = .090
 4-D = 3.910

AUTOCORRELATION COEFFICIENTS

| LAG | R(L) | S.E. | LAG | R(L) | S.E. | LAG | R(L) | S.E. | LAG | R(L) | S.E. | LAG | R(L) | S.E. |
|-----|--------|---------|-----|--------|---------|-----|--------|---------|-----|--------|---------|-----|--------|---------|
| 1 | .9429 | (.1000) | 2 | .8490 | (.1667) | 3 | .7479 | (.2054) | 4 | .6558 | (.2310) | 5 | .5690 | (.2490) |
| 6 | .4818 | (.2616) | 7 | .4032 | (.2704) | 8 | .3478 | (.2763) | 9 | .3076 | (.2807) | 10 | .2649 | (.2840) |
| 11 | .2084 | (.2865) | 12 | .1521 | (.2880) | 13 | .1103 | (.2888) | 14 | .0883 | (.2892) | 15 | .0769 | (.2895) |
| 16 | .0587 | (.2897) | 17 | .0254 | (.2898) | 18 | -.0174 | (.2898) | 19 | -.0607 | (.2898) | 20 | -.1009 | (.2900) |
| 21 | -.1404 | (.2903) | 22 | -.1794 | (.2910) | 23 | -.2072 | (.2921) | 24 | -.2222 | (.2936) | 25 | -.2322 | (.2952) |

Table: 1.7 cont.

SAMPLE NUMBER 7

MEAN RATIOS

| | | | | | | | | | | | | | | | | | | | |
|------|------|------|------|------|------|------|------|------|------|------|------|-------|-------|-------|------|------|------|------|------|
| .860 | .861 | .863 | .867 | .884 | .913 | .915 | .922 | .925 | .897 | .887 | .878 | .875 | .893 | .930 | .919 | .926 | .902 | .890 | .892 |
| .914 | .947 | .911 | .889 | .829 | .735 | .710 | .726 | .696 | .635 | .598 | .597 | .585 | .596 | .649 | .917 | .929 | .926 | .917 | .904 |
| .872 | .805 | .782 | .807 | .876 | .916 | .940 | .975 | .982 | .993 | .989 | .971 | .938 | .924 | .895 | .866 | .856 | .853 | .864 | .892 |
| .912 | .907 | .901 | .915 | .933 | .940 | .940 | .938 | .942 | .986 | .989 | .989 | 1.014 | 1.032 | 1.005 | .870 | .866 | .878 | .982 | .979 |
| .967 | .947 | .935 | .933 | .928 | .925 | .925 | .923 | .917 | .903 | .892 | .888 | .879 | .870 | .875 | .882 | .880 | .871 | .878 | .903 |

MEAN = .888
S.D. = .092
D = .154
4-D = 3.846

AUTOCORRELATION COEFFICIENTS

| LAG | R(L) | S.E. | LAG | R(L) | S.E. | LAG | R(L) | S.E. | LAG | R(L) | S.E. | LAG | R(L) | S.E. |
|-----|--------|---------|-----|--------|---------|-----|--------|---------|-----|--------|---------|-----|--------|---------|
| 1 | .9132 | (.1000) | 2 | .7800 | (.1633) | 3 | .6358 | (.1971) | 4 | .4969 | (.2166) | 5 | .3678 | (.2278) |
| 6 | .2703 | (.2336) | 7 | .2188 | (.2367) | 8 | .1878 | (.2387) | 9 | .1531 | (.2402) | 10 | .1130 | (.2412) |
| 11 | .0915 | (.2417) | 12 | .0807 | (.2421) | 13 | .0618 | (.2423) | 14 | .0357 | (.2425) | 15 | -.0103 | (.2425) |
| 16 | -.0660 | (.2425) | 17 | -.1220 | (.2427) | 18 | -.1606 | (.2433) | 19 | -.1752 | (.2444) | 20 | -.1681 | (.2456) |
| 21 | -.1344 | (.2468) | 22 | -.0939 | (.2475) | 23 | -.0535 | (.2479) | 24 | -.0178 | (.2480) | 25 | .0084 | (.2480) |

SAMPLE NUMBER 8

MEAN RATIOS

| | | | | | | | | | | | | | | | | | | | |
|------|-------|-------|-------|-------|-------|-------|------|------|-------|-------|------|------|------|-------|------|------|------|------|------|
| .991 | 1.004 | 1.034 | 1.063 | 1.055 | 1.029 | 1.007 | .994 | .980 | 1.004 | 1.014 | .995 | .980 | .999 | 1.009 | .989 | .985 | .996 | .984 | .957 |
| .938 | .928 | .931 | .937 | .935 | .931 | .936 | .942 | .933 | .915 | .905 | .911 | .919 | .917 | .915 | .918 | .920 | .917 | .908 | .907 |
| .922 | .936 | .941 | .954 | .932 | .914 | .885 | .875 | .891 | .915 | .930 | .936 | .938 | .938 | .938 | .941 | .947 | .952 | .951 | .948 |
| .944 | .970 | .961 | .958 | .954 | .938 | .886 | .869 | .860 | .845 | .833 | .831 | .829 | .823 | .826 | .827 | .826 | .840 | .865 | .893 |
| .885 | .885 | .861 | .851 | .852 | .862 | .864 | .866 | .873 | .870 | .851 | .847 | .866 | .883 | .897 | .900 | .891 | .909 | .974 | .972 |

MEAN = .924
S.D. = .056
D = .077
4-D = 3.923

AUTOCORRELATION COEFFICIENTS

| LAG | R(L) | S.E. | LAG | R(L) | S.E. | LAG | R(L) | S.E. | LAG | R(L) | S.E. | LAG | R(L) | S.E. |
|-----|-------|---------|-----|-------|---------|-----|-------|---------|-----|--------|---------|-----|--------|---------|
| 1 | .9406 | (.1000) | 2 | .8564 | (.1664) | 3 | .7782 | (.2058) | 4 | .7061 | (.2334) | 5 | .6386 | (.2539) |
| 6 | .5953 | (.2694) | 7 | .5370 | (.2819) | 8 | .4889 | (.2919) | 9 | .4437 | (.3000) | 10 | .3945 | (.3065) |
| 11 | .3410 | (.3115) | 12 | .2996 | (.3152) | 13 | .2736 | (.3181) | 14 | .2441 | (.3204) | 15 | .2057 | (.3223) |
| 16 | .1744 | (.3236) | 17 | .1488 | (.3245) | 18 | .1237 | (.3252) | 19 | .0986 | (.3257) | 20 | .0775 | (.3260) |
| 21 | .0532 | (.3262) | 22 | .0330 | (.3262) | 23 | .0148 | (.3263) | 24 | -.0050 | (.3263) | 25 | -.0299 | (.3263) |

Table 1.7 cont.

SAMPLE NUMBER 9

MEAN RATIOS

| | | | | | | | | | | | | | | | | | | | |
|-------|------|-------|-------|-------|-------|-------|-------|-------|-------|-------|-------|-------|-------|-------|-------|-------|-------|-------|-------|
| .863 | .759 | .626 | .488 | .408 | .397 | .992 | 1.025 | 1.040 | 1.024 | 1.038 | 1.044 | 1.033 | 1.025 | .984 | .959 | .954 | .942 | .925 | .922 |
| .833 | .934 | .933 | .954 | .992 | 1.041 | 1.042 | 1.038 | 1.035 | .976 | .952 | .934 | .941 | .961 | .957 | .945 | .967 | 1.010 | 1.006 | .960 |
| .961 | .978 | 1.017 | 1.023 | 1.027 | 1.025 | 1.011 | .997 | 1.001 | 1.018 | 1.035 | 1.037 | 1.006 | 1.014 | .963 | .960 | .987 | .974 | .959 | .960 |
| .982 | .989 | .973 | .961 | .948 | .935 | .933 | .928 | .934 | .881 | 1.038 | 1.013 | .989 | 1.013 | 1.028 | 1.005 | .995 | 1.024 | 1.046 | 1.040 |
| 1.022 | .984 | .928 | .905 | .924 | .928 | .910 | .912 | .939 | .957 | .951 | .942 | .945 | .949 | .955 | .982 | 1.007 | .994 | .964 | .958 |

MEAN = .957
S.D. = .110
D = .383
4-D = 3.617

AUTOCORRELATION COEFFICIENTS

| LAG | R(L) | S.E. | LAG | R(L) | S.E. | LAG | R(L) | S.E. | LAG | R(L) | S.E. |
|-----|--------|---------|-----|--------|---------|-----|--------|---------|-----|--------|---------|
| 1 | .7970 | (.1006) | 2 | .5345 | (.1507) | 3 | .2794 | (.1686) | 4 | .0889 | (.1731) |
| 6 | -.1206 | (.1737) | 7 | -.1329 | (.1745) | 8 | -.1332 | (.1756) | 9 | -.1127 | (.1766) |
| 11 | -.0492 | (.1777) | 12 | -.0166 | (.1778) | 13 | .0199 | (.1778) | 14 | .0534 | (.1778) |
| 16 | .0898 | (.1783) | 17 | .1017 | (.1787) | 18 | .0947 | (.1793) | 19 | .0611 | (.1798) |
| 21 | -.0497 | (.1800) | 22 | -.0844 | (.1802) | 23 | -.0998 | (.1806) | 24 | -.0752 | (.1811) |
| | | | | | | | | | 25 | -.0333 | (.1814) |

SAMPLE NUMBER 10

MEAN RATIOS

| | | | | | | | | | | | | | | | | | | | |
|------|------|------|------|------|-------|-------|-------|-------|-------|-------|-------|-------|-------|-------|-------|-------|-------|-------|-------|
| .922 | .928 | .940 | .947 | .945 | .945 | .921 | .924 | .909 | .889 | .885 | .885 | .885 | .905 | .930 | .940 | .947 | .962 | .975 | .980 |
| .983 | .982 | .977 | .972 | .973 | 1.008 | 1.007 | .987 | .983 | .966 | .959 | .945 | .945 | .939 | .937 | .929 | .925 | .909 | .877 | .895 |
| .910 | .908 | .934 | .943 | .945 | .925 | .910 | .877 | .867 | .871 | .903 | .849 | .849 | .919 | .937 | .923 | .909 | .909 | .919 | .912 |
| .896 | .880 | .866 | .873 | .896 | .921 | .904 | .914 | .932 | .895 | .867 | .863 | .863 | .869 | .851 | .816 | .829 | .756 | .696 | .684 |
| .669 | .613 | .587 | .623 | .671 | 1.056 | 1.125 | 1.102 | 1.102 | 1.043 | 1.021 | 1.033 | 1.033 | 1.057 | 1.087 | 1.089 | 1.058 | 1.067 | 1.079 | 1.058 |

MEAN = .923
S.D. = .103
D = .184
4-D = 3.806

AUTOCORRELATION COEFFICIENTS

| LAG | R(L) | S.E. | LAG | R(L) | S.E. | LAG | R(L) | S.E. | LAG | R(L) | S.E. |
|-----|--------|---------|-----|--------|---------|-----|--------|---------|-----|--------|---------|
| 1 | .8852 | (.1000) | 2 | .7235 | (.1602) | 3 | .5604 | (.1901) | 4 | .4087 | (.2060) |
| 6 | .2018 | (.2180) | 7 | .1230 | (.2198) | 8 | .0571 | (.2205) | 9 | -.0036 | (.2207) |
| 11 | -.1532 | (.2210) | 12 | -.2074 | (.2221) | 13 | -.2564 | (.2240) | 14 | -.3032 | (.2269) |
| 16 | -.3047 | (.2357) | 17 | -.2501 | (.2396) | 18 | -.1970 | (.2422) | 19 | -.1592 | (.2438) |
| 21 | -.0933 | (.2454) | 22 | -.0773 | (.2458) | 23 | -.0757 | (.2460) | 24 | -.0772 | (.2463) |
| | | | | | | | | | 25 | -.0653 | (.2465) |

Table 1.7 cont.

SAMPLE NUMBER 11

MEAN RATIOS

| | | | | | | | | | | | | | | | | | | | | |
|-------|-------|-------|-------|-------|-------|-------|-------|-------|-------|-------|-------|-------|-------|-------|-------|-------|-------|-------|-------|-------|
| 1.032 | 1.059 | 1.091 | 1.141 | 1.135 | 1.133 | 1.128 | 1.128 | 1.128 | 1.136 | 1.134 | 1.126 | 1.118 | 1.109 | 1.105 | 1.105 | 1.103 | 1.108 | 1.112 | 1.104 | 1.101 |
| 1.061 | 1.038 | 1.016 | .994 | .972 | .973 | 1.004 | 1.008 | 1.016 | 1.016 | 1.017 | 1.005 | .992 | .974 | .952 | .954 | .972 | .971 | .966 | .970 | .959 |
| .944 | .945 | .951 | .936 | .993 | 1.027 | 1.058 | 1.026 | .934 | .876 | .880 | .880 | .890 | .852 | .863 | .843 | .816 | .785 | .764 | .761 | .788 |
| .841 | .885 | .882 | .894 | .900 | .904 | .954 | .980 | .976 | .955 | .950 | .950 | .960 | .966 | .964 | .960 | .964 | .968 | .957 | .949 | .952 |
| .958 | .963 | .972 | .980 | .978 | .969 | .960 | .915 | .905 | .915 | .915 | .932 | .939 | .938 | .959 | .953 | .934 | .954 | .959 | .949 | .948 |

MEAN = .977
S.D. = .087
D = .063
4-D = 3.937

AUTOCORRELATION COEFFICIENTS

| LAG | R(L) | S.E. | LAG | R(L) | S.E. | LAG | R(L) | S.E. | LAG | R(L) | S.E. | LAG | R(L) | S.E. |
|-----|-------|---------|-----|-------|---------|-----|-------|---------|-----|-------|---------|-----|-------|---------|
| 1 | .9562 | (.1000) | 2 | .8911 | (.1692) | 3 | .8210 | (.2102) | 4 | .7556 | (.2401) | 5 | .7010 | (.2628) |
| 6 | .6535 | (.2809) | 7 | .6051 | (.2957) | 8 | .5495 | (.3078) | 9 | .4894 | (.3175) | 10 | .4246 | (.3249) |
| 11 | .3626 | (.3304) | 12 | .3138 | (.3344) | 13 | .2820 | (.3373) | 14 | .2623 | (.3397) | 15 | .2467 | (.3417) |
| 16 | .2253 | (.3435) | 17 | .1940 | (.3450) | 18 | .1614 | (.3460) | 19 | .1328 | (.3468) | 20 | .1080 | (.3473) |
| 21 | .0886 | (.3476) | 22 | .0746 | (.3479) | 23 | .0645 | (.3480) | 24 | .0589 | (.3481) | 25 | .0564 | (.3482) |

SAMPLE NUMBER 12

MEAN RATIOS

| | | | | | | | | | | | | | | | | | | | |
|-------|-------|-------|-------|-------|-------|-------|-------|-------|-------|-------|-------|-------|-------|-------|-------|-------|-------|-------|-------|
| 1.009 | 1.041 | 1.033 | 1.029 | 1.021 | .998 | .938 | .920 | .913 | .940 | .939 | .944 | .945 | .951 | .962 | .933 | .935 | .935 | .935 | .972 |
| .941 | .935 | .944 | .979 | .929 | .908 | .902 | .918 | .936 | .936 | .932 | .927 | .915 | .915 | .933 | .931 | .902 | .876 | .880 | .905 |
| .910 | .879 | .842 | .818 | .809 | .814 | .839 | .886 | .911 | .910 | .856 | .754 | .626 | .550 | .526 | .533 | .578 | 1.059 | 1.018 | .960 |
| .950 | .951 | 1.004 | 1.036 | 1.043 | 1.027 | 1.020 | 1.022 | 1.015 | 1.007 | 1.020 | 1.050 | 1.120 | 1.110 | 1.072 | 1.056 | 1.083 | 1.128 | 1.115 | 1.091 |
| 1.082 | 1.089 | 1.102 | 1.074 | 1.062 | 1.089 | 1.119 | 1.147 | 1.144 | 1.133 | 1.089 | 1.086 | 1.111 | 1.175 | 1.153 | 1.125 | 1.120 | 1.114 | 1.097 | 1.087 |

MEAN = .969
S.D. = .131
D = .192
4-D = 3.808

AUTOCORRELATION COEFFICIENTS

| LAG | R(L) | S.E. | LAG | R(L) | S.E. | LAG | R(L) | S.E. | LAG | R(L) | S.E. | LAG | R(L) | S.E. |
|-----|-------|---------|-----|--------|---------|-----|--------|---------|-----|--------|---------|-----|--------|---------|
| 1 | .8904 | (.1000) | 2 | .7601 | (.1608) | 3 | .6427 | (.1934) | 4 | .5510 | (.2137) | 5 | .4915 | (.2275) |
| 6 | .4570 | (.2379) | 7 | .4401 | (.2465) | 8 | .4353 | (.2542) | 9 | .4284 | (.2616) | 10 | .4086 | (.2685) |
| 11 | .3656 | (.2746) | 12 | .3226 | (.2795) | 13 | .2908 | (.2832) | 14 | .2689 | (.2861) | 15 | .2465 | (.2887) |
| 16 | .2057 | (.2908) | 17 | .1617 | (.2922) | 18 | .1215 | (.2931) | 19 | .0867 | (.2936) | 20 | .0506 | (.2939) |
| 21 | .0171 | (.2939) | 22 | -.0075 | (.2940) | 23 | -.0279 | (.2940) | 24 | -.0485 | (.2941) | 25 | -.0666 | (.2941) |

Table 1.7 cont.

SAMPLE NUMBER 13

MEAN RATIOS

| | | | | | | | | | | | | | | | | | | | |
|-------|-------|-------|------|------|------|------|------|------|------|------|------|------|------|------|------|------|-------|-------|-------|
| .944 | .920 | .910 | .904 | .880 | .848 | .815 | .789 | .792 | .808 | .821 | .836 | .859 | .883 | .890 | .835 | .812 | .843 | .882 | .857 |
| .791 | .697 | .660 | .659 | .670 | .701 | .730 | .731 | .735 | .776 | .815 | .829 | .846 | .875 | .896 | .900 | .900 | .908 | .915 | .912 |
| .923 | .940 | .910 | .865 | .871 | .884 | .862 | .859 | .884 | .892 | .885 | .885 | .889 | .897 | .904 | .906 | .904 | .909 | .920 | .920 |
| .884 | .892 | .908 | .943 | .907 | .891 | .880 | .879 | .892 | .919 | .942 | .953 | .958 | .964 | .967 | .963 | .968 | 1.014 | 1.020 | 1.017 |
| 1.018 | 1.016 | 1.007 | .995 | .979 | .929 | .913 | .908 | .910 | .904 | .899 | .906 | .952 | .964 | .965 | .965 | .962 | .924 | .910 | .905 |

MEAN = .887
S.D. = .077
D = .093
4-D = 3.907

AUTOCORRELATION COEFFICIENTS

| LAG | R(L) | S.E. | LAG | R(L) | S.E. | LAG | R(L) | S.E. | LAG | R(L) | S.E. |
|-----|-------|---------|-----|-------|---------|-----|-------|---------|-----|-------|---------|
| 1 | .9408 | (.1000) | 2 | .8478 | (.1664) | 3 | .7553 | (.2051) | 4 | .6722 | (.2313) |
| 6 | .5106 | (.2636) | 7 | .4363 | (.2733) | 8 | .3701 | (.2802) | 9 | .3171 | (.2850) |
| 11 | .2663 | (.2913) | 12 | .2621 | (.2937) | 13 | .2671 | (.2960) | 14 | .2804 | (.2984) |
| 16 | .2755 | (.3037) | 17 | .2602 | (.3062) | 18 | .2419 | (.3084) | 19 | .2152 | (.3103) |
| 21 | .1869 | (.3128) | 22 | .1436 | (.3138) | 23 | .1107 | (.3145) | 24 | .0723 | (.3149) |
| | | | | | | | | | 5 | .5892 | (.2500) |
| | | | | | | | | | 10 | .2826 | (.2885) |
| | | | | | | | | | 15 | .2846 | (.3010) |
| | | | | | | | | | 20 | .1881 | (.3118) |
| | | | | | | | | | 25 | .0352 | (.3150) |

SAMPLE NUMBER 14

MEAN RATIOS

| | | | | | | | | | | | | | | | | | | | |
|-------|-------|-------|-------|-------|-------|-------|-------|-------|-------|-------|-------|------|------|------|------|-------|-------|-------|-------|
| .879 | .880 | .915 | .908 | .904 | .892 | .871 | .884 | .916 | .907 | .872 | .870 | .871 | .848 | .834 | .790 | .745 | .698 | .695 | .724 |
| .743 | .758 | .754 | .724 | .676 | .657 | .648 | .700 | .743 | 1.053 | 1.010 | .875 | .947 | .958 | .984 | .997 | .986 | .960 | .965 | 1.030 |
| 1.043 | 1.041 | 1.050 | 1.060 | 1.056 | 1.009 | 1.009 | 1.024 | 1.018 | .997 | .998 | 1.007 | .990 | .962 | .972 | .998 | 1.008 | 1.014 | 1.063 | 1.073 |
| 1.075 | 1.065 | 1.060 | 1.057 | 1.041 | 1.027 | 1.029 | 1.026 | .971 | .946 | .937 | .933 | .917 | .891 | .872 | .879 | .925 | .914 | .891 | .890 |
| .903 | .905 | .870 | .885 | .941 | .947 | .949 | .893 | 1.060 | 1.073 | 1.051 | 1.043 | .975 | .908 | .860 | .866 | .852 | .834 | .812 | .797 |

MEAN = .924
S.D. = .109
D = .143
4-D = 3.857

AUTOCORRELATION COEFFICIENTS

| LAG | R(L) | S.E. | LAG | R(L) | S.E. | LAG | R(L) | S.E. | LAG | R(L) | S.E. |
|-----|--------|---------|-----|--------|---------|-----|--------|---------|-----|--------|---------|
| 1 | .9115 | (.1000) | 2 | .8071 | (.1631) | 3 | .7057 | (.1991) | 4 | .6213 | (.2227) |
| 6 | .4660 | (.2513) | 7 | .4070 | (.2598) | 8 | .3531 | (.2661) | 9 | .3053 | (.2707) |
| 11 | .2051 | (.2766) | 12 | .1520 | (.2781) | 13 | .1026 | (.2789) | 14 | .0606 | (.2793) |
| 16 | .0020 | (.2795) | 17 | -.0118 | (.2795) | 18 | -.0244 | (.2795) | 19 | -.0325 | (.2795) |
| 21 | -.0374 | (.2796) | 22 | -.0537 | (.2796) | 23 | -.0705 | (.2797) | 24 | -.0736 | (.2799) |
| | | | | | | | | | 5 | .5392 | (.2394) |
| | | | | | | | | | 10 | .2594 | (.2741) |
| | | | | | | | | | 15 | .0295 | (.2794) |
| | | | | | | | | | 20 | -.0343 | (.2795) |
| | | | | | | | | | 25 | -.0726 | (.2801) |

Table 1.7 cont.

SAMPLE NUMBER 15

MEAN RATIOS

| | | | | | | | | | | | | | | | | | | | |
|------|------|------|------|------|------|------|------|------|------|------|------|------|------|------|------|------|------|------|------|
| .886 | .923 | .938 | .945 | .940 | .934 | .930 | .913 | .894 | .895 | .912 | .931 | .942 | .944 | .942 | .940 | .928 | .905 | .896 | .908 |
| .917 | .919 | .927 | .933 | .935 | .942 | .945 | .910 | .908 | .944 | .949 | .940 | .912 | .916 | .912 | .913 | .882 | .872 | .871 | .878 |
| .870 | .852 | .848 | .840 | .821 | .828 | .875 | .910 | .948 | .957 | .966 | .968 | .972 | .979 | .987 | .986 | .982 | .971 | .952 | .936 |
| .933 | .937 | .906 | .889 | .875 | .877 | .884 | .906 | .903 | .911 | .895 | .883 | .867 | .875 | .890 | .907 | .904 | .925 | .934 | .877 |
| .851 | .852 | .863 | .862 | .867 | .886 | .882 | .856 | .844 | .847 | .855 | .858 | .831 | .792 | .773 | .779 | .802 | .799 | .768 | .753 |

MEAN = .898
S.D. = .050
D = .116
4-D = 3.884

AUTOCORRELATION COEFFICIENTS

| LAG | R(L) | S.E. | LAG | R(L) | S.E. | LAG | R(L) | S.E. | LAG | R(L) | S.E. |
|-----|--------|---------|-----|--------|---------|-----|--------|---------|-----|--------|---------|
| 1 | .8903 | (.1000) | 2 | .7518 | (.1608) | 3 | .6397 | (.1928) | 4 | .5482 | (.2129) |
| 6 | .3562 | (.2354) | 7 | .2757 | (.2407) | 8 | .2162 | (.2439) | 9 | .1600 | (.2458) |
| 11 | .0269 | (.2472) | 12 | -.0290 | (.2472) | 13 | -.0536 | (.2472) | 14 | -.0532 | (.2474) |
| 16 | -.0320 | (.2476) | 17 | -.0037 | (.2476) | 18 | .0233 | (.2476) | 19 | .0338 | (.2476) |
| 21 | .0332 | (.2477) | 22 | .0631 | (.2477) | 23 | .0816 | (.2479) | 24 | .0843 | (.2482) |
| | | | | | | | | | 25 | .0899 | (.2485) |

SAMPLE NUMBER 16

MEAN RATIOS

| | | | | | | | | | | | | | | | | | | | |
|-------|-------|-------|-------|-------|-------|-------|-------|-------|-------|-------|-------|-------|-------|-------|-------|-------|-------|-------|------|
| .962 | .954 | .941 | .934 | .918 | .893 | .869 | .847 | .830 | .826 | .817 | .798 | .787 | .797 | .810 | .818 | .829 | .840 | .846 | .853 |
| .878 | .904 | .939 | .945 | .962 | .938 | .932 | .927 | .924 | .914 | .904 | .907 | .918 | .916 | .894 | .878 | .879 | .888 | .891 | .869 |
| .845 | .857 | .874 | .872 | .904 | .880 | .863 | .841 | .838 | .846 | .843 | .818 | .732 | .629 | .537 | .514 | .529 | .562 | .572 | .538 |
| 1.103 | 1.111 | 1.123 | 1.094 | 1.055 | 1.013 | .989 | .958 | .955 | .992 | 1.020 | 1.036 | 1.091 | 1.090 | 1.085 | 1.070 | 1.030 | 1.034 | 1.036 | |
| 1.085 | 1.088 | 1.069 | 1.063 | 1.087 | 1.106 | 1.055 | 1.018 | 1.003 | 1.010 | 1.035 | 1.062 | 1.080 | 1.113 | 1.110 | 1.109 | 1.103 | 1.088 | 1.016 | .999 |

MEAN = .925
S.D. = .142
D = .196
4-D = 3.804

AUTOCORRELATION COEFFICIENTS

| LAG | R(L) | S.E. | LAG | R(L) | S.E. | LAG | R(L) | S.E. | LAG | R(L) | S.E. |
|-----|-------|---------|-----|--------|---------|-----|--------|---------|-----|--------|---------|
| 1 | .8910 | (.1000) | 2 | .7779 | (.1609) | 3 | .6487 | (.1949) | 4 | .5193 | (.2154) |
| 6 | .3045 | (.2345) | 7 | .2424 | (.2385) | 8 | .2208 | (.2409) | 9 | .2265 | (.2429) |
| 11 | .2279 | (.2472) | 12 | .2115 | (.2493) | 13 | .1708 | (.2511) | 14 | .1290 | (.2522) |
| 16 | .0658 | (.2532) | 17 | .0498 | (.2534) | 18 | .0421 | (.2535) | 19 | .0329 | (.2536) |
| 21 | .0033 | (.2536) | 22 | -.0130 | (.2536) | 23 | -.0318 | (.2536) | 24 | -.0578 | (.2537) |
| | | | | | | | | | 25 | -.0962 | (.2538) |

Table 1.7 cont.

SAMPLE NUMBER 17

MEAN RATIOS

| | | | | | | | | | | | | | | | | | | | |
|------|------|------|------|------|------|------|------|------|------|------|------|------|------|------|------|------|------|-------|------|
| .988 | .978 | .964 | .938 | .918 | .912 | .910 | .913 | .931 | .952 | .952 | .949 | .962 | .972 | .968 | .962 | .968 | .989 | 1.000 | .993 |
| .987 | .981 | .960 | .945 | .954 | .976 | .983 | .961 | .937 | .943 | .967 | .977 | .972 | .969 | .971 | .969 | .963 | .962 | .966 | .968 |
| .963 | .958 | .962 | .960 | .939 | .916 | .918 | .931 | .926 | .907 | .896 | .907 | .931 | .941 | .927 | .913 | .917 | .926 | .936 | .938 |
| .927 | .916 | .916 | .923 | .923 | .894 | .951 | .961 | .961 | .956 | .965 | .903 | .880 | .873 | .857 | .846 | .850 | .874 | .866 | .863 |
| .835 | .839 | .845 | .858 | .884 | .926 | .929 | .933 | .938 | .947 | .917 | .902 | .894 | .901 | .903 | .899 | .902 | .907 | .902 | .903 |

MEAN = .931
S.D. = .039
D = .166
4-D = 3.834

AUTOCORRELATION COEFFICIENTS

| LAG | R(L) | S.E. | LAG | R(L) | S.E. | LAG | R(L) | S.E. | LAG | R(L) | S.E. |
|-----|-------|---------|-----|-------|---------|-----|-------|---------|-----|-------|---------|
| 1 | .8941 | (.1000) | 2 | .7571 | (.1612) | 3 | .6411 | (.1935) | 4 | .5593 | (.2137) |
| 6 | .4276 | (.2376) | 7 | .3949 | (.2452) | 8 | .3709 | (.2515) | 9 | .3444 | (.2569) |
| 11 | .2754 | (.2651) | 12 | .2440 | (.2679) | 13 | .2241 | (.2701) | 14 | .2274 | (.2720) |
| 16 | .3134 | (.2766) | 17 | .3374 | (.2801) | 18 | .3300 | (.2841) | 19 | .3035 | (.2879) |
| 21 | .2402 | (.2935) | 22 | .2075 | (.2955) | 23 | .1767 | (.2969) | 24 | .1483 | (.2980) |
| | | | | | | | | | 25 | .1390 | (.2987) |

SAMPLE NUMBER 18

MEAN RATIOS

| | | | | | | | | | | | | | | | | | | | |
|-------|-------|-------|-------|-------|-------|-------|-------|-------|-------|-------|-------|-------|-------|-------|-------|-------|-------|-------|-------|
| .872 | .875 | .890 | .885 | .881 | .892 | .885 | .874 | .884 | .881 | .833 | .732 | .631 | .507 | .442 | .415 | 1.065 | 1.060 | 1.026 | 1.001 |
| .995 | 1.005 | 1.025 | 1.052 | 1.055 | 1.056 | 1.001 | .980 | .989 | .999 | .985 | .967 | .967 | .993 | 1.019 | 1.020 | 1.049 | 1.053 | 1.056 | 1.061 |
| 1.072 | 1.098 | 1.088 | 1.117 | 1.151 | 1.116 | 1.102 | 1.095 | 1.106 | 1.117 | 1.110 | 1.110 | 1.083 | 1.092 | 1.097 | 1.112 | 1.083 | 1.061 | 1.051 | 1.038 |
| 1.023 | 1.012 | 1.010 | 1.010 | 1.002 | .996 | .980 | .986 | .981 | .959 | .938 | .941 | .953 | .955 | .948 | .942 | .944 | .936 | .915 | .917 |
| .952 | .971 | .966 | .969 | .981 | .990 | .996 | 1.000 | 1.003 | 1.006 | 1.012 | 1.008 | .980 | .959 | .984 | 1.016 | 1.011 | 1.012 | 1.037 | 1.045 |

MEAN = .980
S.D. = .124
D = .324
4-D = 3.676

AUTOCORRELATION COEFFICIENTS

| LAG | R(L) | S.E. | LAG | R(L) | S.E. | LAG | R(L) | S.E. | LAG | R(L) | S.E. |
|-----|--------|---------|-----|--------|---------|-----|--------|---------|-----|--------|---------|
| 1 | .8243 | (.1000) | 2 | .6437 | (.1536) | 3 | .4918 | (.1785) | 4 | .3938 | (.1916) |
| 6 | .3072 | (.2050) | 7 | .2891 | (.2096) | 8 | .2536 | (.2135) | 9 | .2102 | (.2165) |
| 11 | .1646 | (.2199) | 12 | .1560 | (.2212) | 13 | .1387 | (.2223) | 14 | .1077 | (.2231) |
| 16 | .0250 | (.2238) | 17 | .0311 | (.2239) | 18 | .0273 | (.2239) | 19 | .0100 | (.2239) |
| 21 | -.0401 | (.2239) | 22 | -.0660 | (.2240) | 23 | -.0865 | (.2242) | 24 | -.1001 | (.2245) |
| | | | | | | | | | 25 | -.1117 | (.2250) |

SAMPLE NUMBER 19

MEAN RATIOS

| | | | | | | | | | | | | | | | | | | | |
|-------|------|------|------|------|------|-------|------|-------|------|------|------|------|-------|-------|-------|-------|-------|-------|-------|
| .866 | .894 | .916 | .923 | .927 | .961 | .968 | .981 | .970 | .970 | .958 | .962 | .984 | 1.022 | 1.022 | 1.018 | 1.013 | 1.010 | 1.011 | 1.007 |
| .999 | .994 | .967 | .969 | .973 | .976 | 1.003 | .998 | .998 | .998 | .961 | .945 | .933 | .921 | .919 | .926 | .928 | .923 | .928 | .935 |
| .932 | .931 | .924 | .911 | .925 | .950 | .956 | .949 | .939 | .946 | .969 | .998 | .988 | .959 | .934 | .903 | .887 | .916 | .838 | .847 |
| .940 | .911 | .881 | .885 | .851 | .708 | .603 | .562 | .526 | .525 | .606 | .727 | .990 | 1.005 | .999 | .983 | .958 | .968 | 1.021 | 1.071 |
| 1.039 | .944 | .821 | .932 | .935 | .923 | .834 | .998 | 1.048 | .992 | .976 | .990 | .971 | .948 | .968 | 1.011 | 1.087 | 1.085 | 1.082 | 1.083 |

MEAN = .940
S.D. = .104
D = .166
4-D = 3.834

AUTOCORRELATION COEFFICIENTS

| LAG | R(L) | S.E. | LAG | R(L) | S.E. | LAG | R(L) | S.E. | LAG | R(L) | S.E. | LAG | R(L) | S.E. |
|-----|--------|---------|-----|--------|---------|-----|--------|---------|-----|--------|---------|-----|--------|---------|
| 1 | .8959 | (.1000) | 2 | .7209 | (.1614) | 3 | .5300 | (.1909) | 4 | .3536 | (.2051) | 5 | .2130 | (.2111) |
| 6 | .1121 | (.2132) | 7 | -.0519 | (.2138) | 8 | -.0157 | (.2140) | 9 | -.0259 | (.2140) | 10 | -.0513 | (.2140) |
| 11 | -.0561 | (.2141) | 12 | -.0562 | (.2143) | 13 | -.0528 | (.2144) | 14 | -.0415 | (.2145) | 15 | -.0303 | (.2146) |
| 16 | -.0375 | (.2147) | 17 | -.0663 | (.2147) | 18 | -.0817 | (.2149) | 19 | -.0831 | (.2152) | 20 | -.0877 | (.2156) |
| 21 | -.0897 | (.2159) | 22 | -.0807 | (.2163) | 23 | -.0635 | (.2166) | 24 | -.0527 | (.2168) | 25 | -.0716 | (.2169) |

SAMPLE NUMBER 20

MEAN RATIOS

| | | | | | | | | | | | | | | | | | | | |
|-------|-------|-------|-------|-------|-------|-------|-------|-------|-------|-------|-------|-------|-------|-------|-------|------|------|------|------|
| 1.049 | 1.068 | 1.090 | 1.094 | 1.085 | 1.079 | 1.072 | 1.069 | 1.070 | 1.057 | 1.035 | 1.025 | 1.013 | 1.001 | 1.006 | 1.004 | .982 | .963 | .954 | .942 |
| .933 | .897 | .913 | .900 | .900 | .890 | .867 | .848 | .849 | .857 | .851 | .845 | .869 | .904 | .918 | .916 | .907 | .907 | .930 | .945 |
| .928 | .909 | .911 | .919 | .908 | .869 | .870 | .934 | .935 | .838 | .762 | .769 | .824 | .856 | .846 | .879 | .957 | .977 | .962 | .974 |
| .971 | .937 | .912 | .910 | .909 | .889 | .871 | .877 | .893 | .898 | .891 | .852 | .849 | .883 | .885 | .889 | .884 | .869 | .867 | .872 |
| .873 | .879 | .886 | .883 | .877 | .876 | .848 | .848 | .848 | .847 | .851 | .852 | .848 | .856 | .868 | .874 | .889 | .916 | .923 | .908 |

MEAN = .916
S.D. = .072
D = .101
4-D = 3.899

AUTOCORRELATION COEFFICIENTS

| LAG | R(L) | S.E. | LAG | R(L) | S.E. | LAG | R(L) | S.E. | LAG | R(L) | S.E. | LAG | R(L) | S.E. |
|-----|-------|---------|-----|-------|---------|-----|--------|---------|-----|--------|---------|-----|--------|---------|
| 1 | .9227 | (.1000) | 2 | .8142 | (.1644) | 3 | .7309 | (.2007) | 4 | .6650 | (.2258) | 5 | .5796 | (.2446) |
| 6 | .4777 | (.2579) | 7 | .3963 | (.2666) | 8 | .3471 | (.2725) | 9 | .2995 | (.2769) | 10 | .2391 | (.2801) |
| 11 | .1876 | (.2821) | 12 | .1561 | (.2834) | 13 | .1323 | (.2842) | 14 | .1054 | (.2848) | 15 | .0738 | (.2852) |
| 16 | .0471 | (.2854) | 17 | .0310 | (.2855) | 18 | .0190 | (.2855) | 19 | .0125 | (.2855) | 20 | .0139 | (.2855) |
| 21 | .0138 | (.2855) | 22 | .0115 | (.2856) | 23 | -.0064 | (.2856) | 24 | -.0255 | (.2856) | 25 | -.0433 | (.2856) |

Table 1.7 cont.

if we restrict ourselves to one point sampled at random per orbit we will find instead a standard deviation of

$$s' = \sqrt{\frac{\sum_{j=1}^{n_o} (Y_j - \bar{Y})^2}{n_o - 1}}$$

The relative standard deviations in the two cases

1) oversampling, and 2) actual, are thus in the ratio

$$\sqrt{\frac{n}{n \cdot n_o - 1}} \quad \text{to} \quad \sqrt{\frac{1}{n_o - 1}}$$

Take a typical case of 30 orbits with 4 samples per orbit. The apparent standard deviation to the true standard deviations are in the ratio

$$\sqrt{\frac{4}{119}} \quad \text{to} \quad \sqrt{\frac{1}{29}}$$

or 1.3% lower than actual.

1.6.5 Conclusion

We conclude that while the data do appear to be correlated in time, this has little or no impact on the magnitude of the standard deviations as they are currently being calculated. However, it does impact the "degrees of freedom" associated with the standard deviations which will impact any confidence or prediction intervals that may be calculated from these statistics.

1.7 AE-E Local Time Effect

Since the AE/S3-1 data is characterized by greater local time coverage than the SETA-1 data, it has been suspected that unmodeled local time variations in the density contribute significantly to the higher variabilities (standard deviations) of the AE/S3-1 measured to model ratios. Therefore an analysis of variance, similar to that described in Section 1.6, was conducted for the AE-E data, which has the most extensive local time coverage, to assess the significance of unmodeled local time variations, and to see if elimination of these variations could bring the AE/S3-1 and SETA variabilities into agreement. Results are given in Tables 1.8, 1.9 for the data to Jacchia 71 model ratio and the data to MSIS 83B model ratio. These results show that, while the unmodeled local time variations are significant for the AE-E data, their elimination reduces the AE-E variability only to around 12%, still well above the SETA variabilities. Note also that the unmodeled local time variations are more significant for the Jacchia 71 model ratios than for the MSIS 83B ratios, indicating that the local time variations for the AE-E data are better represented by the MSIS 83B model than by the Jacchia 71 model.

Table: 1.8 ONE WAY ANALYSIS OF VARIANCE FOR AE-E LOCAL TIME EFFECT

JACCHIA 71 MODEL

MODEL: $LN(R(I,J)) = MU + LT(I) + E(I,J)$ $I=1,24, J=1,N(I)$

| SOURCE OF VARIATION | SUM OF SQUARES | DEGREES OF FREEDOM | MEAN SQUARE | F STATISTIC | PR(F>1009.8) |
|---------------------|----------------|--------------------|-------------|-------------|--------------|
| TOTAL | 826.262 | 35628 | .02306 | | |
| LOCAL TIME | 326.112 | 23 | 14.178 | 1009.8 | 0.0* |
| RESIDUAL | 500.150 | 35605 | .01404 | | |

* WITHIN OUR ABILITY TO COMPUTE THE RELEVANT PROBABILITY LEVEL.

OVERALL MEAN MU = .0144
TOTAL VARIANCE = .02306
TOTAL STANDARD DEVIATION = .1523

| I | LOCAL TIME (HOURS) | N(I) | MU + LT(I) | VARIANCE WITHIN | S.D. WITHIN |
|----|--------------------|------|------------|-----------------|-------------|
| 1 | 0-1 | 1138 | .1501 | .01861 | .1364 |
| 2 | 1-2 | 1111 | .1378 | .02030 | .1425 |
| 3 | 2-3 | 1116 | .1417 | .01552 | .1246 |
| 4 | 3-4 | 1138 | .1772 | .01859 | .1363 |
| 5 | 4-5 | 1061 | .1754 | .01787 | .1336 |
| 6 | 5-6 | 1662 | .1919 | .01773 | .1332 |
| 7 | 6-7 | 1980 | .1689 | .01357 | .1165 |
| 8 | 7-8 | 2183 | .1647 | .01356 | .1164 |
| 9 | 8-9 | 1996 | .1149 | .01142 | .1069 |
| 10 | 9-10 | 2018 | .0433 | .01182 | .1087 |
| 11 | 10-11 | 1797 | .0090 | .01130 | .1063 |
| 12 | 11-12 | 1587 | -.0239 | .00897 | .0947 |
| 13 | 12-13 | 1593 | -.0432 | .00856 | .0926 |
| 14 | 13-14 | 1485 | -.0764 | .01107 | .1052 |
| 15 | 14-15 | 1449 | -.1029 | .01215 | .1102 |
| 16 | 15-16 | 1372 | -.0698 | .00983 | .0992 |
| 17 | 16-17 | 1320 | -.0559 | .01327 | .1152 |
| 18 | 17-18 | 1338 | -.0602 | .01205 | .1098 |
| 19 | 18-19 | 1401 | -.0143 | .01845 | .1358 |
| 20 | 19-20 | 1452 | .0778 | .01506 | .1227 |
| 21 | 20-21 | 1389 | .1322 | .01183 | .1088 |
| 22 | 21-22 | 1397 | .1252 | .02194 | .1481 |
| 23 | 22-23 | 1397 | .1251 | .01643 | .1282 |
| 24 | 23-24 | 1249 | .1224 | .01564 | .1251 |

RESIDUAL VARIANCE = .01404
RESIDUAL STANDARD DEVIATION = .1185

Table: 1.9 ONE WAY ANALYSIS OF VARIANCE FOR AE-E LOCAL TIME EFFECT

MSIS 83B MODEL

MODEL: $\ln(R(I,J)) = \mu + LT(I) + E(I,J)$ $I=1,24, J=1,N(I)$

| SOURCE OF VARIATION | SUM OF SQUARES | DEGREES OF FREEDOM | MEAN SQUARE | F STATISTIC | PR(F>319.6) |
|---------------------|----------------|--------------------|-------------|-------------|-------------|
| TOTAL | 619.688 | 35628 | .01739 | | |
| LOCAL TIME | 106.082 | 23 | 4.612 | 319.6 | 0.0* |
| RESIDUAL | 513.606 | 35605 | .01443 | | |

* WITHIN OUR ABILITY TO COMPUTE THE RELEVANT PROBABILITY LEVEL.

OVERALL MEAN μ = .0144
TOTAL VARIANCE = .01739
TOTAL STANDARD DEVIATION = .1319

| I | LOCAL TIME (HOURS) | N(I) | $\mu + LT(I)$ | VARIANCE WITHIN | S.D. WITHIN |
|----|--------------------|------|---------------|-----------------|-------------|
| 1 | 0-1 | 1138 | .0554 | .02179 | .1476 |
| 2 | 1-2 | 1111 | .0447 | .02195 | .1481 |
| 3 | 2-3 | 1116 | .0480 | .01319 | .1148 |
| 4 | 3-4 | 1138 | .0747 | .01650 | .1284 |
| 5 | 4-5 | 1061 | .0433 | .02015 | .1419 |
| 6 | 5-6 | 1662 | -.0027 | .01666 | .1291 |
| 7 | 6-7 | 1980 | -.0347 | .01594 | .1262 |
| 8 | 7-8 | 2183 | -.0362 | .01309 | .1144 |
| 9 | 8-9 | 1996 | -.0461 | .01143 | .1068 |
| 10 | 9-10 | 2018 | -.0584 | .01391 | .1144 |
| 11 | 10-11 | 1797 | -.0316 | .01320 | .1149 |
| 12 | 11-12 | 1587 | -.0258 | .00992 | .0996 |
| 13 | 12-13 | 1593 | -.0348 | .00798 | .0893 |
| 14 | 13-14 | 1485 | -.0363 | .01213 | .1101 |
| 15 | 14-15 | 1449 | -.0240 | .01165 | .1079 |
| 16 | 15-16 | 1372 | .0416 | .00798 | .0893 |
| 17 | 16-17 | 1320 | .0467 | .01222 | .1105 |
| 18 | 17-18 | 1338 | .0312 | .01118 | .1057 |
| 19 | 18-19 | 1401 | .0569 | .01589 | .1260 |
| 20 | 19-20 | 1452 | .1235 | .01442 | .1200 |
| 21 | 20-21 | 1389 | .1399 | .01256 | .1121 |
| 22 | 21-22 | 1397 | .0795 | .02224 | .1491 |
| 23 | 22-23 | 1397 | .0421 | .01868 | .1366 |
| 24 | 23-24 | 1249 | .0288 | .01933 | .1390 |

RESIDUAL VARIANCE = .01443
RESIDUAL STANDARD DEVIATION = .1201

References

1. Jacchia, L.E., Revised Static Models of the Thermosphere and Exosphere with Empirical Temperature Profiles, Special Report No. 332, Smithsonian Astrophysical Observatory, Cambridge, Massachusetts, 1971.
2. Hedin, A.E., "A Revised Thermospheric Model based on Mass Spectrometer and Incoherent Scatter Data:MSIS-83," Journal of Geophysical Research, Vol. 88, No. A12, 10170-10188, December 1983.
3. Marcos, F. A., Robinson, E. C., Bass, J. N., and Bryant, C. M., Jr., "Atmospheric Density Variability at Low Satellite Altitudes", in preparation.
4. Forbes, J.M., "Thermosphere Structure Variations during High Solar and Magnetic Activity Conditions", AFGL Technical Report 86-0009, Air Force Geophysical Laboratory, Hanscom AFB, Massachusetts, 30 September 1985, ADA171350.
5. Noonan, J.P., Fioretti, R.W., and Hass, B., "Digital Filtering Analysis Applied to the Atmosphere Explorer-C Satellite MESA Accelerometer Data", AFCRL Technical Report 75-0293, Air Force Cambridge Research Laboratories, Hanscom AFB, Massachusetts, 15 February 1975, ADA015765.
6. Marcos, F.A., Swift, E.R., "Application of the Satellite Triaxial Accelerometer Experiment to Atmospheric Density and Wind Studies", AFGL Technical Report 82-0091, Air Force Geophysics Laboratory, Hanscom AFB, Massachusetts, 4 March 1982. ADA120852
7. "Analysis and Programming for Research in the Physics of the Upper Atmosphere", Logicon, Inc., Final Report, AFGL-TR-84-0066, 1984, ADA144203.
8. Bhavnani, K. H., and McInerney, R. E., "SUATEK Interactive User Guide".
9. Snedecor, George W., and Cochran, W.G., Statistical Methods, 6th ed., Iowa State University Press, Ames, Iowa, 1967.
10. Gibbons, Jean D., Nonparametric Statistical Inference, McGraw-Hill, New York, 1971.
11. Draper, Norman, and Smith, H., Applied Regression Analysis, 2nd ed., Wiley, New York, 1981.
12. Bass, J. N., and Robinson, E. C., "Private Communication."

References (cont'd)

13. Box, G.E.P. and Jenkins, G.M., Time Series Analysis, Forecasting and Control, Holden-Day 1970, pp. 30-36.
14. Draper, N.R., and Smith, H., Applied Regression Analysis 2nd ed., Wiley, 1981, pp. 162-169.
15. Guttman, I., Wilks, S.S., and Hunter, J.S., Introductory Engineering Statistics, 2nd ed., Wiley, 1971, pp. 371-377.
16. Mendenhall, W., Introduction to Linear Models and the Design and Analysis of Experiments, Duxbury Press, 1968, pp. 337-354.
17. Snedecor, G.W., and Cochran, W.G., Statistical Methods, 6th ed., Iowa State University Press, 1967, pp. 258-298.

2.0 Ionospheric Scintillation Data Processing Systems

2.1 Overview

Two radio wave scintillation data processing systems, developed by SRI International, known as AFSATCOM (SDS)^(1,2) and Fleetsatcom (FLT)⁽³⁾ routinely process radio wave scintillation data from near stationary polar beacons and geostationary satellites, respectively. Data are collected using an Intel 8080 microprocessor system at Goose Bay, Labrador, Thule, Greenland, Tromso, Norway, and Malvik, Scotland, for SDS and at Ascension Island for the FLT system. The format of the field tapes is shown in Table 2.1. Data reduction and analysis takes place at AFGL and involves unpacking the raw data, separating it into its phase and intensity components, extracting that portion of total phase ascribable to propagation effects, and deriving certain statistical properties of the propagation data (See Table 2.2 and Figures 2.1, 2.2, 2.4, and 2.5). In the process, the data are spectrum analyzed and plots of the power spectrum of the data are part of the output of the SDS and FLT systems. Statistics on each block of data are accumulated, usually on a monthly basis, and summary statistics are generated using the STATSDS and STATFLT programs (See Figures 2.3 and 2.6). In addition, SUATEK plots of parameters of interest are part of the period end processing (See Table 2.3).

Table 2.1 Field Tape Data Format

| <u>Byte #</u> | <u>Meaning</u> |
|---------------|--|
| 0 | record type (1 = data, 2 = calibration) |
| 1 | pass number |
| 2-3 | record serial number (1.s. byte first) |
| 4 | seconds |
| 5 | minutes |
| 6 | hours |
| 7-8 | days |
| 9 | year |
| 10 | system configuration word |
| 11-12 | receiver status (1.s. byte first) |
| 13 | mode |
| 14 | chart speed |
| 15 | chart flag |
| 16-27 | most recent HP-IB tuning command string (ASCII) |
| 28 | number of channels in A/D list, number of samples/burst |
| 29 | offset into list for cosine channel |
| 30 | offset into list for sine channel |
| 31-46 | list of A/D channels in sequence |
| 47 | divide factor for 10 ms clock |
| 48-49 | hour, minute to open window |
| 50-51 | hour, minute to close window |
| 52 | hour, minute to close window |
| 53-63 | blank, spare space |
| 64-1663 | A/D converter samples, 2 bytes/sample |

(INTEL 8080 format: 16 bit, two's complement,
least significant byte first)

Table 2.2 Unpacked Data Format

| <u>Word</u> | <u>Meaning</u> |
|-------------|---------------------------|
| 1-800 | (intensity, phase) pairs* |
| 801 | time in seconds |
| 802 | day number |
| 803 | sampling frequency, Hz |
| 804 | channel #1 frequency, Hz |
| 805 | channel #2 frequency, Hz |
| 806 | channel #3 frequency, Hz |
| 807 | pass number |
| 808 | record serial number |
| 809 | system configuration word |
| 810 | receiver status |
| 811 | mode |

* Note: For mode 3 data, the intensity (I) and phase pairs for the three channels are interleaved (i.e. $(I_{1i}, P_{1i}), (I_{2i}, P_{2i}), (I_{3i}, P_{3i}), i=1,133$), with two extra "dummy" values at the end to pad the array out to 800 words.

Note: Mode 5 data consists of intensity data only.

Table 2.3 SDS and FLT Plots

SDS Plots

- | | |
|---|---|
| 1. Kp | vs Magnetic Local Time |
| 2. RMS Phase Deviation | vs Magnetic Local Time |
| 3. Phase Spectral Slope | vs Magnetic Local Time |
| 4. Phase Spectral Strength | vs Magnetic Local Time |
| 5. S ₄ | vs Magnetic Local Time |
| 6. Intensity Spectral Strength | vs Magnetic Local Time |
| 7. Log ₁₀ (Decorrelation Time) | vs Magnetic Local Time (Night and Day) |
| 8. Phase Spectral Slope | vs S ₄ |
| 9. Phase Spectral Slope | vs RMS Phase Deviation |
| 10. Phase Spectral Slope | vs Phase Spectral Strength |

FLT Plots

- | | |
|-------------------------|---|
| 1. Decorrelation Time | vs S ₄ (Pre and Post Midnight) |
| 2. Phase Spectral Slope | vs RMS Phase Deviation |
| 3. Decorrelation Time | vs Phase Spectral Strength |
| 4. Phase Spectral Slope | vs Phase Spectral Strength |

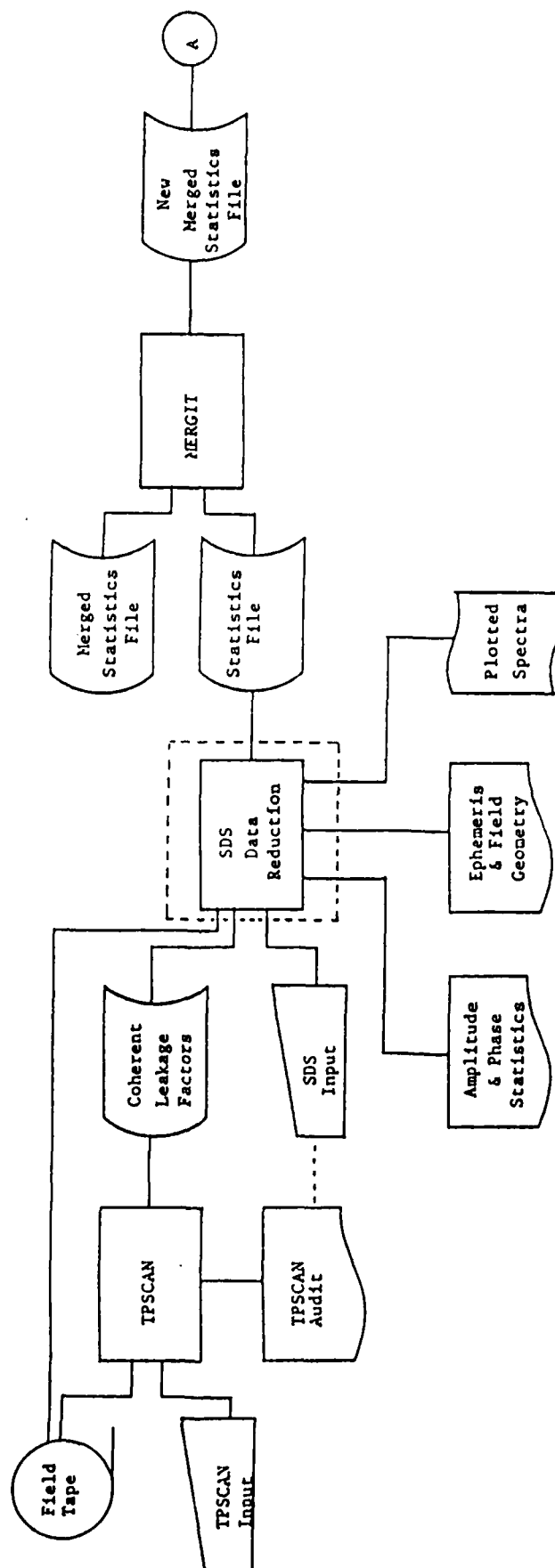


Figure 2.1 SDS Ionospheric Scintillation Data Processing System

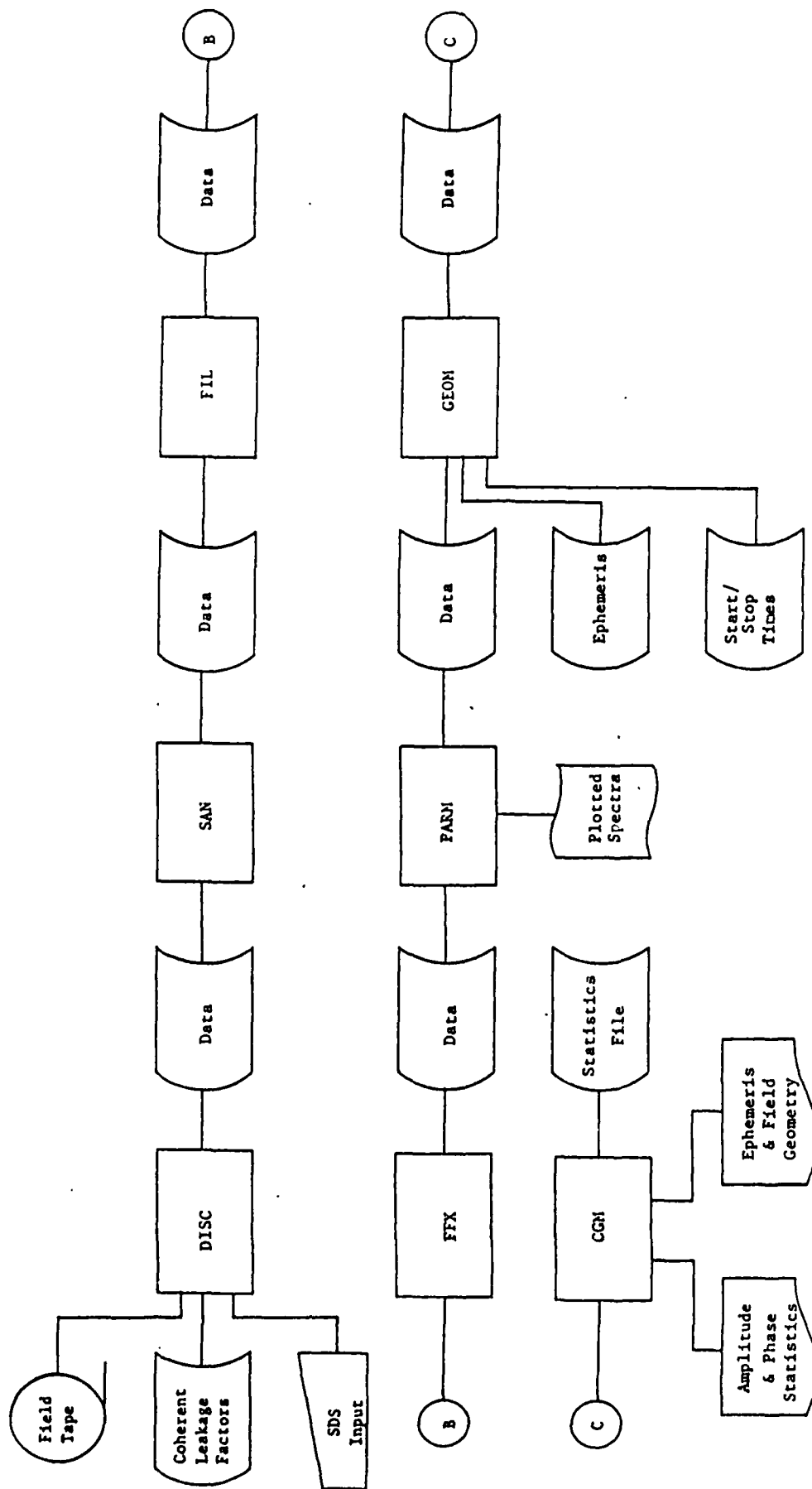


Figure 2.2 SDS Data Reduction System

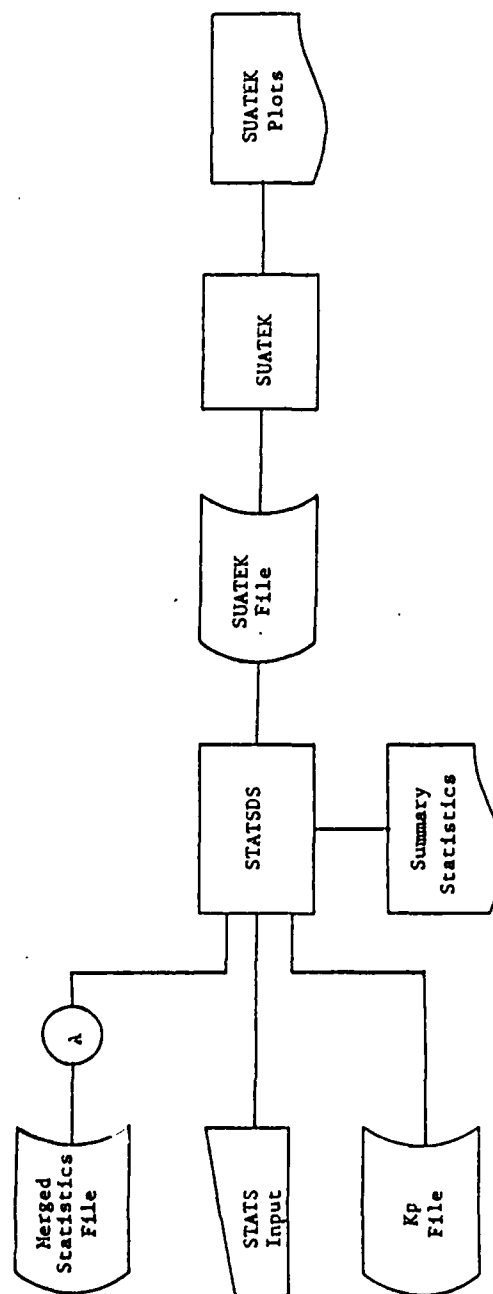


Figure 2.3 SDS Period-end Statistics Processing

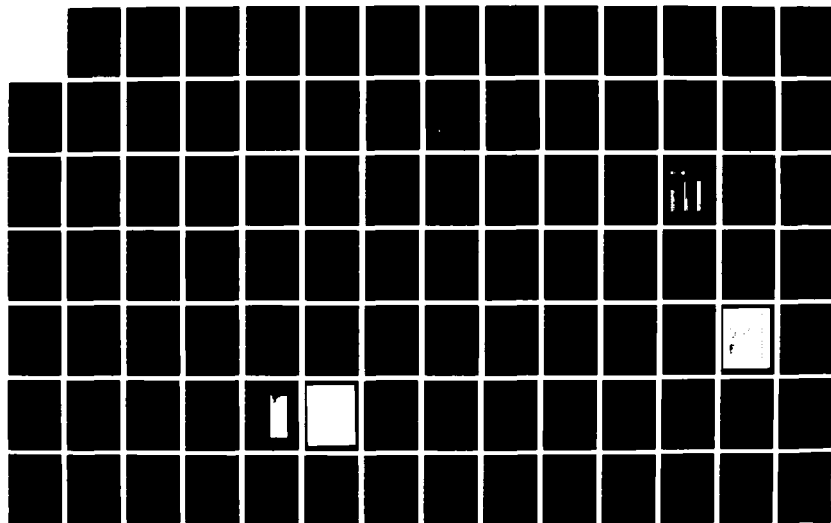
AD-A185 748

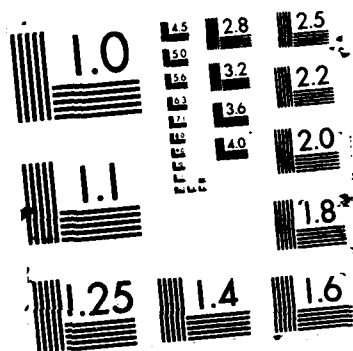
INTEGRATED SYSTEMS WITH APPLICATIONS TO THE
MULTI-PHASES OF THE EPHEMERID. (U) RADEX INC CARLISLE
MA J N BASS ET AL. 27 FEB 87 RX-870227 AFOL-TR-87-0064
F19628-83-C-0134 F/G 4/1

2/3

UNCLASSIFIED

NL





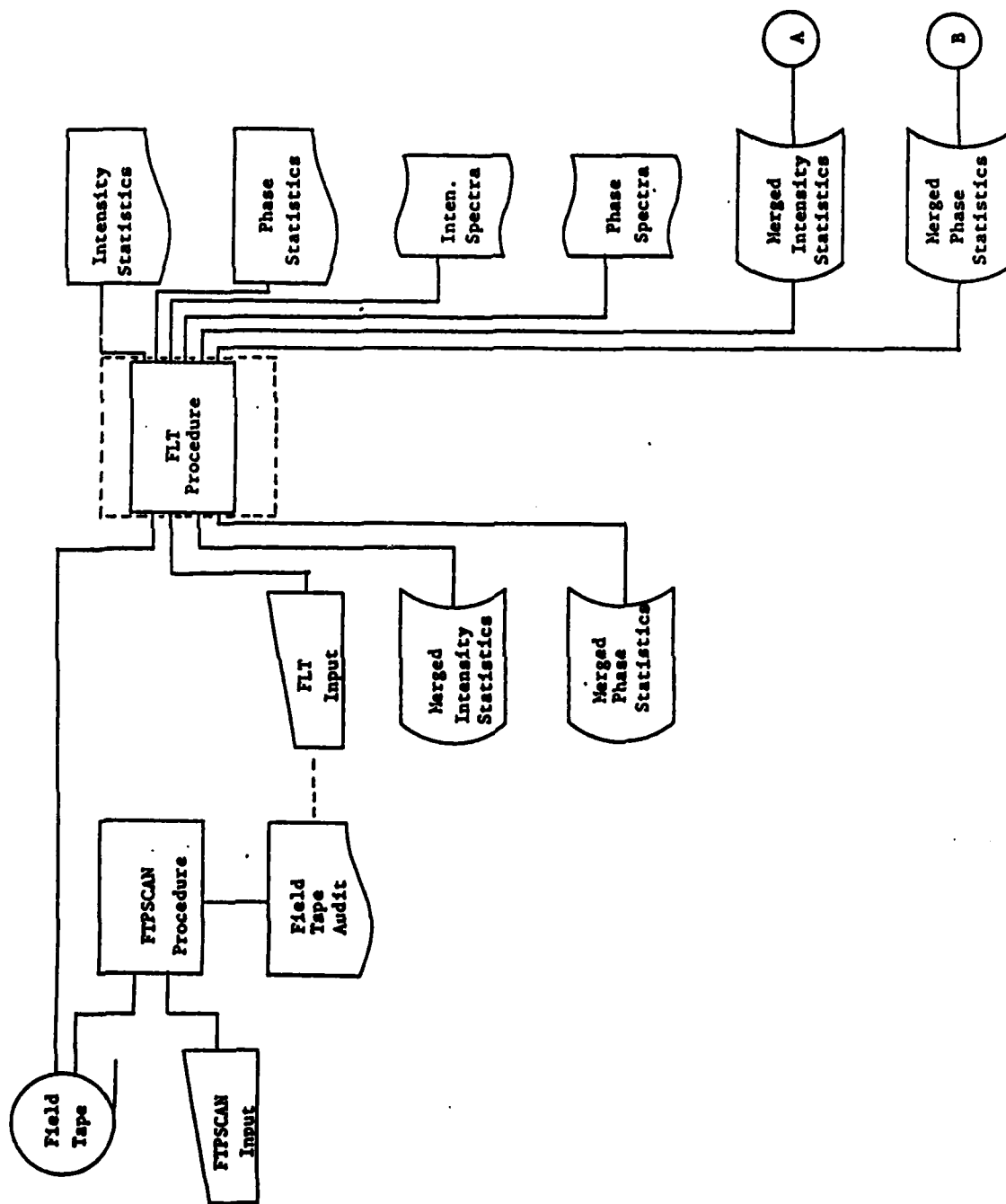


Figure 2.4 FLT Ionospheric Scintillation Data Processing System

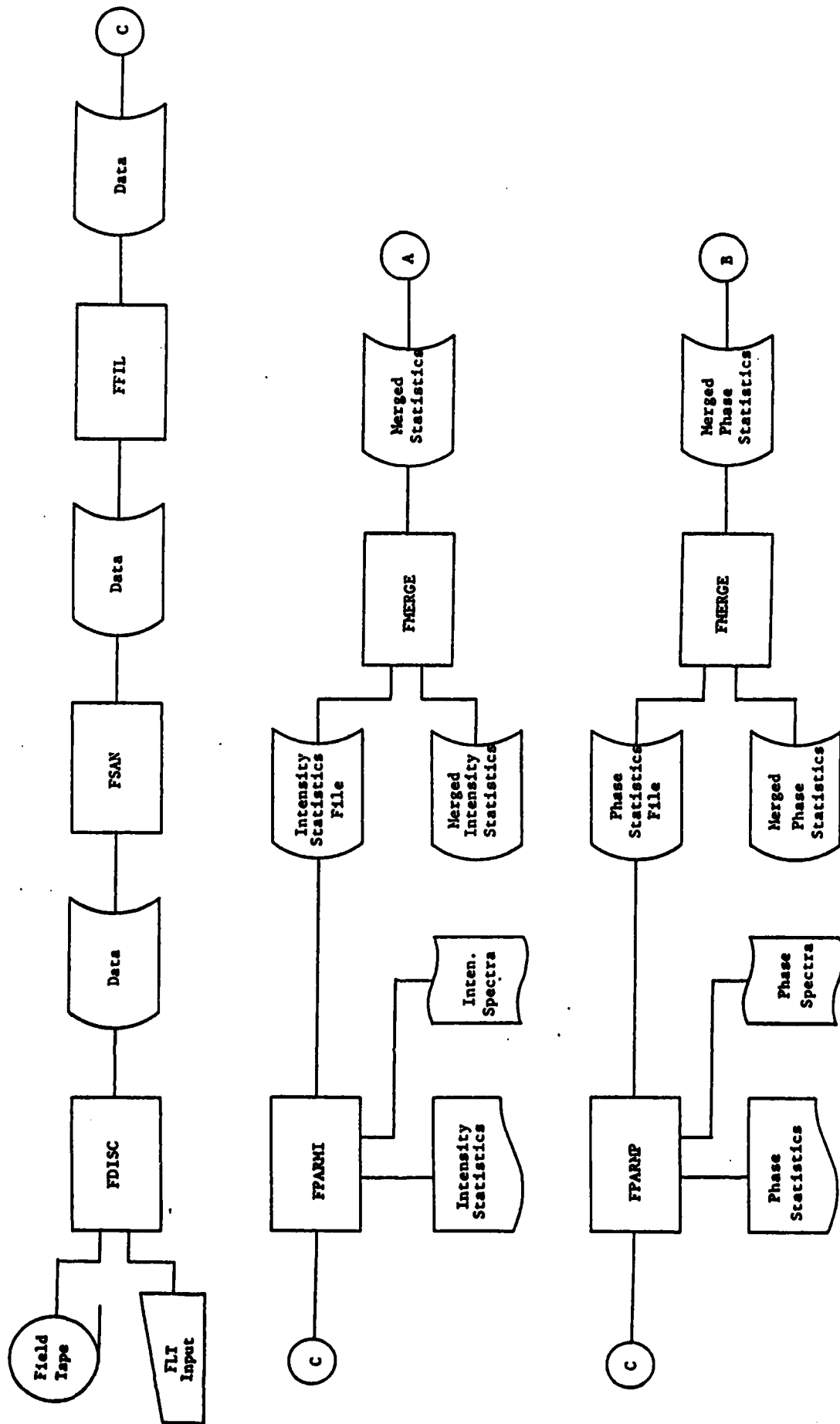


Figure 2.5 FLT Data Reduction System

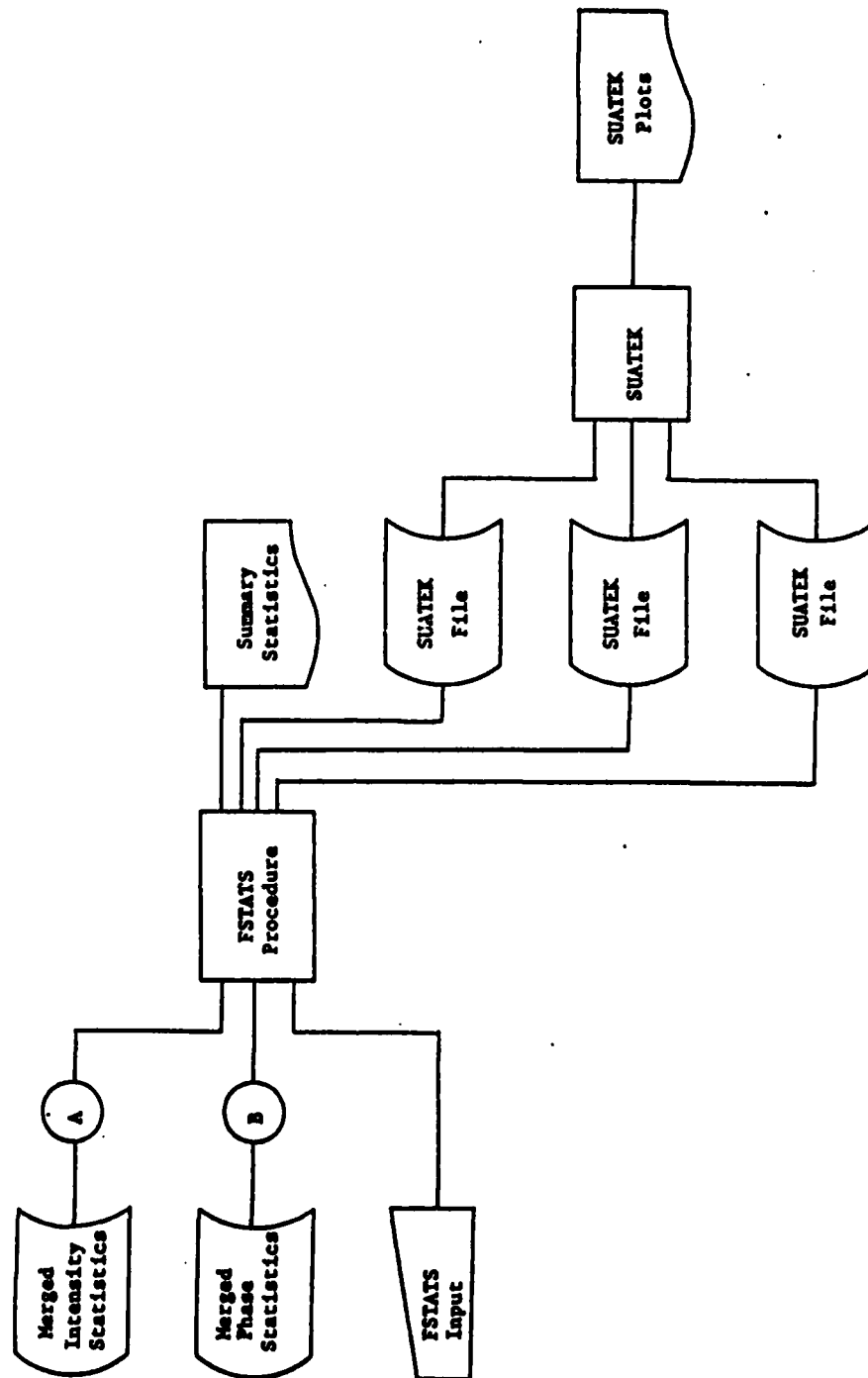


Figure 2.6 FLT Period-End Statistics Processing

2.2 Description of Procedures

Procedures were written to perform all of the SDS and FLT data processing functions (plus some additional functions not previously available, useful in diagnosing anomalous data). Each of the processing functions is now operationally much simpler, and any maintenance and/or program changes are transparent to the user.

2.3 Discrete Fourier Transform Window/MEM Study

The process of Fourier analysis is subject to a number of contaminating effects. To insure reliability of conclusions from the resulting spectra, it is important to minimize the impact of such spurious effects.

Leakage is one of the major contributors to contamination of Fourier spectra. It is a consequence of the fact that, in practice, one deals with data samples of finite length which the Fourier processor treats as being periodic. The computed spectrum then corresponds to that of a finite duration sample repeated periodically from $-\infty$ to $+\infty$. The cause of the leakage effect is the convolution of the rectangular "boxcar" function representing the finite time duration sample with an assumed signal extending from $-\infty$ to $+\infty$. In the frequency domain, the consequence of this effect is that spectral power at one frequency contributes a certain amount of spurious power at other frequencies in addition to whatever power already exists at those frequencies. Depending on the relative magnitudes of the already occurring and spurious power at a given frequency, the computed spectrum may be seriously in error.

Leakage has its most serious impact in those cases in which it is necessary to observe weak contributions at a certain set of frequencies in the presence of relatively high level contributions at nearby frequencies. The contribution of spurious power at one frequency to its neighbor goes as $\sin(x)/x$, where x is proportional to the difference in frequencies. The $1/x$ fall-off implies that nearby neighbors are most severely affected. In the current application, the most serious contamination occurs in the case of very steep roll-offs at relatively low frequencies.

The standard approach to the problem of leakage is the use of window functions.⁽⁴⁾ Their utility lies in their suppressing the magnitude of the artifact discussed above. However, a window is itself an artifact and has its own disadvantage, i.e. the transform of the window function is convolved with the unwindowed spectrum, tending to smear and/or broaden individual features of the resulting spectrum. The result is a loss of spectral resolution. In general, the better a window function suppresses leakage, the poorer the resulting resolution. Hence, a tradeoff is necessary depending on the character of the data being analyzed.

Another, approach is to replace discrete Fourier analysis, with its implicit assumption of periodicity, by the Maximum Entropy Method (MEM).^(5,6) The MEM avoids the assumption of periodicity of the Fourier method.

To assess the effect of different windows on the current application and to make a comparison of the MEM with the windowed DFT, a synthetic signal and Tromso Day 61 were processed by a suite of windows and the MEM. The candidate windows are given in Table 2.4. As a result of this study, and at the request of the initiator, the -74 dB 4 term Blackman-Harris window was implemented in the SDS system as an option.

Table 2.4 DFT Window Candidates

1. No window
2. End matching
3. \cos
4. \cos^2
5. \cos^3
6. \cos^4
7. -92 dB 4 term Blackman-Harris
8. -74 dB 4 term Blackman-Harris
9. 4 sample Kaiser-Bessel
10. Subtract mean

2.4 Statistics Programs

There are two statistics programs which produce period end reports from the merged statistics files, namely STATSDS and STATFLT (See Figures 2.3 and 2.6). STATFLT is an entirely new program, while STATSDS was rewritten to simplify program maintenance. Both programs produce a listing of the accumulated statistics on the merged statistics files and a report summarizing the accumulated statistics for the period of interest. A sample output of the STATSDS program is given in Table 2.5. STATFLT performs a similar function to STATSDS, but for the FLT system. Since there are two separate merged statistics files in this case, one for intensity and one for phase, STATFLT sorts the files by day number and start time and checks for duplicate and/or missing intensity and/or phase records. The output of STATFLT is similar to that of STATSDS.

Table 2.5 Sample STATSDS Output

TROMSO, NOVEMBER 1986 SUMMARY STATISTICS

DAYS 307/86 - 331/86

KP = < 3.5

NUMBER OF RECORDS IN ANALYSIS = 1796

| | 21<GMLT=<3 | | | | | 3<GMLT=<9 | | | | | 9<GMLT=<15 | | | | | 15<GMLT=<21 | | | | | | | | | |
|-----------------------|-----------------|--------|--------|-------|--------|---------------|--------|------|------|--------|-----------------|--------|-------|--------|--------|-----------------|-------|------|-----|------|------------|------|----|-----|------|
| | BIN COUNT = 308 | | | | | BIN COUNT = 2 | | | | | BIN COUNT = 682 | | | | | BIN COUNT = 804 | | | | | | | | | |
| | PERCENTILE | MEAN | ST | DEV | 90TH | PERCENTILE | MEAN | ST | DEV | 90TH | PERCENTILE | MEAN | ST | DEV | 90TH | PERCENTILE | MEAN | ST | DEV | 90TH | PERCENTILE | MEAN | ST | DEV | 90TH |
| RMS PHASE DEVIATION | 2.46 | 3.57 | 2.72 | 1.04 | 2.06 | 2.06 | 2.38 | 2.06 | .45 | 1.08 | 2.07 | 1.39 | 1.32 | 2.37 | 2.94 | 2.52 | | | | | | | | | |
| PHASE SPEC STRENGTH | -24.67 | -17.59 | -24.78 | 6.09 | -35.35 | -33.41 | -35.35 | 2.74 | 2.74 | -29.35 | -21.96 | -28.70 | 5.16 | -24.22 | -17.87 | -24.85 | 5.90 | | | | | | | | |
| PHASE SPEC SLOPE | -2.07 | -2.82 | -2.15 | .30 | -2.69 | -2.91 | -2.69 | .31 | .31 | -2.11 | -2.58 | -2.18 | .31 | -2.05 | -2.55 | -2.13 | .25 | | | | | | | | |
| S4. INT SCINTILLATION | .06 | .13 | .08 | .07 | .05 | .05 | .05 | .05 | .01 | .05 | .09 | .06 | .03 | .05 | .08 | .06 | .03 | | | | | | | | |
| INT SPEC STRENGTH | -40.07 | -33.69 | | | -41.34 | -39.58 | -41.34 | 2.49 | 2.49 | -49.78 | -33.44 | | | -40.59 | -33.83 | | | | | | | | | | |
| INT SPEC SLOPE | -1.59 | -2.83 | -1.77 | 1.76 | -.86 | -1.07 | -.86 | .29 | .29 | -1.79 | -3.48 | -1.85 | 2.11 | 2.11 | -.96 | -2.77 | -1.32 | 3.04 | | | | | | | |
| DECORRELATION TIME | .12 | .02 | .35 | .80 | .05 | .02 | .05 | .04 | .04 | .04 | .02 | .35 | .97 | .97 | .04 | .02 | .25 | .68 | | | | | | | |

KP >= 3.6

NUMBER OF RECORDS IN ANALYSIS = 287

| 21<GMLT=<3 | | | | | 3<GMLT=<9 | | | | | 9<GMLT=<15 | | | | | 15<GMLT=<21 | | | | |
|-----------------------|--------|--------|--------|------|---------------|------|------|------|------|---------------|------|------|------|------|-----------------|------|------|------|------|
| BIN COUNT = 102 | | | | | BIN COUNT = 0 | | | | | BIN COUNT = 0 | | | | | BIN COUNT = 185 | | | | |
| PERCENTILE | MEAN | ST | DEV | 90TH | PERCENTILE | MEAN | ST | DEV | 90TH | PERCENTILE | MEAN | ST | DEV | 90TH | PERCENTILE | MEAN | ST | DEV | 90TH |
| RMS PHASE DEVIATION | 2.35 | 5.13 | 2.83 | 1.39 | 0.00 | 0.00 | 0.00 | 0.00 | 0.00 | 0.00 | 0.00 | 0.00 | 0.00 | 0.00 | 0.00 | 0.00 | 0.00 | 0.00 | 0.00 |
| PHASE SPEC STRENGTH | -22.54 | -15.65 | -23.43 | 6.76 | 0.00 | 0.00 | 0.00 | 0.00 | 0.00 | 0.00 | 0.00 | 0.00 | 0.00 | 0.00 | 0.00 | 0.00 | 0.00 | 0.00 | 0.00 |
| PHASE SPEC SLOPE | -2.03 | -2.63 | -2.12 | .27 | 0.00 | 0.00 | 0.00 | 0.00 | 0.00 | 0.00 | 0.00 | 0.00 | 0.00 | 0.00 | 0.00 | 0.00 | 0.00 | 0.00 | 0.00 |
| S4. INT SCINTILLATION | .07 | .16 | .10 | .08 | 0.00 | 0.00 | 0.00 | 0.00 | 0.00 | 0.00 | 0.00 | 0.00 | 0.00 | 0.00 | 0.00 | 0.00 | 0.00 | 0.00 | 0.00 |
| INT SPEC STRENGTH | -38.78 | -33.08 | -39.96 | 8.55 | 0.00 | 0.00 | 0.00 | 0.00 | 0.00 | 0.00 | 0.00 | 0.00 | 0.00 | 0.00 | 0.00 | 0.00 | 0.00 | 0.00 | 0.00 |
| INT SPEC SLOPE | -1.49 | -2.84 | -1.87 | 1.12 | 0.00 | 0.00 | 0.00 | 0.00 | 0.00 | 0.00 | 0.00 | 0.00 | 0.00 | 0.00 | 0.00 | 0.00 | 0.00 | 0.00 | 0.00 |
| DECORRELATION TIME | .35 | .05 | .69 | .77 | 0.00 | 0.00 | 0.00 | 0.00 | 0.00 | 0.00 | 0.00 | 0.00 | 0.00 | 0.00 | 0.00 | 0.00 | 0.00 | 0.00 | 0.00 |
| | | | | | | | | | | | | | | | | | | | |
| | | | | | | | | | | | | | | | | | | | |
| | | | | | | | | | | | | | | | | | | | |
| | | | | | | | | | | | | | | | | | | | |
| | | | | | | | | | | | | | | | | | | | |
| | | | | | | | | | | | | | | | | | | | |
| | | | | | | | | | | | | | | | | | | | |
| | | | | | | | | | | | | | | | | | | | |
| | | | | | | | | | | | | | | | | | | | |
| | | | | | | | | | | | | | | | | | | | |
| | | | | | | | | | | | | | | | | | | | |
| | | | | | | | | | | | | | | | | | | | |
| | | | | | | | | | | | | | | | | | | | |
| | | | | | | | | | | | | | | | | | | | |
| | | | | | | | | | | | | | | | | | | | |
| | | | | | | | | | | | | | | | | | | | |
| | | | | | | | | | | | | | | | | | | | |
| | | | | | | | | | | | | | | | | | | | |
| | | | | | | | | | | | | | | | | | | | |
| | | | | | | | | | | | | | | | | | | | |
| | | | | | | | | | | | | | | | | | | | |
| | | | | | | | | | | | | | | | | | | | |
| | | | | | | | | | | | | | | | | | | | |
| | | | | | | | | | | | | | | | | | | | |
| | | | | | | | | | | | | | | | | | | | |
| | | | | | | | | | | | | | | | | | | | |
| | | | | | | | | | | | | | | | | | | | |
| | | | | | | | | | | | | | | | | | | | |
| | | | | | | | | | | | | | | | | | | | |
| | | | | | | | | | | | | | | | | | | | |
| | | | | | | | | | | | | | | | | | | | |
| | | | | | | | | | | | | | | | | | | | |
| | | | | | | | | | | | | | | | | | | | |
| | | | | | | | | | | | | | | | | | | | |
| | | | | | | | | | | | | | | | | | | | |
| | | | | | | | | | | | | | | | | | | | |
| | | | | | | | | | | | | | | | | | | | |
| | | | | | | | | | | | | | | | | | | | |
| | | | | | | | | | | | | | | | | | | | |
| | | | | | | | | | | | | | | | | | | | |
| | | | | | | | | | | | | | | | | | | | |
| | | | | | | | | | | | | | | | | | | | |
| | | | | | | | | | | | | | | | | | | | |
| | | | | | | | | | | | | | | | | | | | |
| | | | | | | | | | | | | | | | | | | | |
| | | | | | | | | | | | | | | | | | | | |
| | | | | | | | | | | | | | | | | | | | |
| | | | | | | | | | | | | | | | | | | | |
| | | | | | | | | | | | | | | | | | | | |
| | | | | | | | | | | | | | | | | | | | |
| | | | | | | | | | | | | | | | | | | | |
| | | | | | | | | | | | | | | | | | | | |
| | | | | | | | | | | | | | | | | | | | |
| | | | | | | | | | | | | | | | | | | | |
| | | | | | | | | | | | | | | | | | | | |
| | | | | | | | | | | | | | | | | | | | |
| | | | | | | | | | | | | | | | | | | | |
| | | | | | | | | | | | | | | | | | | | |
| | | | | | | | | | | | | | | | | | | | |
| | | | | | | | | | | | | | | | | | | | |
| | | | | | | | | | | | | | | | | | | | |
| | | | | | | | | | | | | | | | | | | | |
| | | | | | | | | | | | | | | | | | | | |
| | | | | | | | | | | | | | | | | | | | |
| | | | | | | | | | | | | | | | | | | | </ |

* 10TH PERCENTILE FOR PHASE SPECTRAL SLOPE, INTENSITY SPECTRAL SLOPE, AND DECORRELATION TIME.

TOTAL NUMBER OF RECORDS = 2226
 TOTAL NUMBER OF RECORDS ELIMINATED = 143
 TOTAL NUMBER OF FIELDS ELIMINATED = 0
 NUMBER OF DUPLICATE RECORDS ELIMINATED = 110
 NUMBER OF RECORDS ELIMINATED DUE TO TIME DIFFERENCE BETWEEN SUCCESSIVE RECORDS < 160 SECONDS = 25
 NUMBER OF RECORDS ELIMINATED DUE TO RMS PHASE DEVIATION > 50. = 0
 NUMBER OF RECORDS ELIMINATED DUE TO S4 > 1.4 = 0
 NUMBER OF RECORDS ELIMINATED DUE TO RMS PHASE DEVIATION/S4 > 25. AND S4 >= 0.2 = 8
 NUMBER OF FIELDS ELIMINATED DUE TO PHASE SPECTRAL SLOPE < -5. = 0
 NUMBER OF FIELDS ELIMINATED DUE TO PHASE SPECTRAL STRENGTH < -60. = 0

Table 2.5 (Cont.) Sample STATSDS Output

TROMSO, NOVEMBER 1986 SUMMARY STATISTICS

. DAYS 307/86 - 331/86

ALL KP

NUMBER OF RECORDS IN ANALYSIS = 2083

| | 21<GMLT=<3 | | | | 3<GMLT=<9 | | | | 9<GMLT=<15 | | | | 15<GMLT=<21 | | | |
|----------------------|-----------------|--------|---------------|------|-----------------|--------|-----------------|------|-----------------|--------|-----------------|------|-----------------|--------|-----------------|------|
| | BIN COUNT = 410 | | BIN COUNT = 2 | | BIN COUNT = 682 | | BIN COUNT = 989 | | BIN COUNT = 682 | | BIN COUNT = 989 | | BIN COUNT = 989 | | BIN COUNT = 989 | |
| | PERCENTILE | MEAN | ST | DEV | PERCENTILE | MEAN | ST | DEV | PERCENTILE | MEAN | ST | DEV | PERCENTILE | MEAN | ST | DEV |
| | 50TH | 90TH | | | 50TH | 90TH | | | 50TH | 90TH | | | 50TH | 90TH | | |
| RMS PHASE DEVIATION | 2.42 | 3.61 | 2.75 | 1.14 | 2.06 | 2.38 | 2.06 | .45 | 1.08 | 2.07 | 1.39 | 1.32 | 2.39 | 3.07 | 2.55 | .98 |
| PHASE SPEC STRENGTH | -23.96 | -16.82 | -24.44 | 6.28 | -35.35 | -33.41 | -35.35 | 2.74 | -29.35 | -21.96 | -28.70 | 5.16 | -24.09 | -17.76 | -24.71 | 5.93 |
| PHASE SPEC SLOPE | -2.06 | -2.62 | -2.15 | .29 | -2.69 | -2.91 | -2.89 | .31 | -2.11 | -2.58 | -2.18 | .31 | -2.05 | -2.55 | -2.14 | .26 |
| S4 INT SCINTILLATION | .08 | .14 | .08 | .07 | .05 | .05 | .05 | .01 | .05 | .09 | .06 | .03 | .05 | .10 | .06 | .04 |
| INT SPEC STRENGTH | -39.74 | -33.51 | | | -41.34 | -39.58 | -41.34 | 2.49 | -48.78 | -33.44 | | | -40.15 | -32.47 | | |
| INT SPEC SLOPE | -1.53 | -2.76 | -1.74 | 1.62 | -1.86 | -1.07 | -1.86 | .29 | -1.79 | -3.48 | -1.85 | 2.11 | -1.03 | -2.60 | -1.35 | 2.86 |
| DECORRELATION TIME | .18 | .02 | .44 | .81 | .05 | .02 | .05 | .04 | .04 | .02 | .35 | .97 | .08 | .02 | .27 | .64 |

* 10TH PERCENTILE FOR PHASE SPECTRAL SLOPE, INTENSITY SPECTRAL SLOPE, AND DECORRELATION TIME.

TOTAL NUMBER OF RECORDS = 2226
 TOTAL NUMBER OF RECORDS ELIMINATED = 143
 TOTAL NUMBER OF FIELDS ELIMINATED = 0
 NUMBER OF DUPLICATE RECORDS ELIMINATED = 110
 NUMBER OF RECORDS ELIMINATED DUE TO TIME DIFFERENCE BETWEEN SUCCESSIVE RECORDS < 168 SECONDS = 25
 NUMBER OF RECORDS ELIMINATED DUE TO RMS PHASE DEVIATION > 80. = 0
 NUMBER OF RECORDS ELIMINATED DUE TO S4 > 1.4 = 0
 NUMBER OF RECORDS ELIMINATED DUE TO RMS PHASE DEVIATION/S4 > 25. AND S4 > 0.2 = 8
 NUMBER OF FIELDS ELIMINATED DUE TO PHASE SPECTRAL SLOPE < -8. = 0
 NUMBER OF FIELDS ELIMINATED DUE TO PHASE SPECTRAL STRENGTH < -60. = 0

2.5 SDS Scintillation Processing System User's Guide

The SDS Scintillation Processing System, originally developed by Stanford Research Institute International, is used in order to process radio wave scintillation data collected using transmissions from beacons on board satellites. Procedures that are needed to acquire the field tapes, and the subsequent processing for plots, statistics, and evaluation are described.

2.5.1 Introduction

It is the intent of this document to describe the input necessary to run the various processing capabilities of the SDS Scintillation Processing System. It is not the intent of this document to describe in detail the mathematical computations involved. For those details, the reader is referred to Reference 2.

All of the SDS processing functions are now handled by NOS procedures. Hopefully, this will provide for ease of use by the user. A description of the input necessary to run the SDS Scintillation Processing System follows.

2.5.2 SDS Tape Scan

Field tapes are submitted first to the TPSCAN procedure, which provides a printed listing of the contents of the files on that tape. Figure 2.7 is a typical tape scan output. The start and end times for one file have been identified. The TPSCAN program also writes a file, TAPE19, which may be SAVED for use in later processing. The TAPE19 file contains information used in removing an unwanted receiver artifact

| FILE 1 | 675 | 1 | 67 | 105 | 3:33.5 | 105 | 4 | 0:57 | 1215F409 | RECORDS 1 | IMPROUGH | 475 |
|--------------------------|----------------------|---|----|-----|--------|-----------------|---------|----------|-----------|-----------|----------------|-----|
| (CALIBRATION FILE 2) | | | | | | | | | | | | |
| 1 EMPTY FILES | | | | | | | | | | | | |
| PROBLEM CODE | TIME STEP 6T 6 SEC:6 | | | | | REPEATED TIME:R | | | | | PARITY ERROR:P | |
| 14655. | 0 | 0 | 0 | 0 | 0 | 0 | 0 | 0 | 0 | 0 | 0 | 0 |
| 14823. | 0 | 0 | 0 | 0 | 0 | 0 | 0 | 0 | 0 | 0 | 0 | 0 |
| 14991. | 0 | 0 | 0 | 0 | 0 | 0 | 0 | 0 | 0 | 0 | 0 | 0 |
| 15159. | 0 | 0 | 0 | 0 | 0 | 0 | 0 | 0 | 0 | 0 | 0 | 0 |
| 15327. | 0 | 0 | 0 | 0 | 0 | 0 | 0 | 0 | 0 | 0 | 0 | 0 |
| 15495. | 0 | 0 | 0 | 0 | 0 | 0 | 0 | 0 | 0 | 0 | 0 | 0 |
| 15663. | 0 | 0 | 0 | 0 | 0 | 0 | 0 | 0 | 0 | 0 | 0 | 0 |
| 15831. | 0 | 0 | 0 | 0 | 0 | 0 | 0 | 0 | 0 | 0 | 0 | 0 |
| 15999. | 0 | 0 | 0 | 0 | 0 | 0 | 0 | 0 | 0 | 0 | 0 | 0 |
| 16167. | 0 | 0 | 0 | 0 | 0 | 0 | 0 | 0 | 0 | 0 | 0 | 0 |
| 16335. | 0 | 0 | 0 | 0 | 0 | 0 | 0 | 0 | 0 | 0 | 0 | 0 |
| 16503. | 0 | 0 | 0 | 0 | 0 | 0 | 0 | 0 | 0 | 0 | 0 | 0 |
| 16671. | 0 | 0 | 0 | 0 | 0 | 0 | 0 | 0 | 0 | 0 | 0 | 0 |
| 16839. | 0 | 0 | 0 | 0 | 0 | 0 | 0 | 0 | 0 | 0 | 0 | 0 |
| 17007. | 0 | 0 | 0 | 0 | 0 | 0 | 0 | 0 | 0 | 0 | 0 | 0 |
| 17175. | 0 | 0 | 0 | 0 | 0 | 0 | 0 | 0 | 0 | 0 | 0 | 0 |
| 17343. | 0 | 0 | 0 | 0 | 0 | 0 | 0 | 0 | 0 | 0 | 0 | 0 |
| 17511. | 0 | 0 | 0 | 0 | 0 | 0 | 0 | 0 | 0 | 0 | 0 | 0 |
| 17679. | 0 | 0 | 0 | 0 | 0 | 0 | 0 | 0 | 0 | 0 | 0 | 0 |
| 17847. | 0 | 0 | 0 | 0 | 0 | 0 | 0 | 0 | 0 | 0 | 0 | 0 |
| FILE 4 | 416 | 1 | 67 | 105 | 4:4:15 | 105 | 4:59:51 | 1215F409 | RECORDS 1 | IMPROUGH | 413 | |
| 2 EMPTY FILES | | | | | | | | | | | | |
| mode start time end time | | | | | | | | | | | | |

Figure 2.7: A Typical Scan Output

from the intensity and phase spectra (See Reference 7).
Input to TPSCAN consists of the visual serial number (VSN) of the tape.

Input to TPSCAN:

| Card | Columns | Description |
|------|---------|-------------------|
| 1 | 1-6 | VSN of field tape |

A sample deck setup is shown in Figure 2.8. This deck is available as CCSDS1/UN=BRYANTW.

```
<TOP OF FILE>
BRYANT,T=700.  SDS TAPE SCAN
USER,BRYANTW,BRYANTW.
CHARGE,5501,4643.
GET,PROCFIL/UN=BRYANTW.
LABEL,TAPE1.VSN=M91,WT.D=PE.F=S,LB=KU,PO=R.
BEGIN.TPSCAN,,T194044.
EXIT.
EOR
TR4044
<BOTTOM OF FILE>
```

Figure 2.8: An Example of Deck Setup for Tape Scan

2.5.3 Normal SDS Processing

A complete description of the data processing involved in normal SDS processing is given in Reference 2. Briefly, the data are read from a field tape, are unpacked and reduced. The reduced data is spectrum analyzed and various statistics are calculated. The output of the normal SDS processing procedure consists of a printed listing of the statistics for the files and time periods of interest. Plots of intensity and phase spectra are produced. Either micro-fiche or penplots are available. Finally, the calculated statistics are written to TAPE3 which may be SAVED for later processing (See Sections 2.5.4 and 2.5.5).

Input for Normal SDS Processing:

| Card | Description |
|------|--|
| 1 | VSN of field tape |
| 2 | file, station #, channel, year, window option. |
| 3 | start time (day number, hour, minute, second) |
| 4 | end time (day number, hour, minute, second) |

The file is the actual file number from a tape scan run.

The station numbers are as follows:

| Station # | Location |
|-----------|-----------|
| 2 | Goose Bay |
| 3 | Thule |
| 4 | Tromso |
| 5 | Malvik |

Set the window option=0 for no windowing, or window option=1 for the -74 dB 4-term Blackman-Harris window (See Reference 4). All quantities are INTEGER and in free format (i.e. list directed format), except for VSN which is alphanumeric.

Input for multiple file processing should be separated by end of record marks (EORs). The default medium for SDS plots is microfiche. Pen plots may be obtained by specifying PEN=YES on the BEGIN,SDS statement (i.e. BEGIN,SDS,,PEN=YES). A sample deck setup is given in Figure 2.9. This deck is available as CCSDS2/UN=BRYANTW.

2.5.4 Merging SDS Data Files

The TAPE3 data files saved during normal SDS processing may be merged using the MERGIT procedure. The easiest way to do this is to run the MERGIT procedure interactively. An example of this is given in Figure 2.10. The user's typeins have been underlined in Figure 2.10. Note that the user must GET the procedure file PROCFIL/UN=BRYANTW before executing the procedure MERGIT.

2.5.5 End of the Month Statistics

End of the month statistics on the merged data files are produced by the STATS procedure. A listing of the data on the merged file is produced along with the report shown in Figure 2.11. A plot file suitable for plotting by SUATEK is also produced. This plot file contains geomagnetic local time, Kp, rms phase deviation, phase spectral slope, phase spectral strength, S4, intensity spectral slope, intensity spectral strength, decor- relation time, log10(decorrelation time), and a day/night indicator. Day is considered to be geomagnetic local time between the hours of 0900 to 2100.

```

<TOP OF FILE>
BRYANT.T=1500.  NORMAL SDS PROCESSING
USER.BRYANTU,BRYANTU.
CHARGE.5501,4643.
GET,PROCFIL/UN=BRYANTU.
GET.TAPE19=T194044/UN=BRYANTU.
LABEL,TAPE7,USN=M91,NT,D=PE,F=S,LB=KU,P0=R.
BEGIN.SDS.
REPLACE.TAPE3=T4044F1.
BEGIN.SDS.
REPLACE.TAPE3=T4044F4.
BEGIN.SDS.
REPLACE.TAPE3=T4044F7.
EXIT.
END
TR4044
1.4.1.84
61.21.31.0
62.1.10.44
END
TR4044
4.4.1.84
62.9.15.52
62.13.14.48
END
TR4044
7.4.1.84
62.21.31.13
63.1.10.49
<BOTTOM OF FILE>

```

Figure 2.9: An Example of Deck Setup for Normal SDS Processing

get.procfil/un=brvantu
/begin,mergit

WELCOME TO THE SDS MERGING PROCEDURE.

Enter PFN2 SDS FILE NAME TO BE MERGED? T4044F1
Enter PFN3 SDS OR OLD MERGED FILE NAME ? T4044F4
Enter PFN4 NEW MERGED FILE NAME? T4044
15.17.31. USER DAYFILE PROCESSED.
15.17.31.COMMENT. *****
15.17.31.COMMENT. * SDS MERGING PROCEDURE *
15.17.31.COMMENT. *****
15.17.31.BEGIN,GETPFN,,T4044F1.
15.17.33.IF,%0%.EQ.%0%,LABEL1.
15.17.33.GET,T4044F1/NA.
15.17.33.ELSE,LABEL1.
15.17.33.ENDIF,LABEL1.
15.17.34.IF,FILE(T4044F1,AS).REVERT.
15.17.34.REVERT.
15.17.34.RENAME,TAPE2=T4044F1.
15.17.34.BEGIN,GETPFN,,T4044F4.
15.17.35.IF,%0%.EQ.%0%,LABEL1.
15.17.35.GET,T4044F4/NA.
15.17.36.ELSE,LABEL1.
15.17.36.ENDIF,LABEL1.
15.17.36.IF,FILE(T4044F4,AS).REVERT.
15.17.36.REVERT.
15.17.36.RENAME,TAPE3=T4044F4.
15.17.36.GET,MERGITB/UN=BRYANTU.
15.17.36.MERGITS.
15.17.40. CH LWA+1 = 20711B, LOADER USED 36400B
15.17.41.***KEY EXTRACTION USED
15.17.43. ** INSERTIONS DURING INPUT *****0
15.17.43. ** DELETIONS DURING INPUT *****0
15.17.43. ** TOTAL RECORDS SORTED *****158
15.17.43. ** INSERTIONS DURING OUTPUT *****0
15.17.43. ** DELETIONS DURING OUTPUT *****0
15.17.43. ** TOTAL RECORDS OUTPUT *****158
15.17.43. ** MERGE ORDER USED *****11
15.17.43. **END SORT RUN
15.17.43. END MERGIT
15.17.43. 050200 MAXIMUM EXECUTION FL.
15.17.43. 0.099 CP SECONDS EXECUTION TIME.
15.17.43.RENAME,T4044=TAPE4.
15.17.44.SAVEDI,T4044.
15.17.45.REPLACE,T4044.
15.17.46.REVERT. SAVE (INDIRECT)
15.17.46.CHANGE,T4044/CT=PU.
15.17.46.DAYFILE.
0REVERT.CCL

Figure 2.10: An Example of the Interactive Use of the MERGIT Procedure

06/89 - 06/19 SATU .

[illegible]

TOTAL NUMBER OF RECORDS - 231

167 0 50874 4 32600 7101

TOTAL NUMBER OF FILES ELIMINATED -

SECRET

NUMBER OF PERSONS ESTIMATED TO HAVE BEEN EXPOSED TO THE DUST

[illegible]

NUMBER OF RECORDS ELIMINATED DUE TO SA > 1.0 = 0

ALL INFORMATION CONTAINED HEREIN IS UNCLASSIFIED
DATE 07-11-2008 BY 60322 UCBAW

POWER OF FIELDY CLIMATIZED BY TO PHASE SPECTRAL SLOPE - 5.0

SECRET

CONFIDENTIAL

Continuation of previous fig.

1877

100

Continuation of previous Fig.

Input to the STATS procedure consists of a title card:

| Card | Columns | Description |
|------|---------|-------------|
| 1 | 1-80 | Title |

An example of a deck setup is given in Figure 2.12. This deck is available as CCSDS3/UN=BRYANTW.

2.5.6 SDS Time Series Plots

It is possible to obtain pen plots of the time series at any point in the normal SDS processing cycle (see Reference 2) using the SDSPLOT procedure. Time series plots can be obtained after processing by DISC, SAN, FIL, or FFX. The default is FIL. Figure 2.13 shows a typical time series plot after processing by FIL. Input to the SDSPLOT procedure consists of the normal SDS processing input (Section 2.5.3) plus two other parameters, the number of seconds per inch and the maximum absolute value for phase.

Input to SDSPLOT procedure:

Record 1 - Normal SDS input (see Section 2.5.3)

| Record 2 - Card | Description |
|-----------------|--------------|
| 1 | SCPRIN, PMAX |

where SCPRIN is seconds per inch, and PMAX is maximum absolute value for phase. Both quantities are REAL and in free format (i.e. list directed). An example of a deck setup for SDS time series plots is given in Figure 2.14. This deck is available as CCSDS4/UN=BRYANTW.

```
<TOP OF FILE>  
BRYANT.  SDS STATISTICS  
USER.BRYANTU.BRYANTU.  
CHARGE,5501.4643.  
SET,PROCFIL/UN=BRYANTU.  
BEGIN.STATS.,T4044.SUA4044.  
EXIT.  
EOR  
TROMSO TEST CASE  
<BOTTOM OF FILE>
```

Figure 2.12 Example of Deck Setup for End of the Month Statistics

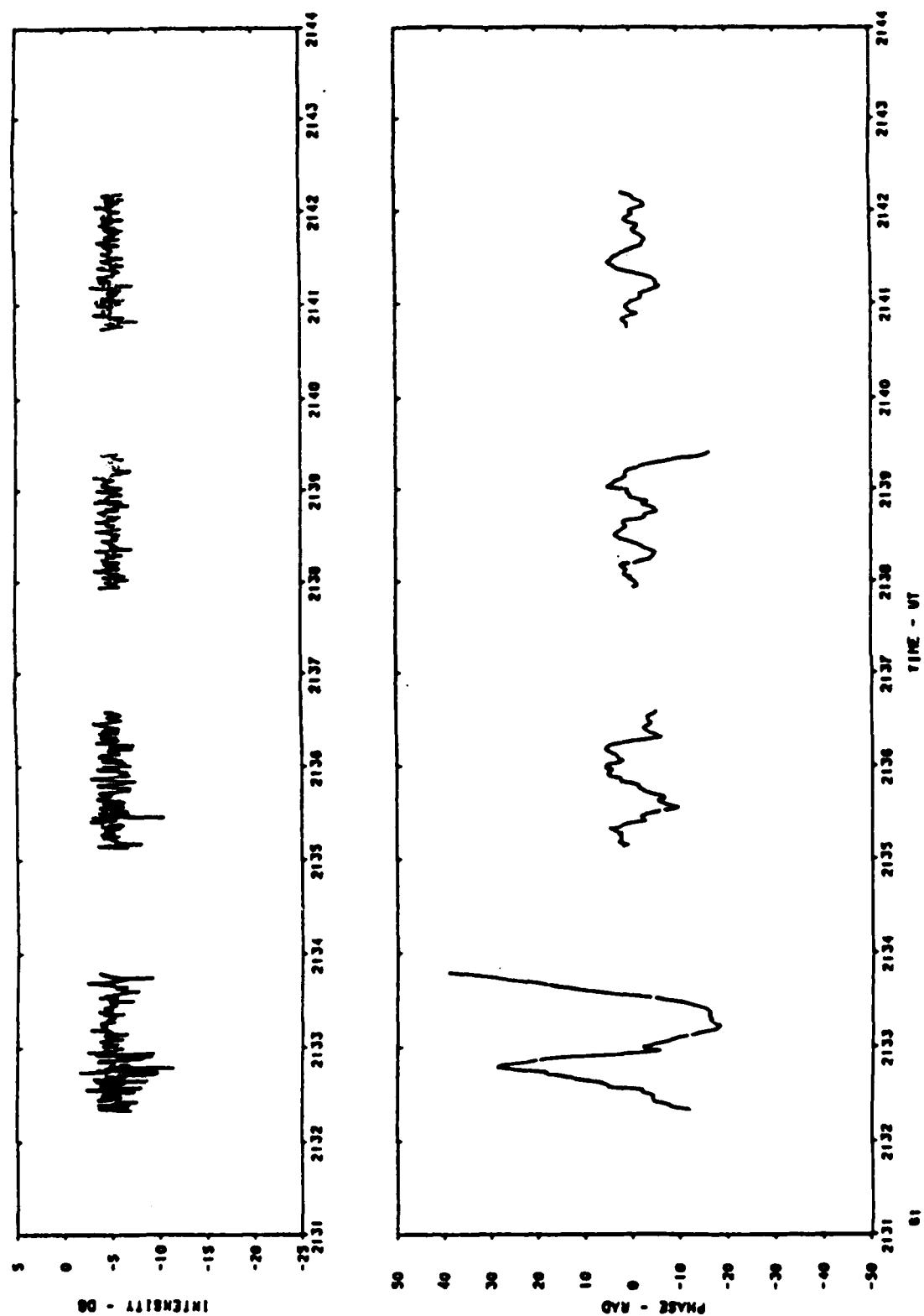


Figure 2.13 Typical SDS Time Series Plot after Processing by FIL

2.5.7 Dumping SDS Field Tapes

It is possible to examine the data on SDS field tapes using the SDSDUMP procedure. The data are converted to intensity and phase, but no detrending or correction for receiver artifacts has been applied. Input to the SDSDUMP procedure consists of the normal SDS input (See Section 2.5.3). An example of a deck setup for SDSDUMP is given in Figure 2.15. This deck is available as CCSDS5/UN=BRYANTW. Bear in mind when dumping files that each 8 second time block produces 2 pages of output.

```
<TOP OF FILE>
BRYANT.  SDS TIME SERIES PLOTS
USER,BRYANTW,BRYANTW.
CHARGE,5504,6670.
GET,PROCFIL/UN=BRYANTW.
GET,TAPE19=T194044/UN=BRYANTW.
LABEL.TAPE7.VSN=M91,NT,D=PE,F=S,LB=KU,PO=R.
BEGIN,SDSPLOT,,FIL.
EXIT.
EOR
TK4044
1,4.1,84
61,21,31.0
61,21.43.0
EOR
60.,50.
<BOTTOM OF FILE>
```

Figure 2.14 **An Example of Deck Setup for SDS Time Series Plots**

References

1. Basu, Sunanda, Basu, S., Mackenzie, E., and Whitney, H.E. "Morphology of the Phase and Intensity Scintillations in the Auroral Oval and Polar Cap", Radio Science, Vol. 20, No. 3, pp. 347-356, May-June 1985.
2. Roberts, F. R., "Software for Processing Scintillation Data from Satellites in Eccentric Orbits", Private Communication, April 7, 1983.
3. Basu, Sunanda, Basu, S., Livingston, R.C., Mackenzie, E., and Whitney, H.E. "Phase and Amplitude Scintillation Statistics at 244 MHz from Goose Bay Using a Geostationary Satellite", AFGL-TR-82-0222, 28 March 1986. ADA124291
4. Harris, Frederic J. "On the Use of Windows for Harmonic Analysis with the Discrete Fourier Transform," Proceedings of the IEEE, Vol. 66, No. 1, pp. 51-83, November 1981.
5. Burg, J.P., "Maximum Entropy Spectral Analysis," Proceedings of the 37th Meeting of the Society of Exploration Geophysicists (Oklahoma City, Oklahoma), October 31, 1967.
6. Fougere, P.F., "On the Accuracy of Spectrum Analysis of Red Noise Processes Using Maximum Entropy and Periodogram Methods: Simulation Studies and Application to Geophysical Data," Journal of Geophysical Research, Vol. 90, No.A5, pp. 4355-4366, May 1, 1985.
7. Bass, J. N., and Roberts, F. R., "Artifacts in SPA Observations of Radio Wave Scintillations", AFGL-TR-84-0066, Analysis and Programming for Research in the Physics of the Upper Atmosphere, February 1984, ADA144203.

3.0 Study of Magnetic Fields

AFGL's research emphasizes investigations of the ionosphere and magnetosphere. In this environment Earth's magnetic field is recognized as a key controller in the global distribution and movement of particles, including pitch angle dependencies, mirroring, drift, and dissipation. At AFGL, research is sponsored on satellites such as DMSP, SCATHA and CRRES, where experimental instruments measure the particle environment and plasma interactions. This chapter describes the installation and investigation of magnetic field models for support of related AFGL research.

3.1 Magnetic Field Models

Below a few earth radii, Earth's internal magnetic field is the predominant component. The internal field is represented through the magnetic field potential V which, at any point in space, is expressed in a spherical harmonic expansion:

$$V = a \sum_{n=1}^N \left(\frac{a}{r}\right)^{n+1} \sum_{m=0}^n (g_n^m \cos m\phi + h_n^m \sin m\phi) P_n^m(\sin \lambda)$$

where

a = radius of earth, ϕ = longitude, λ = latitude

and

$P_n^m(\sin \lambda)$ = associated Legendre polynomial

The vector components of the field at the point of interest are given by:

$$B_r = -\frac{\delta V}{\delta r} = -Z \quad (\text{the vertical field component})$$

$$B_\lambda = -B_\theta = -\frac{1}{r} \frac{\delta V}{\delta \lambda} = +X \quad (\text{the North field component})$$

$$B_\phi = \frac{1}{r \sin \lambda} \frac{\delta V}{\delta \phi} = +Y \quad (\text{the East field component})$$

The external magnetic field modifies the internal field further from Earth. Since this contribution is due to ring, tail, and magnetopause currents, it must be expressed in solar oriented coordinates.

The Earth-centered dipole magnetic field, based on a $1/r^2$ potential, is the simplest but still useful representation. The Mead⁽¹⁾ model adds a symmetric compression as well as a single azimuthally asymmetric term to the dipole field, and the Mead-Williams⁽²⁾ model includes a term for tail currents; they are suitable for qualitative studies of the outer zone. Full scale models may be static, ie. with no model for geomagnetic variations, such as the Olson-Pfitzer BFLD⁽³⁾ model used for SCATHA studies; or they may allow variations due to geomagnetic activity, eg. the Tsyganenko-Usmanov⁽⁴⁾ model.

3.2 Magnetic Field Package MFP

More than 10 years ago, AFGL/LCY developed and integrated a geomagnetic field package⁽⁵⁾ MFP, for general use at the Lab. The routines provide B and L values, and are capable of field line tracing. A spherical harmonic field model such as GSFC or IGRF is input as Gauss normalized coefficients representing the zonal and tesseral harmonics. This package has served most of the lower altitude research needs, where the external field is negligible. It has the capability of calculating, for a given geodetic or geocentric position:

- Field components including total field
- Field at equator crossing & conjugate point
- L-shell value
- Latitude & longitude of conjugate point
- Coordinates & field values at North & South crossings of a specified altitude

A separate routine LINTRA performs the field line tracing to specified altitudes, using routine FIELD from FIELDG, but is not used for L-shell calculations.

3.3 Magnetic Field Package BFLD

The magnetic field code BFLD was developed by Aerospace Corp. primarily for the SCATHA satellite orbit environment. It contains the Barraclough⁽³⁾ model, epoch 1975, for the main internal field, and an Olson-Pfitzer model for the field due to external currents. The external field is calculated using coefficients that are functions of the dipole tilt, and this routine BXYZMU is called only beyond 2 Re. For determining L-shell, field lines are traced to the conjugate point using a Runge Kutta 4th order method, and the invariant integral I is computed using Simpson's rule. L is then empirically computed from I and the magnetic field strength.

3.4 Magnetic Field Package Tsyganenko-Usmanov Model

Coordinate Systems and Rotations

The T-U model adds Kp dependence to the Ring, Tail, and Magnetopause contributions of the external field. These components are formulated in different coordinate systems, all Earth centered. Therefore, the program initially calculates the rotation matrix transformations that will be applicable. Five basic coordinate systems and two aberrated (optional) systems are involved:

Tsyganenko-Usmanov Model (cont'd)

| <u>Coordinate System</u> | <u>Primary Axis</u> | <u>Secondary Axis</u> |
|------------------------------|--|--|
| Geographic (G) | x: Greenwich, Uniform, precession | z: North free rotation assumed |
| Dipole (D) | z_d : N mag. pole. | x_d : Geog. meridian of N. Mag. pole |
| Celestial (C) | z_c : North (=z), | x_c : 1st point of Aries |
| Solar Ecliptic (S) | z_s : 23.4333° incl. to ecliptic | x_s : points to sun (Keplerian orbit) |
| Solar Magnetospheric (SM) | x_{sm} : towards sun, | z_{sm} : North in plane of x_{sm} , z_d |

Note: z_{sm} rocks 11.2° daily about x_s , and can be inclined as much as 34.6° ($23.4+11.2$) to the (x_s, z_s) plane at equinox.

OPTIONAL (aberrated coordinates)

Solar Wind (SW) resembles Solar Ecliptic (S) coordinates, but x_{sw} : points to solar wind; e.g. 400 km/s solar wind and 20 km/s Earth orbital velocity gives an aberration angle of 4.3° .

Solar Wind Mag. (SWM) similarly corresponds to SM.

Tsyganenko-USmanov Model (cont'd)

Coordinate Rotations

15 coordinate rotations (and their inverses) between the above systems are available, and the transformation desired is activated by a call to ROTATE with the appropriate value of K.

| K | Transformation (K+1 is the inverse) |
|-------|-------------------------------------|
| 1 | S → G |
| 3 | G → D --- time independent |
| 5 | S → D |
| 7 | S → SM |
| 9 | G → SM |
| 11 | SM → D |
| 13 | S → C |
| 15 | C → G |
| ----- | |
| 17 | SW → S |
| 19 | G → SWM |
| 21 | SWM → D |
| 23 | SM → SWM |
| 25 | S → SWM |
| 27 | SW → D |
| 29 | SW → SWM |

The External Magnetic Field Components

Ring Current Magnetic Field

The magnetic vector potential is represented by

$$A\phi = 4 B_0^3 \rho_0^2 \rho^2 [z^2 + \rho^2 + 4\rho_0^2]^{-3/2}$$

in the cylindrical geodipole system (ρ, ϕ, z) with $2\rho_0$ = the loop's radius. B_0 and ρ_0 are Kp dependent model parameters $B_0 = -12.5$ nT (lowest Kp) to -48.1 (highest Kp) but ρ_0 is held constant at 4Re.

In terms of normalized variables $\rho' = \rho/\rho_0$ and $z' = z/\rho_0$ this gives

$$B_z = 4B_0 (2z'^2 + 8 - \rho'^2)/u$$

$$B_\rho = 2B_0 \rho' z' / u$$

in Dipole coordinates, where $u = (\rho'^2 + z'^2 + 4)^{5/2}$

Note that this field vanishes at $z' = 0$, $\rho' = 2^{3/2}$.

Tail Current Magnetic Field

An infinite sheet of current filaments is assumed parallel to the y-axis, "hinged" or offset a distance z_0 on the z-axis due to the dipole tilt. Kp dependent model parameters define the current per unit length of the sheet in a linear relationship:

$$I(x_0) = c/2\pi (B_N + \Delta B_{x_0} - \frac{x^N}{S})$$

where $S = x_N - x_F$ and N and F refer to the near and far limits of integration. The far limit is fixed at 50 Re.

A shaping function multiplier $[1 + (y/\Delta y)^2]^{-1}$ is included to make the current flow lines curve towards the sunward edge and approximate the ring current pattern. A closed form solution for B_x , B_y and B_z has been derived in SM coordinates.

Magnetopause Current Magnetic Field

B_x , B_y and B_z are expressed in SM coordinates as polynomial functions of y , z , $\exp(x/\Delta x)$, and $\sin\psi$. Δx ranges between 15 and 20 Re and characterizes the gradient of the external magnetic field; ψ is the tilt angle. 18 Kp dependent parameters are the coefficients in these functions, but 4 are mutually related due to the imposition of the $\text{Div } \underline{B} = 0$ condition.

Organization of the GTUBFD program

A number of control parameters are entered in an array, and activate various options (or defaults) throughout the program. A flow chart shows the steps and routines employed when x, y, and z are input in SM coordinates.

Input

x, y, z
(SM coordinates)

Routine BFELD

one-time call
unless reactivated

READY (fixed values)

CONSTU (Kp)

TRANS3 (rotations)

Routine POINT

Rotation

ROTATE coordinates SM→G 10

NSCALE Truncate Harm. Expan.

MAINB Main field

ROTATE B G→SM 9

ROTATE coordinates SM→D 11

RING B_R

ROTATE B_R D→SM 12

Add B_R to B

TAIL B_T in SM coordinates

MPAUSE B_M in SM coordinates

Add B_T and B_M to B

Note:

If SWM coordinates
were desired,
Rotations 20, 19, 21,
and 22 would have
been used instead

Output

B_x, B_y, B_z
in SM coordinates.

References

1. Mead, G.D., "Deformation of the Geomagnetic Field by the Solar Wind", J.Geophys. Res. 69, p. 1181, 1964.
2. Williams, D.J. and Mead, G.D., "Night-side Magnetospheric Configuration as Obtained from Trapped Electrons at 1100 Kilometers", J.Geophys. Res. 70, p. 3017, 1965.
3. Barraclough, et.al. Geophys.J.R., Astro. Soc., 43, pp. 645-659 (1975).
4. Tsyganenko, N.A. and Usmanov, A.V., "Determination of the Magnetospheric Current System Parameters and Development of Experimental Geomagnetic Field Models Based on Data from IMP and HEOS Satellites", Planet. Space Sci., 30, 985, 1982.
5. McInerney and Abelowitz, "MFP Magnetic Field Package for Theoretical Magnetic Field Calculations", AFCRL-TR-73-0356, June 1973, AD766208.

4.0 Radiation Belt Studies

The high energy charged particles in the earth's radiation belts threaten successful operation of microelectronic circuits of satellites operating in that region. AFGL has conducted research on the radiation belts with the DMSP⁽¹⁾ satellites at low altitudes and the SCATHA⁽²⁾ satellite at geosynchronous altitudes. In this section we summarize the software developed for analysis of SCATHA data and display of radial, pitch angle, and energy distributions of trapped particles, and display of measured/model magnetic field comparisons.

The SCATHA SC-5 instrument measured electron and ion fluxes in the energy ranges 50 eV to 1 MeV and 50 eV to 7 MeV, respectively ⁽²⁾. The SC11 instrument measured the magnetic field. The satellite orbited in the L-shell range 5.3-8.5 R_E in a near-geosynchronous orbit. Software was developed to form and display orbital data bases consisting of averaged detector counts by L-shell/pitch angle bins and averaged magnetic field values by L-shell bins, with the corresponding ephemeris parameters appropriate to each L-shell bin. Subsequently these data bases have been used in a study⁽³⁾ of adiabatic variations of the trapped particles for the purpose of developing schemes which might be used in the analysis of CRRES⁽⁴⁾ data.

4.1 Statistical Analysis

Six electron energy channels, from 23 keV to 1 MeV, and 11 ion channels, from 23 keV to 5 MeV, were chosen for this analysis. The data for these channels are available at one second intervals as counts per .2 second, along with the pitch angle at 6° resolution (satellite rotates at 360 deg/min). At the beginning of the data tape (one tape per day) are header records indicating the detector energies,

geometric factors, and degradation factors. These are defined so that the fluxes can be computed from the counts by

$$F = GDC$$

where F is the flux in particles/(cm²-sec-sr-eV), G is the geometric factor, D is the degradation factor, and C is the counts per .2 second. The degradation factors account for variation (degradation) in detector sensitivity in time, and effect only the ESA channels below 100 keV. Periodic updates of the degradation factors occur on the data tape as short records (i.e. they may be detected in processing by their short length). An ephemeris file for each orbit accompanies the data. This includes magnetic field parameters based on the Olson-Pfizer quiet model.⁽⁵⁾

Program SC5STAT was developed to process this data. Data are sorted into L-shell bins .05 R_E wide. Each L bin is in general encountered twice, in the ascending and descending half of the orbit, respectively. These are treated as separate bins, and so labeled. The data for a particular such bin will thus be encountered in one continuous period in time. Thus the data can be processed one bin at a time. Using the ephemeris file, SC5STAT detects which L bin the satellite is in initially and begins accumulating the necessary statistical sums for that bin. When the satellite leaves that bin, these sums are stored on a temporary file, and the process repeated for the next L bin. Within each L bin, the data are sorted into the 10 deg. pitch angle bins, and separate sums accumulated for each, along with the count of the number of samples. When the end of the data is reached, SC5STAT executes a second pass, in which the statistical sums are converted to averages and standard deviations. The relevant ephemeris values for the L bin are computed by interpolation of the data on the ephemeris file at the average universal time of the bin. The output record for each L bin then consists of:

4.2 Display

Several programs were written for display of the data. Program PLOTFIL extracts the 40° and 90° pitch angle data for an ascending or descending portion of an orbit and creates a separate file of this data suitable for plotting with program SUATEK⁽⁶⁾. The data bases for two consecutive days must be used since the requested ascending or descending portion may not lie within one day. If the data requested extends past a day boundary, the bin at the end of the first day may be for the same L as the first bin for the second day, i.e. that L bin is continued into the second day. In this case, the means of the combined bin are computed as the weighted means of the separate portions, using the sample counts that had been saved for the separate portions.

Program SIPILOT is a specialized version of SUATEK developed to stack plots sideways for up to 11 detectors. (Figures 4.1 and 4.2) For each detector the 40° and 90° counts are placed in a single panel. A separate version of SIPILOT similarly displays the measured and model magnetic field vector components, magnetic field magnitudes and magnetic pressures.

Program SPECFIL develops spectral plot files for a specified L bin, or specified group of selected L bins, for a specified detector and pitch angle. The data on this file can be plotted with SUATEK. Either the flux or the distribution function may be plotted. The flux is computed as described previously. If the distribution function is desired, it is computed from:

$$D = F\lambda Q(E)/E,$$

where:

$$F = \text{flux};$$

$\lambda = .1617$ for electrons, 5.45×10^5 for ions;

E = energy;

$Q(E) = 1/[1+E/(2E_0)]$;

E_0 = rest mass energy, 5.11×10^5 eV for electrons,
 9.4×10^8 eV for ions;

In the above, the flux is in particles/(cm²-sec-sr-eV), the energies are in eV, and the distribution function is in sec³/km⁶. The factor $Q(E)$ is a relativistic factor which differs significantly from unity, for the energies considered, only for electrons. Otherwise the distribution function given here is identical to that given for velocity space in Ref. 2. Since, due to relativistic effects, the momentum distribution function is not related to the velocity distribution function by simple multiplication by a constant, we have chosen to use the relativistic momentum distribution function, multiplied by the cube of the rest mass, so that it is in the same units as the velocity distribution function quoted in Ref. 2, and reduces to it when relativistic effects are negligible.

Spectral analysis programs have been developed in Fortran IV on the CYBER to display measurements from SCATHA in color on the Tektronix 4100 series terminals. Particle measurement and ephemeris data are read from the SC5STAT output data tape, interpolation is performed and the data are arranged into files appropriate for plotting using color graphics programs to interface with the Tektronix terminals. The spacecraft measurements corresponding to electron and ion flux distributions in space are thus displayed in a form ready for photographing.

Figure 4.3 shows a sample electron spectrogram generated by

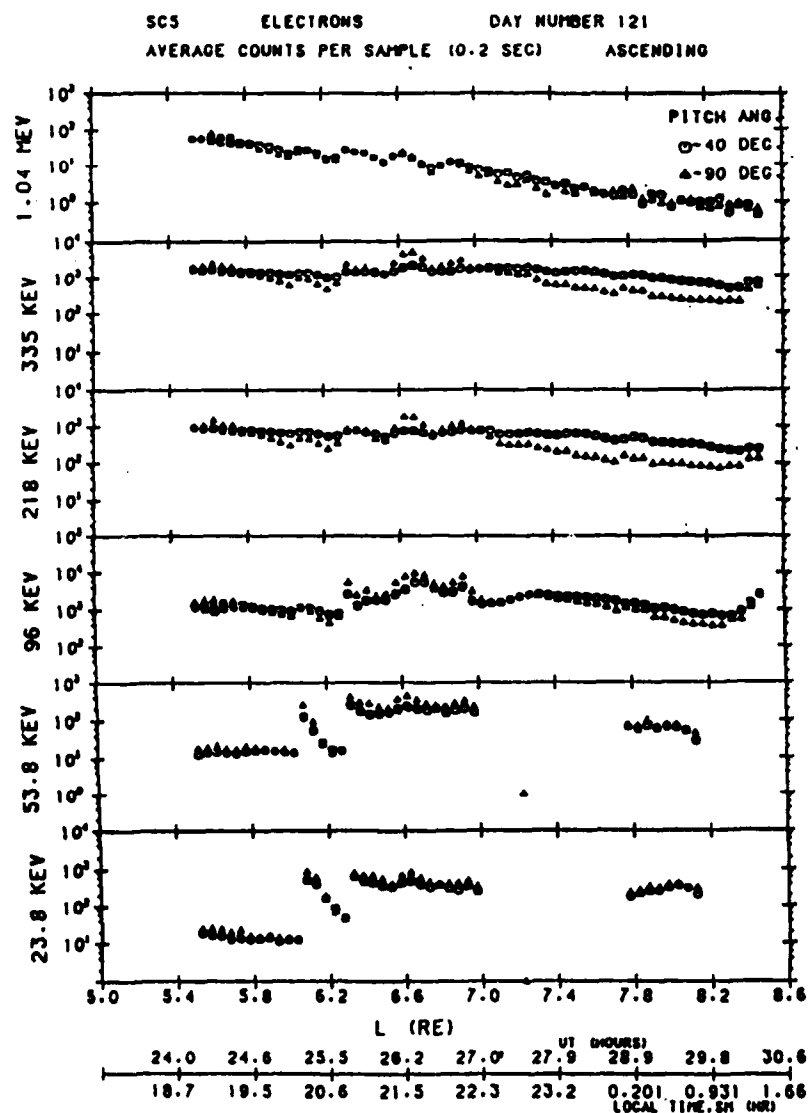


Figure 4.1 L-Shell Variations of Electron Counts for 40 and 90 Degree Pitch Angles

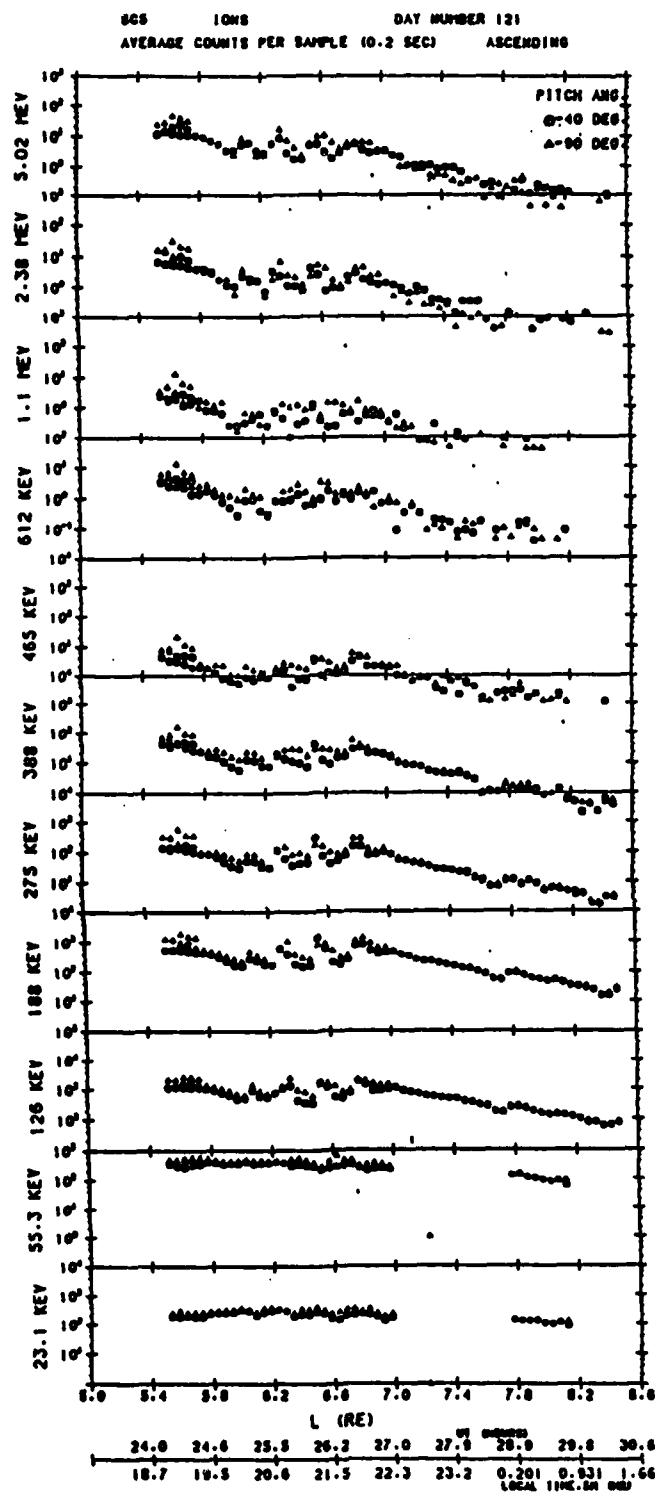
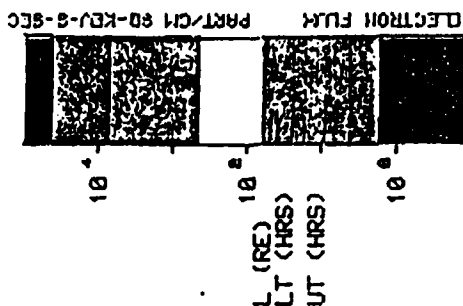


Figure 4.2 L-Shell Variations of Ion Counts for 40 and 90 Degree Pitch Angles

SCATHA ELECTRONS



DAY 110
20 APRIL 1979
ASCENDING

EACH .05 RE IS
FURTHER DIVIDED
INTO 19 PITCH
ANGLES RANGING
FROM 0 TO 180 DEG.

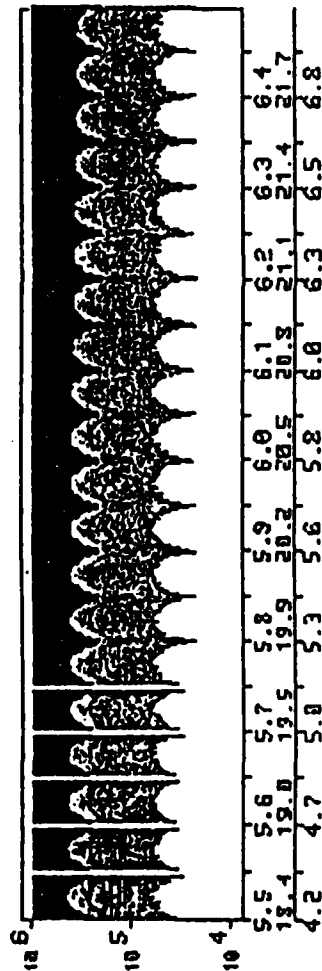
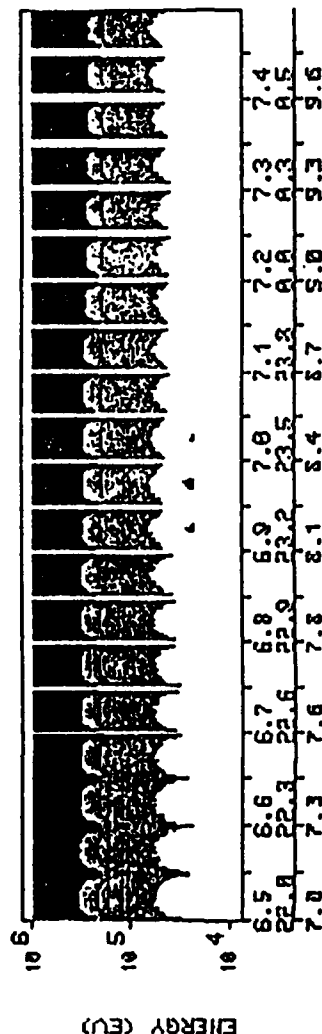
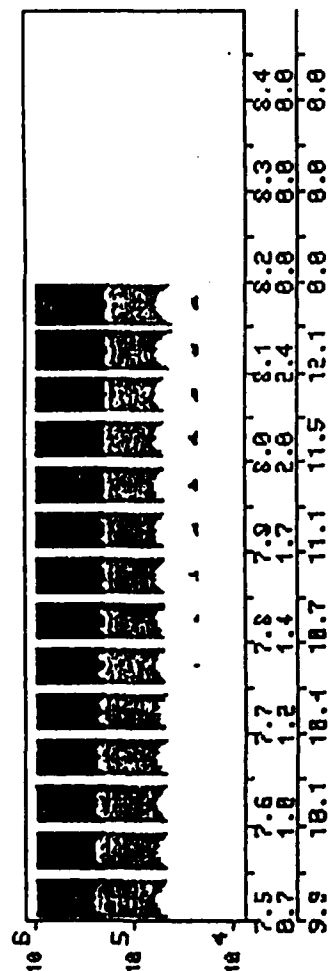


Figure 4.3 Spectrogram Depicting Electron Flux Measured by SCATHA as a Function of L-Shell and Pitch Angle.

this software. In this case the particle measurements used cover seventeen energy channels and ranges from 5.5 to 8.5 Re. The data are divided into 60 L-bins, each equal to .05 Re. Each L-bin is further divided into 10^0 pitch angle bins. The flux value for the particles in each energy channel, L-bin and pitch angle bin is read from the SC5STAT cutput data base and is stored in a direct access file. This data are then arranged for graphics. Each pixel in the plot must be assigned a color to display the flux at that point. The y-axis on each plot represents the particle energies, and the x-axis provides sequential particle binning data, i.e. all pitch angle bins per L-shell bin. Since there are only six electron energy channels and 11 ion energy channels, and the resolution of the energy axis is 90 pixels, the flux values between these channels are interpolated to obtain a flux value for each of the 90 pixels. The entire data set is displayed as two sets of three plots -- one for electron measurements (Figure 4.3) and the other for ion measurements. Each set of three plots range from 5.5 to 6.5 Re, 6.5 to 7.5 Re, and 7.5 to 8.5, respectively. The x-axis for each plot is 380 pixels long, so there is a pixel for each flux value in each L-bin and pitch angle bin, therefore no interpolation between flux values is done in this direction. After a flux value for each pixel is calculated, 15 flux bins are defined over the entire range of fluxes and a bin number replaces each flux value. The bin numbers represent the color index number which is associated with each pixel. This color index, ranging from 0 to 15, defines the color which represents each flux bin. (The color index for black is zero. This index represents when there is no data or when the flux value equals zero.) The final data set of flux color index numbers are then stored in a direct access data files to be used with the plotting program, SPECPLT.

Program PTCHFIL performs a function similar to SPECFIL, with respect to pitch angle distributions, i.e., it prepares plot files for the generation of pitch angle distribution plots.

References

1. Gussenhovem, M. S., Filz, R. C., Lynch, K. A., Mullen, E. G., and Hanser, F. A., Space Radiation Dosimeter SSJ* for the Block 5D/Flight 7 DMSP Satellite: Calibration and Data Presentation, Tech. Report, AFGL-TR-86-0065, Air Force Geophysics Laboratory, Hanscom Air Force Base, MA, 1986, ADA172178.
2. Mullen, E. G., and Gussenhoven, M. S., SCATHA Environmental Atlas, Tech. Report, AFGL-TR-83-0002, ADA131456, Air Force Geophysics Laboratory, Hanscom Air Force Base, MA, 1983.
3. Bass, J. N., Gussenhoven, M. S., and Redus, R. H., "The Importance of Adiabatic Variations in Trapped Particle Distributions Observed by the SCATHA Satellite", to be submitted to J. Geophys. Res.
4. Gussenhoven, M. S., Mullen, E. G., and Sagalyn, R. C., CRRES/SPACERAD Experiment Descriptions, Tech. Report, AFGL-TR-85-0017, Air Force Geophysics Laboratory, Hanscom Air Force Base, MA, 1985, ADA160504.
5. Olson, W. P., and Pfitzer, K. A., "A Quantitative Model of the Magnetospheric Magnetic Field", J. Geophys. Res., Vol. 79, No. 25, Pp. 3739-3748, 1974.
6. Bhavnani, K. H., and McInerney, R. E., "SUATEK Interactive Graphics User Guide".

5. Investigation of Auroral Electron Precipitation Data

Electron precipitation flux measurements are made on board the DMSP series of polar orbiting satellites that are flown at around 840 km altitude. The data bases are preprocessed and made available for a number of research investigations. Radex personnel have conducted computational and analytical work for statistically interpreting the data, and providing estimates for observational planning purposes of instruments that might be placed on shuttle or other spacecraft missions. For these studies it was determined by the researchers that the midnight equatorward auroral boundary, which can be calculated in real time from the satellite, provided a superior measure of geomagnetic activity which should be used for correlation.

A different line of endeavor consisted in developing analytical models of four auroral properties viz. electron energy and number flux, and the Peterson and Hall conductivities. This effort led to functional fits using spherical harmonic and Epstein functions requiring a relatively small number of coefficients. Through contour plots, the results were shown to match the data extremely well, and could be used both for editing irregularities in the data base, and for prediction.

These investigations have required accessing large data bases, and progressively accumulating and managing the reduced data for the analysis and presentation purposes. Both the probabilistic and the analytical modeling efforts were successfully completed, using F2, F4, F6, F7 DMSP data bases on individual studies, and additional runs were then requested and completed on other data bases.

5.1 Probabilistic Modeling of Auroral Electron Precipitation

This work was initiated with the goal of improving the

quality of the observation of bright discrete auroral events through the calculation of the probability of occurrence of such events as a function of magnetic activity and of geomagnetic location. With such knowledge, one could concentrate observational activities only during periods of magnetic activity consistent with a high probability of sight and could focus attention during these periods on regions of the sky with the highest probabilities. Two large scale studies were carried out, the first on data from DMSP/F2 and DMSP/F4 over a period of about 300 days⁽¹⁾ and the second on data from DMSP/F6 and DMSP/F7 for the years 1983 and 1984 respectively.⁽²⁾ The major difference between these two studies was the way in which magnetic activity was introduced. In the first, the Kp index was used and in the second, the latitude of the midnight extrapolated equatorward boundary of diffuse aurora was used. The correspondence between Kp and midnight extrapolated boundary has been established.⁽³⁾

This second study came about because it was realized that, since equatorward boundary is a quantity calculated in real time for each DMSP polar pass,⁽⁴⁾ it would be more reliable to refer to it when making decisions as to when to look for high energy events. This, coupled with the fact that the second study drew upon almost twice as much data and was derived from higher resolution instrumentation, means that for practical purposes, the second study superseded the first. We will thus concentrate this discussion on the second study.

The data is derived from DMSP/F6 and F7 satellites. F6 was launched in December 1982 into a 840 km circular polar orbit, sun-synchronous in the dawn-dusk meridian plane. The F7 satellite was launched in November 1983 in a similar orbit in the 1030-2230 meridian. The orbital periods of both are approximately 101 minutes. Although both are sun-synchronous, the spatial coverage for the two taken together is quite large, due to the rotation of the geomagnetic pole

about the geographic pole. Figure 5.1 shows the coverage for the periods used in this study.

The SSJ/4 sensors on F6 and F7 are identical in design and measure the flux of electrons and ions in 20 energy channels in a range from 30 to 30,000 eV. For the electrons, with which we will be concerned here, this is accomplished by means of two cylindrical plate electrostatic analyzers, one for low energy and one for high. These return a complete electron spectrum once per second. A more complete description of the experiment has been given⁽⁵⁾ along with results of the calibration necessary in conversion from counts to flux level. The DMSP satellites are non-spinning and the sensors are mounted such that their look directions are oriented radially outward from the earth at all times.

The data base is maintained on the AFGL Cyber system as a series of tapes. With one exception, each is a multi-file containing either five for F7 or six for F6 files. Each file itself contains one half month of data from the first to the fifteenth or from the sixteenth to the end of the month.

Each block on a file contains 5000 60-bit CDC words, except for the final block of each day. This is a variable length block with a zeroed block of length two immediately before it. This means that if one wishes to read past a day, one must look for a block of length two and then read one additional block before reading the first block of the next day. Each minute of data comprises an entity of variable length within the fixed length block. A set of ephemeris is assigned to the first second of each minute interval. This variation is due to the fact that missing data within a single record is not zero filled. The arrangement leads to two complications. The fact that ephemeris for latitude and magnetic local time appears each minute means that it must be interpolated by some means more accurate than linear to obtain the precision we require. This was done by the law of

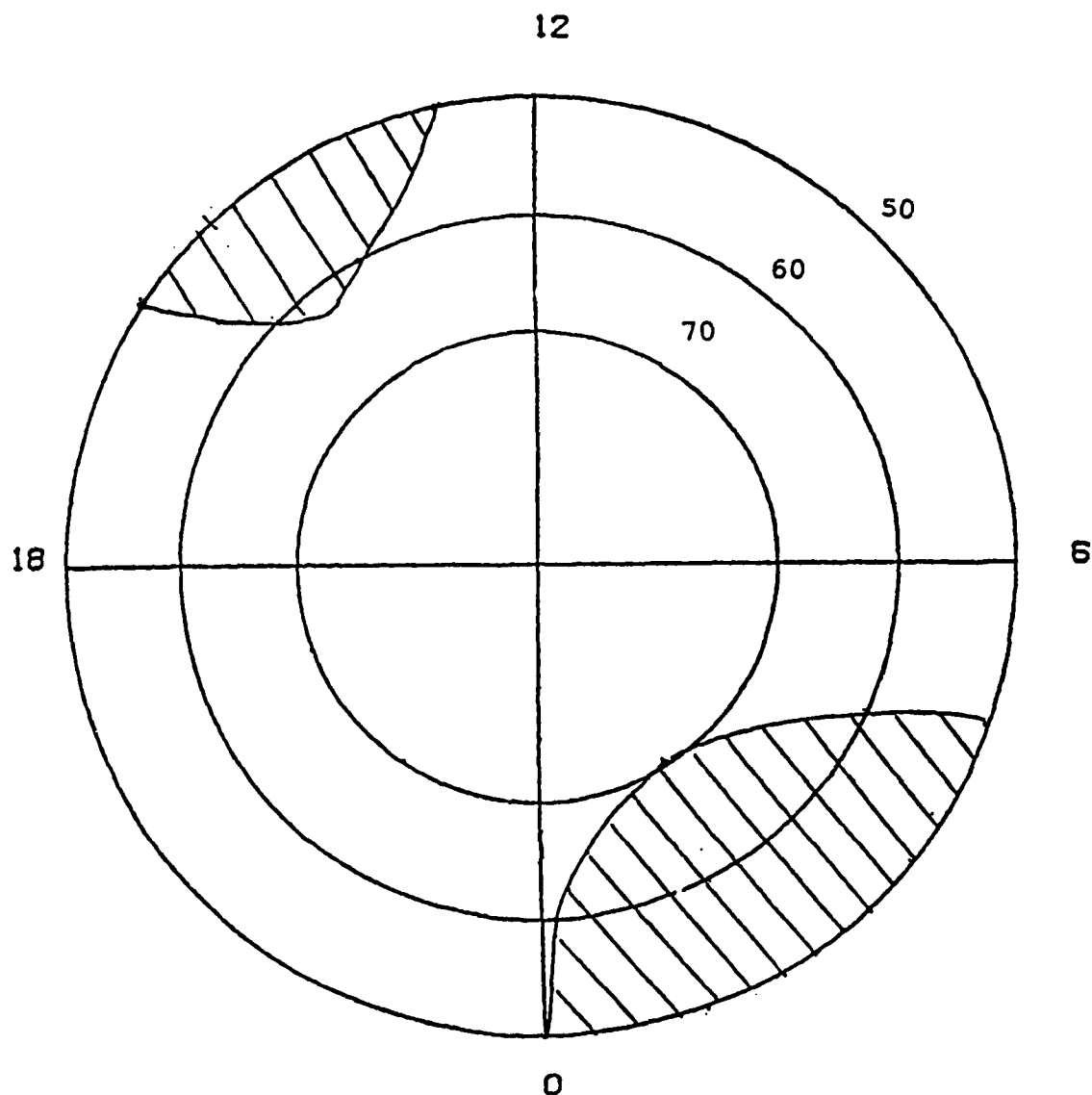


Figure 5.1 Magnetic Latitude - Local-time Coverage by DMSP/F6 and F7 Satellites. (Regions not covered are shaded)

cosines as outlined in the next section.

Also, the fact that each minute of data is of varying length means that minutes overlap blocks, making the logic for decoding complicated. We have created a routine which returns a fully decoded minute as well as the ephemeris for the next minute each time called. With this subroutine in hand, we can ignore the complexities of the data base for the remainder of the work.

Once each minute of data is sorted out, the nine bits representing each channel and the bits for the ephemeris are separated and channel counts are converted to flux by the calibration factors mentioned above.

5.1.1 Processing Algorithms

In order to assign a midnight extrapolated boundary to each DMSP pass, it was necessary first to carry out the extrapolation. The boundaries themselves were obtained from the Hardy/Holeman boundary code in a series of files, one month per file.⁽⁴⁾ These were extrapolated to midnight local time by the relation developed by Gussenhoven et.al.⁽⁶⁾ The equatorward midnight boundary is given in their notation by

$$\Lambda_M = (\Lambda_{OM} - \alpha_M/\alpha_i \Lambda_{O_i}) + \alpha_M/\alpha_i \Lambda_{CGM}$$

where Λ is the intercept and α is the slope of the Kp dependence fit for the boundary. OM refers to MLT 0, O_i refers to the measured MLT, and Λ_{CGM} is the measured boundary. The result Λ_M is the measured boundary extrapolated to its equivalent latitude as if the MLT had been midnight. The slopes and intercepts are given in Reference 6.

Each boundary, morning and evening side, was calculated

separately in the Hardy/Holeman code and thus there were two for each pass. We could use only one, since a midnight boundary had to be assigned to an entire pass. We chose to use the evening boundary since this is expected to be the sharpest and most well defined of the two. It was necessary to edit the boundaries to remove some poorly determined points. This process consisted of three tests. The first was made in the boundary code itself, which rejected poorly determined cases. Secondly, we required the extrapolated midnight boundary to agree with that predicted on the basis of Kp to within two standard deviations. The predicted midnight boundary, also from Reference 6, is given by

$$\Lambda_M = \Lambda_{OM} + \alpha_M Kp$$

Lastly, we required that a boundary appear as part of a morning/evening pair, that is, that both the morning and evening boundaries of each pair passed the above tests.

There was another complication that arose because we wished to include data at all latitudes above 50 degrees. The UT associated with the boundaries, however, was the UT at the boundary which was usually well above 50 degrees. In order to determine the UT when DMSP passed 50 degrees on the way to encountering each boundary, we used the following algorithm.

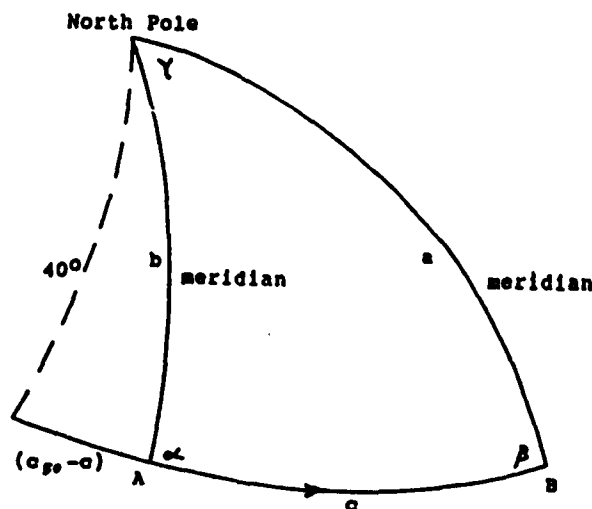


Figure 5.2 Geometry of 50° Latitude Crossing

Referring to Figure 5.2, let A and B be the two known points in the orbit given in the boundary file, i.e. the position of the morning and evening boundary. Let a, b and c be the internal angles, measured to the origin of the sphere. A and b are thus the colatitudes of the known points. Further, the angle γ is given by the difference in MLT's of the two known points. The law of cosines gives us

$$\cos(c) = \cos(b)\cos(a) + \sin(b)\sin(a)\cos(\gamma)$$

We also know that the angle c must vary linearly in time since the satellite orbits at a constant rate and constant radial distance. In order to solve the problem, we need to find the c for which a is 50 degrees. First, we calculate α from the law of cosines. The value of α will always be the same no matter how large c becomes, so from here, we solved iteratively for the proper c to give a value of 50 degrees. We could then find the crossing time from

$$UT_{50} = UT_B - (UT_B - UT_A)c_{50}/c$$

A similar algorithm was used to interpolate the latitudes and local times between the once per minute ephemeris given in the DMSP tapes.

5.1.2 Quantities Calculated

The major probabilities of interest are what we call per pass and per second probabilities. The per second probabilities are defined as simply the fraction of seconds in which an

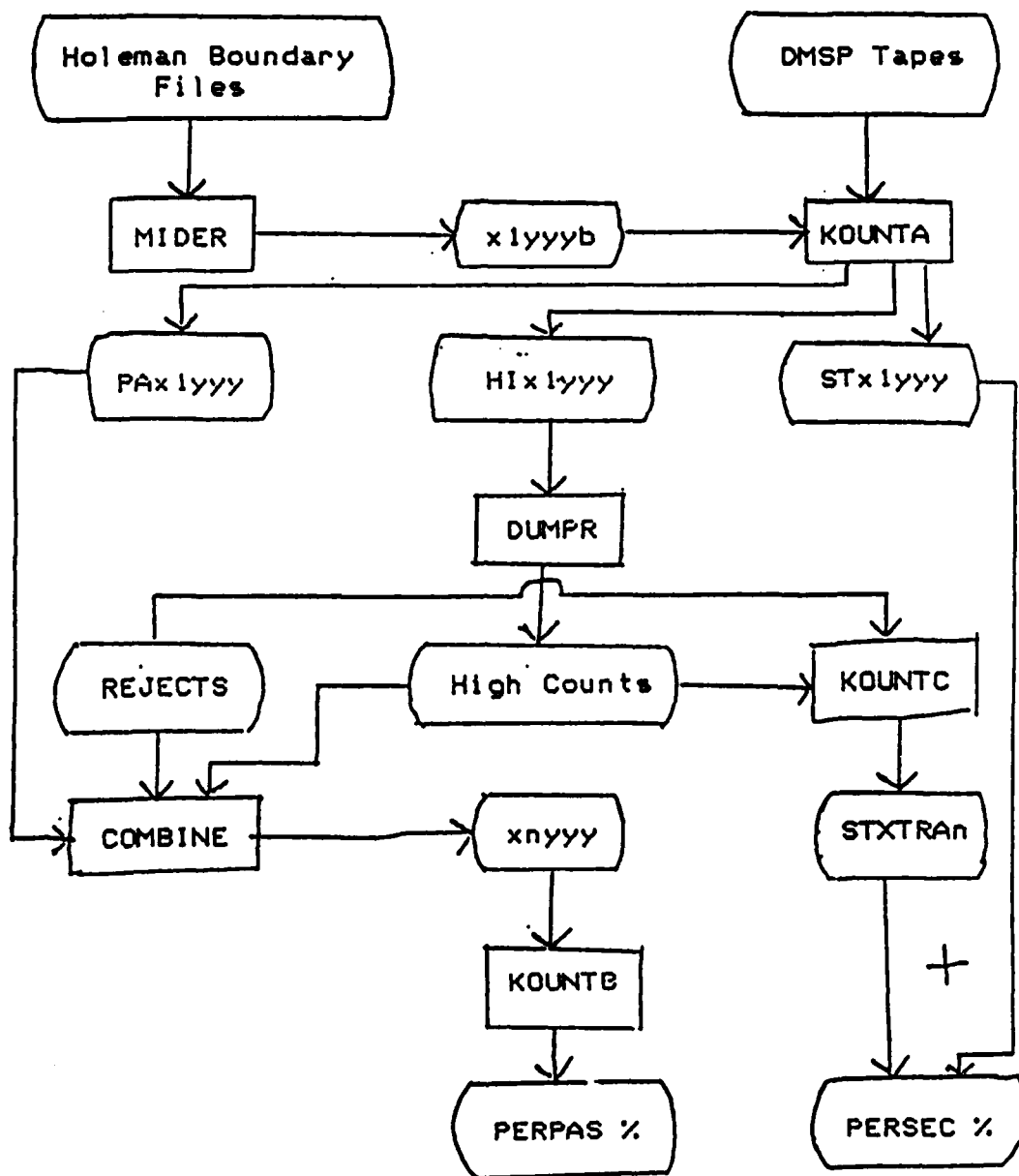
event in a given energy and flux bin was observed, divided by the total number of seconds spent in a particular geomagnetic division. The per pass probabilities are a little less straightforward. These give the fraction of passes through a particular geomagnetic bin in which a particular energy flux level was achieved, divided by the total number of passes through the geomagnetic bin. In order to qualify as a pass, it was decided that the satellite must spend at least five seconds in a given bin.

The processing system requires several passes, as diagrammed in Figure 5.3. First, the program MIDER examines the boundary file, editing out poor boundaries, and creates a second file of boundaries for a particular half month. The program KOUNTA then uses this file and the DMSP tapes to produce three files. The first is an accumulation of per second data, which is binned over fixed geomagnetic locations and midnight equatorward boundaries. Second, all records that contain counts greater than 30,000 are excluded from this count and dumped to another file for visual examination and editing. Third, a file is created which is a record of each geomagnetic bin encountered. This file contains two words for each bin crossing of the form

DDDTTTT,MMMLLTXXN

where DDD is the day, TTTT is the UT in seconds, MMM is the equatorward midnight boundary times 10, LL is the latitude bin from one to twenty and TT is the mlt bin from one to forty-eight. X is the maximum flux level encountered in the bin from one to six and NN is the total number of seconds in that pass through the bin.

Moving to the next level in the flow chart, the program DUMPR reads and edits the high counts, creating the file High



x = B for beginning (day 1 - 15) or E for end
 yyy = JAN or FEB or etc
 n = 6 for F6 or 7 for F7

Figure 5.3 Probabilistic Model Processing System

Counts which contains those deemed good data. These are injected into both the per second data and the bin crossing data files through the programs called KOUNTC and COMBINE respectively. The per second data is then combined to yield the final per second probabilities. Yet another program is then used on the files called xnyyy, the records of bin crossings, to calculate the per pass probabilities. The beauty of the per pass probability calculated in this way is that one can partition the count over any arrangement of midnight boundaries or over any arrangement of geomagnetic bins without recourse to the DMSP data base itself. We have used this system for both these variations on the original theme.

5.1.3 Results and Deliverables

The results of both these studies were of numerous forms. The most significant were contour plots of probability. There were four sets in all. The first came from the per second probabilities, calculated over midnight boundaries chosen to correspond to the thresholds 2,4 and 6 in Kp. The second set was the per pass version, calculated over the same boundary divisions. A third set was produced calculated over four boundary divisions that were chosen such that each division contained roughly the same number of passes. The fourth set was calculated over five divisions selected in the same way for more resolution.

In making these plots, it was necessary to fill in the small regions of space which were covered either poorly or not at all by the orbits of DMSP F7 and F6. Additionally, a mild form of smoothing was performed on the data before plotting. This consisted of averaging over each set of three local times for a constant latitude. A typical example of such a contour plot is shown in Figure 5.4.

PERPAS EF>4.0E8 (2.KRAL) 63.7->65.7 DEG

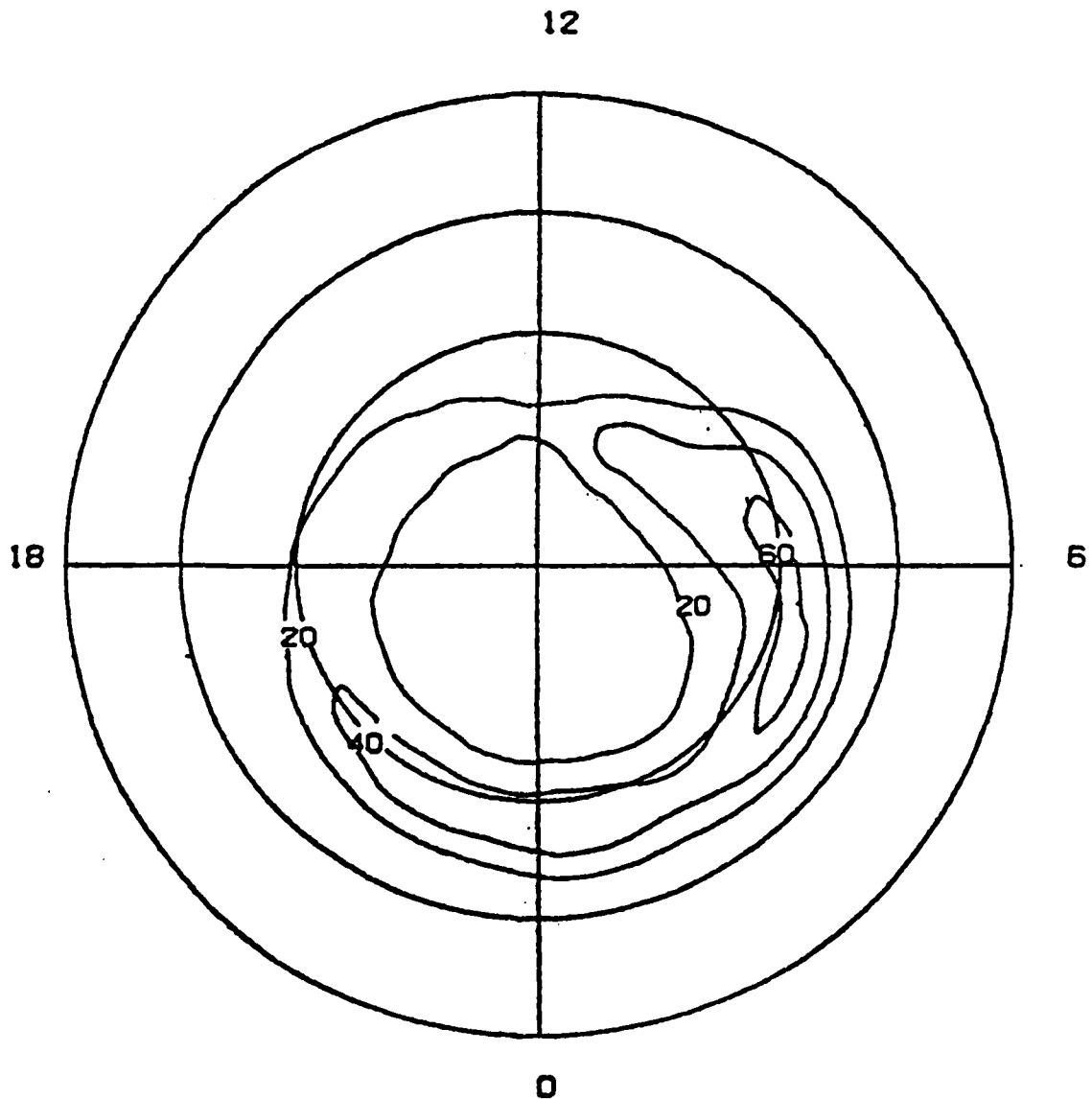


Figure 5.4 Example of Per-Pass Probability Contours

Another result of interest was histograms of the duration or spatial extent of each high flux event. A typical example is shown in Figure 5.5. Tables of numerical values for probability were also produced. Finally, the secondary data base discussed above was used to calculate a rather different probability, the probability of sighting an arc greater than or equal to a given intensity anywhere in the auroral region during a given pass at fixed equatorward boundary. Seven divisions of boundary were selected for this study and the results are shown in Table 5.1. We note again that without the secondary data base that this work produced, such a calculation would have had to rely on the DMSP tapes, which would have required weeks instead of a few hours to complete.

A by-product of these two studies was the substantiation of the correlation of Kp with midnight equatorward boundary. This correlation was borne out by the qualitative similarity of the results of the first and second study.

5.1.4 Further Work

Interest has been expressed in the initiation of other counting studies on the DMSP data. The major difference between these and the previous ones would be the concentration on the overall structure of the aurora in regard to energy flux and average energy rather than to focus only on high energy events as was previously done. This could be carried out by increasing the number of energy and flux bins and by lowering the thresholds so that the probability became distributed over several bins instead of concentrated in the lowest of the bins. Binning by average energy and flux would then show which regions of the sky exhibited high energy electrons as well as a high level of flux. Results of such a study would be of interest in understanding the detailed structure of the aurora as opposed to determining when and where a bright event might occur.

DURATION OF FLUX 0 < KP < 2 MLT ZONE=1800-2200

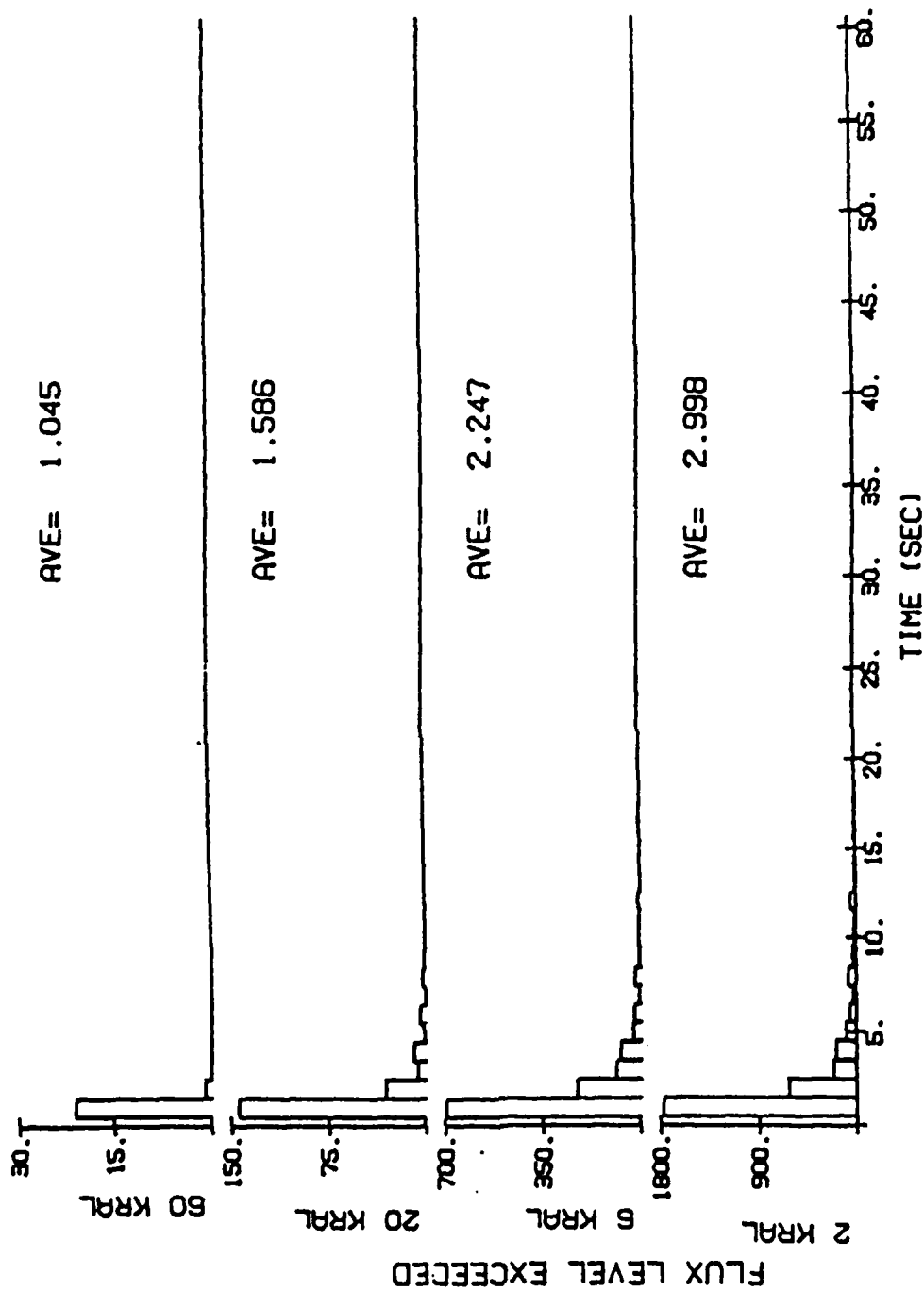


Figure 5.5 Example of Flux Event Duration Histograms

Table 5.1 Probabilities of Encountering a Flux Event Above Level Shown on Any Single Auroral Pass for Various Extrapolated Midnight Auroral Boundaries

| | 2 | 3 | 4 | 5 | 6 |
|-----------------|-----------------|-----------------|------------------|------------------|-------------------|
| <u>Boundary</u> | <u>>2 KR</u> | <u>>6 KR</u> | <u>>20 KR</u> | <u>>60 KR</u> | <u>>200 KR</u> |
| 90.0-67.8 | .812 | .420 | .123 | .022 | .007 |
| 67.8-65.7 | .943 | .666 | .222 | .062 | .013 |
| 65.7-63.7 | .987 | .839 | .394 | .107 | .022 |
| 63.7-61.6 | .998 | .941 | .593 | .205 | .043 |
| 61.6-59.5 | 1.000 | .973 | .711 | .298 | .061 |
| 59.5-57.5 | 1.000 | .990 | .774 | .335 | .073 |
| 57.5-50.0 | .999 | .994 | .870 | .436 | .099 |

Total Number of Passes

| <u>Boundary</u> | <u>Total</u> |
|-----------------|--------------|
| 90.0-67.8 | 543 |
| 67.8-65.7 | 1785 |
| 65.7-63.6 | 2366 |
| 63.6-61.6 | 2604 |
| 61.6-59.5 | 2075 |
| 59.5-57.5 | 1241 |
| 57.5-50.0 | 857 |

This effort could be accomplished relatively easily using the existing processing system, which is tailored for DMSP/F6 and F7 data, since the problems involving access, decoding and assigning the equatorward boundaries to each polar pass have been encountered and successfully solved in the study above.

5.2 Modeling of Averaged Auroral Properties

Another area of attention in regard to the investigation of electron precipitation data was the modeling of averaged auroral properties by simple functional forms. Four properties were studied; the integral and energy flux and the Hall and Peterson conductivities. These properties were calculated by Hardy, et.al. from DMSP F2 and F4 data.⁽⁷⁾ Their model averaged over time at a series of Kp values, using 48 divisions of magnetic local time and 30 divisions of latitude. A total of 15 months of data was used, chosen so as to provide a uniform distribution over seasonal variations. The properties to be fit were obtained as a matrix of 1350 values at seven integral values of Kp from zero to six. Each matrix contained data at 48 magnetic local times and 30 geomagnetic latitudes. In general, the data was statistically excellent, although occasional irregularities did exist. One purpose of this modeling was to smooth out these irregularities, although the most important objective was to reduce the data to a more manageable size via the functional fits. The rationale was that if the large arrays could be reduced to a small number of coefficients, the data could be employed on microcomputers in the field for predictive purposes.

Overall, the properties as viewed as a function of latitude at fixed local time resemble two straight lines that converge smoothly to a maximum at a characteristic mid-latitude. This regular pattern was a considerable aid in choosing the fit functions.

5.2.1 Methods of Representing the Properties

Our first attempt at the creation of a model used a spherical harmonic expansion. A software system was created to interpolate the values onto a 49 x 49 point grid and to calculate the expansion coefficients by direct integration of the product of the function to be modeled and each of the spherical harmonics. This particular grid was chosen because it gave an accurate result for the mean square integral of all spherical harmonics up to order seven and yet was not too time consuming.

The representation of spherical harmonics used was

$$\log_{10}f(T,X) = \sum_{n=1}^7 \sum_{m=-n}^n C_n^m b_n^m Y_n^m(T,X)$$

where

$$Y_n^m = \cos(2\pi T/24) P_n^m(X)$$

$$Y_n^{-m} = \sin(2\pi T/24) P_n^m(X)$$

and

T is the magnetic local time in hours

X is (latitude - 70)/20

and

C_n^m is the calculated expansion coefficient

b_n^m is a coefficient that makes the square integral of each spherical harmonic unity.

The use of C and b is convenient because, when normalized by b, the expansion coefficient is simply the value of the integral of the spherical harmonic and the function to be fit. Its use does mean, however, that one must carry along all the b's in the generating routine. To avoid this in the implementation of the model, we have reported coefficients both as the C and as the product of b and C in the above equation.

This scheme was used to expand the base ten logarithm of the energy and number flux to produce a total of 64 coefficients at each value of Kp. The conductivities were not so amenable to fitting with spherical harmonics and this approach was discarded in their case in favor of a second fit function, Epstein transition functions.

In our implementation, the Epstein function was taken to be

$$e(h) = r + s_1(h-h_0) + (s_2-s_1)\ln[1-s_1/s_2\exp(h-h_0)]/[1-s_1/s_2]$$

where h is the latitude and e is comprised of four parameters: the maximum value r, the latitude where the maximum occurs h_0 , and two slopes s_1 and s_2 on either side of the maximum. Some distance from h_0 , the Epstein function is nearly a straight line with slope s_1 or s_2 . Near h_0 , these two lines meet in an arc which reaches maximum r at h_0 . This is a special adaptation of the more general Epstein function.⁽⁸⁾

Fitting was done in two passes. First, the maximum latitude and value were chosen from the data and a least squares optimum value for s_1 and s_2 was calculated for all points above a cutoff. In order to inspect the quality of these fits, an interactive graphics system was developed to page through each local time and Kp, overlaying the original data and fit function. If a fit were judged visually to be something less than the best possible, any of the four

parameters could be modified in one of several ways and new least squares fits could be performed over variable ranges of latitude. Such modification was found to be necessary in about twenty percent of the cases.

When fitting was complete, we were left with 192 coefficients for each level of Kp. Since the local time dependence of the coefficients showed a slow and regular variation, we felt that the set could be represented by expansion of the Epstein coefficients in a Fourier series in local time. We took this series to order six.

$$\alpha(T) = \sum_{n=0}^6 [C_n \cos(2\pi T/24) + S_n \sin(2\pi T/24)]$$

where

T is MLT in hours and

α is r or h_0 or s_1 or s_2 above.

5.2.2 Results and Deliverables

The main result of this work were the sets of coefficients and software to implement them. As support, contour plots of original data and model, and histograms and plots of percent error were produced. A typical contour plot is shown in Figure 5.6 and a histogram of fractional deviation is shown in Figure 5.7. Also, tables of coefficients were supplied. In the case of the Epstein functions, these coefficients were doubly useful in that they could be used to give directly the position of the maximum and the minimum value. This study has been documented⁽⁹⁾ and is being prepared for submission to the Journal of Geophysical Research.⁽¹⁰⁾

ENERGY FLUX ORIGINAL DATA KP= 5

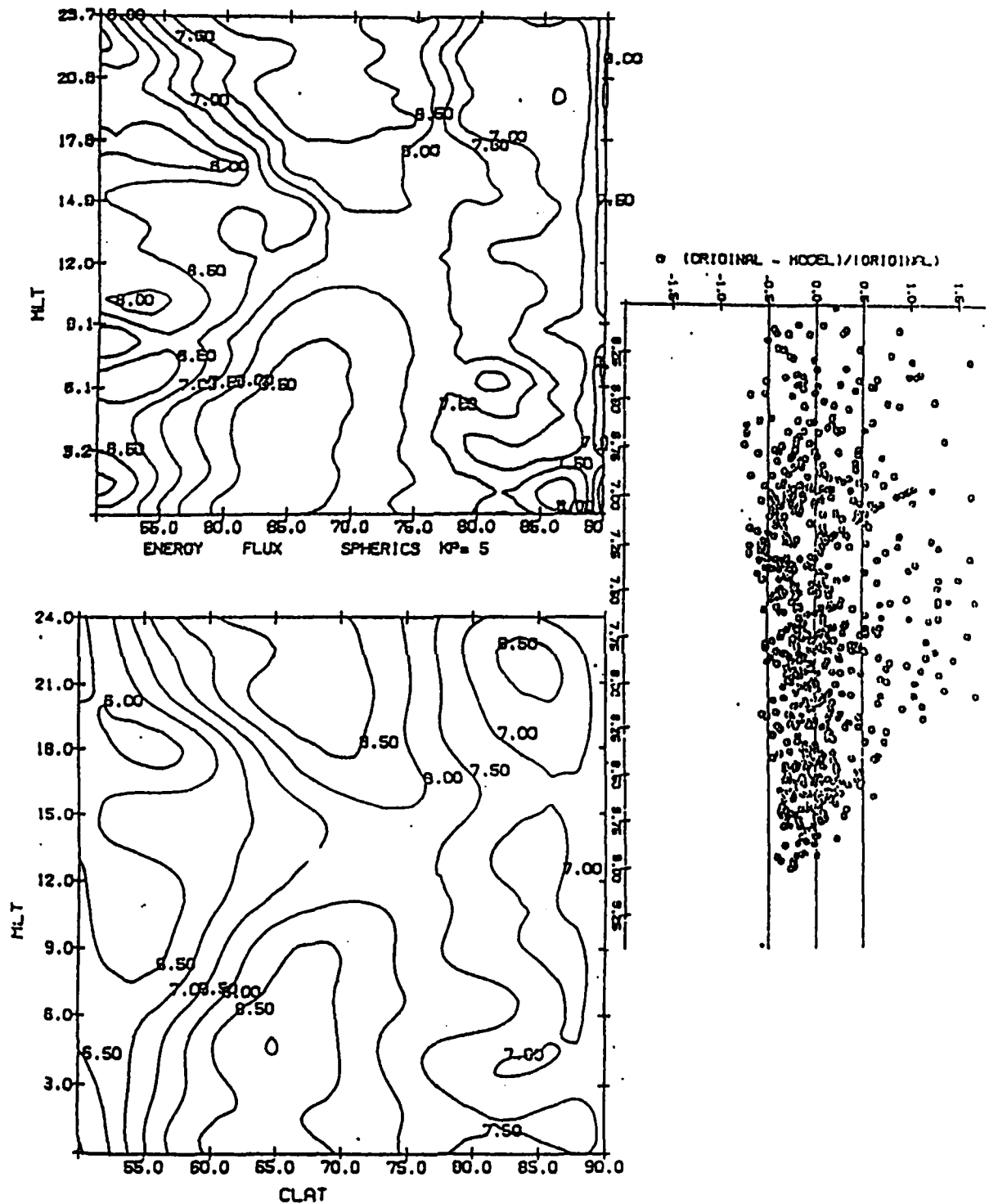


Figure 5.6 Example of Contours from Original Energy Flux Data (top), Spherical Harmonic Model (bottom), and Fractional Deviation as a Function of Value (right)

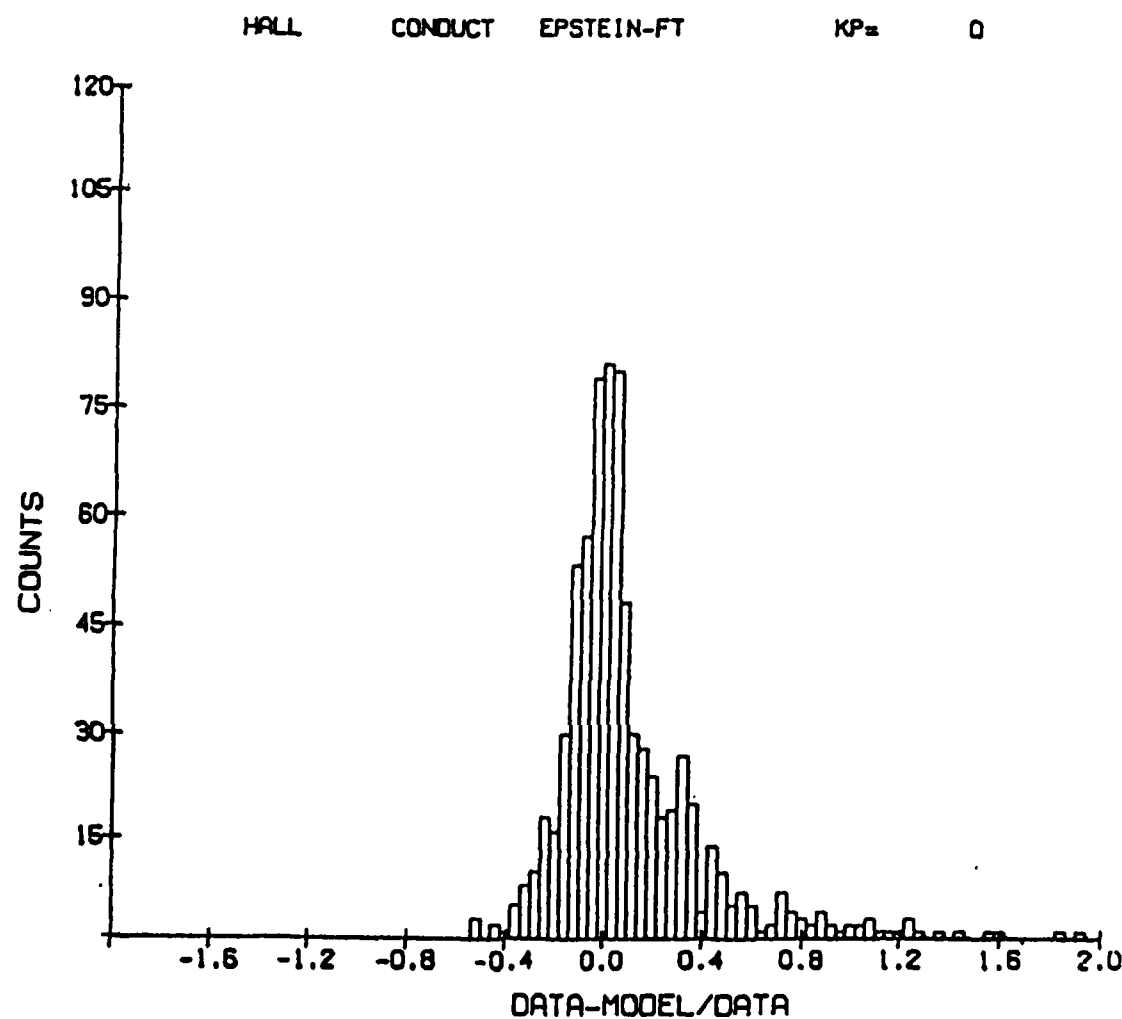


Figure 5.7 Histogram of Fractional Deviation of Epstein-Fourier Model from Original Data

References

1. McNeil, W.J., Hardy, D.A., and O'Neil, R.R., Private Communication.
2. McNeil, W.J. and Hardy, D.A., Private Communication.
3. Gussenhoven, M.S., et al., "1978 Diffuse Auroral Boundaries and a Derived Auroral Boundary Index," AFGL-TR-82-0398, ADA130175.
4. Hardy, D.A., and MacKean, R., "An Algorithm for Determining the Boundary of Auroral Precipitation Using Data from the SSJ/3 Sensor," AFGL-TR-80-0028, ADA084482.
5. Hardy, D.A., et. al., Private Communication.
6. Gussenhoven, M.S., Hardy, D.A., and Heineman, N., "Systematics of the Equatorward Diffuse Auroral Boundary," J. Geophys. Res., 88, 5692, 1983.
7. Hardy, D.A., Gussenhoven, M.S., and Holeman, E., "A Statistical Model of Auroral Electron Precipitation," J. Geophys. Res., 90, 4229 (1985).
8. Rawer, K. et. al., "International Reference Ionosphere IRI 79," World Data Center A for Solar-Terrestrial Physics, NOAA, Report UAG-82, November 1981.
9. McNeil, W.J. and Hardy, D.A., Private Communication.
10. Hardy, D.A., Gussenhoven, M.S., Raistrick, R., O'Neil, R.R., and McNeil, W.J., "Statistical and Functional Representation of ?? Patterns of Energy Flux, Number Flux and Conductivity," J. Geophys. Res., (submitted for publication August 1986).

6.0 The AFGL Interactive Targeting System

6.1 Introduction

The AFGL Interactive Targeting System (AITS) was designed to provide pre-mission and on-orbit planning support for the CIRRIS-1A project. It is a computer based system which displays shuttle position and sensor line of sight in various formats. Color graphic displays are used to depict the world map, the celestial sphere, and the probability of auroral activity. This system is required to provide researchers with the tools needed to evaluate, in near realtime, the shuttle and the sensor orientation during data gathering portions of the orbit, and to view the dynamics of the shuttle attitude and the auroral oval conditions. It also provides information on sensor line of sight and field of view for earth and space targets. The system is user friendly and provides the researcher with an interactive menu to select the desired computation or display.

The AITS system was developed to support the CIRRIS-1A project, however, the system can be applied toward any orbiting sensor whose pointing direction can be calculated. The system is especially useful for sensors whose pointing direction can be controlled.

6.2 General Description

6.2.1 System Application

The upper atmosphere is highly dynamic and exhibits infrared spectral and spatial structure which can interfere with Air Force systems' detection of infrared targets. The purpose of CIRRIIS-1A is to measure and characterize the spectral and spatial properties of the earth limb atmosphere. Specific objectives include: infrared radiation from atmosphere airglow, auroral emissions, targets of opportunity, and effects of local shuttle contamination.

CIRRIIS-1A will measure the spectral and spatial characteristics of the 30-300 km earthlimb over a range of latitudes, day/night conditions, and geomagnetic activity. This data will form the basis of an earthlimb model of spectral signatures and spatial clutter which can be used by designers to optimize the performance of their operational systems. Secondary objectives are to measure targets of opportunity and to demonstrate the role of a military payload specialist (Manned Spaceflight Engineer - MSE) in on-orbit shuttle operations.

To obtain this data, the CIRRIIS-1A measurement modes include vertical, horizontal, and stare scans of the earthlimb using various interferometer, radiometer, optical filters, and scan pattern combinations. For example, an earthlimb scan be entirely pre-programmed as to where the sensor will step through a sequence of tangent heights to provide a vertical atmospheric profile. On the other hand, for transitory observations, the payload specialist will track auroral or other targets of opportunity using a low light level TV (LLTV) co-aligned with the sensor telescope, and a joystick controller in the orbiter aft flight deck.

This report provides a functional description of the ground based flight support computer system. The intended uses of the system are to provide the following:

1. Provide the tools required for the AFGL researcher to effectively manage the data measurement periods available to the CIRRIS payload on orbit.
2. Provide support to the payload specialists as required for the targets of opportunity.
3. Provide limited preflight mission planning.
4. Provide limited post flight ancillary data analysis.

6.2.2 System Requirements

The AITS software operates on a Digital Equipment Corporation (DEC) VAX 11-750 computer system. The computer system configuration consists of a 456 Mega-byte fixed hard disk for database storage; a 9-track magnetic tape drive for permanent archive of databases generated and for initial loading of the AITS and system software; a system printer for hard copy output of selected computations; color graphic terminals for use in the generation of mission required displays; and a color ink jet hard copy unit to obtain copies of the graphic terminal displays for archive and for use in mission planning.

6.3 Operations Support Functions

The AITS software system provides researchers with the capability to compute and display information relevant to the operation of probes flown on the space shuttle. Data displays are used for long and short range operations planning, and post pass evaluation of data taking conditions. The processes calculate, for the CIRRIS-1A payload, the sensor's line of sight and orientation needed to view target locations. The CIRRIS-1A payload is a multi-sensor gimbal mounted system with the sensor's orientation requirements determined by the data gathering operation being performed. A description of the processes and displays and their use in the planning function is given below.

6.3.1 Vehicle Flight Simulation

This procedure provides displays of shuttle ground tracks on latitude and longitude grids with continental outlines. This can be either a linear or polar coordinate display. Also, the Feldstein⁽¹⁾ auroral oval and Hardy/Gussenhoven^(2,3,4) probability contours, described in Section 6.4.4 of this report, and the day/night terminator locations at 0 km, 100 km, and satellite altitude are projected onto these maps. A GMT and MET time scale is shown on the bottom of the display along with a one day mission time line containing planned sensor modes of operation. These displays can be used by the researchers to determine ground tracks of the past and upcoming orbits; present time and position of the vehicle; line of sight fan of the instrument relative to the auroral oval and probability contours; and when the next instrument operation mode will occur.

Figure 6.1 shows the linear world map projection display that is used to monitor the position of the vehicle. The day/night terminators, Feldstein auroral ovals, Hardy/Gussenhoven contours, and the vehicle's ground track are recalculated and displayed at a rate of every 5 minutes during the monitoring process. The ground track position is shown on the terminal display in white, directional arrows depict where the vehicle was for the past 30 minutes. The portion in red with directional arrows shows where it will be in the next 120 minutes. The point representing the vehicle's location, at the displayed time, is depicted with a flashing image of the vehicle on the ground track. The image of the vehicle is repositioned every minute to represent the actual movement of the vehicle as a function of time. The shuttle pointer below the time scale shows the present time and the instrument operation occurring.

The user can select one of three vehicle attitude orientations; Belly to Ram (BTR), Gravity Gradient South (GGS), or Gravity Gradient North (GGN) when determining the region for the gimbaled sensor's field of view. The sensor's field of view is displayed at each directional arrow as gimbal scan regions. Each gimbal scan region is displayed on the terminal in either white depicting where the scan region was in the past 30 minutes, or red depicting where the scan region will be in the next 120 minutes.

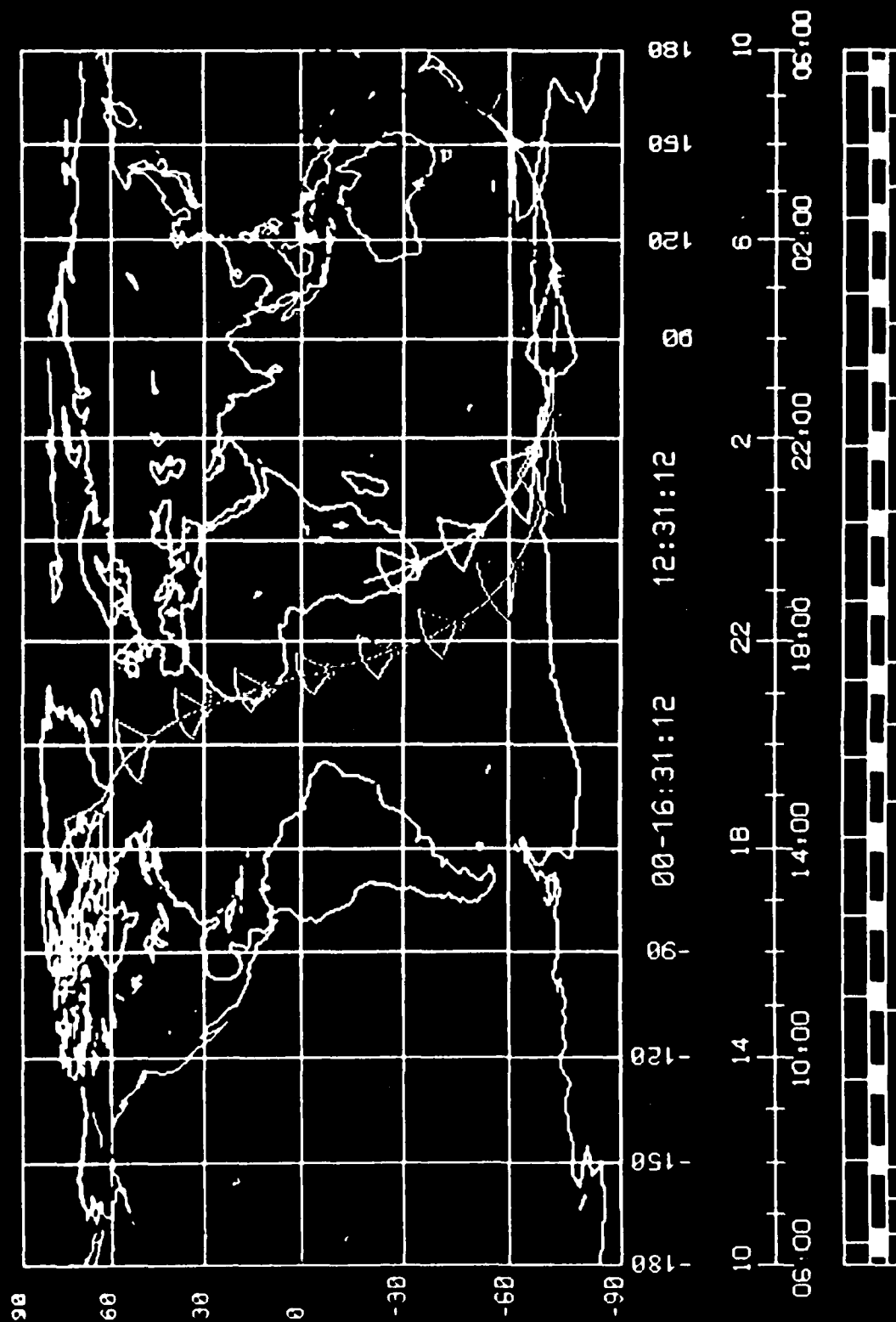


Figure 6.1 Vehicle Flight Simulation (Linear Projection)

6.3.2 Ephemeris Computations

Orbit parameter computation is done using a software package derived from the ephemeris calculation program LOKANGL.^(5,6) The package interpolates between orbital elements to compute satellite position, or extrapolates from an orbital element set for cases of thrust or lack of further elements. In interpolation or extrapolation, the package uses the six elements (a, the semi-major axis; e, eccentricity; N, the right ascension of the ascending node; w, the argument of perigee; i, the inclination; and M, the mean anomaly) along with their derivatives to compute sub-satellite position.

The condensing and retailoring of the LOKANGL package so that it is included in the software system, minimizes the need for pregenerated ephemeris information and the amount of computer storage. The major advantage of these independent ephemeris computations arises when online updating of the satellite position elements occurs. Regeneration of data files to incorporate the change is unnecessary since the routines access the orbital position elements directly. Initial orbital elements are entered prior to launch and are updated as they become available during on-orbit operations.

6.3.2.1 Trajectory

Ephemeris computations performed include calculation of vehicle position in geodetic and geocentric coordinates and corrected geomagnetic coordinates. Vehicle position information may be generated in the form of hardcopy listing or as a graphical display). The graphical display provides the user with the geographic projection of the position of the vehicle for the time span selected. Modified mercator, linear, or polar projections of the world map may be used to depict the geographic outline of the land masses and the vehicle's position.

6.3.2.2 Station Look Angle

The station look angle option provides the user with the capability to compute and display information when the shuttle is within the field of view of ground stations. NASA, SCF, and ADCOM ground station coordinates reside in permanent storage and may be selected, or the coordinates of any ground station may be entered. The user selects the desired minimum elevation for the station viewing of the vehicle during the time span selected.

A tabular output containing start and end times of viewing, and the maximum elevation time at each station is generated (Figure 6.2). Graphical displays of modified mercator, linear, or polar projection of the world map can be chosen by the user. These displays contain the vehicle's ground track along with the chosen station's conical viewing region determined by the altitude of the vehicle and the minimum viewing elevation selected.

6.3.3 Celestial Support Functions

The AITS software uses various displays, symbols and colors to represent the celestial sphere and stellar sources. Stellar intensities are denoted by various colors, and symbol sizes within a color. Each display shows for the time period selected, the celestial ecliptic plane, and the planets. The vehicle's orbital path for the time period selected is projected onto the celestial sphere with directional arrows at 5 minute intervals. The celestial sphere and computed information can be depicted as spherical, aitoff, or linear display projections. These displays can be used to show what the instrument will view in the celestial background.

| YR/MN/DY | GMT | START OF VIEWING | | | GMT | END OF VIEWING | | | RANGE | | | GMT | RANGE | | | GMT | PEAK ELEVATION | | | DURATION | STATION |
|----------|----------|------------------|--------|--------|----------|----------------|--------|--------|----------|------|--------|--------|-------|----------|----|-------|----------------|----|---------|----------|---------|
| | | EL | AZ | RANGE | | EL | AZ | RANGE | | EL | AZ | RANGE | | EL | AZ | RANGE | EL | AZ | SECONDS | | |
| 86/ 3/21 | 13:29:00 | 19.5 | 50.6 | 777.8 | 13:31:00 | 15.7 | 118.5 | 928.8 | 13:30:00 | 21.8 | 88.3 | 730.1 | 120. | GSTDN75 | | | | | | | |
| 86/ 3/21 | 13:29:00 | 19.4 | 51.4 | 781.2 | 13:31:00 | 15.4 | 118.5 | 939.0 | 13:30:00 | 21.5 | 88.9 | 738.4 | 120. | ADCOM354 | | | | | | | |
| 86/ 3/21 | 14:16:00 | 17.4 | -112.6 | 1084.5 | 14:19:00 | 15.6 | -32.6 | 1116.1 | 14:17:00 | 22.5 | -87.4 | 904.0 | 180. | ADCOM334 | | | | | | | |
| 86/ 3/21 | 15:49:00 | 21.5 | -106.4 | 927.4 | 15:51:00 | 21.4 | -42.3 | 907.3 | 15:50:00 | 25.8 | -74.7 | 806.1 | 120. | GSTDN24 | | | | | | | |
| 86/ 3/21 | 15:49:00 | 20.8 | -108.3 | 948.1 | 15:51:00 | 21.9 | -44.6 | 893.1 | 15:50:00 | 25.6 | -77.6 | 810.3 | 120. | SCF37 | | | | | | | |
| 86/ 3/21 | 14:03:00 | 25.6 | -149.2 | 923.3 | 14:07:00 | 20.6 | 7.4 | 1058.3 | 14:05:00 | 66.1 | -47.5 | 487.2 | 240. | GSTDN37 | | | | | | | |
| 86/ 3/21 | 18:10:00 | 24.5 | -12.1 | 742.8 | 18:13:00 | 25.1 | 155.9 | 765.2 | 18:11:00 | 56.4 | -0.6 | 413.5 | 180. | GSTDN54 | | | | | | | |
| 86/ 3/22 | 03:48:00 | 19.2 | 137.2 | 1115.6 | 03:50:00 | 18.2 | 87.8 | 1146.8 | 03:49:00 | 21.1 | 112.1 | 1047.4 | 120. | GSTDN54 | | | | | | | |
| 86/ 3/21 | 16:25:00 | 16.0 | -11.7 | 817.6 | 16:28:00 | 23.1 | 159.1 | 651.6 | 16:27:00 | 62.0 | 141.9 | 314.1 | 180. | ADCOM363 | | | | | | | |
| 86/ 3/21 | 16:22:00 | 30.9 | -38.7 | 497.3 | 16:24:00 | 24.8 | 178.9 | 599.8 | 16:23:00 | 58.4 | -129.8 | 316.0 | 120. | GSTDN02 | | | | | | | |
| 86/ 3/21 | 16:22:00 | 30.9 | -38.7 | 497.3 | 16:24:00 | 24.8 | 178.9 | 599.8 | 16:23:00 | 58.4 | -129.8 | 315.9 | 120. | ADCOM466 | | | | | | | |
| 86/ 3/21 | 16:19:00 | 23.2 | -22.4 | 621.1 | 16:22:00 | 15.5 | 158.8 | 835.9 | 16:20:00 | 67.3 | -23.8 | 291.4 | 180. | ADCOM387 | | | | | | | |
| 86/ 3/21 | 17:54:00 | 25.8 | -44.7 | 572.0 | 17:56:00 | 25.8 | -169.2 | 582.8 | 17:55:00 | 47.9 | -108.1 | 360.0 | 120. | ADCOM399 | | | | | | | |
| 86/ 3/21 | 17:55:00 | 15.4 | -76.5 | 835.2 | 17:56:00 | 18.0 | -111.1 | 757.9 | 17:56:00 | 18.0 | -111.1 | 757.9 | 60. | GSTDN71 | | | | | | | |
| 86/ 3/21 | 16:19:00 | 32.1 | -18.5 | 483.3 | 16:21:00 | 26.2 | 154.2 | 569.2 | 16:20:00 | 77.6 | 126.5 | 276.2 | 120. | SCF36 | | | | | | | |
| 86/ 3/22 | 05:40:00 | 15.5 | 131.8 | 1060.9 | 05:42:00 | 15.1 | 78.7 | 1043.0 | 05:41:00 | 17.8 | 105.5 | 954.5 | 120. | ADCOM387 | | | | | | | |
| 86/ 3/21 | 19:24:00 | 25.9 | 11.3 | 567.6 | 19:26:00 | 23.8 | 129.6 | 612.3 | 19:25:00 | 43.5 | 74.9 | 382.3 | 120. | GSTDN28 | | | | | | | |
| 86/ 3/21 | 19:25:00 | 15.3 | -60.8 | 832.6 | 19:27:00 | 19.3 | -137.2 | 717.5 | 19:26:00 | 22.7 | -95.2 | 632.7 | 120. | SCF99 | | | | | | | |
| 86/ 3/21 | 19:26:00 | 21.8 | -91.1 | 650.7 | 19:27:00 | 19.7 | -133.3 | 706.6 | 19:26:00 | 21.8 | -91.1 | 650.7 | 60. | SCF90 | | | | | | | |
| 86/ 3/21 | 23:34:00 | 18.8 | -93.5 | 929.4 | 23:36:00 | 17.5 | -32.2 | 942.4 | 23:35:00 | 21.7 | -62.5 | 827.0 | 120. | ADCOM337 | | | | | | | |
| 86/ 3/21 | 20:18:00 | 17.3 | 129.2 | 1130.9 | 20:20:00 | 16.7 | 80.0 | 1136.5 | 20:19:00 | 19.3 | 104.5 | 1047.1 | 120. | SCF38 | | | | | | | |
| 86/ 3/21 | 19:23:00 | 22.2 | 33.5 | 641.7 | 19:25:00 | 15.9 | 115.6 | 818.0 | 19:24:00 | 25.3 | 81.5 | 582.6 | 120. | ADCOM388 | | | | | | | |
| 86/ 3/21 | 22:31:00 | 26.0 | 43.8 | 573.8 | 22:33:00 | 15.7 | 128.4 | 844.4 | 22:32:00 | 26.9 | 97.6 | 564.3 | 120. | GSTDN12 | | | | | | | |
| 86/ 3/21 | 22:31:00 | 27.8 | 25.8 | 545.6 | 22:33:00 | 20.5 | 132.7 | 701.5 | 22:32:00 | 37.4 | 90.9 | 438.0 | 120. | SCF35 | | | | | | | |
| 86/ 3/22 | 02:38:00 | 17.8 | -90.2 | 951.7 | 02:40:00 | 16.4 | -31.0 | 969.3 | 02:39:00 | 20.4 | -60.2 | 854.9 | 120. | GSTDN22 | | | | | | | |
| 86/ 3/22 | 03:20:00 | 21.2 | 6.1 | 831.1 | 03:23:00 | 24.5 | 137.1 | 788.2 | 03:22:00 | 43.7 | 104.8 | 504.5 | 180. | GSTDN37 | | | | | | | |
| 86/ 3/22 | 01:38:00 | 20.5 | -76.6 | 714.3 | 01:40:00 | 15.6 | -149.9 | 887.0 | 01:39:00 | 22.9 | -118.4 | 667.7 | 120. | ADCOM334 | | | | | | | |
| 86/ 3/22 | 00:52:00 | 19.9 | 129.5 | 1076.0 | 00:54:00 | 17.7 | 77.9 | 1105.3 | 00:53:00 | 20.9 | 103.2 | 1000.6 | 120. | GSTDN75 | | | | | | | |
| 86/ 3/22 | 00:52:00 | 18.7 | 129.4 | 1085.9 | 00:54:00 | 17.5 | 78.3 | 1112.6 | 00:53:00 | 20.6 | 103.4 | 1010.0 | 120. | ADCOM354 | | | | | | | |
| 86/ 3/22 | 12:57:00 | 19.5 | 134.6 | 1108.9 | 12:59:00 | 17.2 | 86.5 | 1192.0 | 12:58:00 | 20.5 | 109.4 | 1069.0 | 120. | GSTDN37 | | | | | | | |
| 86/ 3/22 | 03:09:00 | 17.5 | -92.0 | 794.8 | 03:10:00 | 16.5 | -126.1 | 838.5 | 03:09:00 | 17.5 | -92.0 | 794.8 | 60. | GSTDN24 | | | | | | | |
| 86/ 3/22 | 03:09:00 | 17.0 | -94.4 | 809.0 | 03:10:00 | 15.6 | -127.4 | 867.6 | 03:09:00 | 17.0 | -94.4 | 809.0 | 60. | SCF37 | | | | | | | |
| 86/ 3/22 | 07:14:00 | 19.3 | -75.7 | 886.2 | 07:15:00 | 18.9 | -44.2 | 884.8 | 07:14:00 | 19.3 | -75.7 | 886.2 | 60. | SCF36 | | | | | | | |
| 86/ 3/22 | 07:09:00 | 18.1 | -105.7 | 988.9 | 07:11:00 | 20.5 | -44.3 | 882.2 | 07:10:00 | 23.0 | -77.2 | 828.3 | 120. | GSTDN71 | | | | | | | |
| 86/ 3/22 | 05:34:00 | 18.8 | 171.7 | 1006.1 | 05:36:00 | 16.2 | 36.4 | 1044.8 | 05:35:00 | 44.8 | 100.4 | 524.8 | 240. | ADCOM362 | | | | | | | |
| 86/ 3/22 | 08:41:00 | 21.4 | -137.0 | 877.1 | 08:44:00 | 24.8 | -7.1 | 752.5 | 08:43:00 | 44.6 | -44.0 | 495.9 | 180. | SCF99 | | | | | | | |
| 86/ 3/22 | 08:41:00 | 21.8 | -133.8 | 866.2 | 08:44:00 | 23.2 | -8.3 | 789.3 | 08:43:00 | 41.0 | -42.3 | 526.9 | 180. | SCF90 | | | | | | | |
| 86/ 3/22 | 05:22:00 | 15.7 | -80.4 | 1252.3 | 05:24:00 | 15.7 | -80.4 | 1252.3 | 05:23:00 | 15.7 | -80.4 | 1252.3 | 0. | GSTDN54 | | | | | | | |
| 86/ 3/22 | 10:15:00 | 16.3 | -106.1 | 1021.1 | 10:17:00 | 21.4 | -45.0 | 823.3 | 10:16:00 | 22.2 | -79.6 | 817.2 | 120. | ADCOM388 | | | | | | | |
| 86/ 3/22 | 08:41:00 | 15.7 | 150.0 | 1078.2 | 08:44:00 | 16.5 | 64.2 | 998.6 | 08:43:00 | 22.9 | 91.7 | 813.5 | 180. | GSTDN28 | | | | | | | |
| 86/ 3/22 | 09:19:00 | 16.0 | -59.5 | 885.6 | 09:21:00 | 22.1 | -132.4 | 729.6 | 09:20:00 | 24.0 | -91.1 | 676.4 | 120. | SCF38 | | | | | | | |
| 86/ 3/22 | 09:08:00 | 24.0 | -46.9 | 603.7 | 09:10:00 | 26.4 | -167.1 | 566.9 | 09:09:00 | 45.1 | -102.9 | 373.4 | 120. | ADCOM337 | | | | | | | |
| 86/ 3/22 | 11:41:00 | 23.2 | -162.1 | 863.7 | 11:45:00 | 15.7 | 15.0 | 1054.8 | 11:43:00 | 72.8 | 3.1 | 891.0 | 240. | GSTDN12 | | | | | | | |
| 86/ 3/22 | 11:41:00 | 23.1 | -149.6 | 866.4 | 11:44:00 | 22.0 | -1.3 | 703.1 | 11:43:00 | 57.9 | -38.8 | 438.2 | 180. | SCF35 | | | | | | | |
| 86/ 3/22 | 13:55:00 | 24.4 | -63.1 | 670.5 | 13:57:00 | 22.5 | -153.5 | 737.0 | 13:56:00 | 32.8 | -111.5 | 544.2 | 120. | GSTDN75 | | | | | | | |
| 86/ 3/22 | 13:55:00 | 24.9 | -63.2 | 661.3 | 13:57:00 | 22.5 | -154.4 | 738.2 | 13:56:00 | 33.3 | -112.6 | 539.3 | 120. | ADCOM354 | | | | | | | |
| 86/ 3/22 | 12:11:00 | 20.5 | -73.6 | 679.9 | 12:13:00 | 16.3 | -153.9 | 809.3 | 12:12:00 | 24.6 | -118.6 | 595.8 | 120. | GSTDN22 | | | | | | | |
| 86/ 3/22 | 14:42:00 | 20.7 | 139.3 | 960.2 | 14:44:00 | 22.3 | 75.9 | 887.6 | 14:43:00 | 25.7 | 109.2 | 813.7 | 120. | GSTDN24 | | | | | | | |
| 86/ 3/22 | 14:42:00 | 20.1 | 141.4 | 976.4 | 14:45:00 | 15.4 | 55.7 | 1111.3 | 14:43:00 | 25.7 | 112.2 | 813.2 | 180. | SCF37 | | | | | | | |
| 86/ 3/22 | 14:30:00 | 16.0 | -99.2 | 1241.9 | 14:32:00 | 15.8 | -55.3 | 1246.0 | 14:31:00 | 17.8 | -77.2 | 1166.4 | 120. | GSTDN37 | | | | | | | |

Figure 6.2 Station Look Angle (Example Listing #1)

A spherical projection of the celestial sphere consists of approximately one fourth of the sphere, where the focal point of the projection is user determined. The central region of a spherical projection supplies the user with an actual representation of the celestial area viewed. This type of projection allows the user to obtain necessary information about the LOS or FOV of the sensor as it tracks along a specific region of the celestial sphere during that orbit.

Aitoff and linear projections allow the user to display the complete celestial sphere and all the computed information on one display. An aitoff projection minimizes distortion of the polar regions. Both types of displays show a full orbit projection and also all the regions that the sensor's LOS or FOV encounter. The aitoff and linear display are the most useful type of display when performing gimbal angle determination for a celestial target sighting. These projections allow the user to view all the gimbal angles necessary at each point in the orbit.

6.3.4 Camera Computations

6.3.4.1 Camera View Simulation at an Instant

The AITS system process for Camera View Simulation allows the user to graphically display the camera field of view (FOV) at a given instant in the mission. The user selects the time desired along with the vehicle attitude and gimbal orientation of the camera to be used for the simulation. The graphic display contains land masses, stars, planets, and a simulation of the auroral boundary that would be encountered at that time in the mission (Figure 6.3). The FOV is annotated with a crosshair that marks the line of sight (LOS) of the camera and the angular dimension of the FOV. The display is annotated with either the geographic location of the LOS tangency or the intersection with the earth. In the cases where the camera FOV does not contain any portion of the earth, the display is annotated with the celestial coordinates for the LOS.

6.3.4.2 Camera Celestial Target Tracking

This process allows the user to select a celestial target location and obtain the gimbal angles required to maintain the target within the camera's FOV. The user selects the period of interest in the mission and a constant vehicle attitude for that period. The process then computes the gimbal angles required for the camera to view the target location over the span of time selected. This information is shown across the bottom of the display as XY graphs (Figure 6.4). The top of the display contains the celestial region that the gimbal tolerances allow the camera to view.

| | | | | | | | | | | | | | |
|-------|-----|-----|---|------|-----|-------|----------|----------|-------|-----------|--------|----------|------|
| PITCH | 268 | YAW | 0 | ROLL | 180 | GP- 5 | GP- -19 | LATITUDE | 45.12 | LONGITUDE | -71.85 | T.H. ALT | 0.00 |
| | | | | | | | 16:22:30 | | | | | | |

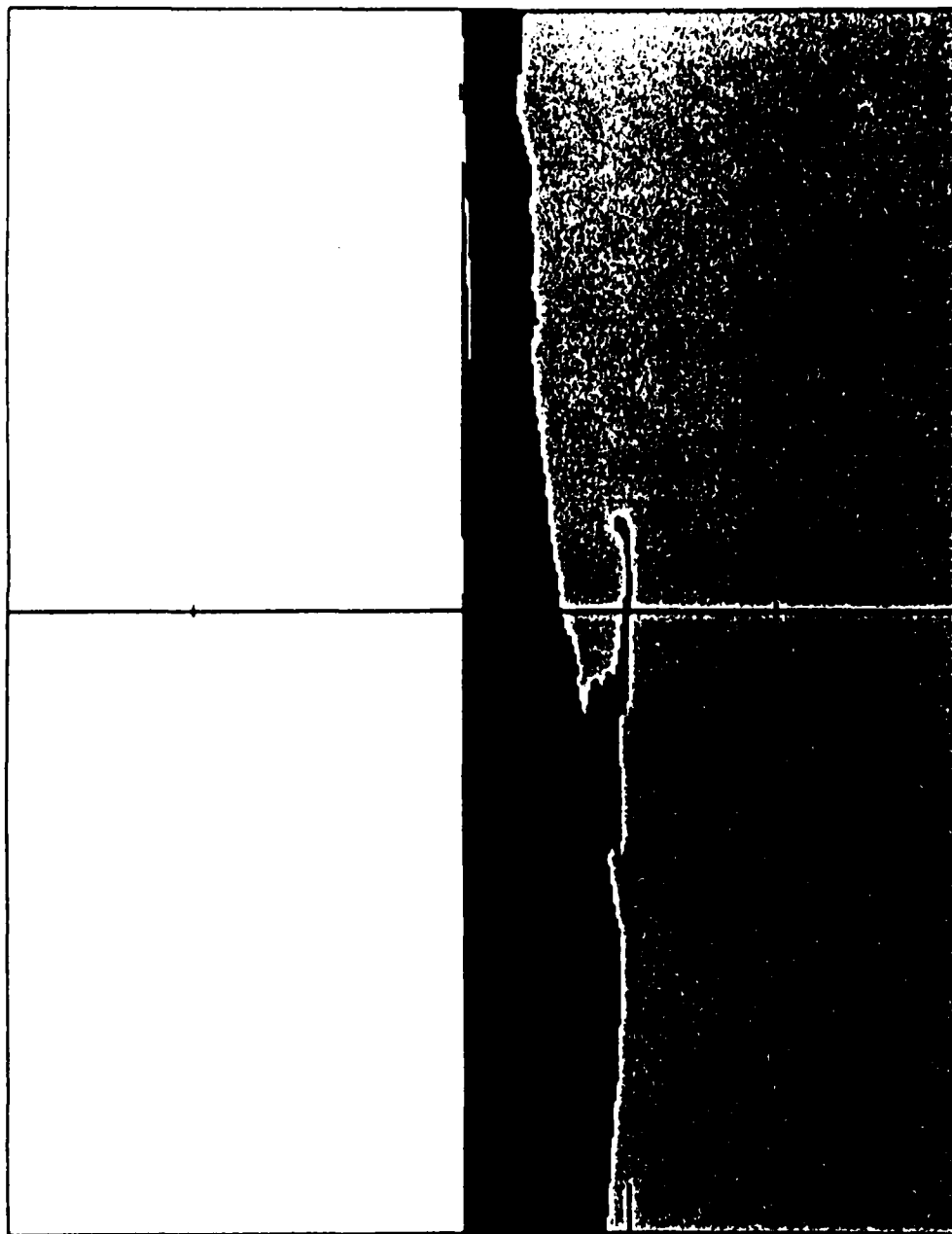
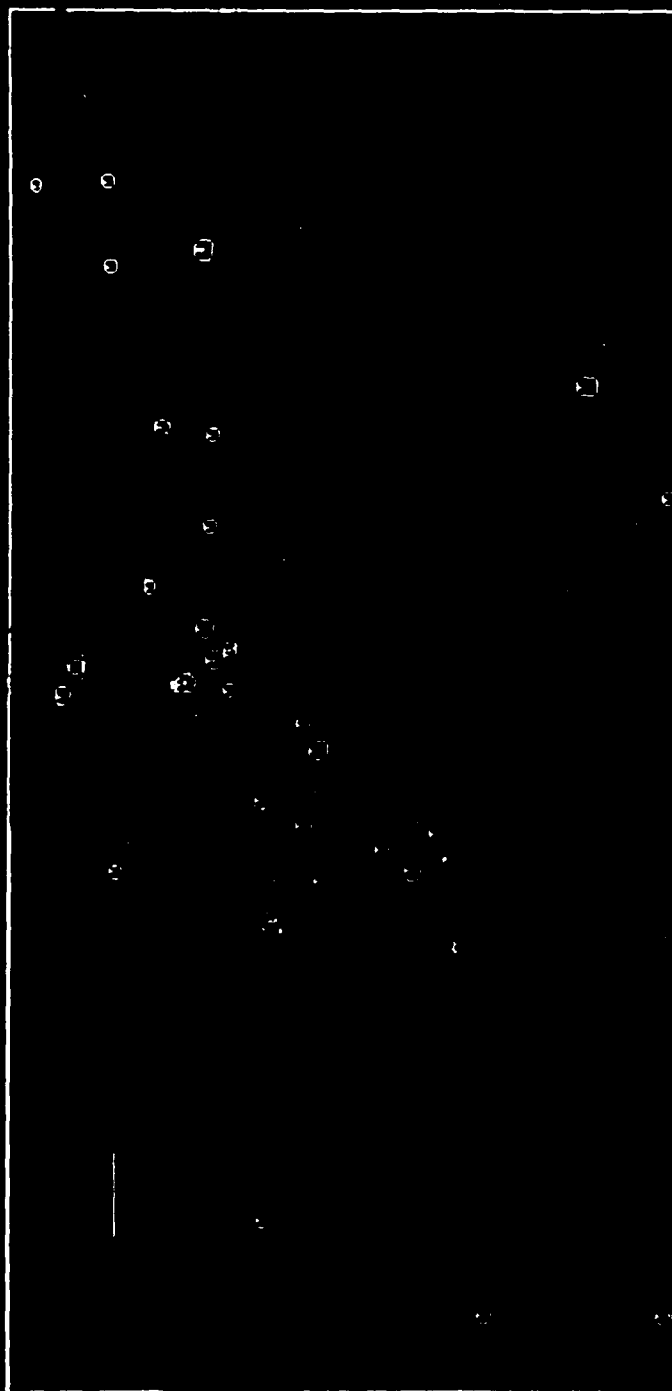


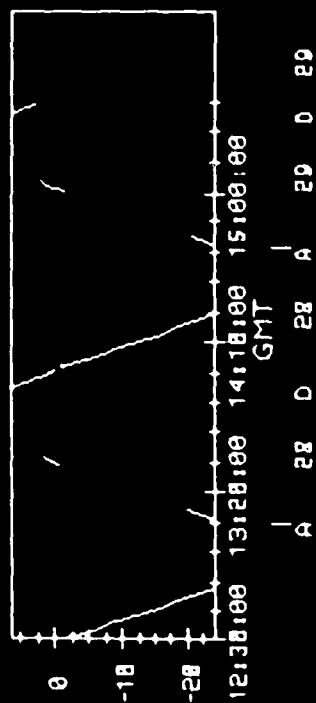
Figure 6.3 Camera View Simulation at an Instant

TARGET RA 264.00 DEC -34.00

PITCH 110 YAW 10 ROLL 110



GIMBAL PITCH



GIMBAL ROLL

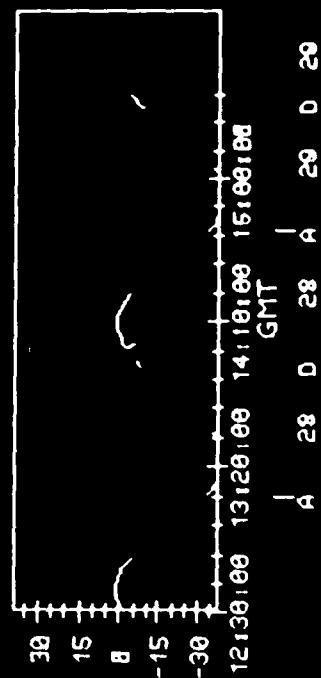


Figure 6.4 Camera Celestial Tracking

The actual camera's FOV location for the selected time is displayed within the gimbal region with a red outline. The user may then step forward in time to view the camera's FOV and gimbal region at another instant using the same attitude and target parameters. The gimbal region display contains the stars and planets viewed and, for cases of earth intersection, a brown spherical representation of the earth's region. The gimbal angles, vehicle attitude, and the time period in the mission are stored as part of the user defaults during this process. This allows the user the option of implementing the Camera View Simulation process to generate a camera FOV display with the earth land masses, stellar values, and auroral region encountered.

6.3.5 Gimbal/Off-Track Calculations

6.3.5.1 Ground & Celestial Target Gimbal Angle Determination

This process determines the gimbal angles required to view either a ground target, auroral region, or a celestial target location for a user entered constant vehicle attitude. An auroral region is defined by the geometric center (centroid) of a selected Hardy Auroral Probability Contour. The results of the computation performed for the selected span of time are tabulated on print-outs to aid the researcher in the selection of gimbal angles to use with other processes. The Local Vertical Local Horizontal (LVLH) angles of azimuth and elevation from the vehicle to the target; the local time at the target; and the geodetic position of the vehicle are tabulated for each of the target calculations. LVLH elevation is referenced positive down from the local horizontal toward the earth. LVLH azimuth is positive about the local vertical from the negative velocity vector on the local horizontal plane.

6.3.5.2 Ground & Celestial Target LVLH Angle Determination

This process determines the LVLH angles required to view a ground location or a celestial target. The user supplies the type of target and its coordinates, the span of time desired to process, and the type of output product desired. The process creates either a tabulated print-out of the information or a graphic display of the LVLH angles versus time.

The print-out values for both geographic and celestial target calculations contain the geodetic and corrected geomagnetic coordinates of the vehicle's position, and the LVLH azimuth and elevation. The display consists of the azimuth and elevation versus time, with the angular quantities of azimuth and elevation drawn in white for the periods that the earth did not obstruct the viewing of the target location. For periods of obstruction the angles are drawn in red. Each display will contain the length of time selected between a maximum of 12 hours and a minimum of 1 hour. Periods greater than 12 hours are shown as multiple displays.

6.4 AITS Databases

Various databases are utilized by the AITS system to generate graphical displays and determine LOS, FOV, and vehicle position. The users create their own set of parameters by defining attitude angles to use, auroral contours, gimbal orientation angles, and time periods for use in each of the analyses. This database is the only one that the user is allowed to alter during the use of the AITS system processes. All other databases used by the AITS system are resident on the computer system as a master directory to prevent inadvertent alteration. Sensor specific information concerning the sensor's mount angles and FOV dimensions are not alterable from process to process since this information is specific to the sensor.

6.4.1 SAO Stellar Catalog

The Smithsonian Astronomical Observatory (SAO) stellar catalog consists of 258,997 star locations referenced for the equinox of 1950⁽⁷⁾. Associated with each data location is a visual magnitude and coefficients to correct for the yearly motion from 1950. The SAO catalog has been modified to create a working database for access by the AITS software package. This working database consists of almost 10,000 stellar locations converted to the year and month of launch. The major criterion for the deletion of stellar locations in the creation of the working database was the inability to view these locations without utilizing specially designed optical sensors. The database structure created requires minimal computer time to display the stellar locations that are within the FOV. This is accomplished by the use of a direct access database where each element of the database defines a 10 by 20 degree grid.

6.4.2 World Map

The earth's land mass representation is obtained with the use of two separate databases, continental outlines and rasterized panels for each land mass. These were both created from a database maintained by the Data Systems Branch at the Air Force Geophysics Laboratory. The rasterized world map database was generated from the original by separating the database into grids of latitude and longitude to allow for individual grid panel rasterization. This database is designed as a direct access database with each grid panel being accessed as a separate element allowing greater access capability by the camera simulation portion of the AITS software.

6.4.3 Planned Mission and Updated Kepler Elements

The AITS system requires availability of the planned mission state-vector elements. These are obtained from either the Johnson Space Center (JSC) Super-Tape microfiche output or from the Satellite Control Facility (SCF). The updating of the element database is performed on-orbit by the user interactively entering the actual vehicle state-vectors at specific times.

6.4.4 Hardy/Gussenhoven Auroral Probabilities

This database consists of information on the probability of observing high flux auroral energy for a single orbital pass of the auroral region. The database contains two categories of probability for magnetic/solar activity level, Kp per pass and Equatorward Boundary (EQ) per pass^(1,2,3). The database was obtained from the analysis of sensor data derived from DMSP satellites. The difference from the EQ probability binning was the use of midnight auroral boundary in place of Kp.

The database structure consists of 16 different contours for the Kp probability and 25 different contours for the EQ probability. Each contour represents a particular probability condition of auroral energy, binned by the appropriate criteria at either two or three percentage levels. The storage format allows for alteration of the database given new contours from future probability study information.

6.4.4.1 Feldstein Auroral Oval

This database consists of eight auroral oval representations of inner and outer boundary per Feldstein derived auroral region⁽¹⁾. Each oval is stored in geomagnetic coordinates of local time and latitude. These coordinates are converted and displayed by the Flight Simulation process.

6.4.5 DMSP Satellite Images

This database is created by the user, during on-orbit support, from Global Weather Center (GWC) communications consisting of DMSP satellite auroral images. Analysts at GWC evaluate the DMSP auroral image and transmit, via telephone, information on the auroral activity region viewed by DMSP satellites. This information is interactively entered into the system by the user to create a contour database for display by the Flight Simulation process. These contours are archived on the AITS computer system database directory.

6.4.6 Mission Timeline

This information is entered prior to launch and updated during the mission as required. The database consists of all the information relevant to the times for each of the sensor measurements.

6.4.7 Station Coordinates

Latitude and longitude of SCF, GSTDN, and ADCOM Radar Tracking Stations (RTS) are maintained at the AITS system master directory. These locations can be displayed on world maps projections if required, or accessed by the user as ground target locations.

6.5 Coordinate Systems

The AITS software system utilizes a number of coordinate system in the generation of sensor FOV, LOS, and vehicle position. The most used systems and transformation matrixes are described below.

6.5.1 Local Vertical Local Horizontal (LVLH)

This coordinate system is referenced to the vehicle's position and direction of travel (velocity vector). The primary application is in the conversion of vehicle orientation to ECI coordinates. The LVLH coordinate system is a right-handed system with the geocentric radius to the vehicle and the velocity vector defining the orbital plane at that instant in time (Figure 6.5). The LVLH z-axis lies along the geocentric radius vector to the vehicle and is positive toward the center of the earth. The LVLH y-axis is the normal to the orbital plane and is determined by the cross-product of the LVLH z-axis and the vehicle's velocity vector. The cross-product of the LVLH y-axis and the LVLH z-axis generates the LVLH x-axis, completing the right-handed coordinate system. The vehicle's body orientation is transformed by the LVLH matrix to determine the vehicle's coordinates in an ECI coordinate system.

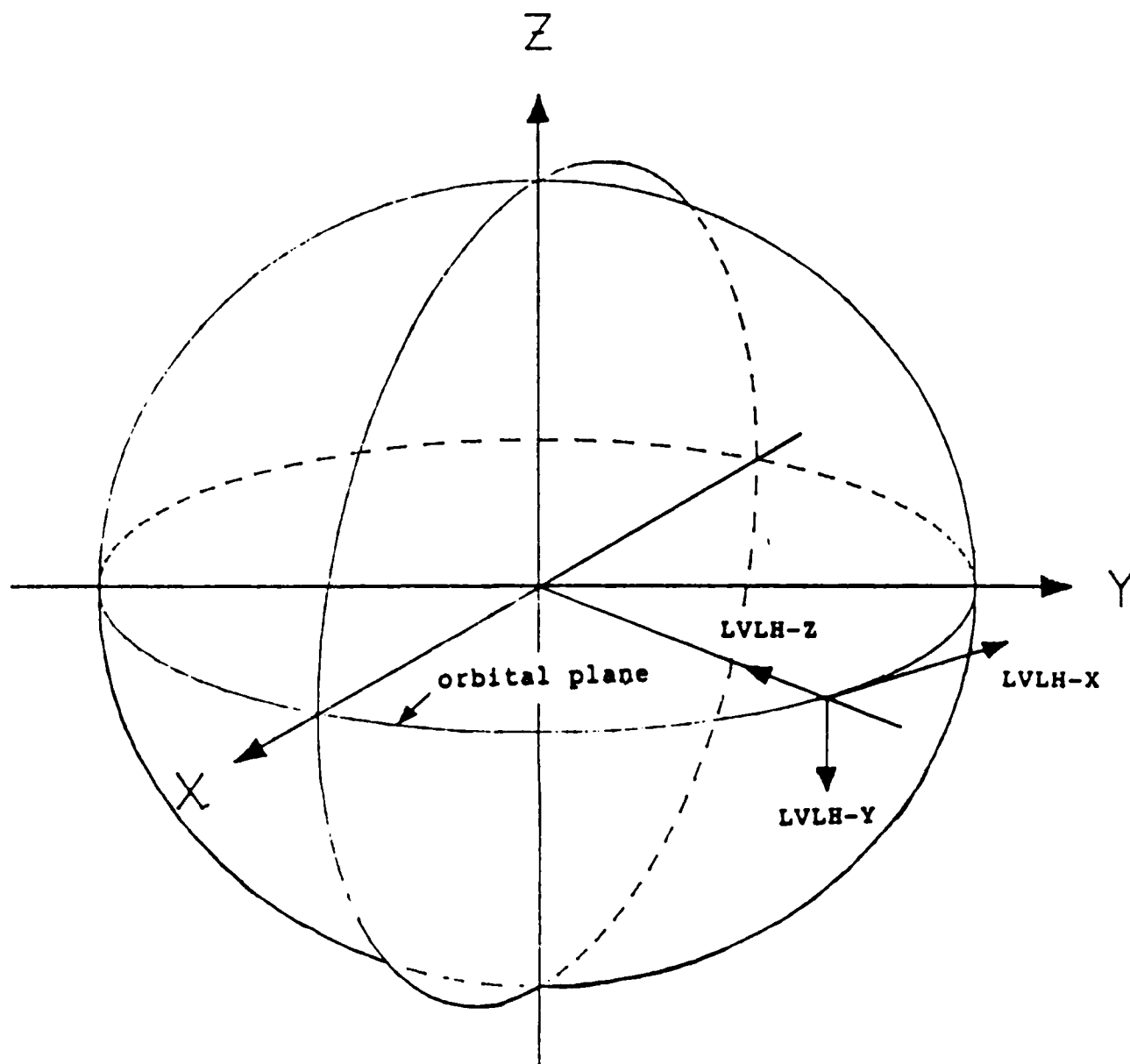


Figure 6.5 LVLH Coordinate System

6.5.2 Vehicle Body Orientation System (VBO)

The Euler rotation for the shuttle attitude is a pitch, yaw, and roll sequence. The shuttle's body coordinate system is a right handed system with the x-axis parallel to the vehicle's structural body axis (positive toward the shuttle nose), z-axis parallel to the vehicle's plane of symmetry and perpendicular to the x-axis (positive down with respect to the shuttle fuselage), and y-axis completing the right-handed system (positive toward the shuttle's right wing). The Euler angles for the shuttle are measured positive as follows: pitch up (positive x-axis to negative z-axis), yaw right (positive x-axis to positive y-axis), and roll clockwise (positive y-axis to positive z-axis) (Figure 6.6).

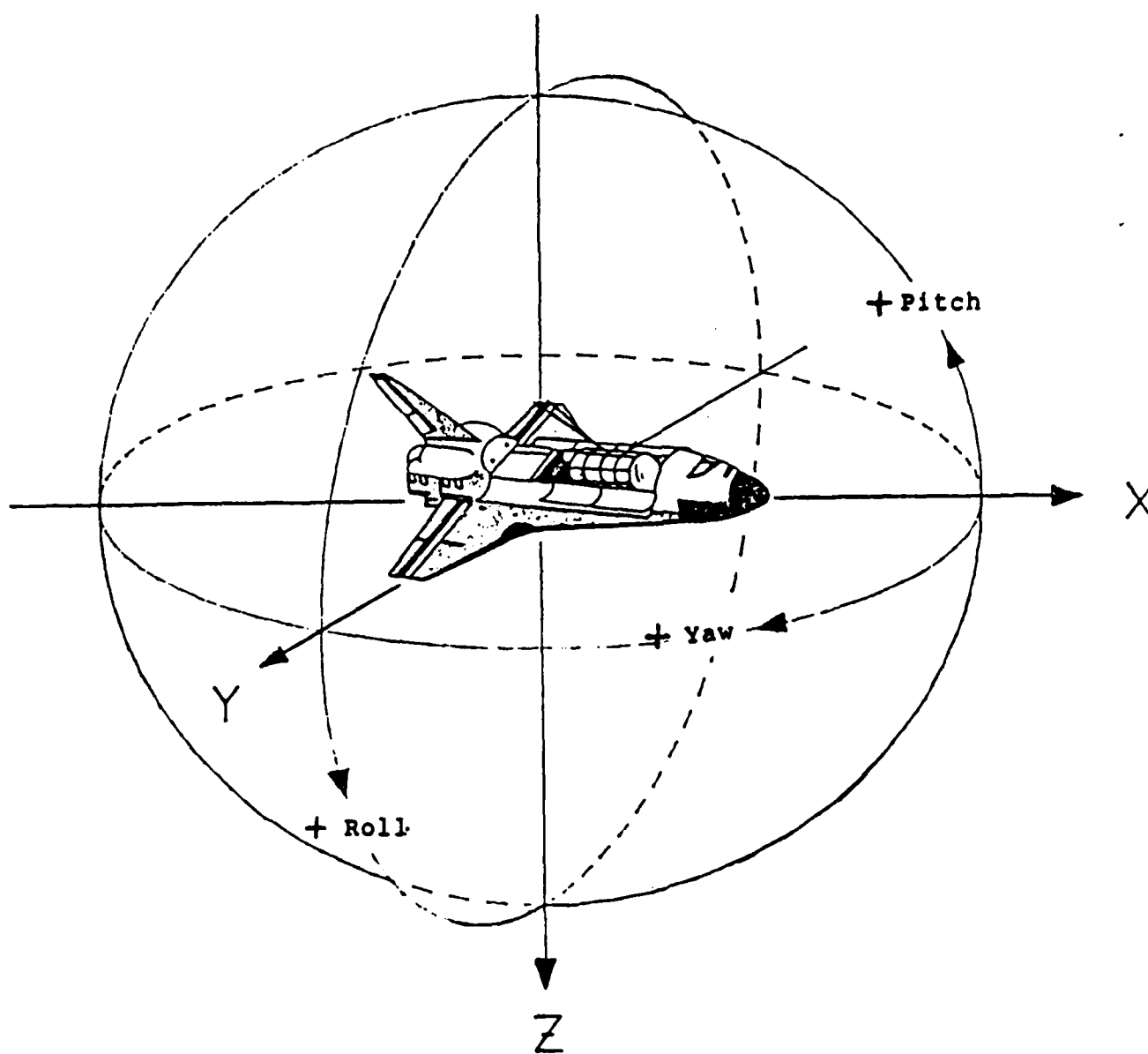


Figure 6.6 Vehicle Body Coordinate System and Rotation

6.6 User's Guide

The AITS software system is an interactive menu driven package that allows the user to select options and enter numeric values with great ease. The AITS menus require a terminal device that is Digital Video Terminal (VT) compatible. The AITS system utilizes terminal function and cursor movement keys in the selection of values for the processes. The menus allow the user to either use the default values that are displayed or to alter the value before continuing to the next menu option. The use of cursor movement keys allows the user to go forward or backward in the menu sequence to alter or verify the parameters entered.

The AITS system is initiated by the user entering the command "AFGL" at the VAX operating system prompt "\$" after login on the VAX. The main menu is then displayed for the user to select the desired process (Figure 6.7). The menu display will contain the AFGL logo if the terminal is a Tektronix model 4109. The following section defines the processes that the user may select from the main menu.



REAL-TIME FLIGHT SUPPORT SYSTEM

MAIN MENU

- 1 - VEHICLE FLIGHT SIMULATION
- 2 - EPHEMERIS CALCULATIONS
- 3 - CELESTIAL OPERATIONS SIMULATION
- 4 - CAMERA SIMULATION
- 5 - GIMBAL/OFF-TRACK ANGLES
- 6 - SPECIAL APPLICATIONS
- 9 - RETURN TO VAX/VMS

PROCESS DESIRED =

Figure 6.7 AITS Main Menu

References

1. James A. Whalen: Auroral Oval Plotter and Nomograph Determining Corrected Geomagnetic Local Time, Latitude, and Longitude for High Latitudes in the Northern Hemisphere. Environmental Research Papers, No. 327, AFCRL-70-0422, July 1970, AD713170.
2. W.J. McNeil, D.A. Hardy, R.R. O'Neil: Private Communication.
3. W.J. McNeil, D.A. Hardy, R.R. O'Neil: Private Communication.
4. M.S. Gussenhoven, D.A. Hardy, N. Heineman: Systematics of the Equatorward Diffuse Auroral Boundary, Journal for Geophysical Research, 88, 5692, 1983.
5. K. Minka: Orbit Determination and Analysis by the Minimum Variance Method. Martin Company, Baltimore Division, Er 13950. Prepared for AFCRL, OAR (CRMXA), USAF. AFCRL-65-579, August 1965, AD625453.
6. K. Minka: Orbit Determination and Ephemeris Computation. Martin Company, Baltimore Division. Prepared for AFCRL, OAR (CRMXA) USAF. AFCRL-66-259, May 1966, AD637206.
7. Star Catalog: Positions and Proper Motion of 258,997 Stars for the Epoch and Equinox of 1950.0. Smithsonian Institution, Washington, D.C., 1966.

7.0 Ephemeris Computation for Double Thrust Situations

7.1 Introduction

Program TTLOK, an adaptation of the standard AFGL satellite ephemeris program LOKANGL, provides the ability to compute ephemerides for the double thrust situation. A double thrust is defined as two successive impulsive thrusts between which no intermediate Keplerian elements or P/V (position/velocity) vectors are available. Under these circumstances, the standard LOKANGL program is unable to provide valid ephemeris calculations for the time interval between successive thrusts. Experimenters' need for coverage during this period has prompted the development of TTLOK to fill the void.

7.2 Functional Description

The reader should refer to Reference 1 for an overview of the basic LOKANGL program. The focus of activity in the TTLOK modifications to LOKANGL is preparation of a suitable TAPE4 file. As discussed in the reference, TAPE4 data represents a transformation from inputted standard Keplerian element sets or P/V (position/velocity) vector sets to a related set of mean Keplerian elements and their associated time derivatives, by use of which element values can be derived for any arbitrary time of interest. The purpose of the TTLOK modification is to provide the information needed for spanning the time interval between two successive thrusts during which no orbital measurements are available.

Once all this type of information has been extracted from the input (element cards or P/V vector cards) and captured in suitable format on TAPE4, TTLOK (or LOKANGL) rewinds the

TAPE4 file and reads the first record. Each record consists of a set of elements, their derivatives, their epoch, and the latest value of time thru which these data are to be applied to ephemeris calculations. TAPE4 records are ordered chronologically in increasing value of epoch for the associated mean element set.

For each instant of time for which ephemeris data is requested, beginning with the earliest and proceeding sequentially with increasing values of time, LOKANGL employs these elements and their temporal derivatives in a Taylor's series expansion to calculate mean elements for each of the requested instants of time. The instantaneous values of mean elements are then transformed to coordinate values defining the vehicle's instantaneous location and velocity (i.e., the ephemeris). When time, the independent variable, has advanced to the end of the region of applicability of the first record on TAPE4, the next record, which has a later cut-off time than its predecessor, is read in. The forgoing process then continues cyclically until the entire span of time for which calculations have been requested has been covered. (The last record on TAPE4 is assigned a cut-off time of essentially infinity, permitting calculations to extend as far as desired beyond the epoch of the last entry on TAPE4.)

Standard LOKANGL is unable to provide ephemeris values between successive thrusts having no intermediate point of orbit measurement. TTLOK eliminates this limitation by providing entries on TAPE4 which provide computational coverage of the inter-thrust period. The procedure for generating these new TAPE4 entries involves modeling the thrust process as follows:

- The duration of the thrust is assumed infinitesimal. Thus the thrust is represented as an acceleration impulse occurring at the nominal thrust time.
- The thrust impulse (or equivalently, the resultant discontinuous change in vehicle velocity) is assumed to have the direction of the vehicle velocity immediately before thrusting.

It is assumed that numerical values for the time of thrust and the associated increment in velocity are available from the satellite tracking agency. The entries on TAPE4 associated with the double thrusting should satisfy the requirements that:

- At each of the two instants at which thrusting occurs there should be discontinuous changes in mean elements.
- The discontinuities in the new elements should reflect the requisite jump in value of the vehicle velocity at the time of thrust.
- Vehicle position should remain continuous across each of the thrust times.

7.3 Punched Card Changes from Standard LOKANGL

Input cards are identical to those for standard LOKANGL except for the thrust card, to which is added the increment in velocity in columns 34-43 shown below. In addition, there are now two successive thrust cards.

| <u>Card</u> <u>No.</u> | <u>Variable</u> <u>Name</u> | <u>Card</u> <u>Col.</u> | <u>Format</u> | <u>Variable Description</u> |
|---------------------------|--------------------------------|----------------------------|---------------|--|
| 2+ | IYTH year of thrust | 19-20 | I2 | Two digit value of |
| | IDTH (or IDTH2) | 21-23 | I3 | Three digit value of day number of thrust |
| | SECTH (or SECTH2) | 24-33 | F10.3 | Thrust time in seconds of day |
| | DELV1 (or DELV2) | 34-43 | F10.3 | Increment in velocity in feet per second |

Note the restriction that, as presently implemented, TTLOK requires that the sequence of input element (or P/V) set cards includes at least two element sets prior to the first thrust card and at least two element sets subsequent to the second thrust card. This requirement is not a fundamental limitation, but rather is a consequence of the particular design approach which has been implemented.

7.4 Output

Ephemeris output from TTLOK is identical to the standard LOKANGL print options (Reference 1). The header has been modified to accommodate two thrusts and to indicate the velocity increment for each. Elements used in the inter-thrust period, and associated derivatives, are printed out in standard LOKANGL format.

7.5 Mathematical or Logical Procedures

As noted previously, each record on the TAPE4 file provides mean Keplerian elements, their derivatives, the epoch, and DELDAX, a time interval which is to be added to the epoch to obtain the latest time for which data in the record is to be used to compute an ephemeris.

a. Background

To familiarize the reader with operation of the LOKANGL system several simple situations will be illustrated. Consider the sequence diagram of Figure 7.1. There is only one set of element cards in the input deck. They are denoted by X and have epoch t_1 . Correspondingly, there is one entry on TAPE4 and its DELDAX is essentially infinite. Derivatives of the elements are estimated based on geopotential and drag modules internal to the program. This single TAPE4 entry is used for calculations for all times.

Next consider the case of two element sets as illustrated in Figure 7.2. DELDAX for the first entry on TAPE4 equals $t_2 - t_1$. The derivatives for the first entry represent an interpolation between element values at t_1 and those at t_2 . The second entry on TAPE4 has an infinite DELDAX. Thus its usage extends from t_2 to infinity. The derivatives for the second TAPE4 record are obtained, not from interpolation, but from the internal models.

Consider now the case of a single thrust shown in the sequence diagram of Figure 7.3. Standard element cards again represented by X , and the thrust card by T . There are two element sets preceding and two following the thrust. The first entry on TAPE4 has t_1/t_2 interpolated derivatives; it is used between minus infinity and $t=t_2$. The second entry has model-computed derivatives and is used between t_2 and t_3 .

X \leftrightarrow Standard Elements
T \leftrightarrow Thrust Event

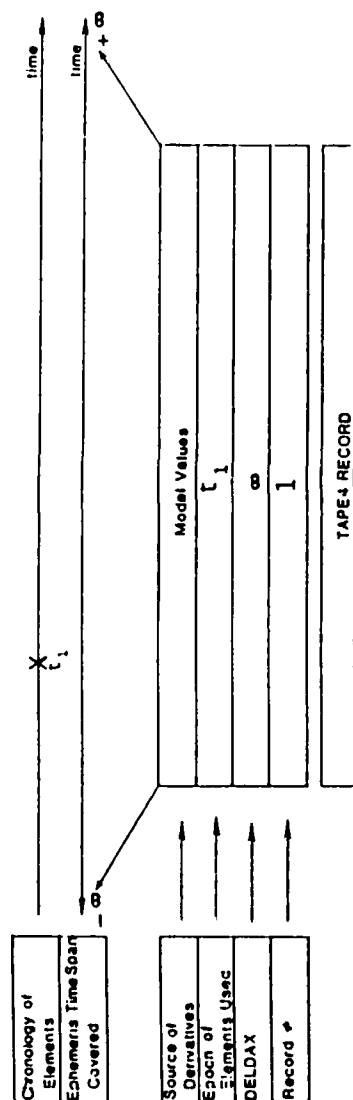


Figure 7.1 TAPE4 Structure for the Case of a Single Element Set

X \leftrightarrow Standard Elements
T \leftrightarrow Thrust Event

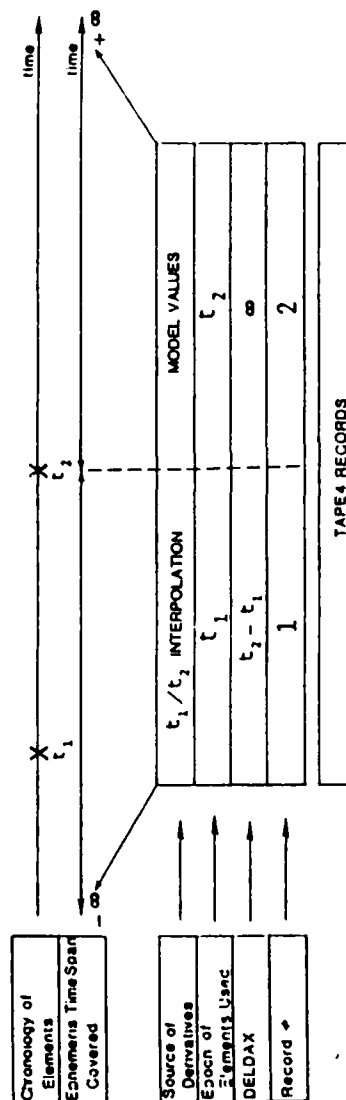


Figure 7.2 TAPE4 Structure for the Case of Two Element Sets

The third entry has derivatives based on t_4/t_5 interpolation and is used for computations between t_3 and t_5 . The fourth entry is used from t_5 onward and employs model derivatives.

The forgoing examples illustrate the general rule regarding applicability of element sets and derivatives contained in a given TAPE4 record: The range of applicability begins at the cut-off point of the preceding record (minus infinity for the first record in the file) and extends up to $t_e + \text{DELDAX}$ where t_e is the epoch for the given record.

b. Double Thrust Outside the Inter-thrust Interval

The sequence diagram for the case of a double thrust is shown in Figure 7.4. Standard cards with epochs t_1 and t_2 are handled in the usual fashion on TAPE4: i.e., a t_1 epoch with t_1/t_2 derivatives and $\text{DELDAX} = t_2 - t_1$. But when, next, TTLOK recognizes that the t_2 element cards are followed by two successive thrust cards, the same elements and derivatives are written a second time to TAPE4, but in this case with $\text{DELDAX} = t_3 - t_1$. This repeated record written to TAPE4 provides coverage within the pre-thrust interval from t_2 to t_3 using t_1/t_2 interpolated derivatives. Note that this differs from the corresponding situation in the single thrust case where model derivatives are used to provide coverage between the epoch of thrust and the epoch of the preceding element set.

The sequence of input element cards depicted in the figure results in 5 records being written to TAPE4. The first two, as noted, differ only in their values of DELDAX . The third record covers the inter-thrust period and is discussed below.

Finally, the post-thrust TAPE4 records of epochs t_5 and t_6 are similar in content and usage to the two-card case of Figure 7.2. The only difference is that, in the present case, usage of the t_5, t_6 pair begins, not at minus infinity, but immediately following t_4 , the time of the second thrust.

X → Standard Elements

T → Thrust Event

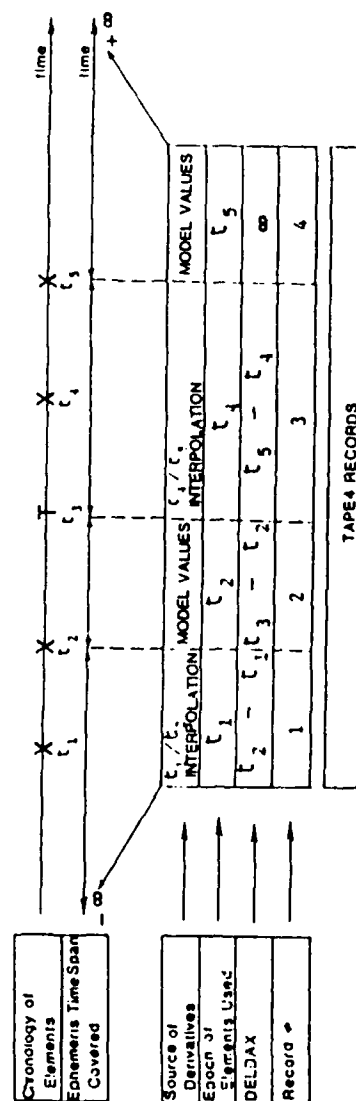


Figure 7.3 TAPE4 Structure for a Single Thrust

X → Standard Elements

T → Thrust Event

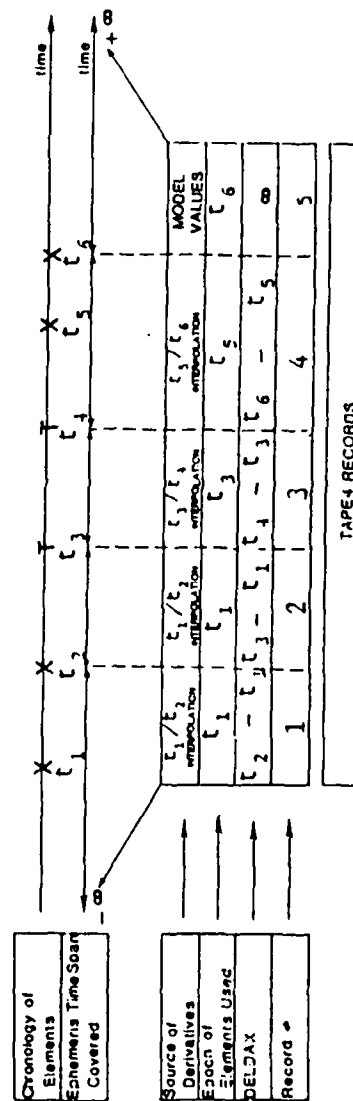


Figure 7.4 TAPE4 Structure for Double Thrust

c. Coverage of the Inter-Thrust interval

The procedures for obtaining element coverage up to t_3 (first thrust) and beyond t_4 (second thrust) have been described. Needed now is coverage within the interval from t_3 to t_4 . t_1/t_2 extrapolated elements are evaluated for the time just prior to t_3 and are converted to osculating P/V vectors; and similarly for the time just following t_4 . LOKANGL routine MNTOPV is used for this purpose. Next, it is assumed that the thrusts create increments in vehicle velocity which are aligned vectorially with the pre-thrust velocity vector. The V's in the P/V sets at t_3 and t_4 are incremented (decremented) accordingly. These new osculating P/V sets are then transformed by LOKANGL routine PVTOMN to equivalent mean elements.

Next, derivatives valid in the t_3 to t_4 interval are calculated using the standard LOKANGL code for evaluation of derivatives of elements. An entry is then written to TAPE4 with the elements being the post-thrust #1 values with epoch t_3 ; derivatives are as just described; and $DEL DAX = t_4 - t_3$. The flow of the overall procedure is illustrated in Figure 7.5.

The procedure for handling the inter-thrust period is mechanized in subroutine XFORM. Given a set of mean elements, their epoch (t), their derivatives, a prescribed time interval (Δt), and a velocity change (ΔV), XFORM performs a transformation in which the given Keplerian elements are converted to a second set, at epoch $t + \Delta t$, for which the magnitude of the vehicle velocity at $t + \Delta t$ has changed by an amount ΔV from the value which would have been calculated using the given elements. LOKANGL routines MNTOPV and PVTOMN are employed in this velocity transformation process. They provide the means for reversibly converting between mean Keplerian elements and equivalent osculating P/V vectors.

AD-A185 748

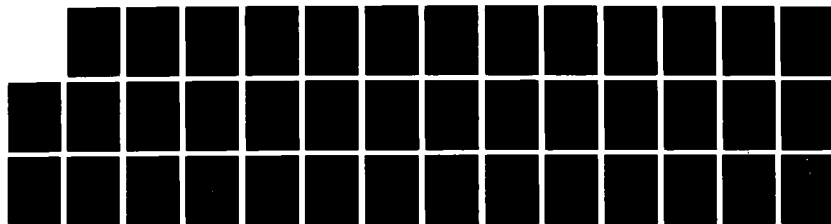
INTEGRATED SYSTEMS WITH APPLICATIONS TO THE
MULTI-PHASES OF THE EPHEMERID. (U) RADEX INC CARLISLE
MA J N BASS ET AL. 27 FEB 87 RX-870227 AFGL-TR-87-0064
F19628-83-C-0134

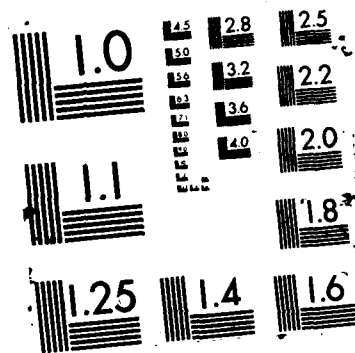
3/3

UNCLASSIFIED

F/G 4/1

NL





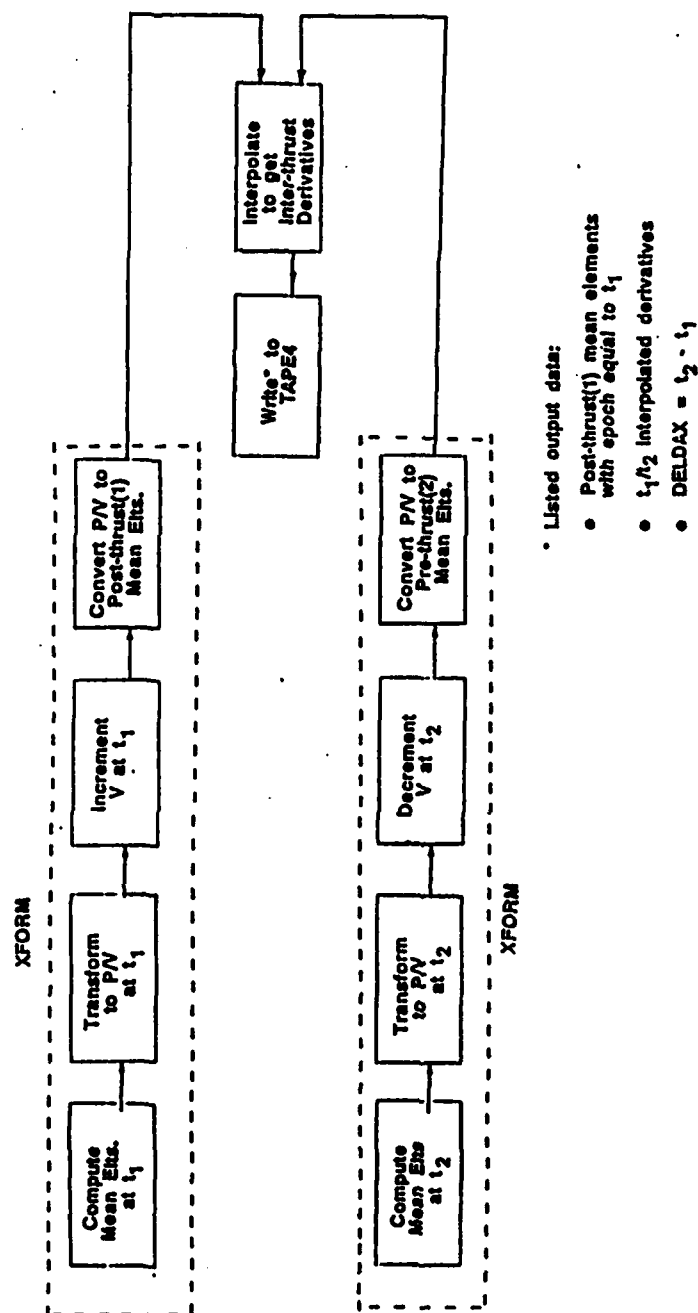


Figure 7.5 Functional Flow Diagram for Double Thrust Analysis

References

1. "Analysis and Programming for Research in the Physics of the Upper Atmosphere", Logicon, Inc., Final Report, AFGL-TR-81-0293, 1981, ADA113932.

8.0 Software for Processing Celestial Aspect Sensor Data

8.1 Introduction

A number of rocket-borne experiments require high accuracy attitude information to successfully interpret in-flight measurements. Instrument line-of-sight is normally determined from gyroscopic systems mounted in the vehicle payload. However, the results from these systems may contain errors that limit the quality of the attitude information. For certain demanding applications, gyro system measurements, alone, fail to satisfy the requirements for precision. In such cases, sun, horizon, and celestial aspect sensors can be used to provide correction factors to be applied to gyroscopic measurements to create more accurate attitude profiles. This report contains a general description of the techniques designed and implemented to calculate corrected line of sight information for a payload which carried a Celestial Aspect Sensor (CAS).

Utilization of the CAS measurements required the development of a software processing system, the CAS Processor (CASP), to convert the raw CAS data into corresponding corrections to the nominal vehicle attitude parameters. Suitably combined with the gyro measurements, these CAS updates provide an attitude database of improved accuracy. This upgraded attitude profile is then used for precise calculations of the tangent height (and related geometrical parameters) associated with the field of view of the prime sensor, an instrument which is oriented along the payload body axis.

The software for processing of CAS data has been developed in two stages. The first of these is documented in Reference 1, a technical memorandum. The second stage, which is the

subject of the present report, represents an extension of that earlier work and is based upon a data processing algorithm proposed by Dr. H.A. Miranda and Dr. R. Miranda, both formerly of Epsilon Co, the fabricators of the CAS instrument. The effort to collect and process CAS data was performed in support of the Elias rocket experiment, a flight which collected IR measurements of auroral radiation.

There are three primary types of data upon which operation of the CASP system is based. In addition to the star detections provided by the CAS instrument itself, the other databases are the vehicle gyro measurements and the Smithsonian Astronomical Observatory (SAO) star catalog. The latter is a listing (stored on magnetic tape) of stars, together with their magnitudes and locations on the celestial sphere (i.e., right ascension, declination). The CASP system utilizes attitude data from the gyros to evaluate the approximate orientation of the CAS and the corresponding field of view. The star catalog data can then be used to identify those stars which should fall within the field of view of the CAS, together with their locations expressed in CAS instrument coordinates. Under ideal conditions (no instrument calibration errors, no detection false-alarms, perfect gyro data, and completeness of the catalog) all of the instrument detections should, in principle, precisely overlay a subset of the totality of catalog stars within the field of view. In practice, a displacement is expected between the spatial pattern of the star catalog items and the corresponding pattern of the CAS detections; i.e., the set of catalog items and the set of detections should share a common pattern of geometrical interrelationships among their individual members, but there is a displacement between these two geometrically similar patterns. For purposes of data analysis, it is assumed that such displacements are due totally to gyro measurement error (i.e., the CAS instrument, as calibrated, performs perfectly). The objective of the analysis performed by CASP system is to evaluate attitude

corrections which will bring the catalog data into "minimum offset" agreement with the detections. Graphical CRT displays which superimpose both the SAO catalog items and the reported detections onto the CAS field of view are used to illustrate the effect of deviation between the actual vehicle attitude and the attitude deduced from (uncorrected) gyro measurements. An example is shown in Figure 8.1.

8.1.1 Description of Sensor

The Celestial Aspect Sensor (CAS) is a scanning instrument with a rectangular field of view of approximately 21 by 25 degrees. The instrument uses a sawtooth drive to scan a mirror up and down the 21 degree y-axis of the field of view. As the mirror scans, it reflects the stellar emissions into the sensor. The optical path from the mirror passes through an objective lens to an image intensifier, and subsequently through a relay lens to the Charged Coupled Device (CCD) detector. The CCD detector, a 256 element linear array with an S25 light intensity response, creates individual raster lines oriented along the 25 degree x-axis direction of the instrument. The mirror requires 0.4 seconds to complete a full scan and thereby to create a 256 by 256 pixel field of view of the instrument. Figure 8.2 is a cut-away view of the construction of the CAS.

Every 0.1 seconds the on board processor determines the x,y locations of the eight highest intensity pixel responses located in the one-fourth of a field-of-view swept over in this partial scan. For each selected detection location, the processor then calculates three quantities: the magnitude of intensity, delta-x, and delta-y. Delta-x and delta-y are position corrections for detections that straddle pixels, and are used to obtain sub-pixel location accuracy for each detection.

Figure 8.3 illustrates a typical pixel-straddling image. The

TAL = 129.268 SCAN DIR. UP

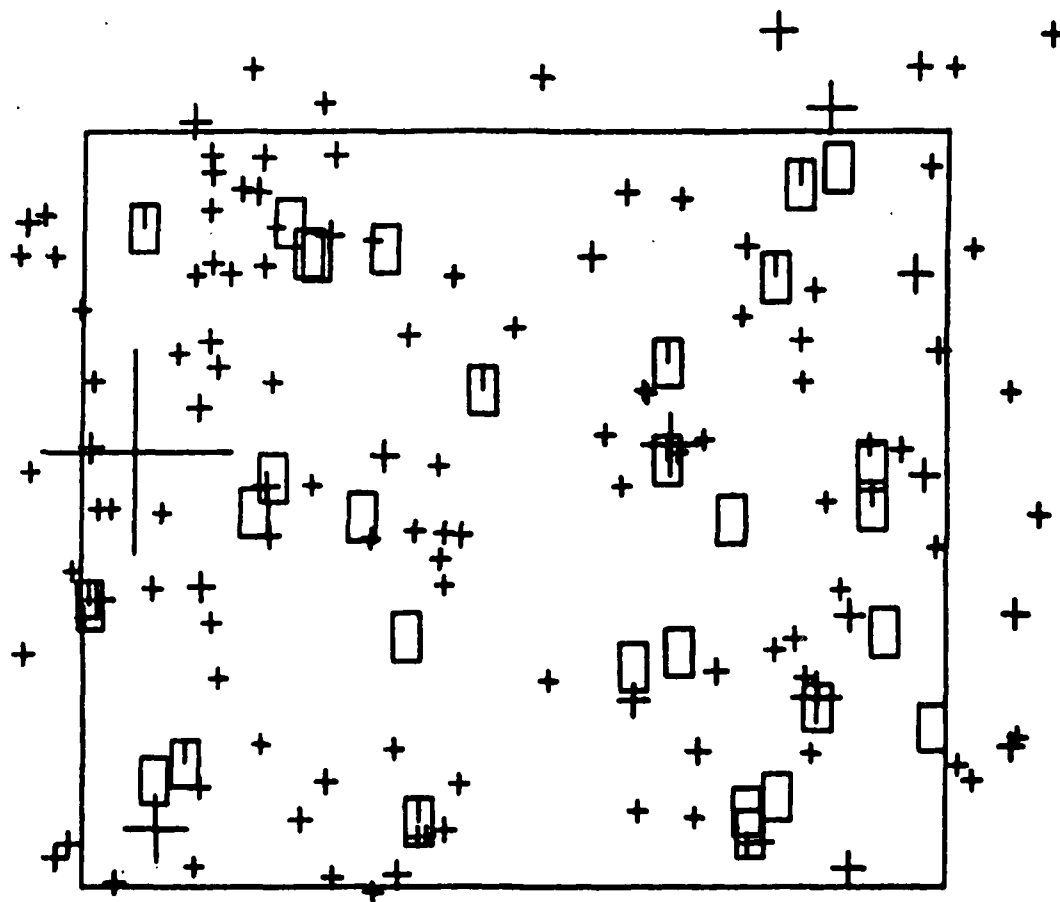


Figure 8.1 CRT Display of Field of View of CAS (bounded by rectangular frame) Showing Star Catalog Entries ('+'s) and 30 Detections (at centers of small rectangular boxes).

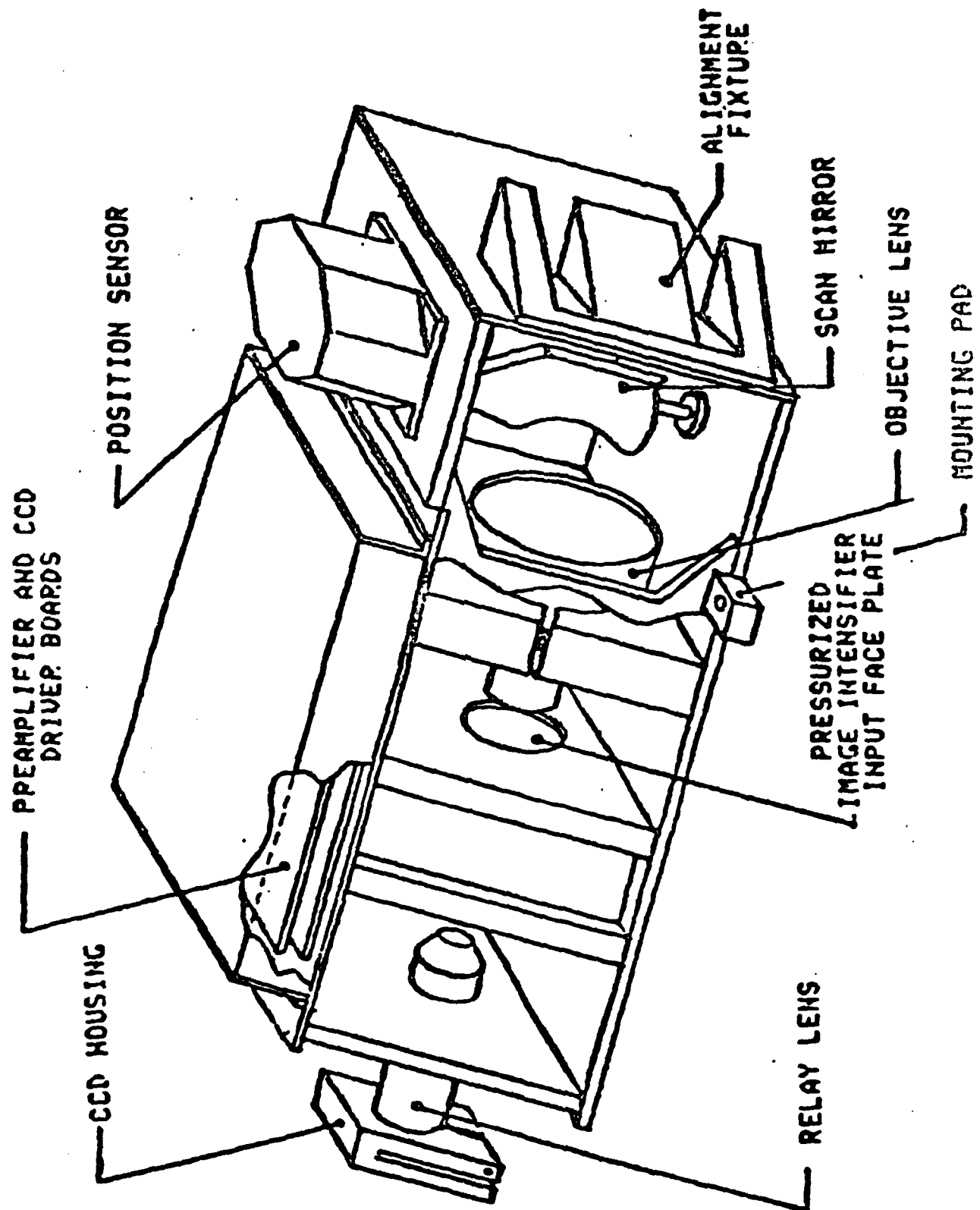


Figure 8.2 Celestial Aspect Sensor Cut-out View

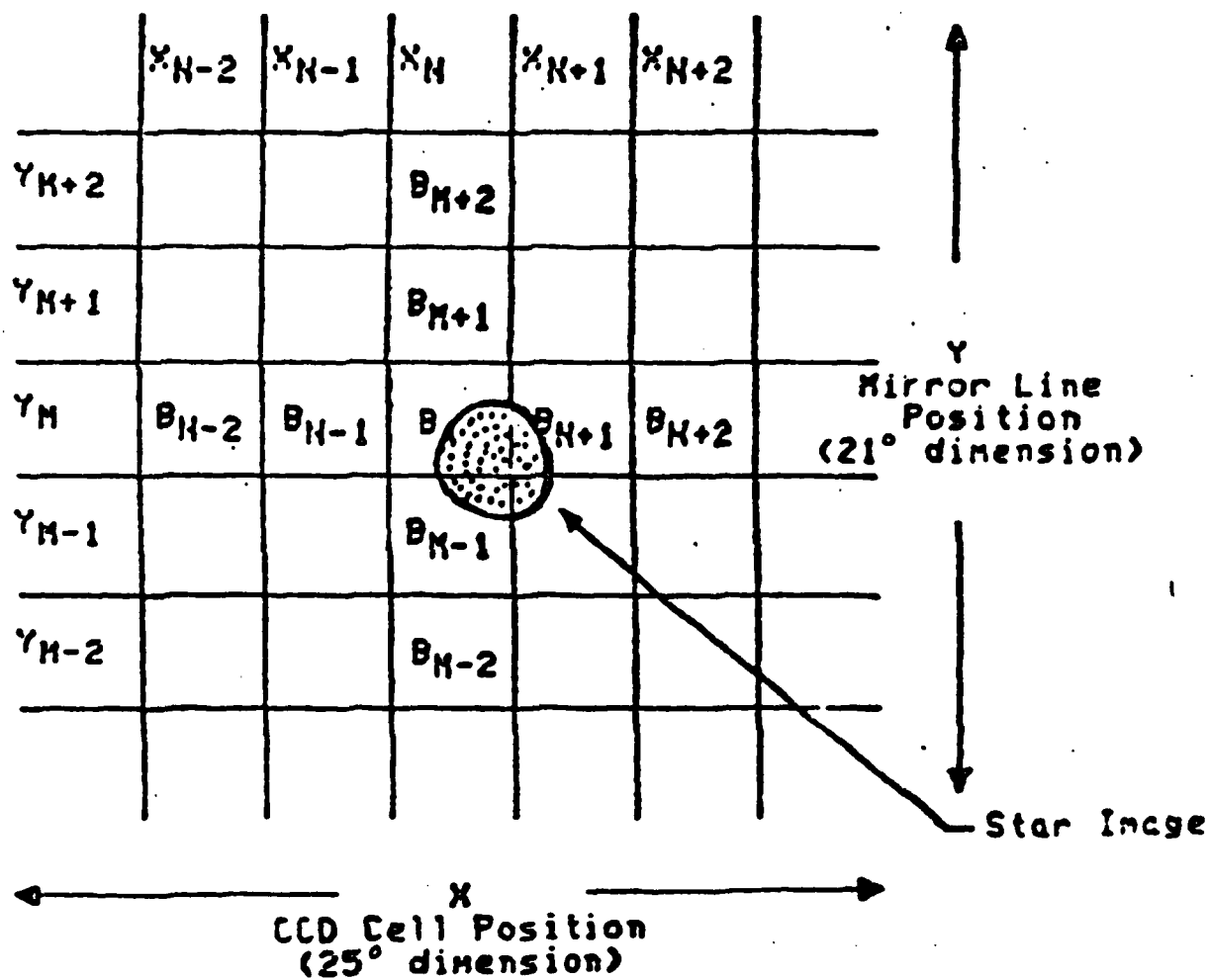


Figure 8.3 Image Element Configuration

following relations are used by the on-board processor to calculate parameters for each image:

$$\text{Delta-x} = B_{N,1} - B_{N,1}$$

$$\text{Delta-y} = B_{M,1} - B_{M,1}$$

$$\text{Magnitude of Intensity} = (B_M + B_{M-1}) - (B_{M+1} + B_{M+2})$$

A full scan field of view consists of 32 detection coordinates created from four consecutive scan segments of the same direction of mirror rotation. Two of those 32 sets of detection coordinates are obtained from fixed LEDs (light emitting diodes) mounted on the cover lens of the instrument. These are calibration sources used to adjust the pixel field of view for mirror deviation and fluctuation introduced by the mechanical drive system of the mirror.

Pulse Code Modulation (PCM) telemetry is used to transmit data from the vehicle to the ground station. Within each telemetry frame, the instrument packs and transmits data for a single $\frac{1}{4}$ -scan segment of the field-of-view. The frames occur at a rate of one every 0.1 seconds. A telemetry frame consists of eight sets of the following data: detection x and y coordinates, magnitude of stellar intensity, delta-x, and delta-y. The structure of the telemetry frame is illustrated in Figure 8.4.

8.1.2 Reduction of Raw Data

The flight data was recorded on instrumentation tape at the rocket range and sent to the Telemetry Data Processing Section of AFGL to create formatted raw sensor data tapes. These are unpacked, and their quality is checked to create working databases for use by data reduction software.

The tracking data is processed by trajectory determination software to produce a database of standard position

ONE PCM TELEMETRY FRAME (422 BITS EVERY 0.1 SECONDS)

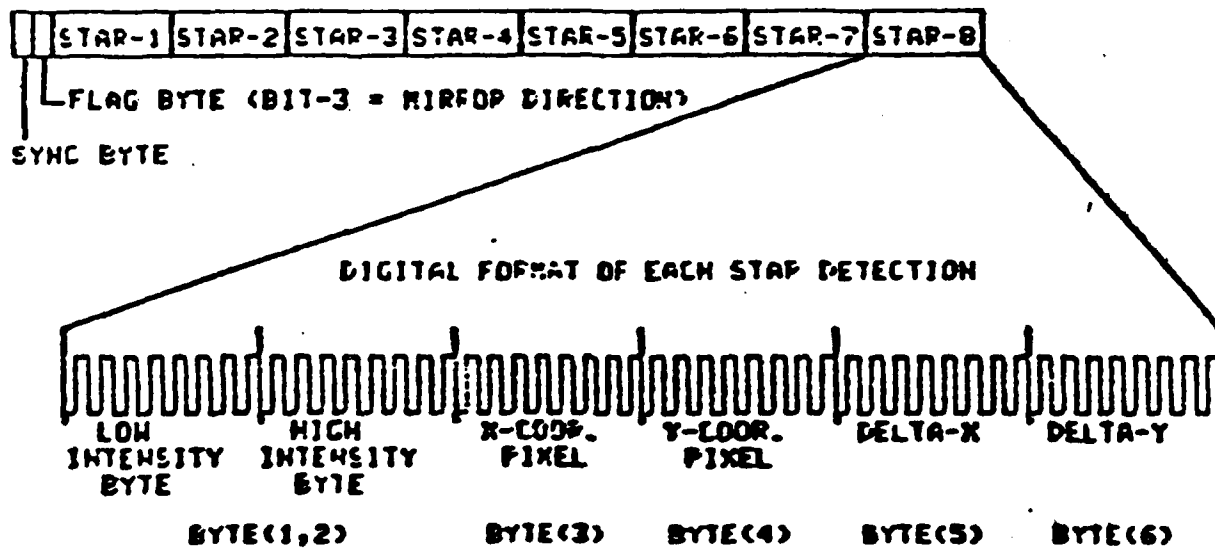


Figure 8.4 PCM Telemetry Format

parameters. The trajectory data and the raw database of gyroscopic measurements are used by existing attitude determination software to produce a preliminary flight history of attitude defining the line of sight for each of the sensors on the payload.

The SAO star catalog is unpacked, and each entry is calibrated to an S25 light intensity response range. The epoch for the flight and nominal Celestial Aspect Sensor (CAS) fields-of-view during the flight are used to define a subset of the full SAO catalog known as the SAO working database. The CAS working database is calibrated and adjusted to permit reconstruction of fields of view of the CAS during the flight.

Figure 8.5 presents an overview of the data flow supporting the operation of the CASP software system. To initiate processing of CAS data, the CASP software system extracts, from the CAS working database, four consecutive telemetry frames of the same scan direction to reconstruct a CAS field of view of a segment of the celestial sphere.

Note that delta-x and delta-y corrections have already been applied to the detection readouts by an on board processor to yield interpolated coordinates for detections that straddle adjacent pixels; equations 1, 2, and 3 of Table 8.1 illustrate how these adjustments are applied.

Each field is corrected for mirror misalignment using the two reference star coordinates contained in the field of view (Eq. 4, 5). The remaining readouts are calibrated into instrument degrees and corrected for magnification distortion in the x-axis direction and mirror mounting angle skewness in the y-axis direction (Eq. 6, 7, 8).

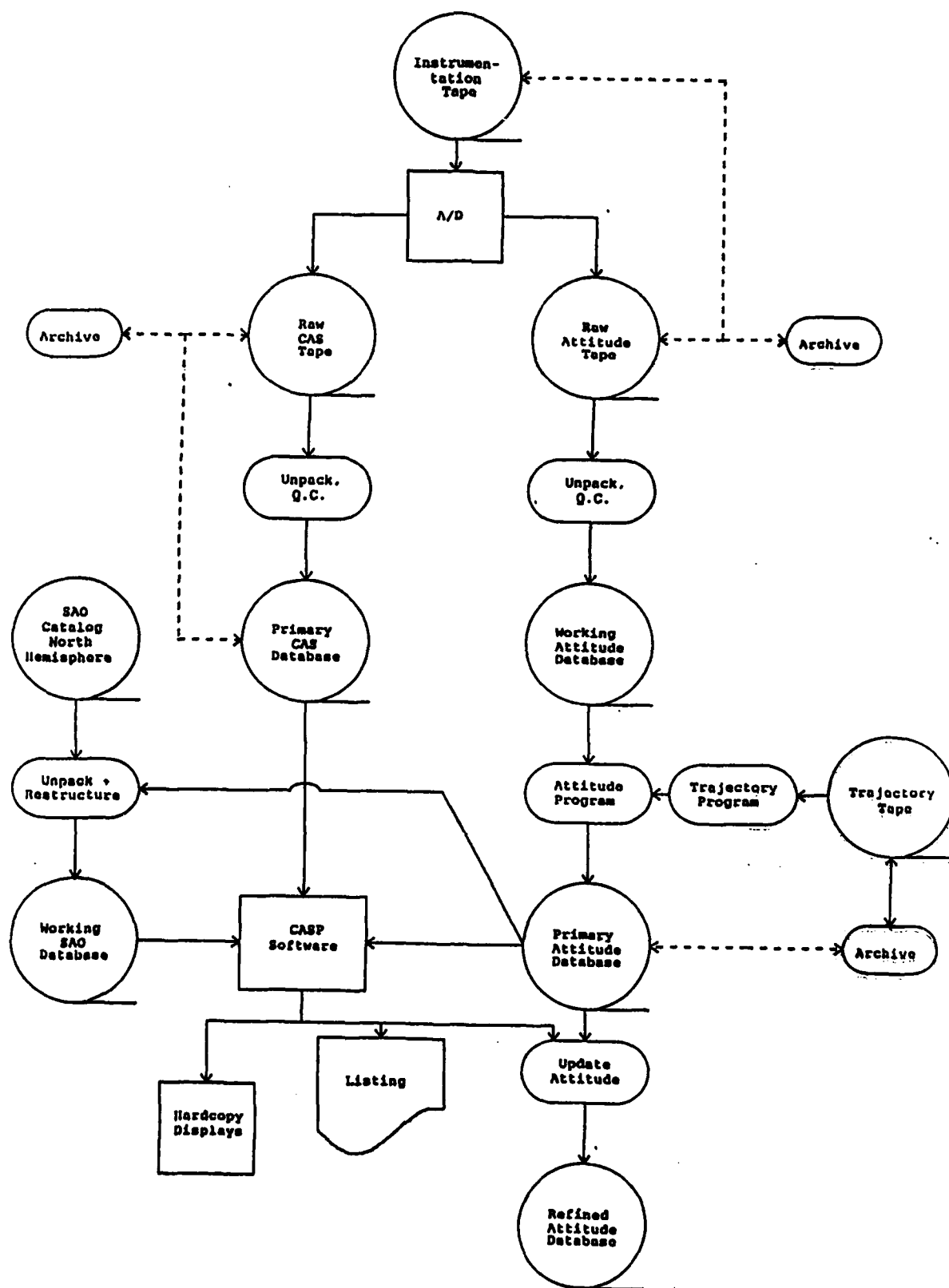


Figure 8.5 Top Level Data Flow for Processing CAS Data

Table 8.1
Calibration Equations

Eq. 1. If byte(6) <= 128:

CM = byte(6)

Else:

CM = byte(6) - 256

SM = byte(1) + (256)(byte(2))

Eq. 2. If byte(6) <= 128:

Cdelta-y = [byte(6)/(2(byte (1,2)) +
byte(6)/(4(byte(1,2) - byte(6))))]

Else:

Cdelta-y = [(byte(6)-256)/(4(byte(1,2) -
(CM))) + (byte(6)-256)/(2(byte(1,2)
- 2(CM)))]

Eq. 3. If direction bit = 1 : Sign = 1

Else: Sign = -1

Correct-Y' = byte(4) + Sign(Cdelta-y)

Correct-X' = byte(3) - f(byte(5)/SM)

where f is the function defined in Table 8.2

Eq. 4. Ref1-X = X-coordinate of LED #1

Ref2-X = X-coordinate of LED #2

Ref1-Y = Y-coordinate of LED #1

Ref2-Y = Y-coordinate of LED #2

Adj-X = (Ref1-X + Ref2-X)/2 - 208

Adj-Y = (Ref1-Y + Ref2-Y)/2 - 113

Eq. 5. Correct-X'' = Correct-X' - Adj-X

Correct-Y'' = Correct-Y' - Adj-Y

Table 8.1
(continued)

- Eq. 6. $\text{Correct-X} = \text{Correct-X}' - 1.863\text{E-}6(|\text{Correct-X}' - 140|^3)$
- Eq. 7. $\text{Correct-Y} = \text{Correct-Y}' - 0.01375(\text{Correct-X}' - 140)$
- Eq. 8. $\text{Deg-X} = \text{Correct-X}(0.001719)180/\pi$
 $\text{Deg-Y} = (255 - \text{Correct-Y})(0.001417)180/\pi$
- Eq. 9. $\text{LOSDEC} = \text{declination from gyro calculation}$
 $\text{LOSRA} = \text{right ascension from gyro calculation}$
 $\text{Fi} = \tan^{-1}(\text{Deg-X} - 13.2992772902)/$
 $(\text{Deg-Y} - 13.9406770361))$
 $\text{Rads} = (\text{Deg-X} - 13.2992772902)\cos(\text{Fi})$
- Eq. 10. $\text{Inst-DEC} = \text{LOSDEC} + (\text{Rads})\sin(\text{Fi} - \text{Alpha})$
- Eq. 11. $\text{Inst-RA} = \text{LOSRA} + (\text{Rads})\cos(\text{Fi} - \text{Alpha})$

Table 8.2
Discrete Points Defining Function f

| x | f |
|-----------|-----|
| .6 to .99 | 2.0 |
| .55 | 1.9 |
| .51 | 1.8 |
| .46 | 1.7 |
| .41 | 1.6 |
| .35 | 1.5 |
| .29 | 1.4 |
| .23 | 1.3 |
| .16 | 1.2 |
| .08 | 1.1 |
| .0 | 1.0 |

8.2 Processing Software For The CAS

A celestial aspect sensor (CAS) was flown on the Elias rocket flight to provide high precision attitude data to augment the data collected using horizon sensor and gyro instruments. At the most rudimentary level, the CAS may be described as consisting of a linear array of 256 CCD elements together with a rotating (actually rocking) mirror which provides a scanning capability. The period of the scan is 0.4 seconds, and the scan direction is reversed on successive frames.

Each scan provides a two-dimensional image of a section of the celestial sphere. It is assumed that the CAS and the rocket body jointly constitute a single, perfectly rigid body of precisely known geometry. Thus, if the orientation of the CAS is known, the attitude of the vehicle is deducible; and conversely. Further, it is assumed that at each instant of time of interest, the attitude data deduced from gyro measurements is sufficiently accurate to ensure that calculated expected locations of stars within the viewing field of the CAS are of "ballpark" caliber. Basically, the processing system evaluates these expected star locations, forms pair-wise associations between detections and catalog stars, evaluates the displacements between the observed star detections and their respective star catalog counterparts, and calculates the increments in attitude angles needed to bring the two sets of points as close to overall coincidence as possible. Thus, it is tacitly assumed that mismatch between calculated star locations and the corresponding detection points is caused solely by error in the gyro measurements. Hence, the increments in attitude angles needed to achieve optimum coincidence can be viewed as corrective updates to the gyro data base, valid at the time corresponding to that of the CAS scan. (Actually scanning is not an instantaneous process, but occurs over a finite period of time, during which the payload attitude may vary. See Section 8.2.2 where this effect is taken into account.)

8.2.1 Operation Of The CAS Processor (CASP) System

The operation of CASP is based on a frame-by-frame analysis of the CAS data, coupled with feed-forward updating. Attitude data deduced from gyro measurements, alone, is never of sufficient accuracy to yield perfect alignment between star catalog data and the corresponding CAS detections. However, if the correct attitude were somehow known for frame N , then that attitude data could be updated to the time of frame $N+1$ using available rate gyro data in a Taylor's series expansion. It is assumed that attitude data obtained by updating from an adjacent frame is of sufficient accuracy to yield near-coincidence between CAS detections and their corresponding catalog items (if any). Reported detections failing to have a nearby catalog counterpart can be assumed to be noise and can be ignored. Thus a small acceptance cell can be erected about each reported detection. (These are the 30 rectangles evident in Figure 8.1. Each detection can then be matched to that star (if any) falling within its acceptance cell. If more than one catalog item falls within a given cell, the most probable is selected (e.g., on the basis of star magnitude). Small attitude adjustments are then evaluated which minimize the overall misalignment of detections and stars. This completes the analysis of frame $N+1$. The process is then repeated for frame $N+2$.

The forgoing process is the basis for the automatic mode of operation of the CASP system. Figure 8.6 illustrates the operation of the automatic mode. Once initiated, this mode is designed to process successive frames sequentially, provided only that the quality of the raw CAS data is adequate to sustain the operation. The caliber of the data can be judged on the basis of the percentage of the 30 detections reported per frame which represent legitimate star detections. If their number is too few, the system will have only noise to which to lock and the results will be erratic

DIRECTION OF FLOW OF TIME

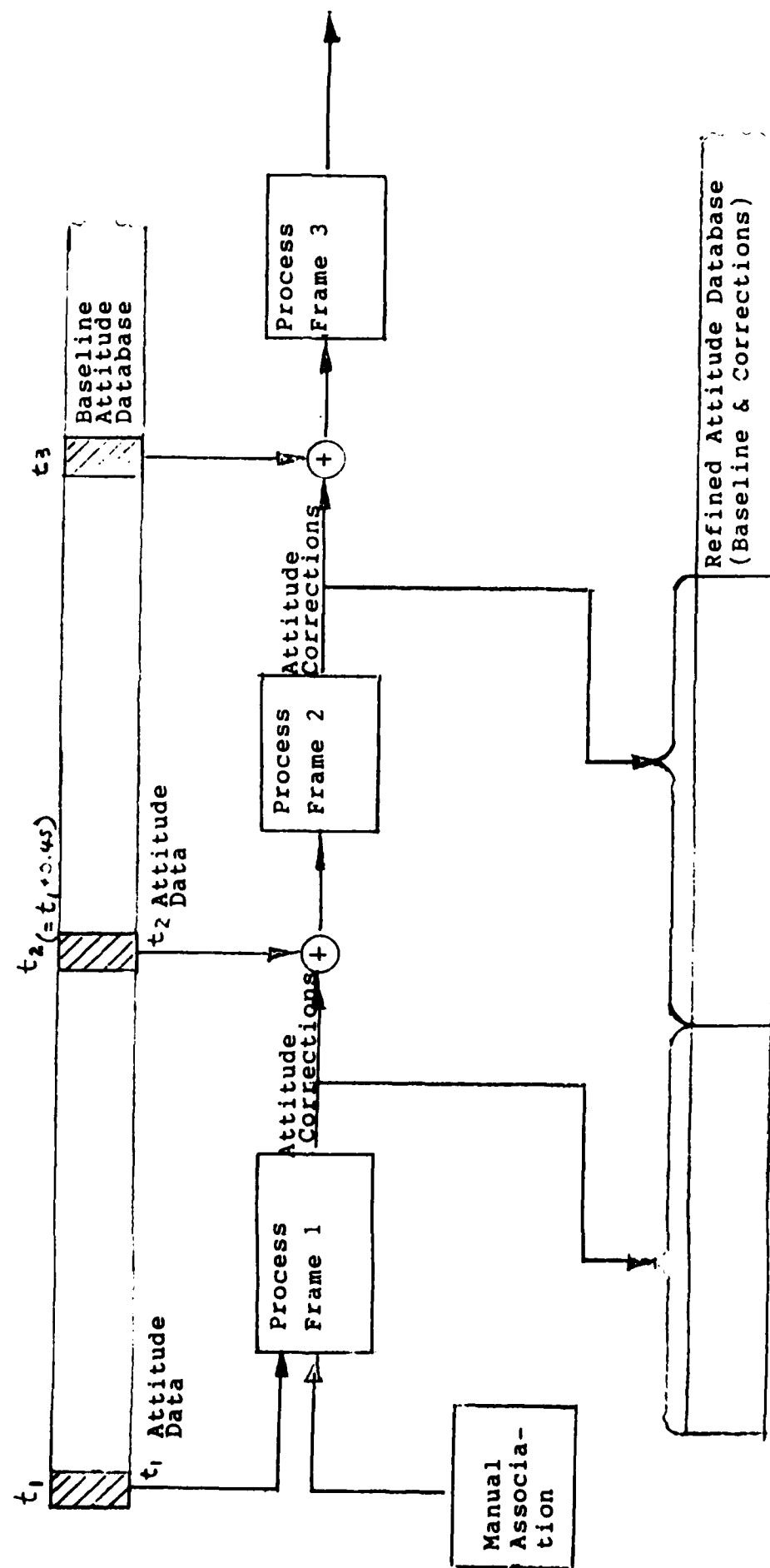


Figure 8.6: Highly Schematic Representation of Normal Initiation and Subsequent Automatic Mode of CASP Operation

and erroneous. Internal tests have been provided to identify this situation and to terminate automatic processing when it occurs.

As noted above, gyro data alone is too inaccurate to ensure near-coincidence of individual detections with their corresponding catalog items. How then can the automatic mode be initiated? The solution is a manual designation process. The analyst is provided with a CRT graphic display showing both the catalog stars and the detections plotted on the CAS field of view, as shown in Figure 8.1. The operator judges which detections are real and, using a cursor, manually associates them with the corresponding stars. CASP then evaluates the attitude corrections needed to minimize the overall star/detection offset, and automatic processing can then proceed unaided. There are two basic differences between the manual and the automatic mode. The first relates to the gyro data used in coordinate transformations. For the manual mode, only raw gyro data is employed. In the automatic mode, the attitude data employed is an amalgam of the raw gyro data together with corrective upgrades obtained from the processing of a time-adjacent frame. The second difference relates to the process of associating detections with star catalog items. In the manual mode, the operator designates matching pairs using a graphic display together with a cursor. In the automatic mode, the process is automatically performed using a criterion based upon the acceptance cell concept.

The following subsections provide more detailed background on the operation of CASP.

8.2.2 Software System Overview

Figure 8.7 illustrates the major functions performed in the processing of a single frame of CAS data. The process involves transforming the coordinates of each candidate star

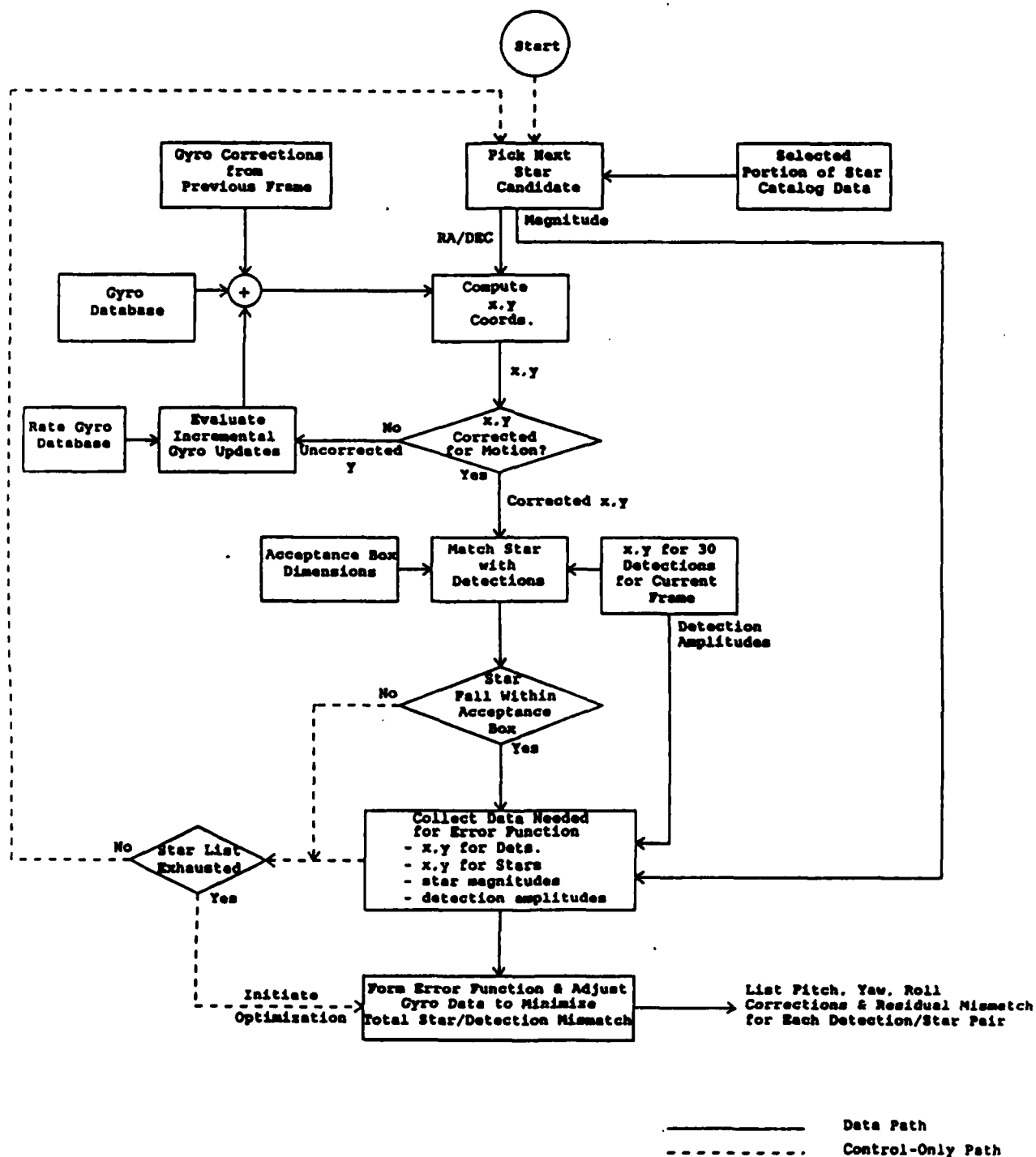


Figure 8.7 Flow Diagram for the Processing of a Single Frame of CAS Data

from the right ascension/declination inertial system to instrument coordinates (x,y) appropriate for the given time. This transformation is a function of the attitude of the vehicle at the given time. It should be recognized that 0.4 second of time elapses during the collection of one frame of data. This is the time required for the mirror to complete the y-direction scan. During this period the vehicle attitude can vary appreciably. In order to identify what attitude values apply for a given catalog star, its time of "detection" must be evaluated. But time within a scan can be measured in proportion to the amount of mirror rotation experienced: i.e., in terms of the y coordinate.

Inter-frame motion is treated by performing a two-pass coordinate transformation. On the first pass, attitude data corresponding to the start-time of the frame is used. This defines an approximate y-coordinate. That value of y, being obtained through the process of mirror rotation, defines the approximate proportion of the 0.4 sec scan period elapsed at the instant when the star would be detectable by the CAS.

With this new time-reference available, the attitude values for use with each individual star are updated to the "time of detection". The coordinate transformation for each catalog star is then performed a second time using as input the attitude appropriate for the time of detection. The result is a set of x,y coordinates for each star which have been corrected for inter-frame motion. In principle, the process could be repeated iteratively, with successively more exact results. In practice, though, one correction is sufficient.

The process of calculating an attitude correction from a given frame of data begins with centering an acceptance box on each of the 30 star detections reported for the frame. Each catalog star is examined to determine whether it falls within any of these boxes. Box occupancy serves to define the association between the catalog star and the

corresponding detection.

Once all associations have been identified, a mismatch error function is defined as shown in Figure 8.7. This function serves as an objective function for the subsequent optimization (minimization) process. The basic form of the error is given by the expression

$$\text{Mismatch Error} = \sum_i [W_{xi}(X_{\text{star}} - X_{\text{det}})_i^2 + W_{yi}(Y_{\text{star}} - Y_{\text{det}})_i^2]$$

where the index i identifies individual associated star/detection pairs, the summation is over all such pairs, $(x_{\text{star}} - x_{\text{det}})_i$ and $(y_{\text{star}} - y_{\text{det}})_i$ are the x, y star/detection coordinate differences for the i -th star/detection association, and the W 's are weighting factors. The mismatch error is functionally dependent on the vehicle attitude parameters. For a perfect CAS instrument and a set of observed detections that represent only valid star "hits" and no noise-induced "false alarms", the mismatch error function reduces (in principle) to a minimum value of zero when evaluated for those attitude parameters which represent the true orientation of the vehicle.

The final step in processing a CAS frame of data is a formal optimization procedure which yields incremental corrections to the pitch, yaw, and roll attitude parameters, jointly evaluated to minimize the total mismatch error.

8.2.3 Transformations between Coordinate Systems

Stars are organized and identified in the Smithsonian Catalog by their ECI-based right ascension and elevation. However their physical manifestations are observed by the CAS in the instrument's field-of-view coordinates. Correlating those two bodies of data entails conversion to a common coordinate

system. The major instrument of the ELIAS payload is an IR sensor with its field-of-view oriented in the direction of the rocket axis. This sensor collects data on the IR emissions of the auroral regions toward which it is directed. Consequently, a key input to analysis of the experimental data is identification, as a function of flight time, of the volume of space under observation. This viewing region at any given time is determined by the instantaneous orientation of the rocket body coordinate system, which can be calculated from attitude measurements, referenced to the launcher. Ground-based radar observations of the payload provide its location expressed in coordinates centered at the radar site.

Payload attitude and position data can be combined to yield the tangent height data which is needed to identify the region under observation. The geometry is illustrated in Figure 8.8. Tangent height is defined as the minimum distance between the rocket line-of-sight (LOS) and the surface of the oblate earth. It is specified in terms of that minimum distance together with the longitude and geodetic latitude of the corresponding point on the surface. Here again, the required geometric analysis utilizes multiple coordinate system conversions.

As the forgoing discussion illustrates, the processing of the CAS measurements requires that the software system provide the capability to transform freely among a variety of coordinate systems. The following subsections describe the major transformations implemented in the CASP software.

8.2.3.1 Earth-Centered-Inertial to Inertial-Fixed-Geographic

The earth-centered inertial (ECI) system is defined by an x-axis aligned with the vernal equinox and a z-axis oriented northward along the earth's axis of rotation. Like the ECI, the inertially fixed geographic (IFG) system is earth centered, and employs the earth's rotational axis as its

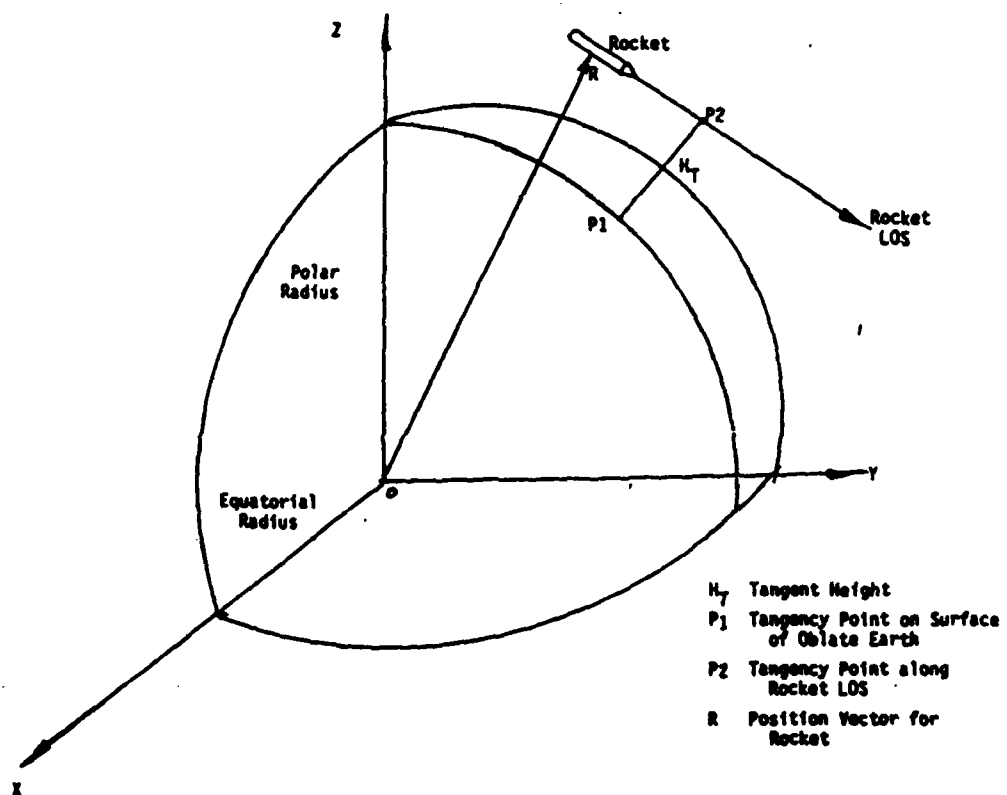


Figure 8-8 Illustration of Tangent Height

z-axis; but its x-axis is positioned in the Greenwich meridian plane at the instant of gyro uncage (taken to be launch time).

Note that because it is defined to be inertial, the IFG system does not rotate with the earth. It coincides with the conventional rotating geographic coordinate system only at gyro uncage time. Figure 8.9 illustrates the relationship between the ECI and the IFG systems.

8.2.3.2 IFG to Vertical-East-North (VEN)

The VEN system is inertially fixed, is centered at the launcher's location (topocentric), and has its axes pointing, respectively:

- ° vertically (i.e., direction of local plumb line on the oblate earth),
- ° east, and
- ° north

Like the IFG system, the VEN system, being inertially fixed, does not participate in the earth's rotation; it, too, is defined in terms of the value of the Greenwich hour angle at the time of uncage. Figure 8.10 illustrates the relationship between the IFG and the VEN systems. Note that account must be taken of the oblateness of the earth in specifying the center of the VEN system.

8.2.3.3 VEN to Launcher System

The VEN and Launcher systems share a common center. The Launcher system is inertially fixed, with axes coincident with the rocket body axes at the uncage time. Thus the launcher system is identical with the body system at launch

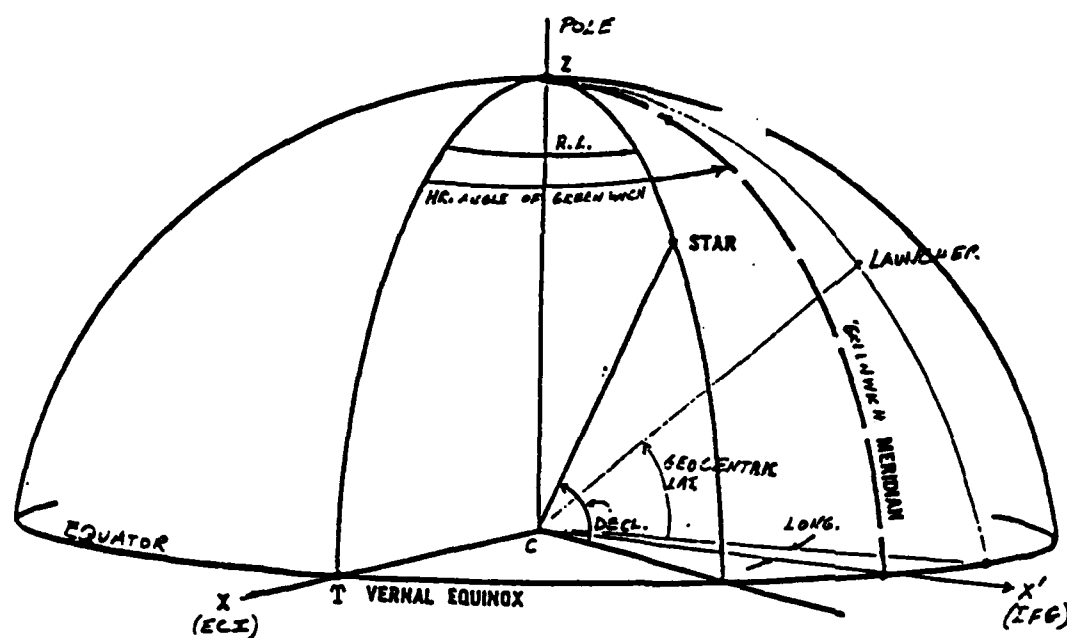


Figure 8.9 Relationship Between the ECI and IFG Coordinate Systems

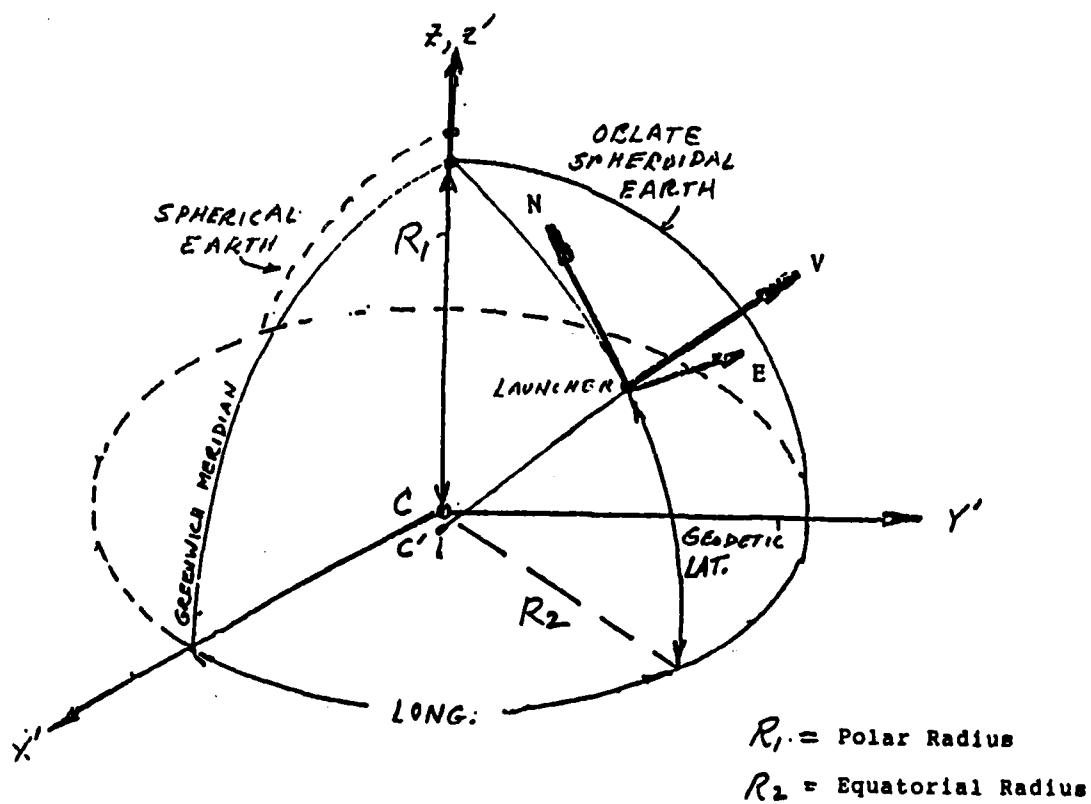


Figure 8.10 Geometry Relating the IFG and the VEN Coordinate Systems
 (V is perpendicular to surface of oblate earth)

time. Subsequently, the rocket body system undergoes rotational and translational motion associated with flight. The launcher system, on the other hand, remains inertially fixed and provides the reference directions against which the gyro system measures in-flight variation in rocket body attitude.

The body system is defined as follows:

- ° x-axis is the roll-axis
- ° y-axis is the pitch-axis
- ° z-axis is the yaw-axis

Figure 8.11 illustrates the geometry.

8.2.3.4 Launcher to Rocket Body System

The orientation of a rigid body can be defined in various ways: direction cosines (9 quantities); quaternions (4 quantities); Euler angles (3 quantities); and the pitch, yaw, and roll attitude angles. Common rocketry practice is to use the attitude angles, which correspond to the minimum number of independent parameters required to uniquely specify attitude. Each of the pitch, yaw, and roll, angles represents a rotation about one of three orthogonal axes. These are finite (i.e., not infinitesimal) angle rotations; and, thus, they do not commute.

In effect, the general transformation matrix, which relates an arbitrary instantaneous attitude of a rigid body to a prescribed reference coordinate system (in our case, the launcher), can be decomposed into the product of three matrices, each of which represents a rotation about an axis through prescribed angles (the pitch, yaw, and roll angles). However, tacitly associated with a given decomposition,

represented as numerical values of pitch, yaw, and roll, is a prescribed sequence in which the corresponding axial rotations must be applied in order to produce the intended body orientation. The non-commuting of these three rotations implies that the correct orientation of a body can be obtained from given values of pitch, yaw, and roll only if the corresponding axial rotations are applied in the proper sequence. For the Elias flight, that sequence is pitch, first, then yaw, and finally roll. Figure 8.12 presents the relationship between the launcher and the body systems.

8.2.3.5 Rocket Body Coordinates to Instrument x,y Coordinates

It will be recalled that the CAS instrument is comprised of a linear array of CCD elements, together with a mirror which provides scanning in the transverse direction. For each of the 30 detections declared per frame, x and y coordinates are provided. Calibrated in terms of angle, these numbers identify an apparent direction of look associated with the corresponding detection. The x,y coordinates are referenced to the CAS boresight and represent an angular offset from that direction. The CAS was mounted on the rocket body such that its boresight direction was in the plane of the body's roll and yaw axes with the x-direction perpendicular to the roll-yaw plane. The boresight was offset by an angle α (nominally 45°) from the roll axis. The mounting arrangement is illustrated in Figure 8.13.

To complete the chain of transformations between the optical measurements and the corresponding star locations defined in an inertial system, we need the transformation between x,y instrument space and the rocket body coordinate system. Figure 8.14 illustrates the geometry. A point $p(x,y)$ represents a detection defined in terms of its instrument coordinates x,y. Contours of constant x are circles whose planes parallel to the plane formed by the yaw and roll axes. Contours of constant y are great circles, the plane

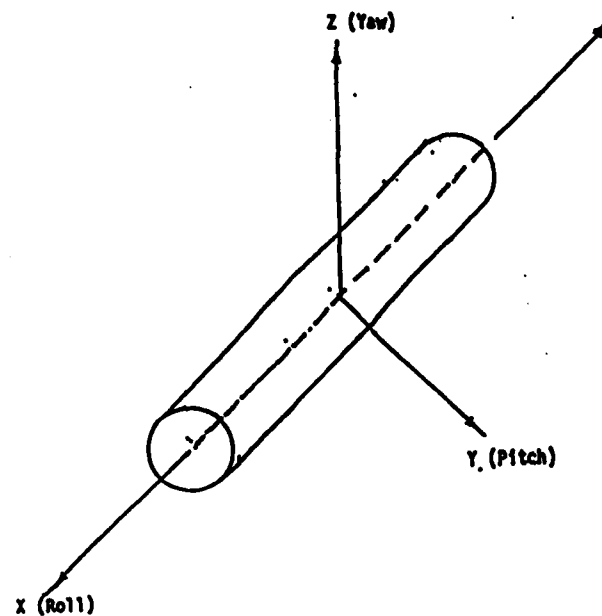


Figure 8-11 The Body Coordinate System

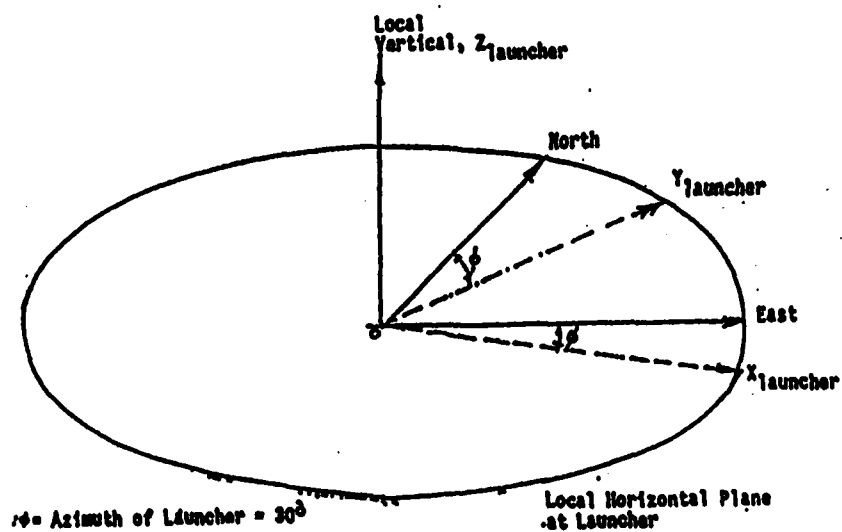


Figure 8-12. Relationship between the Local VEN System and the Launcher Coordinate System (X, Y, Z)

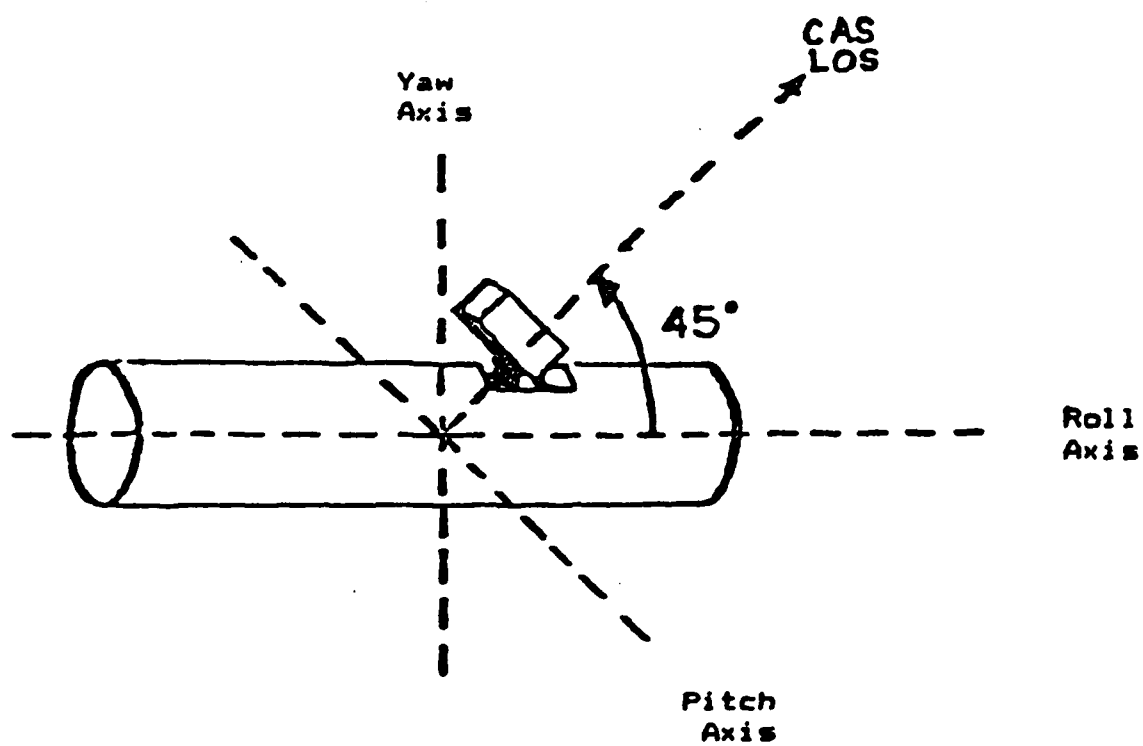


Figure 8.13 CAS Mounting Configuration

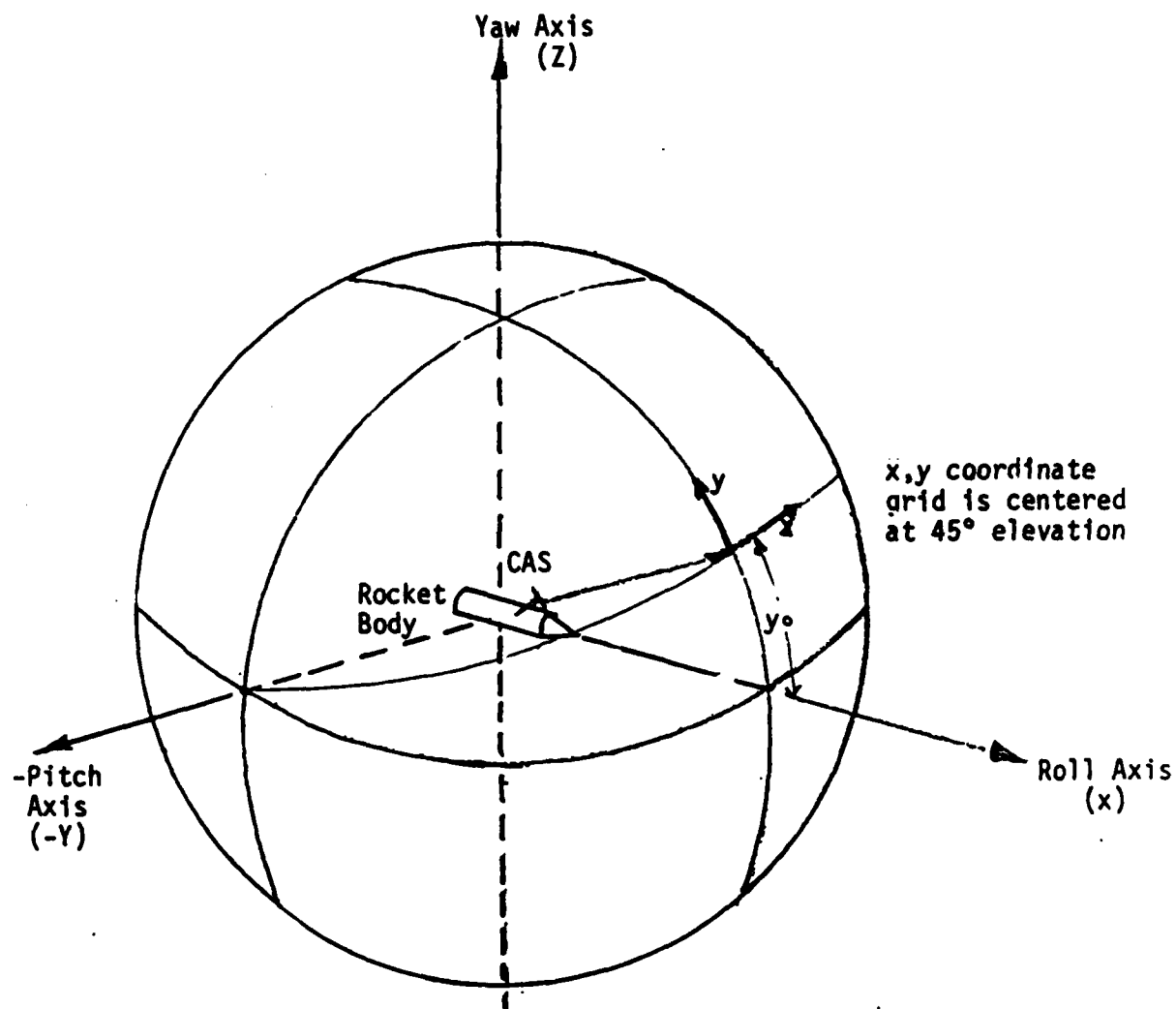


Figure 8-14 Geometrical Relationship between Rocket Body Coordinates and the CAS x-y System.

of each of which contains the body pitch axis, P . The point p also has the body coordinates R_p, P_p , and Y_p . The relationship between the x, y system and the R, P, Y system is given by

$$\begin{aligned}\sin x &= P_p \\ \tan y &= Y_p/R_p\end{aligned}$$

8.2.4 Minimum Displacement Star-to-Detection Fitting: An Optimization Process

The crucial step in utilizing CAS observations to provide corrective updates to gyro-based attitude data is to evaluate those incremental attitude changes which optimally bring the coordinates of the CAS detections into (near) coincidence with the coordinates of the associated catalog stars. The independent variables in the process are the three attitude parameters: pitch, yaw, and roll. The analysis is performed in the field-of-view coordinates of the CAS instrument.

The procedure is to define an analytic "objective" function which quantitatively measures the degree of mismatch. In CASP the objective function is the sum of the squares of the individual displacement distances in the $x-y$ plane of the CAS coordinate space. The Fletcher-Powell optimization algorithm (Reference 2) is then employed to search iteratively for that set of attitude parameters which jointly minimize the objective function. This algorithm belongs to the gradient search class of optimization procedures. When the function to be optimized is ill-behaved, problems can be experienced with this type of approach. However, no difficulty has been encountered in the CASP application.

The user must supply the Fletcher-Powell algorithm with an expression for the objective function, known as FUNCT, by means of which both the function value and the components of

the gradient can be evaluated. Figure 8.15 illustrates the use of FUNCT to compute the data needed to support rapid descent minimization algorithm.

8.2.5 Tangent Height Calculation

The geometry of the problem to be addressed is illustrated in Figure 8.8. The vehicle, located at point V at a radial distance of OV from the center of the earth, O, has its roll axis oriented in the direction R. The problem is to locate the point of closest approach between the surface of the oblate earth and the straight line through point V in the direction of the vehicle's center line, R. At the point of closest approach the perpendicular distance between this line and the earth's surface is defined as the tangent height. In the drawing, the Z axis is the earth's rotational axis and the x-y plane is the earth's equatorial plane.

With the coordinates of point V and the components of R specified, points along the line through V in the direction R are a one parameter family, that parameter, λ , being distance along the line. Similarly, if the surface of the earth is modeled as an oblate spheroid, z coordinates of points on that surface can be represented as functions of their x-y coordinates. An expression can then be written for the distance between an arbitrary point on the line and an arbitrary point on the surface. This function depends on three independent variables: x, y, and distance along the line. The method of solution is to employ this function as an objective function which is to be minimized using the Fletcher-Powell method of rapid descent.

The minimization process is initiated from the spherical earth solution represented by the radial from the center of the earth which is the perpendicular to the tangent line (i.e., R extended). The use of a good first approximation to initialize the process tends to reduce the number iterations

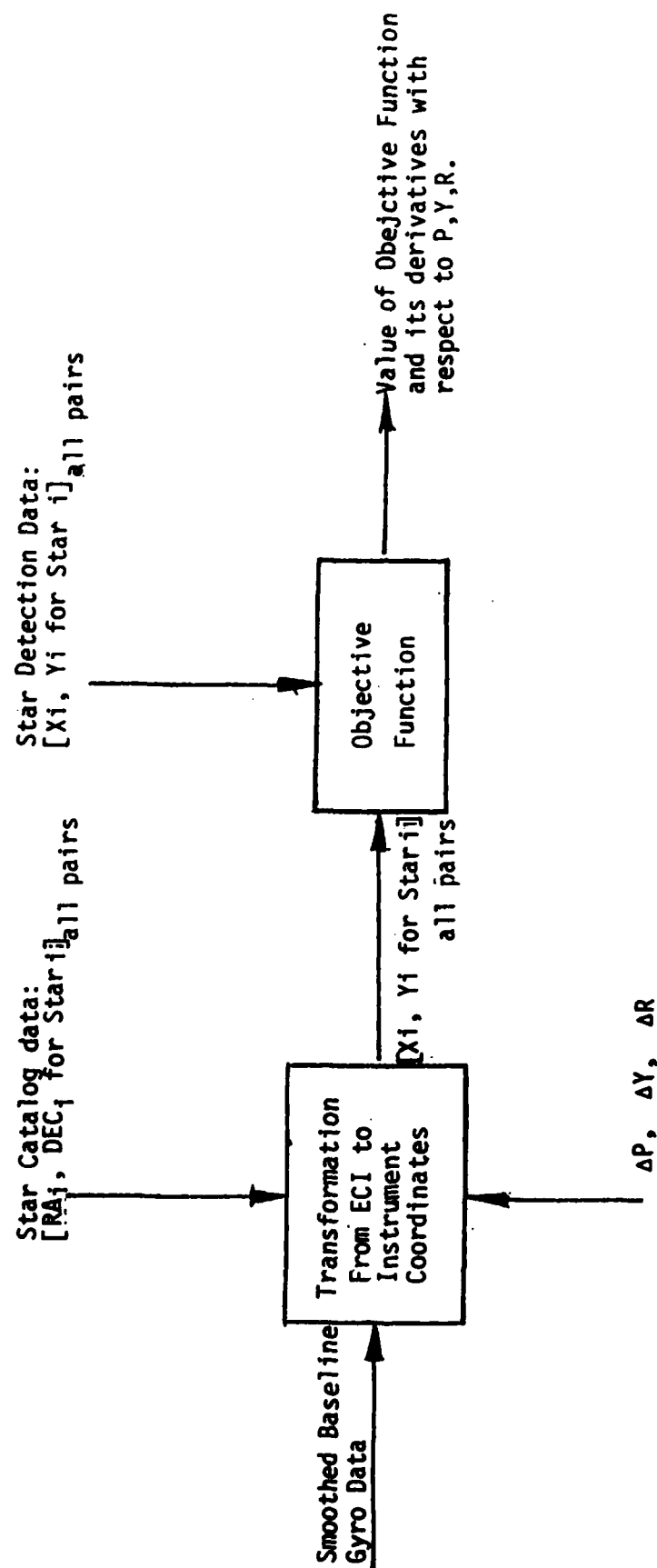


Figure 8-15 Implementation of Subroutine FUNCT. With suitably selected values of ΔP , ΔY , and ΔR (incremental values of attitude parameters), FUNCT is used to provide numerical values of the objective function and its derivatives.

needed to achieve a solution.

Quantities computed are the tangent height, H_t and geodetic and geocentric coordinates of the point on the spheroidal earth below the point of tangency.

8.2.6 Data Quality Considerations

The process of detecting stellar radiation is one which is inherently less than perfect. Viewed simplistically, the level of performance is a function of factors such as the intensity of radiation of the individual stars, the background "noise" level (i.e., the dark-current) of the detectors, the effective integration time, and the level used as a detection threshold. Imperfection in the detection process can manifest itself in several ways: e.g.,

- a) false alarms (noise only events incorrectly declared to be detections)
- b) missed detections
- c) incorrect evaluation of the coordinates for actual and/or apparent pixel-straddling events

The CASP software system performs its functions too far downstream from the detection process to be able to affect either b) or c). However, the fact that the telemetered CAS data involves multiple detection events, coupled with certain necessary conditions which must be met by physically real data, afford the possibility for the CASP software to provide some discrimination against false alarms. Features in the software which capitalize on these principles are discussed in the following four subsections.

8.2.6.1 Roll Rate Discrimination

The possibility exists for the system to lock to real stars on a given frame, but on the succeeding frame to lock to one or more false alarm events, yielding erroneous attitude updates for the second frame. One consequence of this situation would be the likelihood that the magnitude of the change in roll within the time interval between the first and second frames would exceed the bounds imposed by the laws of dynamics governing motion of the vehicle.

A test is performed by CASP to identify excessive inter-frame roll increments. When such an occurrence is detected, automatic frame-to-frame processing is terminated; and manual initiation is needed to re-start the automatic mode of operation.

8.2.6.2 Use of Weighting within the Objective Function

Consider the analysis of data for a frame for which n star-detection associations have been identified. Among the n detections there is a range of detected signal levels. Likewise, there will be variation in optical intensity among the n stars. A crude measure of probability of physical reality of associated pairs is provided by a table such as the following:

| Star Intensity | Detection Level | Probability Event |
|----------------|-----------------|-------------------|
| | | Is Real |
| High | High | High |
| High | Low | Intermediate |
| Low | High | Intermediate |
| Low | Low | Low |

The objective function which is to be minimized in order to evaluate the "true" vehicle attitude is the sum of the squares of the individual mismatch "distances" in x-y space

for each of the identified star-detection associations. To minimize the contributions to this process of likely false alarms, each contribution to the objective function can be weighted in accordance with the table. Choosing actual numerical weights is a largely empirical process based on cut-and-try procedures; values can be specified and adjusted by the user.

A related consideration is the difference in relative accuracies of x and y components of detection location data. Recall that x is determined by position along a one-dimensional CCD array; whereas the y coordinate is deduced from position in the rotational cycle of a scanning mirror. The accuracies of these two physically distinct processes are different. Because x is the more accurate, this coordinate should be accorded more effect in the optimization process. This goal is accomplished by asymmetrical weighting of the x and y contributions to the objective function. Similarly, the dimensioning of the acceptance cell at each detection point must accommodate the greater uncertainty in the y -direction. Accordingly, the box is rectangular, with its y -dimension twice that of x . This asymmetry can be seen in the acceptance cells which are shown in Figure 8.1.

8.2.6.3 Diminishing Size of Acceptance Cells

If, among n identified star-detection associations, n_1 are caused by false alarms, it can be expected that, whenever n_1/n is sufficiently small, the result of the optimization process will be close star-detection spacings for each of the individual $(n-n_1)$ associations corresponding to the real detections; but the spacings for the n_1 cases of false alarms will tend to be substantially greater. It is desirable to window out the false alarms, thereby enabling a more accurate determination of attitude. A procedure to accomplish this employs multiple stages of optimization. At successive

stages the acceptance window is narrowed in both the x and y directions. The concept is that valid star-detection pairs will be relatively closely spaced after the first optimization and will fit within the new, smaller cell. False detection pairs will be more widely spaced and will be rejected by the smaller cell. Optimization can now be repeated, uncorrupted by the false data. The procedure must be truncated whenever $(n-n_1)$ is too small to support a meaningful determination of attitude.

8.2.6.4 Multiple Stars within an Acceptance Cell

In practice more than one star may fall within an acceptance cell centered on a given detection. The choice among the candidate stars is made on the basis of which of them corresponds to the greatest X25 optical intensity.

References

1. Bonito, N.A., Private Communication.
2. Fletcher, R., and M.J.D. Powell, "A Rapid Descent Method for Minimization," Computer Journal, Vol. 6, No. 2, pp 163-168, 1963.

END

12-87

DTIC